Development of advanced biomedical coatings via plasma electrolytic oxidation

By

Arash Mazinani

Supervisors:

Professor Dusan Losic

Dr Md Julker Nine

A thesis submitted in fulfilment of the requirement for the degree of

Doctor of Philosophy

School of Chemical Engineering and Advanced Materials

The University of Adelaide, Australia

July 2021

Table of contents

List of Figures

List of Tables

Declaration

I certify that this work contains no material which has been accepted for the award of any other degree or diploma in my name in any university or other tertiary institution and, to the best of my knowledge and belief, contains no material previously published or written by another person, except where due reference has been made in the text. In addition, I certify that no part of this work will, in the future, be used in a submission in my name for any other degree or diploma in any university or other tertiary institution without the prior approval of the University of Adelaide and where applicable, any partner institution responsible for the joint award of this degree.

The author acknowledges that the copyright of published works contained within this thesis resides with the copyright holders of those works. I give permission for the digital version of my thesis to be made available on the web, via the University's digital research repository, the Library Search and also through web search engines, unless permission has been granted by the University to restrict access for a period of time. I acknowledge the support I have received for my research through the provision of an Australian Government Research Training Program Scholarship.

Arash Mazinani Date: July 18, 2021

Summary

For many decades, the implantation of Ti based biomedical implants has been extensively utilized to improve and restore the patients' quality of life. However, despite advances in technology, failures of the implant do occur. In many cases, the failed Ti implants require immediate removal or correction through surgical operation, which, apart from the substantial economic impact on patients and governments, would cause prolonged suffering for patients. Moreover, the rapid increase in the population's life expectancy necessitates the fabrication and engineering of more reliable orthopaedic implants based on Ti and its allosys for the aged population to address the current issues associated with implant failure. Several factors are involved in bone implant failures, such as bacterial infection and inflammation and poor integration of the bone with the implant surface. Among them, the infection problem requires special attention, as almost two-thirds of the infected implants are not treatable and eventually fail. The emergence of multi-drug resistant (MDR) bacteria is another horrifying issue, which poses a real threat to humankind and is responsible for high mortality rates among vulnerable patients. Fortunately, the emerging advances in nanotechnology and surface engineering can be a promising solution to this crisis. The ideal bone implant should possess antibacterial properties as well as the high bioactivity required for osseointegration improvement. In this regard, novel surface modification treatments such as the plasma electrolytic oxidation technique (PEO) has proven to be effective in the bioactivity improvement of titanium-based implants. However, the development of the PEO treated surface with antibacterial properties is still challenging. This study aims to implement innovative approaches to address the critical factors associated with titanium implant failure by applying post-PEO treatments such as hydrothermal process and

functionalizing the surface with novel 2D materials. This thesis is presented in eight chapters, including a comprehensive literature review and several published, under review or confidential unpublished papers. In brief, the significant contributions of this work fall into four categories as follows:

- Engineering of nanostructured titania surfaces with tunable and mixed topography (paper 1).
- Optimal fabrication of antibacterial titania nanostructures, a combined approach of plasma electrolytic oxidation and hydrothermal treatment (paper 2).
- Antibacterial development of titania surface with the application of graphene oxide and PEO-EPD technique (paper 3).
- Comparative antibacterial activity of 2D materials coated on the porous-titania against gram-positive (*S. aureus*) and gram-negative (*E.coli*) bacteria (paper 4).

Acknowledgment

I would like to extend my heartfelt gratitude to the individuals and organizations mentioned below, whom without their unwavering support and encouragement, I would not have been able to complete my PhD journey:

i. My esteemed principal supervisor **Professor Dusan Losic** for his invaluable support and mentorship during the course of my PhD degree. His guidance into the world of nanotechnology has been a valuable input for this thesis.

ii. I'd like to express my appreciation to **Dr Md Julker Nine**, my PhD co-supervisor, for all of his assistance and invaluable guidance.

iii. My special thanks go to **Prof Reza Ghomashchi, Dr Jacqui McRae**, **Dr Animesh Basak**, **Dr Hadi Rastin**, **Dr Diana Tran**, **Dr Tran Tung, Dr Sanaz Orandi, Dr Shervin Kabiri** and **Prof Sarah Vreugde** who expertly helped me in different stages of my PhD journey.

iv. I also would like to thank the ARC Research Hub for Graphene Enabled Industry Transformation, Adelaide microscopy, School of Chemical Engineering and Advanced Materials, and School of Molecular Life Sciences at the University of Adelaide, the Basil Hetzel Institute for Translational Health Research and Department of Chemistry, Materials and Chemical Engineering "G. Natta" at the Polytechnic University of Milan for providing the support and facilities to proceed with this study.

v. In addition, I would like to express gratitude to **Prof Roberto Chiesa**, **Prof Gabriele Candiani**, **Dr Paolo Tarsini** from the Polytechnic University of Milan and **Mr James Lee**, **Dr Alexandra Tikhomirova** and **Dr Stephen Kidd** from

Adelaide University, who skilfully helped me to run and understand biological and antibacterial studies despite their busy schedule.

vi. Additionally, I would like to thank all my friends and family in Sydney and Adelaide, who gave me the love and strength to carry on during my stay in Australia.

Finally, I will be eternally grateful to my parents for their unparalleled love and unending support throughout my life. Without them, this journey would not have been possible. In particular, I'd like to dedicate this dissertation to my parents and my beloved grandmother.

Arash Mazinani

List of publications

This PhD thesis is submitted as a "thesis by publication" in accordance with the "Specifications for Thesis 2020" of The University of Adelaide.The outcomes generated during my PhD candidature include six published, accepted for publication or under reviewed journal articles (first-authored journal papers: one published, one in review, two under confidential embargo and co-authored journal papers: four, and conference/workshop presentations: three

List of journal publications/protocols (first author):

1. **Arash Mazinani**, Md Julker Nine, Roberto Chiesa, Gabriele Candiani, Paolo Tarsini,Tran Thanh Tung, Dusan Losic. Graphene oxide (GO) decorated on multi-structured porous titania fabricated by Plasma Electrolytic Oxidation (PEO) for enhanced antibacterial performance, Material and Design. 2021; Volume 200; 109443. doi.org/10.1016/j.matdes.2020.109443.
2. **Arash Mazinani**, Hadi Rastin, Md Julker Nine, James Lee, Alexandra Tikhomirova, Tran Thanh Tung, Reza Ghomashchi, Stephen Kidd, Sarah Vreugde, Dusan Losic. Comparative antibacterial activity of 2D materials coated on the porous titania. Royal Society of Chemistry's Journal of Materials Chemistry B, 2021. doi.org/10.1039/D1TB01122G.
3. **Arash Mazinani**, Hadi Rastin, MD Julker Nine, Diana Tran, Tran Thanh Tung, Dusan Losic. Engineering of nanostructured titania surfaces with tunable and mixed topography by combined plasma electrolytic oxidation (PEO) and hydrothermal process. To be published (under confidentiality embargo).
4. **Arash Mazinani**, Md Julker Nine, Hadi Rastin, Roberto Chiesa, Gabriele Candiani, Paolo Tarsini, Dusan Losic. Towards optimal fabrication of antibacterial titania nanostructures via advanced mechano-bactericidal PEO surface. To be published (under confidentiality embargo).

List of journal papers from collaboration (co-author):

1. Maher S, **Mazinani A**, Barati MR, Losic D. Engineered titanium implants for localized drug delivery: recent advances and perspectives of Titania nanotubes arrays. Expert Opin Drug Deliv. 2018; Volume 15; 1021-1037. DOI:10.1080/17425247.2018.1517743

2. Rastin H, Zhang B, **Mazinani A**, Hassan K, Bi J, Tung TT, Losic D. 3D bioprinting of cell-laden electroconductive MXene nanocomposite bioinks. Nanoscale. 2020;12(30):16069-16080. **Featured in journal cover, Recognized as a part of most popular collection papers during 2020 in the Nanoscale journal.** DOI: 10.1039/D0NR02581J

3. Rastin H**,** Ramezanpour M, Hassan K, **Mazinani A**, Tung TT, Vreugde S, Losic D. 3D Bioprinting of a Cell-laden Antibacterial Polysaccharide Hydrogel Composite. Carbohydrate Polymers. 2021:117989. DOI: 10.1016/j.carbpol.2021.117989

4. Rastin H, Mansouri N, Hassan K, **Mazinani A**, Ramezanpour M, Yap P, Yu L, Tran TT, Vreugde S, Losic D. Converging 2D Nanomaterials and 3D Bioprinting Technology: State-of-the-Art, Challenges and Potential Outlook in Biomedical Applications, Small, 2021. DOI.ORG/10.1002/ADHM.202101439

List of conference/workshop presentations:

1. **Arash Mazinani**, MD Julker Nine, Tran Tung, Dusan Losic. Antibacterial activity of GO quantum dots deposited on PEO titanium substrate, third ARC Graphene Research Hub Workshop, 2021. (**Oral presentation**)
2. **Arash Mazinani**, MD Julker Nine, Dusan Losic, Tailoring nanostructured Titania with GO/rGO sheets for biomedical applications**,** second Annual Graphene Hub Workshop (GHW2020) conference paper, Melbourne, Australia, 2020. (**Poster presentation**)
3. **Arash Mazinani**, Diana Tran, Dusan Losic. Plasma Electrolytic Oxidation (PEO) engineered titanium surface combined with Electrophoretic Deposition of Graphene Oxide (GO). First Australian-Europe Graphene Workshop, 2018. (**Poster presentation**)

List of awards and distinctions:

1. **Selected publication by ECMS Director of Academic Excellence as 'high impact' publications and identified as 'Industry Impact – Health Solutions IEP'**. (Paper published in Material and Design. doi.org/10.1016/j.matdes.2020.109443
2. Collaboration in the paper published as a part of a **most popular collection of papers during 2020 in the Nanoscale journal.** DOI: 10.1039/D0NR02581J
3. **One journal covers from my collaboration in the paper** featured in the "Nanoscale" journal. DOI: 10.1039/D0NR02581J

This page is left blank intentionally

Chapter 1

Introduction and motivation

This chapter provides a summary of the current challenges regarding the application of orthopaedic implants worldwide. Different types of bone implants are introduced, and the impact of implant failure and replacement surgery on the patient's health and the government's budget are discussed. Next, the most common factors involved in implant failure and typical infection treatment/prevention methods are briefly reviewed. This chapter also provides information on the current classifications of antibacterial coatings and their pros and cons in the fight against the infection associated with biomedical implants. Moreover, it highlights the necessity to develop new types of antibacterial surface to target multidrug resistant (MDR) bacteria as an immense life-threatening crisis, which requires immediate medical intervention.

1.1. Current challenges with bone implants

Nowadays, metallic orthopaedic and dental implants are widely used to serve the human body and improve patients' quality of life. In general orthopaedic implants can be classified based on their serving life span into two main groups of permanent (such as the knee, joint, dental implants. etc.) and temporary implants (including pins, wire, screws, bars, etc.) [1]. Particularly for permanent orthopaedic implants, long-term successful implantation is vital as the implant must function effectively during the life span of the patients [2, 3]. Therefore, metallic implants, made of titanium or stainless steel, with superior physicial and mechanical stability are widely used as permanent orthopedic implants [1, 4-7]. However, despite advances in technology, bone implant failure still occurs due to various causes such as loosening of the implant, rejection of the implant by the host, poor bone integration around the implant surface and bone infection complications, etc. (**Figure 1.1**) . Moreover, host factors such as patients bone condition including osteomyelitis (OM) or infectious inflammation of bone and osteoporosis (OP) or low bone density are other factors, which adversely reduce the lifetime of implants and result in implant failure [8]. Failed implants need to be replaced or corrected through a surgical operation, which, apart from causing pain for patients, would result in a substantial economic impact on people and governments [9].

Moreover, the common practice for treating musculoskeletal infection is the systemic administration of antibiotics [9]. The antibiotics are also administrated before implantation surgery as a preventive method to tackle peri-operative infection[10]. However, this type of prophylactic antibiotics administration has several drawbacks, such as being ineffective due to the comparatively low antibiotic concentration received

at the affected site, adversely engaging other organs and the need for the administration at the correct time (**Figure 1.1**) [11]. Therefore in several cases, such as deep bone infection, systemic therapy sometimes fails to treat the infection and failed implant required to be removed [12].

Currently, more than 5 % of revision surgeries involving implantation for fracture fixation are associated with infection complications [13]. Moreover, failure in spine surgery due to infections comprises around 5% of cases [11]. The treatment of infected implants may require multiple expensive revision surgeries, which adversely affect the recovery period of patients and may increase the risk of patient's mortality [14]. Furthermore, the emergence of antimicrobial-resistant bacteria drastically has added to the current complexity of medical treatments. It has been reported that Multi-drug resistant (MDR) bacteria take the life of around 700.000 patients each year worldwide [14]. The mortality associated with MDR bacteria can soar up to 10 million in 2050 if the proper action is not taken now [15]. Moreover, the unnecessary application of antibiotics (Intervenous antibiotics) for infection treatment has significantly increased the fear regarding the emergence of new MDR bacteria such as the *methicillin-resistant staphylococcus aureus* (MRSA) worldwide [16]. Different mechanisms are involved in the resistance of MDR bacteria to the current antibiotics while the most important ones are altering the antibacterial agent's uptake, the implication of efflux pump, formation of protective biofilm around bacteria and obtaining resistant genes [17].

Excessive application of antibacterial agents in antimicrobial therapy can also affect the infected site and the surrounding tissues, which may cause treatment side effects such as compromised host responses that can be problematic to the patient

(**Figure 1.1**) [15]. Therefore, studies focus on alternative approaches such as tackling bacterial infection via the development of various antimicrobial surfaces and coatings [10].

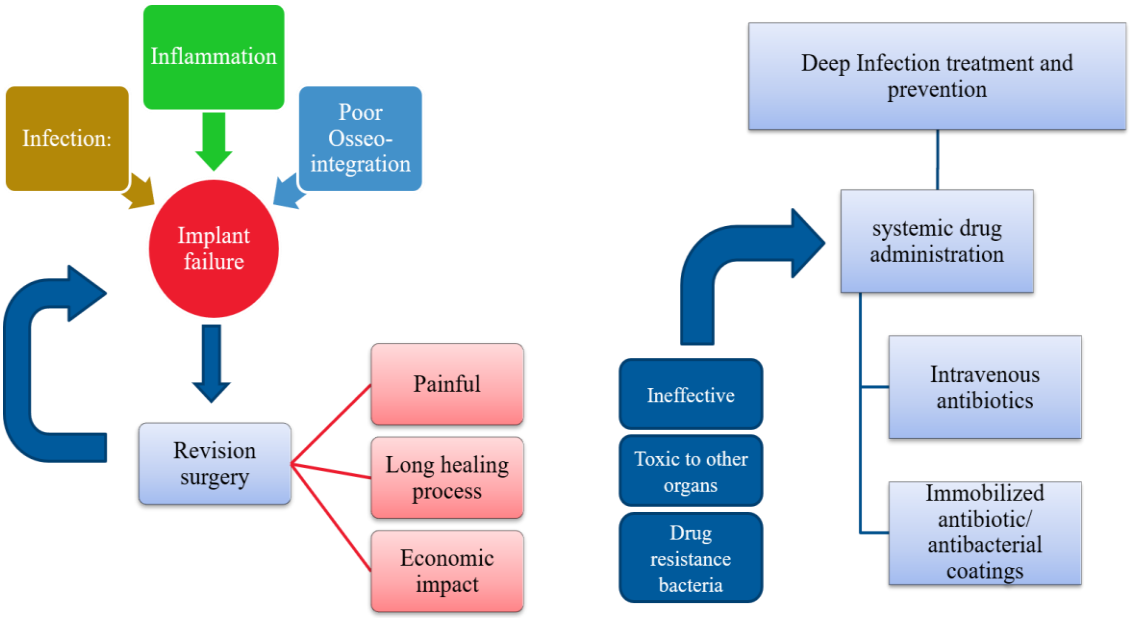

Figure 1.1. Factors involved in the bone implant failure, challenges with the orthopaedic implant and typical infection treatment/prevention methods.

These approaches aim to locally provide the orthopaedic implant with antibacterial properties, where it is most needed and prevent attachment of bacteria or biofilm formation, which eventually may lead to implant-related infections and implant failure [18, 19]. Although there is no universal agreement on a standard classification for antibacterial coating technologies, the current antimicrobial coating approaches can be classified into three main streams (**Figure 1.2**) [21, 22].

A) Passive surface modification treatments (PSM) also known as passive coatings

Passive coatings are designed to address the infection issue by inhibiting or reducing bacterial attachment to the implant surface or killing them upon direct contact with their modified surface. Therefore, no antibacterial agents are involved in the killing process. The engineering of the physiochemical properties of implant surfaces, such as topography, roughness, chemical composition, wettability, and conductivity, significantly influence bacterial adhesion and colonization ability . The desired surface modification treatments are achievable via the application of different techniques such as covalent grafting of bioactive materials to the implant surface, ultraviolet light irradiation of titanium implants, the application of suitable anchors such as silane anchor, catechol anchor, phosphor-based anchor, crystal structure modification and micro-nano texturing [19]. Passive coatings have received significant attention because they can provide bacteriostatic/ bactericidal properties to the target site for a comparatively long time without affecting surrounding body organs, and more importantly, they do not require replenishment of antibacterial agents [10, 23, 24].

However, there are several concerns related to passive coatings in the actual clinical application. Particularly, the achieved robust anti-adhesion properties in some of the engineered passive coatings can negatively interfere with the osseointegration ability of the surface and result in the mechanical loosening of the implant, which eventually may lead to the implant failure . In addition, research showed some passive coatings might be less effective against a specific range of bacteria adhesion, therefore failing to prevent biofilm formation. Moreover, the application of passive coatings in the orthopaedic field

requires further comprehensive in vivo studies to ensure the safe application of this technique in the long-term on the human body [19].

B) Active surface modification (ASM), also known as active coatings

In this approach, antimicrobial agents are pre-incorporated to the implant surface [25]. The antimicrobial compounds can be in the form of antibiotics, nanoparticles such as metal ions,

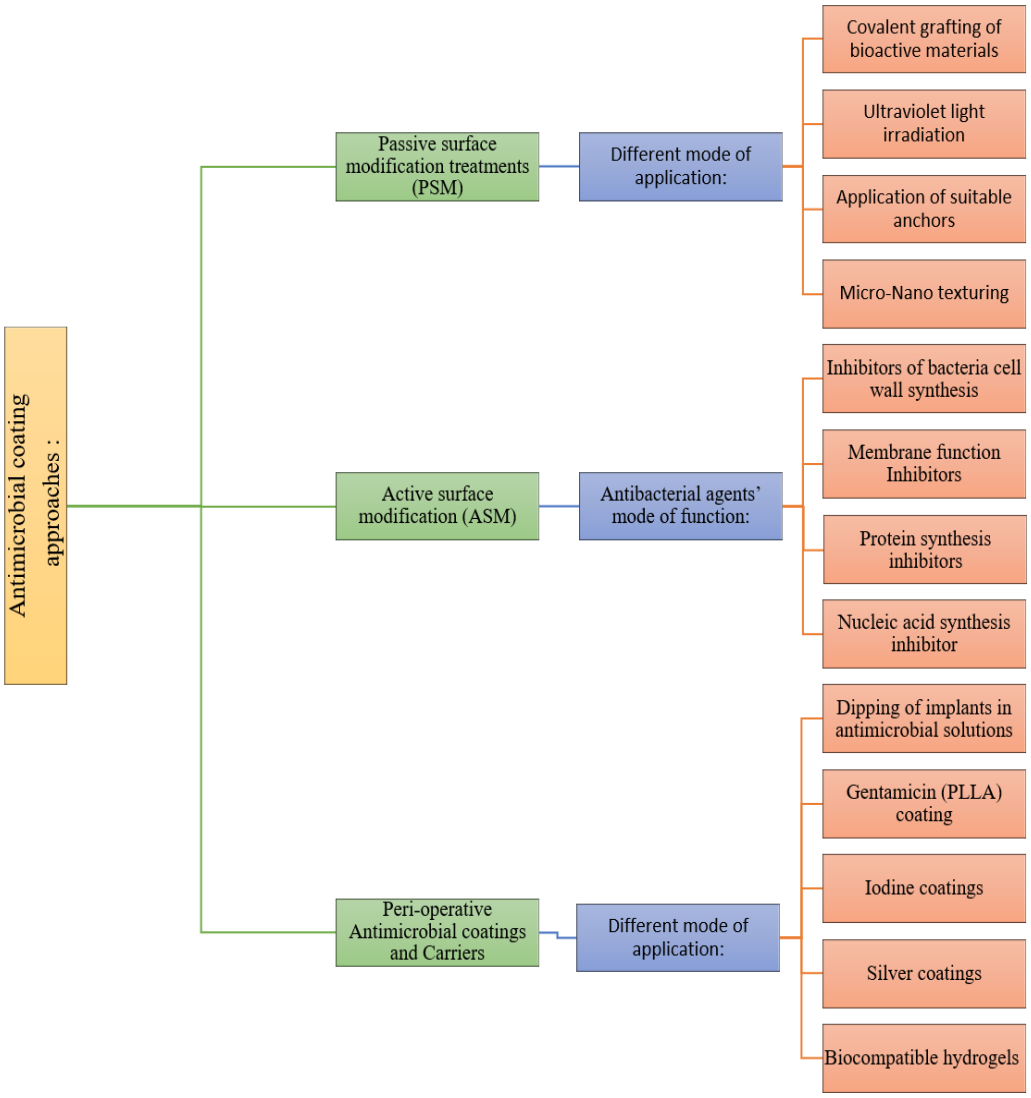

Figure 1.2. Antimicrobial coatings approaches and corresponding mode of application/function.

2D materials, antimicrobial peptides (AMPs) or a combination of other organic and inorganic materials [26-29]. The antibacterial agents can fight against a different type of bacteria with two modes of action:

- Antibacterial agents such as (Penicillins, Gentamicin, Silver nanoparticles, 2D materials, etc.) that can kill bacteria via direct damaging and/or destroying the cell wall/membrane of bacteria are called a bactericidal agent.
- Other antibacterial agents such as Sulphonamides, Tetracycline, Trimethoprim, which slow or block the reproduction and growth of bacteria, are termed as bacteriostatic agents.

In general, bacteriostatic agents may intervene with bacteria multiplying metabolism via preventing nutrients from reaching pathogenic bacteria, blocking protein synthesis, etc. and providing time for the immune system to fight infection [26]. It is worth mentioning that, while this type of classification is accepted by some experts, in reality, when a high dose of antibacterial agents is administrated, it would be difficult to define a clear boundary between these two groups of antibacterial materials [26]. Alternatively, the general antibacterial agents' mode of function for both bactericidal and bacteriostatic materials can be categorized as follow:

- Inhibitors of bacteria cell wall synthesis,
- Membrane function Inhibitors,
- Protein synthesis inhibitors,
- Nucleic acid synthesis inhibitor [10].

Nevertheless, the application of orthopaedic implants with a permanent coating of antibacterial agents has been widely criticized by experts, as it can lead to the emergence

of new MDR bacteria and can affect not only the target area but also surrounding organs, leading to general toxicity and in some cases poor osseointegration [32].

C) Peri-operative antimicrobial coatings and carriers

In this approach, antimicrobial properties of the implant are introduced at the time of surgical operation and before the implantation via various techniques. This method can provide short-term antimicrobial properties that act locally, therefore minimizing side effects such as toxicity of other organs, which is commonly associated with long-term systemic drug administration [10, 21]. This methodology would help decrease the regulatory requirements related to new antibacterial implants' approval for clinical application, which is laborious and costly. Moreover, the combination of antimicrobial agents with currently available implant products can be an economical and straightforward approach to improve implants' antibacterial activity. The practical techniques available for the fabrication of peri-operative antimicrobial coatings comprise the dipping of implants in antimicrobial solutions, gentamicin (PLLA) coating, iodine coatings, silver coatings, biocompatible hydrogels such as fast-resorbable hydrogel coating [19, 21, 32, 34-36].

Although these methods appear promising, there are still some concerns that may limit their application, such as:

- The toxicity of silver ions may damage the implant's surrounding tissues and affect other organs [38].
- Gentamicin (PLLA) coating is currently available solely for few particular designs and does not apply to all type of orthopaedic devices such as screws. Furthermore,

recent studies demonstrate that different bacteria are becoming more resistant to gentamicin [39].

- Antibacterial-loaded hydrogel coatings also require further in vivo studies to guarantee their safe application in the long term for the human body [40].

As discussed earlier, poor bonding of Ti implant surface with bone cells is another major issue in the clinical application of implants. These problems will be discussed in the next chapter in more details.The surface modification treatments of the implant have proved to be a practical approach to enhance the osseointegration properties and improve implants' lifetime. It is worth mentioning that the design and engineering of the implant surface, which possesses both osseointegration and antimicrobial properties, have been constantly one of the major challenges in the development of orthopaedic implants. Recent advances in nanotechnology can be a potential solution to the aforementioned challenges. Nanoparticles, 2D materials and nanostructures are in the size range, negligible to the biological entities and have demonstrated their effectiveness in different bio-applications such as drug delivery [41], infection treatment [42] and biotechnology [43, 44]. Moreover, their application in bone implant development has recently received significant attention. Nevertheless, research in this area is ongoing, and there are plenty of rooms for innovation, fabrication and development of the new generation of bioactive orthopaedic implants with improved antibacterial activity.

1.2. Research aims and objectives

The main aim of the current project was to develop novel biomedical coatings on plasma oxidation treated titanium implants (PEO) to improve osseointegration and antibacterial activity of the surface simultaneously, therefore decrease the chance of

implant failure. To achieve this crucial goal, various aspects of nanotechnology were utilized to form and develop nanostructures, micro-nano porosity and 2D materials on the titanium-based surface in a simple and cost-effective manner. These techniques provided the implant surface with high antimicrobial activity (through passive or active antibacterial modification approaches) while maintaining the original high bioactivity of PEO treated substrates. The above-mentioned primary aim can be further narrowed down into the following objectives :

I. To fabricate a novel type of titania nanostructures on PEO treated substrate through a hydrothermal route that can improve the bioactivity:

- To characterize the fabricated nanostructures' physicochemical properties.
- To investigate the effect of HT duration on the morphology and the bioactivity of the generated nanostructures.

II. To optimize the advanced PEO conditions and develop nanostructures with antimicrobial activity:

- To explore the effect of PEO conditions (such as chemical composition) and HT duration on the morphology and antimicrobial activity of fabricated nanostructures.

III. To explore the application of the advanced electrophoretic techniques for the deposition of graphene oxide (GO) patches on PEO substrate:

- To assess the bioactivity and antibacterial efficiency of the fabricated coating.
- To characterize the mechanical and physicochemical properties of the fabricated coatings.

IV. To investigate the incorporation of other 2D materials such as (hBN, MXene, and GO) on the PEO substrate for potential biomedical implant applications:

- To compare the antibacterial activity of the fabricated samples at different concentrations.
- To assess the bioactivity of the optimized 2D deposited samples.

1.3. Thesis outline

This thesis is comprised of 8 chapters. The following summary provides a brief description of each chapter and its connection to the aforementioned objectives towards the development of a new generation of biomedical implants with antimicrobial and osseointegration properties:

- **Chapter 1**

The introduction provides general information about orthopaedic implants and current challenges regarding the development of bone implants with a focus on antimicrobial coating technologies. This chapter also presents the outline and structure of the thesis.

- **chapter 2**

The literature review provides a more profound and extensive description of the implant failure problem. It discusses various surface modification treatments available to improve osseointegration and antimicrobial activities of the titanium bone implants. This chapter also presents the identified gaps based on the literature data and hypothesis to combine plasma electrolytic oxidation technique with post-surface treatments to address both infection and poor osseointegration issues of titanium implants simultaneously.

- **Chapter 3**

Research Methodology presents the design of PEO set-up, post-treatment process (including the hydrothermal treatment (HT), PEO-EPD, drop-casting techniques, characterization methods, bioactivity and antibacterial assessment protocols.

- **Chapter 4**

Engineering of nanostructured titania surfaces with tuneable and mixed topography by combined plasma electrolytic oxidation (PEO) and hydrothermal treatment (HT). In brief, HT was applied to form and optimize the nanostructures such as nano-roots, nano-blades, nano-spikes, and nano-belt over the PEO substrate. The resulted nano-textures significantly improved the bioactivity of the PEO treated surface.

- **Chapter 5**

Towards optimal fabrication of antibacterial titania nanostructures: A combined approach of plasma electrolytic oxidation and hydrothermal treatment. The PEO substrate was formed in the different chemical electrolytes, and the effect of PEO chemical composition on the formation and growth of titania nanostructures were thoroughly investigated. Optimized samples demonstrated superior antibacterial properties and high bioactivity (paper under confideiality embargo).

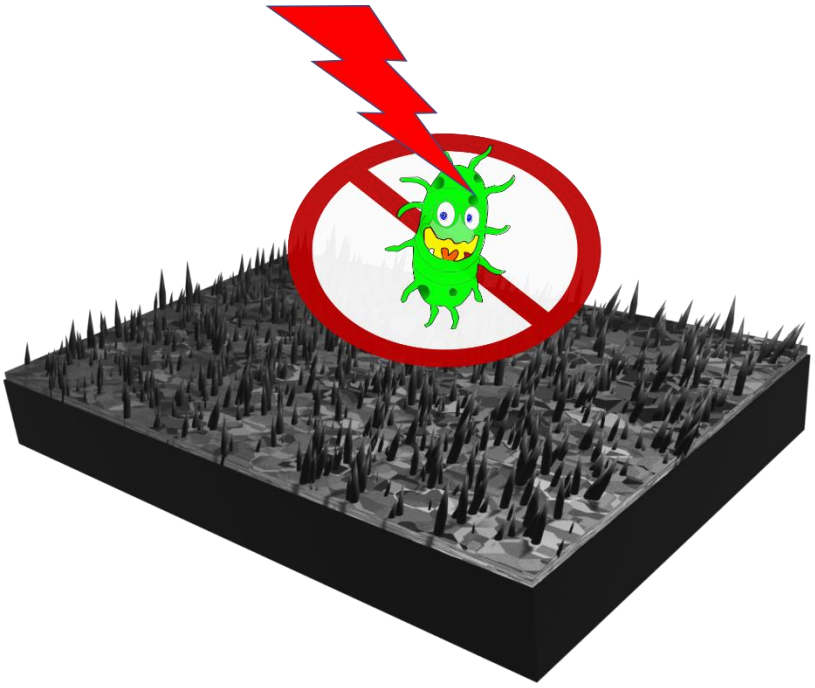

Figure 1.3. Graphical abstract of "Towards optimal fabrication of antibacterial titania nanostructures: A combined approach of plasma electrolytic oxidation and hydrothermal treatment ".

- **Chapter 6**

Antibacterial development of titania PEO surface with PEO-EPD technique. In the novel approach, the high voltage electrophoretic deposition technique, also known as the PEO-EPD technique, was utilized to deposit GO patches on the titania PEO substrate to improve antibacterial properties and bioactivity simultaneously (Published paper).

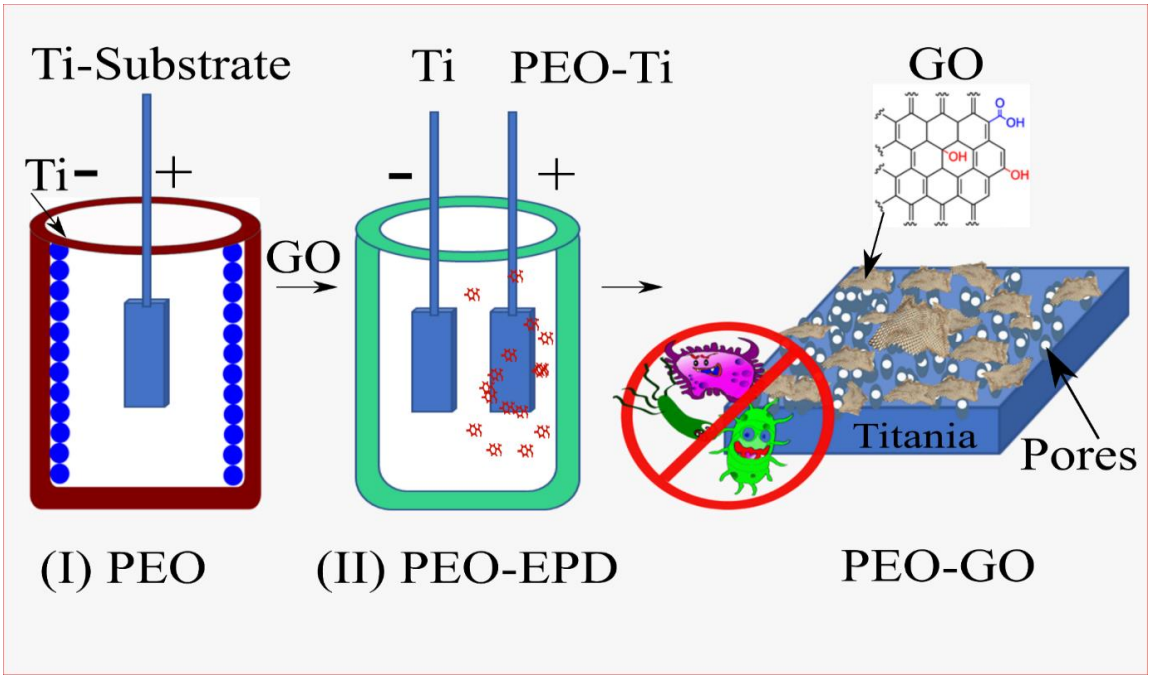

Figure 1.4. Graphical abstract of "Graphene oxide (GO) decorated on multi-structured porous titania fabricated by plasma electrolytic oxidation (PEO) for enhanced antibacterial performance".

- **Chapter 7**

Antibacterial activity and biomineralization ability of modified samples were investigated at different concentration of added 2D materials flakes (Paper submitted for publication).

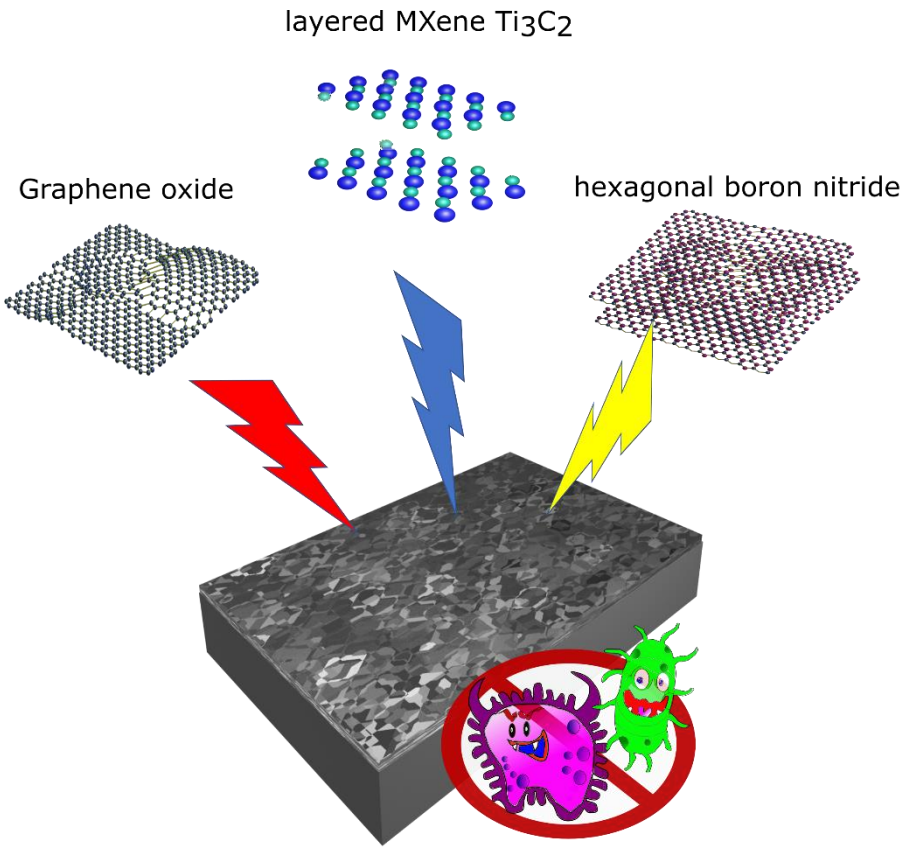

Figure 1.5. Graphical abstract of "Comparative antibacterial activity enhancement study of the porous-titania PEO coatings using various 2D materials".

- **Chapter 8**

  Conclusions and future work highlights the summary of results obtained in this work and recommend future direction of studies on the current topic.

1.4. References

1. Jin, W. and P.K. Chu, *Orthopedic Implants*, in *Encyclopedia of Biomedical Engineering*, R. Narayan, Editor. 2019, Elsevier: Oxford. p. 425-439.
2. Sidambe, A.T.J.M., *Biocompatibility of advanced manufactured titanium implants—A review.* 2014. **7**(12): p. 8168-8188.
3. Losic, D., *Advancing of titanium medical implants by surface engineering: recent progress and challenges.* Expert Opinion on Drug Delivery, 2021: p. 1-24.
4. Lew, D.P. and F.A.J.N.E.J.o.M. Waldvogel, *Osteomyelitis.* 1997. **336**(14): p. 999-1007.
5. Esposito, M., et al., *Biological factors contributing to failures of osseointegrated oral implants,(I). Success criteria and epidemiology.* 1998. **106**(1): p. 527-551.
6. PA, L., et al., *Sensitivity to titanium. A cause of implant failure?* 1991. **73-B**(1): p. 25-28.
7. Darouiche, R.O., *Treatment of infections associated with surgical implants.* N Engl J Med, 2004. **350**(14): p. 1422-9.
8. Camps-Font, O., et al., *Postoperative Infections After Dental Implant Placement: Prevalence, Clinical Features, and Treatment.* Implant Dentistry, 2015. **24**(6).
9. Bratzler, D.W. and P.M.J.C.I.D. Houck, *Antimicrobial prophylaxis for surgery: an advisory statement from the National Surgical Infection Prevention Project.* 2004: p. 1706-1715.
10. Romanò, C.L., et al., *Antibacterial coating of implants in orthopaedics and trauma: a classification proposal in an evolving panorama.* Journal of Orthopaedic Surgery and Research, 2015. **10**(1): p. 157.
11. Kose, N. and A. Ayse Kose, *Chapter 7 - Application of Nanomaterials in Prevention of Bone and Joint Infections*, in *Nanotechnology in Diagnosis, Treatment and Prophylaxis of Infectious Diseases*, M. Rai and K. Kon, Editors. 2015, Academic Press: Boston. p. 107-117.
12. Moriarty, T.F., et al., *Infection in fracture fixation: Can we influence infection rates through implant design?* Journal of Materials Science: Materials in Medicine, 2010. **21**(3): p. 1031-1035.
13. Hickok, N.J. and I.M.J.A.d.d.r. Shapiro, *Immobilized antibiotics to prevent orthopaedic implant infections.* 2012. **64**(12): p. 1165-1176.
14. O'Neill, J., *Tackling drug-resistant infections globally: final report and recommendations.* 2016.
15. Ivanova, E.P., et al., *The multi-faceted mechano-bactericidal mechanism of nanostructured surfaces.* 2020. **117**(23): p. 12598-12605.
16. Khameneh, B., et al., *Breakthroughs in bacterial resistance mechanisms and the potential ways to combat them.* Microb Pathog, 2016. **95**: p. 32-42.
17. Amin Yavari, S., et al., *Combating Implant Infections: Shifting Focus from Bacteria to Host.* 2020. **32**(43): p. 2002962.
18. Salwiczek, M., et al., *Emerging rules for effective antimicrobial coatings.* 2014. **32**(2): p. 82-90.

19. Chouirfa, H., et al., *Review of titanium surface modification techniques and coatings for antibacterial applications.* 2019. **83**: p. 37-54.
20. Chouirfa, H., et al., *Review of titanium surface modification techniques and coatings for antibacterial applications.* Acta Biomaterialia, 2019. **83**: p. 37-54.
21. Romanò, C.L., et al., *Antibacterial coating of implants: are we missing something?* Bone & joint research, 2019. **8**(5): p. 199-206.
22. Losic, D.J.E.O.o.D.D., *Advancing of titanium medical implants by surface engineering: recent progress and challenges.* 2021(just-accepted).
23. Bačáková, L., et al., *Cell adhesion on artificial materials for tissue engineering.* 2004. **53**(Suppl 1): p. S35-S45.
24. Braem, A., et al., *Staphylococcal biofilm growth on smooth and porous titanium coatings for biomedical applications.* 2014. **102**(1): p. 215-224.
25. Liu, X., et al., *Surface modification of titanium, titanium alloys, and related materials for biomedical applications.* 2004. **47**(3-4): p. 49-121.
26. Ullah, H. and S.J.A.a. Ali, *Classification of anti-bacterial agents and their functions.* 2017. **10**.
27. Mahajan, G.B. and L.J.F.B. Balachandran, *Antibacterial agents from actinomycetes-a review.* 2012. **4**(4): p. 240-53.
28. Stoimenov, P.K., et al., *Metal oxide nanoparticles as bactericidal agents.* 2002. **18**(17): p. 6679-6686.
29. Rajavel, K., et al., *Achieving high bactericidal and antibiofouling activities of 2D titanium carbide (Ti3C2Tx) by delamination and intercalation.* 2019. **6**(3): p. 035040.
30. Pankey, G.A. and L.J.C.i.d. Sabath, *Clinical relevance of bacteriostatic versus bactericidal mechanisms of action in the treatment of Gram-positive bacterial infections.* 2004. **38**(6): p. 864-870.
31. Rezaei, M., M. Komijani, and S.M.J.A.S.f.A.A. Javadirad, *Bacteriostatic agents.* 2012: p. 219-234.
32. Romanò, C.L., et al., *Antibacterial coating of implants in orthopaedics and trauma: a classification proposal in an evolving panorama.* 2015. **10**(1): p. 1-11.
33. Bayramov, D.F. and J.A. Neff, *Beyond conventional antibiotics — New directions for combination products to combat biofilm.* Advanced Drug Delivery Reviews, 2017. **112**: p. 48-60.
34. Drago, L., et al., *Does implant coating with antibacterial-loaded hydrogel reduce bacterial colonization and biofilm formation in vitro?* 2014. **472**(11): p. 3311-3323.
35. Darouiche, R.O., *Antimicrobial Approaches for Preventing Infections Associated with Surgical Implants.* Clinical Infectious Diseases, 2003. **36**(10): p. 1284-1289.
36. Darouiche, R.O.J.C.i.d., *Antimicrobial approaches for preventing infections associated with surgical implants.* 2003. **36**(10): p. 1284-1289.
37. Prabhu, S. and E.K.J.I.n.l. Poulose, *Silver nanoparticles: mechanism of antimicrobial action, synthesis, medical applications, and toxicity effects.* 2012. **2**(1): p. 1-10.
38. Dowding, J.E., *Mechanisms of gentamicin resistance in Staphylococcus aureus.* Antimicrobial agents and chemotherapy, 1977. **11**(1): p. 47-50.

39. Drago, L., et al., *Does Implant Coating With Antibacterial-Loaded Hydrogel Reduce Bacterial Colonization and Biofilm Formation in Vitro?* Clinical Orthopaedics and Related Research®, 2014. **472**(11): p. 3311-3323.
40. Spencer, D.S., A.S. Puranik, and N.A.J.C.o.i.c.e. Peppas, *Intelligent nanoparticles for advanced drug delivery in cancer treatment.* 2015. **7**: p. 84-92.
41. Chen, J., et al., *Antibacterial polymeric nanostructures for biomedical applications.* 2014. **50**(93): p. 14482-14493.
42. West, J.L. and N.J.J.C.o.i.B. Halas, *Applications of nanotechnology to biotechnology: Commentary.* 2000. **11**(2): p. 215-217.
43. Lavenus, S., G. Louarn, and P.J.I.j.o.b. Layrolle, *Nanotechnology and dental implants.* 2010. **2010**.
44. Tran, P.A., et al., *Opportunities for nanotechnology-enabled bioactive bone implants.* 2009. **19**(18): p. 2653-2659.

Chapter 2

Literature review

After outlining the current challenges with the implantation of orthopaedic devices and defining the importance of new approaches to overcome implant failure in the previous chapter, this chapter focuses on the recent advances in surface modification of biomedical implants. First, the terminology of biomaterials and particularly titanium as one of the most used biomaterials in the orthopaedic field, is provided. Then, to deliver more profound insight into the implant failure process, a more detailed discussion on factors associated with titanium failure are presented. In the next stage, new materials and approaches to tackle the infection and poor osseointegration issues of titanium implants are discussed, followed by defining the project's knowledge gaps and technical objectives.

2.1. Introduction to the biomaterials in the medical application

The application of biomaterials as an implant is as old as history and can be traced back to around 2500 BC when Egyptians utilized gold wires to fix their unstable teeth (**Figure 2.1**) [1, 2].

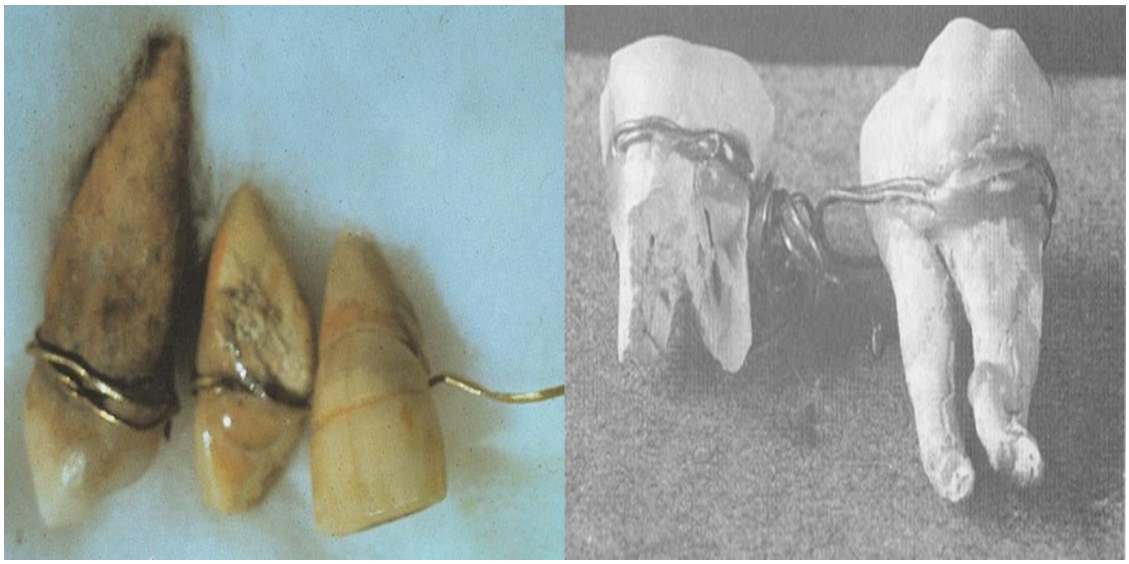

Figure 2.1. Dental work found in ancient Egypt (Image reproduced with permission [3]).

Nevertheless, the implant, as we know it today, was introduced after developments in surgery and general anaesthesia with the application of mineral tooth, pins and plates in the 1800s [4, 5]. In general, biomaterials can be characterized as natural or engineered substance presented into biological systems, such as the human body aimed to improve and support biological function or replace an organ [6, 7]. Selection criteria for biomaterials are mainly governed by their purpose of application and can be categorized as polymeric, metallic (comprised of metal or metal alloys), ceramics, composite materials, etc. [8].

Biomaterials development in the biomedical field has significantly contributed to human longevity and quality of life. **Figure 2.2** demonstrates the typical application of artificial implants in the human body. The traumatic fracture repair or replacement of

bones, artificial leg, arms and skin, biomedical stents and bionic eyes are only a few examples of artificial implants currently being developed to improve the life quality of patients. With the significant increase in life expectancy and population ageing over the past decades, the need for biomaterials product has notably boosted. For older people, the risk of falls increases, which eventually may lead to bone fractures in the knee, hip and joints, etc. [9]. Therefore, in several cases, patients may undergo surgical treatment to receive orthopedic implants such as artificial joints, knees, hips, etc., as part of their medical treatment [10]. The aged population (60+ years old) comprised around 10.0% of the global population in 2000, which recorded as one of the highest levels in the history of humankind [11]. It is expected that the aged population proportion in the global population, particularly in developing countries grows to 32.2% by 2100 [11]. Consequently, a significant portion of the biomaterials being used in the implant industries aims to support, replace or repair organs and tissues such as teeth and bone, blood veins, cartilage etc., for elderly patients [12].

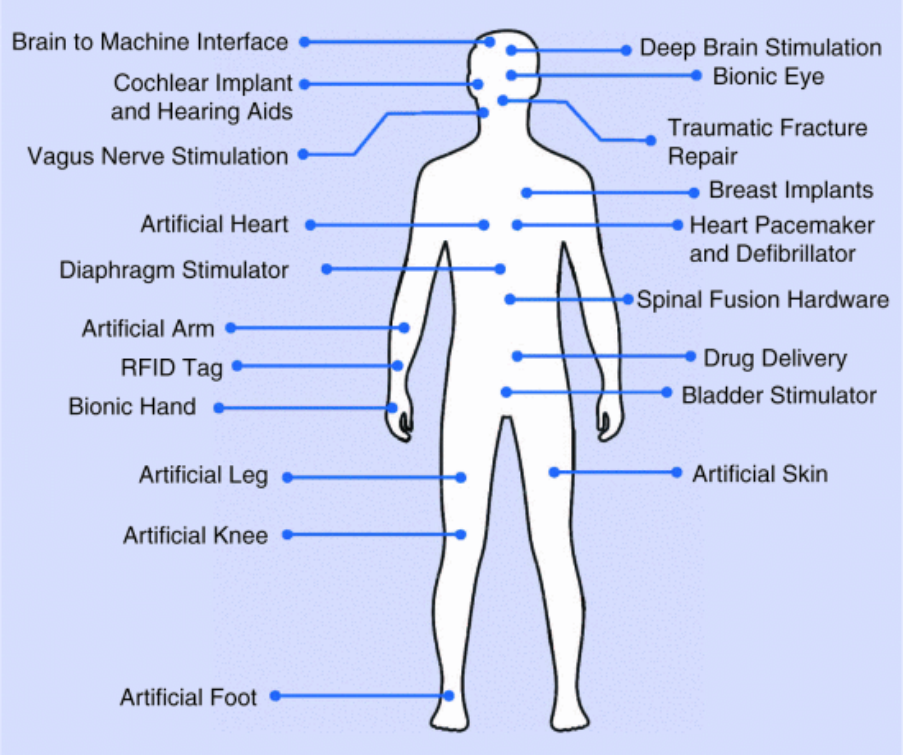

Figure 2.2. Illustration of artificial implants in the human body (Image reproduced with permission from ref [12]).

2.2. Titanium, the wonder material for orthopaedic implants

Orthopaedic implants, also known as bone implants, are defined as implants or reinforcement materials interacting directly with the human skeleton and connective tissues [10]. The common types of orthopaedic implants include artificial joints, knees, hips, dental implants, plates, pins, and screws as structural reinforcement [10]. Nowadays, with the advance of technology, different biomaterials are available for the production of orthopaedic implants. However, these biomaterials should fulfil essential criteria such as suitable mechanical durability, biocompatibility, and physicochemical properties as similar as possible to the surrounding tissues to become an efficient orthopaedic implant [13, 14]. Studies suggest that the share of biomaterials in the global market is around $150 billion in 2021, while the metallic implants market is estimated to gain more than $19 billion by 2026 [15],[16]. Biomaterials such as stainless steel and

other Iron (Fe) based alloys, zirconium-niobium (Zr-Nb), Cobalt Chrome (Co-Cr) alloys, nickel-chromium (Ni-Cr) alloy, Magnesium (Mg), zirconium-niobium (Zr-Nb), Tantalum (Ta) and silver (Ag) are amongst the potential candidates for the fabrication of metallic implants. However, Ti and Ti-based alloys are still the most popular metals in the orthopaedic field and make up the maximum share in the global metal implants market [15, 17]. It is worth mentioning that only in 2005, 1.7 kilotons of titanium and its alloys were utilized to manufacture implants and associated medical devices worldwide [18]. Ti is considered as a valve metal with exceptional physicochemical properties, such as excellent biocompatibility, superb corrosion resistance and in comparison to other available metals in the biomedical market, such as stainless steel, it demonstrates an outstanding strength [19]. At the same time, it is approximately 50% lighter in weight [20-22]. Furthermore, the elasticity modulus for Ti is almost half of the obtained values for other common materials for orthopaedic products such as stainless steel and cobalt-chromium (Co-Cr), which helps to reduce the chance of stress shielding and resorption of bone structure [20-22]. These qualities fulfil the functional requirements and make titanium a suitable candidate for different orthopaedic application [8, 23]. **Table 2.1** summarises the biological impact regarding several elements in the periodic table [23]. This table demonstrates the overall biocompatibility advantage of Ti compared with other transitional metals in the table.

Table 2.1. Biological response of different elements in the periodic table [21].

Periodic position	Element	Biocompatible	Carcinogenic	Genotoxic	Mutagenic	Cytotoxic	Allergenic	Prone to corrosion	Other*
3d	Ti	Yes	No	No	No	Med	No	No	No
	V	No	Yes	Yes	Yes	High	Disputed	No	No
	Cr	No	Disputed	Yes	Yes	High	Yes	No	No
	Mn	No	No	Yes	No	High	No	Yes	No
	Fe	No	No	Yes	Disputed	Med	No	Yes	No
	Co	No	Yes	Yes	Yes	High	Yes	Yes	Yes
	Ni	No	Yes	Yes	Yes	High	Yes	Yes	Yes
	Cu	No	No	Yes	Yes	High	Yes	Yes	Yes
4d	Zr	Yes	No	No	No	Low	No	No	No
	Nb	Yes	No	No	No	Low	No	No	No
	Mo	No	Disputed	Yes	Yes	Low	Yes	Yes	Yes
	Tc	No	- Radioactive -						
	Ru	Yes	No	No	No	Med	No	No	Yes
	Rh	No	Yes	Yes	Yes	High	Unknown	No	No
	Pd	No	Yes	No	Disputed	Med	Yes	No	No
	Ag	No	No	No	No	High	Yes	No	Yes
5d	Hf	Unknown	Unknown	Unknown	Unknown	Med	No	No	Unknown
	Ta	Yes	No	No	No	Low	No	No	No
	W	No	Yes	Yes	No	Med	No	Yes	No
	Re	Unknown	Unknown	Unknown	Unknown	Unknown	No	No	Unknown
	Os	No	Unknown	Yes	Yes	High	No	Yes	No
	Ir	No	No	No	Yes	High	No	No	Yes
	Pt	No	Yes	Yes	Yes	High	Yes	No	No
	Au	Yes	No	No	No	High	No	No	No
Other	Al	No	No	Yes	No	Low	No	No	Yes
	Zn	No	No	No	No	High	No	No	Yes
	Sn	Yes	No	No	No	Low	No	No	Yes

The exceptional performance of titanium is associated with the presence of a protective oxide layer, which is naturally covering its surface [24, 25]. TiO_2 is one of the most common thermodynamically stable states of the oxide layer on titanium. Nevertheless, the Ti/O ratio may differ as a result of oxygen solubility, the addition of other elements (alloying) or the presence of different oxidation states [24, 25]. Titanium dioxide can be found in various crystallographic forms of rutile, anatase or brookite that are frequently used in different biomedical applications (**Figure 2.3**) [26]. Among them, rutile is the most stable form; therefore, anatase and brookite are considered metastable

phases, which can be transferred to the rutile phase in the presence of high temperature [27].

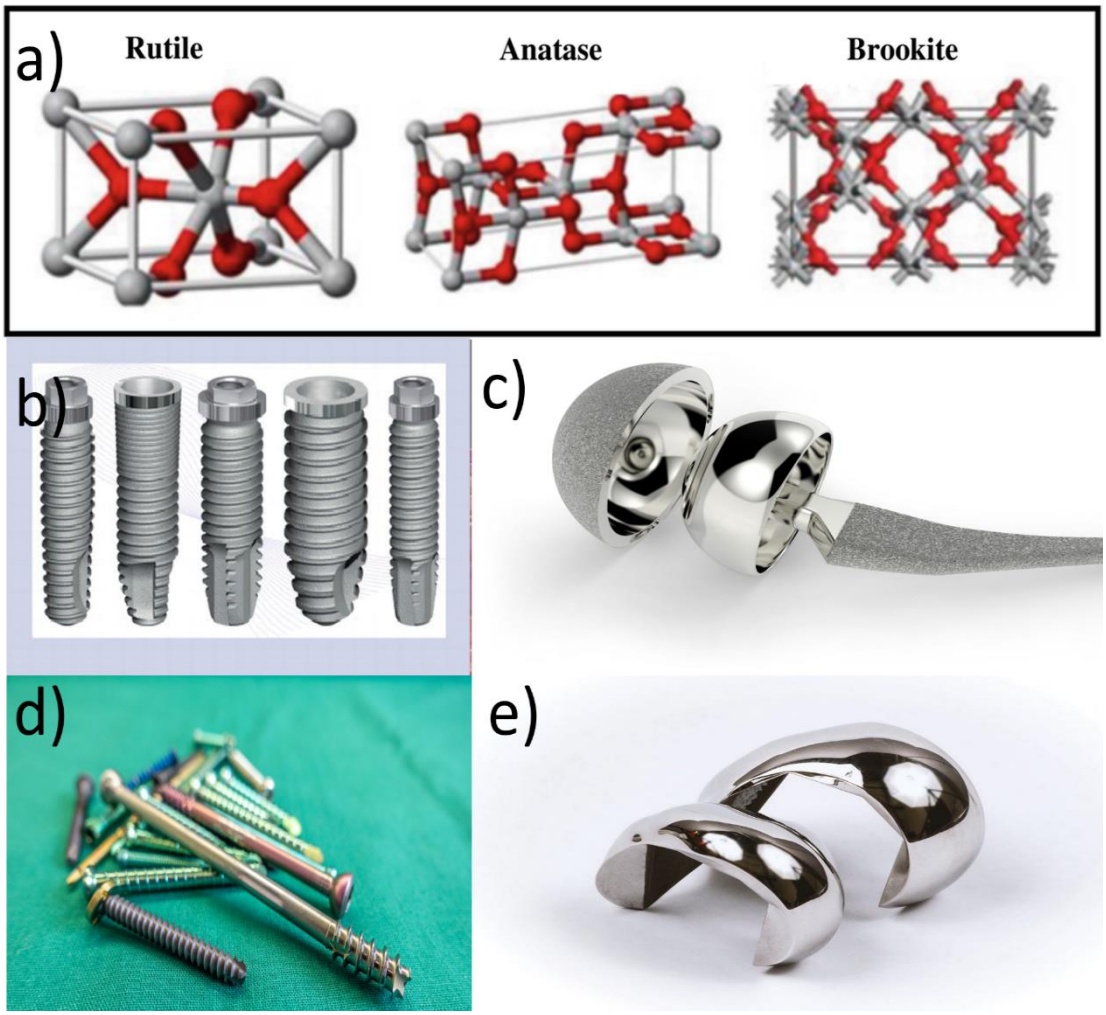

Figure 2.3. a) Crystal structures of TiO_2 adopted with permission [28], an example of Ti application as b) dental implant adopted with permission [29], c) artificial joint, d) surgical screws (Photos courtesy of Gabriel Constantinescu), e) artificial knee (Photos courtesy of Precision ADM).

2.3. Titanium implant failure

Although Ti and Ti alloys have demonstrated a great potential for application as an efficient biomedical implant, the problem with the implant failure remains unsolved. In many typical implants production, the attention is mainly on the mechanical aspects

and their functionality to fix the traumatized or fractured section of bone through a self-healing process [30, 31]. However, the interaction between bone cells with implants surface play an essential role in the life span of implants [32]. Factors associated with titanium implant failure can be classified as biological, mechanical, and infection problems [33]. In the biological failure, the ability of bone tissue to integrate with implant surface decreases and poor osseointegration both in the early or late stage of implantation can result in implant failure [33]. The risk of implant rejection is another issue that occurs due to the body immune system response to the foreign object implantation. This response initially involves biological encapsulation of implant surface, and in severe cases, it can lead to rejection of implants [34, 35].

Bone implants are built to withstand high levels of mechanical stresses induced by everyday activities. However, mechanical failure can happen. This can be due to the poor design or selection of materials, which result in fracture of the implant and its components or as a result of the stress shielding [36]. The stress shielding or stress protection occurs when bone implants demonstrate a noticeably higher elastic modulus compared with bone host tissue, which mechanically damages the bone and results in the reduction in bone density and poor integration [37]. This issue mostly happens in hip implants and bone staples, which increases the risk of implant loosening and failure [38].

2.4. Poor Osseointegration problem

The osseointegration is described as a secure connection between bone cells and implant surface after implantation, in which it does not demonstrate any relative movement between connected surfaces, therefore guarantee a stable fixation (**Figure 2.4**) [39].

.

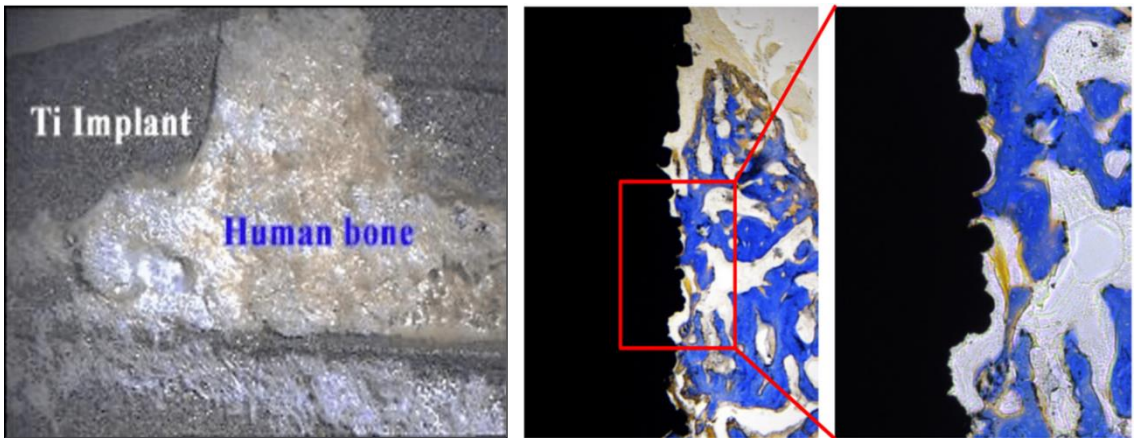

Figure 2.4. Example of successful osseointegration ability of Ti implant (Adopted from [40, 41] reproduced with permission).

This term is considered as the last stage of the bone healing process, which initially starts with nonosseointegration of the woven bone surrounding the implant surface in the first week after implantation, bone cell volume development during the second week, the replacement of woven bone structure with lamellar bone, taking place after two weeks and finally further bone ingrowth after two months post-implantation, which eventually leads to successful osseointegration [39, 42]. Researchers identified two general categories involved in the osseointegration known as systemic factors (such as the effect of anaemia or diabetes) and local factors (interface properties, type of implant, roughness, surface topography, corrosion resistance, etc.) [39, 43, 44]. For instance, titanium implants compared with other implants such as zirconia and DLC showed lower osseointegration properties, while they demonstrated better results compared with aluminium implants which showed local toxicity [45]. Poor osseointegration combined with the loosening of the implant can eventually result in implant failure and rejection of the implant from the body [46]. Among different factors

that are affecting bioactivity and bone-implant integration, the interface properties play the most critical role [39].

2.5. Bacterial infection complication

Nowadays, infection is considered one of the principal problems within the orthopaedic and dental fields. Studies reveal up to 10 % of dental implants would end up with infection issues. Surprisingly, only one-third of affected implants are recovered with applied treatments [47]. Treatment of infected bone implants is even more challenging due to the technical problems associated with poor accessibility to the infected sites. In some severe cases, the treatment ends up with replacement surgery, which otherwise results in amputation or death of the patient [48]. Revision surgeries are costly and create substantial health and economic burden on patients who already are suffering both physically and psychologically in regard to the initial implantation [49-52].

Bacterial infection happens when gram-positive and gram-negative bacteria from different sources enters our body. An opening in the patient's skin can provide a path for bacteria present in the surgical site, medical devices, or clothes to enter the body [53]. In the orthoptic infection, the entered bacteria adhere to the surface of implants and eventually form a biofilm [53]. Produced biofilm is more resistant to medical treatments and can afflict our body in different ways: First, biofilm acts as a new source of bacteria, spreading bacterial colonies to other organs resulting in chronic infection or persistent infection[48]. Second, it can lead to chronic inflammation resulting from the body's intensified response to the infection and subsequent antimicrobial treatments [54]. Implant failure due to the robust biofilm formation and infection can be caused by different bacteria such as *Enterococcus faecalis, E. coli, Pseudomonas aeruginosa,*

Streptococcus viridans, Proteus mirabilis, Klebsiella pneumoniae, Proteus mirabilis [55, 56]. But almost 80% of orthopaedic infections are associated with *Staphylococcus aureus*, *methicillin-resistant Staphylococcus* and *Staphylococcus epidermidis,* which makes *the staphylococci* family the number one enemy in the combat against implant-related infections (**Figure 2.5.)** [55, 56].

Figure 2.5. Example of chronic osteomyelitis (bone infection) in a patient due to *Staphylococcus aureus* (reproduced with permission from ref. [1]).

In order to disable bacteria to form the biofilm or to eliminate an existing biofilm on the surface of implants, different approaches are introduced. Prescription of antibiotics is the most common method to treat implant-associated infection (IAI) which temporarily can kill bacteria and supress infection [57]. However, excessive application of antibiotics to treat disease has significantly increased the fear regarding the emergence of antimicrobial-resistant bacteria such as the *methicillin-resistant Staphylococcus aureus* (MRSA) worldwide [57]. Excessive application of antibacterial agents in antimicrobial therapy can also affect the infected site and the surrounding tissues, which may cause

treatment side effects such as compromised host responses that can be problematic to the patient[58]. Therefore, nowadays, studies are focusing on alternative approaches such as tackling bacterial infection via the development of antimicrobial surfaces [57]. The engineered antibacterial surface can be designed to stop the attachment of bacteria colonies to the surface, which is known as anti-biofouling surfaces or can kill bacteria after contact with the implant surface (biocidal surface) [57]. Biocidal surfaces provide antimicrobial ability either by the presence of an antibacterial coating on their surface or engineering of surface to kill bacteria mechanically upon attachment to the surface[59]. The active ingredient in the antimicrobial coating comprises eluting agents (such as metal ions, nanoparticles [60, 61]), photo bactericidal agents such as photosensitizing dyes, TiO_2, gold nanoparticles (which photosensitize both gram-positive and gram-negative bacteria) [62, 63] and immobilized molecules such as peptides and quats which requires relatively longer contact times to efficiently kill bacteria [64]. In recent years, 2D nanomaterials have received remarkable attention as a new potential source for antibacterial agents. Here, we briefly highlight some of the well-known 2D materials with application in the biomedical fields, which are the focus of the current study.

2.6. Novel candidate 2D materials in the biomedical field

2.6.1. Graphene, the material of the 21st century

The rise of 2D materials began with the discovery of graphene in 2004 [65]. This material provides a range of unique mechanical and physicochemical properties such as very low weight, high Young's modulus and outstanding strength [65, 66]. Since then, different derivatives of graphene such as graphene oxide (GO), reduced graphene oxide (rGO) and functionalized/doped graphene have been discovered and exploited in several

applications such as composites, optics, biomedicine, transport, defence, energy harvest and storage, sensors, capacitors etc. (**Figure 2.6**) [67, 68]. Nevertheless, GO has received more attention in the antimicrobial application, as it exhibited the highest antimicrobial activity towards *E.coli* bacteria compared with rGO, graphite, graphite oxide, and graphene [69]. Besides, studies revealed the coatings benefit from the presence of GO by improving the mechanical stability and reducing micro-cracks formation in the coating [70, 71]. Other research demonstrates a positive response of bone cells to GO, evident from the enhancement of the adhesion and proliferation of bone cells on GO scaffold and related coatings, which results in improved osseointegration and bone healing [72, 73]. There is no consensus on the underlying antibacterial mechanisms of GO. However, studies suggest several fundamental killing mechanisms such as bacteria membrane damage via direct contact with the sharp edge of GO (nano knife effect), oxidative stress by the generation of reactive oxygen species (ROS), interaction with bacterial DNA/RNA, wrapping/trapping bacterial membrane (only in the solution) and charge transfer mechanism, involving GO application as a terminal electron acceptor for bacteria, which eventually kills them [74-77]. Moreover, some other parameters affecting the antimicrobial activity of GO are including lateral size, number of graphene layers, flakes shape and topography, edge characteristics and functional groups, as well as the degree of dispersion [77].

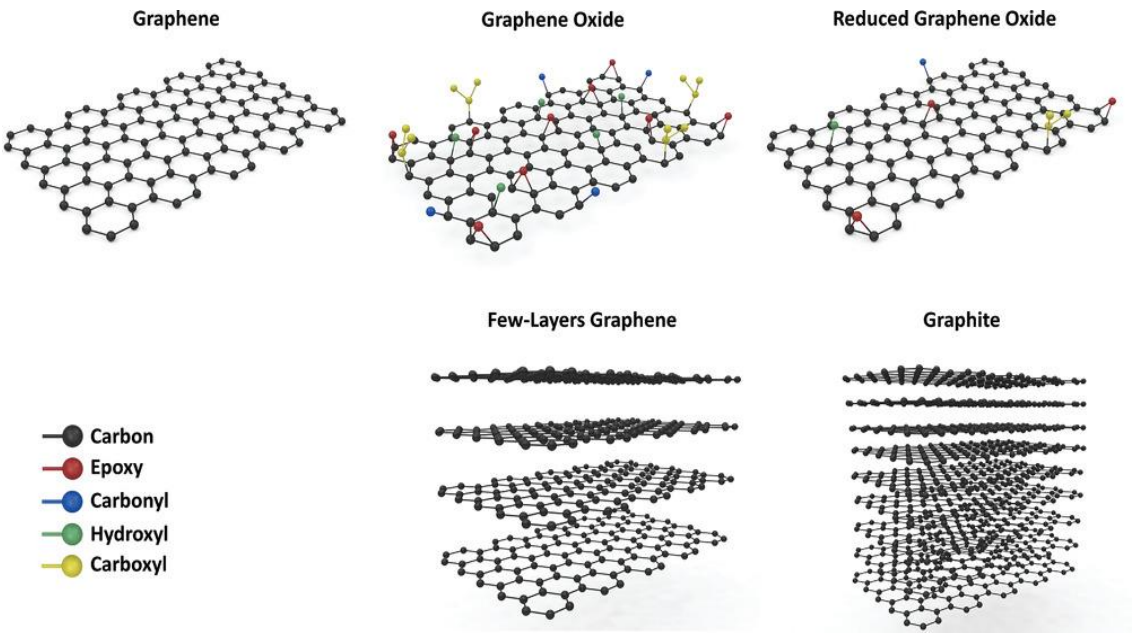

Figure 2.6. Different types of materials in the graphene family (Reproduced with permission from ref. [78]).

Based on the literature data, biocompatibility and toxicity of graphene-based materials are often contradictory and subject of ongoing discussion [79]. One of the main reason for this observation can be found in the different fabrication and functionalization process adopted for the production of GO, which may affect the final physicochemical properties and eventually alter the cytotoxicity of the graphene family [80]. However, in general, fundamental parameters governing the toxicity of 2D materials are size, shape, surface charge and concentration [81]. Apart from physicochemical parameters, the cytotoxicity of GO demonstrates time and dose-dependent behaviour [82]. Therefore, it can be inferred that graphene family can be either safe or deadly to different cells and organs.

2.6.2. Transition metal carbides and carbonitrides (MXene)

After the discovery of GO, gradually, other 2D nanomaterials beyond graphene (2D NBG) such as transition metal carbides and carbonitrides (MXene), layered double

hydroxides (LDHs), laponite (Lap), black phosphorus, hexagonal boron nitride (hBN) and transition metal disulphide (TMD), etc. were discovered. Recent research revealed that some of these 2D materials have antibacterial properties [83-88]. MXene family (were found in 2011) are comprised of carbides and nitrides, which are produced via acid etching (using HF or in-situ HF) and removal of A mid-layers from the bulk crystal MAX phase (where M stands for transition metal such as Ti, Hf, V, Ta and Zr, X represents C or N, and A is an element in A-group such as Al (**Figure 2.7**) [89, 90]. Structural compositions such as Ti_3C_2, Ti_3CN, Ti_4N_3, Ti_2N, Ta_4C_3 and Mo_2C are among 20 stoichiometric MXene compositions identified so far [91]. Several studies showed the successful application of MXene in different sectors such as electronics (photonic diode, batteries, capacitors), water treatment and purification, sensors, composites, and last but not least, the biological application (antibacterial enhancement, cancer treatment, etc. which are in ogoning progress and development) [92-95].

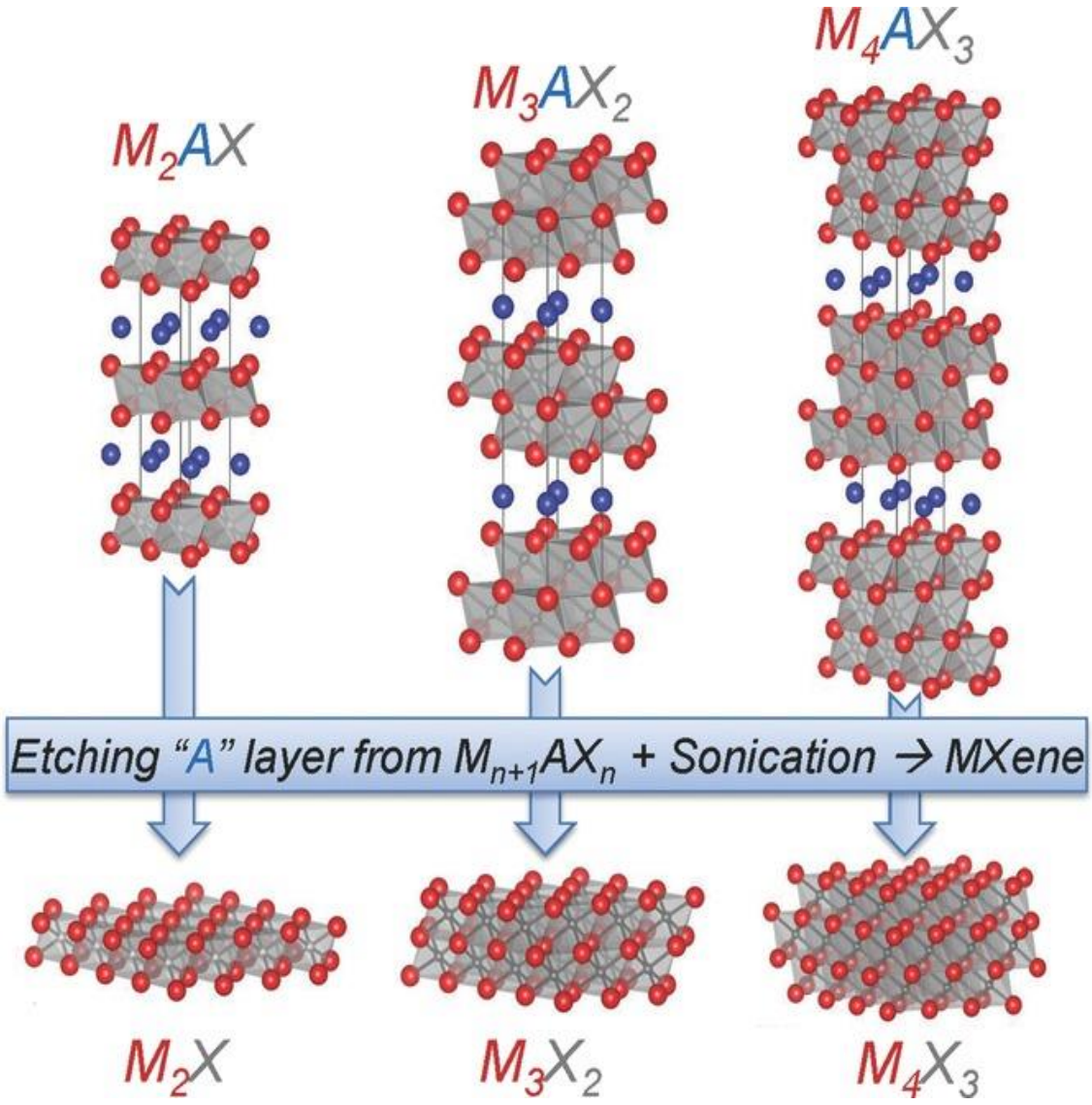

Figure 2.7. Atomic structure of MAX and Mxene phases produced through chemical etching (Reproduced with permission from ref. [96]).

Amongst the MXene family, $Ti_3C_2T_x$ MXene (T_x stands for functional groups) with hexagonal crystal structure has received more attention due to its remarkable antibacterial efficiency (toward both gram-negative and gram-positive bacteria) either as a coating or in a composite material [85, 97]. Moreover, $Ti_3C_2T_x$ MXene exhibits high hydrophilicity due to the presence of -OH, -F and -O functional groups, which enables it to form relatively uniform coatings over the surface [98, 99]. In general, MXene

benefits from good hydrophilicity and metallic conductivity, which makes it more attractive compared to available types of graphene-based materials [95].

2.6.3. hexagonal Boron Nitride (hBN)

Boron nitride (BN) is a synthesized material, which has received great attention for many years in different industries. Its most stable crystalline form, hexagonal crystalline (hBN), is a renowned material in dental cement production and cosmetic products [100, 101]. The hBN possesses a similar structure as graphite; therefore, it is also referred to as "white graphite" [102, 103]. hBN, compared with other available forms of BN such as rhombohedral, cubic, turbostratic and wurtzite, displays superior stability against chemical and oxidation reaction while exhibiting a high thermal conductivity level (**Figure 0.8)** [102, 103]. Although hBN is a well-known material in dental field application, research on its antimicrobial and bioactivity is still naive. Few recent studies demonstrated good antimicrobial properties of hBN against *S. pasteuri* M3, *S. mutans* ATTC 25175, while it was less effective against other types of strains such as *Streptococcus mutans 3.3* and *Candida sp. M25* [100]. Moreover, studies showed that hBN nanoparticles are biocompatible with CRL 2120 fibroblast and Madin Darby Canine Kidney MDCK cells [100].

As mentioned earlier, the antibacterial activity of 2D nanomaterials beyond graphene can be attributed to different mechanisms such as metallic ions release, killing upon contact with the surface, oxidative stress, electron transfer, photo-induced antimicrobial activity or a combination of different mechanisms known as hybrid mechanisms [103].

Regarding BN and its different structure, the underlying physicochemical mechanisms behind the antibacterial efficiency has not been fully understood. Particularly, hBN nanoparticles were more effective against biofilm formation rather than killing bacteria [100]. However, further research reported some sort of morphological disruption and damage to the cell membrane after the direct contact of bacteria with BN-based coatings, suggesting a possible role of physical or chemical stress in the observed antibacterial activity [100, 104].

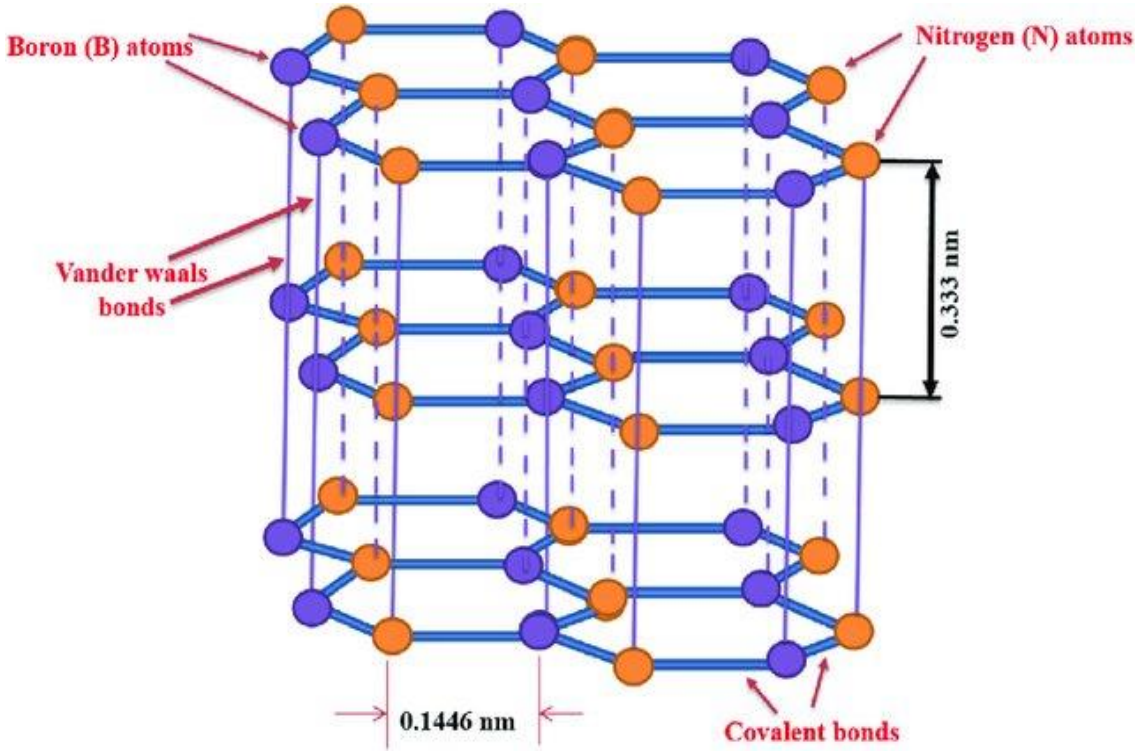

Figure 2.8. Schematic picture of the hexagonal boron nitride (hBN) structure (Reproduced with permission [105]).

2.7. Surface modification treatment to enhance the osseointegration, antibacterial activity or improve drug delivery ability.

With the advance in micro-nano technologies, different strategies have been proposed to modify the surface of implants in order to improve osseointegration

properties, enhance the antibacterial ability. These strategies are listed in **Table 2.2**, with few examples for each cutting-edge technology. In general, available technologies can be categorized into five main groups: Physiochemical modification, Plasma modifications, Electrochemical modification, and Hydrothermal method [52]. Among them, surface treatment via electrochemical modification and hydrothermal treatment (HT) recently have received significant attention. Anodisation and Electrophoretic deposition (EPD) techniques are some of the most well-known methods within the electrochemical group [106]. In the anodization process, the metallic surface is usally placed as the working electrode in the electrolytic cell, while the counter electrode is placed parallel to that [107]. By application of power supply in different modes of Potensio-static or Galvano-static, a protective oxide layer is formed over the metallic surface, which can provide good mechanical and wear properties to the surface. Moreover, this technique significantly enhances the resistance to corrosion of metallic products [108, 109].

Table 2.2. summary of proposed surface modification techniques to improve osseointegration, antimicrobial activity (Adopted from our published paper [51]).

Type of Surface modification	**Osseointegration enhancement**	**Antibacterial/Bacteriostatic**	**Refs.**
Physiochemical modification			
Physical Vapor Deposition (PVD)	✓ Formation of Ti Nano-nodular Structure by Electron-Beam-Physical Vapor Deposition (EB-PVD)	✓ Ti/Ag hard coating	[110]
Chemical Vapour Deposition (CVD) technique	Metal-organic (CVD)	CVD of TiO2/Ag layers	[111]
Acid etching	✓	–	[112]

Magnetron sputtering	Deposition of HAP on Ti ✓	✓ Ag-Ti	[113]
Laser deposition/melting	laser structuring	(e.g. copper–nickel coatings on titanium substrate)	[114, 115]
Spin-coating	✓ Poly(vinyl acetate)/HAP composite nanofibers on Ti implants	Coating Ti with chitosan	[116, 117]
UV treatment	✓	✓	[118, 119]
Grit blasting	Grit blasting with TiO2 Grit blasting + PEO	Ti blasted with zirconia	[120, 121]
Sol-gel	Ca3(PO4)2 deposition on Ti by Discrete Crystalline Deposition	TiO2–Ag composite coating	[122, 123]
Alkaline-heat treatment deposition	Poly (vinyl alcohol) (PVA)/poly (lactide-glycolide acid) (PLGA) NPs	Ti coated with vancomycin containing NPs	[124]
Plasma modifications			
Plasma sprayed hydroxyapatite + Antibacterial agent	✓	Incorporation of Ag	[125-127]
Plasma sprayed hydroxyapatite	✓	–	[127]
Electrochemical Modification			
Electrophoretic Deposition (EPD)	EPD of HAP on Ti	Addition of AgNps during EPD	[128, 129]
Anodization (TNTs formation, Nanopitting)	✓	Combined with antibacterial materials such as ZnO, Ag	[116, 130, 131]
Plasma Electrolytic Oxidation (PEO)	✓	Alkaline etching/antibacterial agents doping	[132, 133]
Cathodic polarisation	✓	Binding doxycycline onto titanium	[134]
Hydrothermal method			
Hydrothermal treatment + MAO	✓ Ca-based electrolyte, HT in Na3PO4 aqueous solution	✓ Zn-doped TiO2 coatings	[135, 136]

Hydrothermal treatment/alkaline etching	✓ Combined with electrochemical methods to form Apatite	Combined with Anodisation and formation of Na2TiO3	[133, 137]

2.7.1. Plasma Electrolytic Oxidation (PEO)

The Plasma Electrolytic Oxidation technique (PEO), also known as Micro Arc Oxidation (MAO), is one of the most critical scalable surface treatment techniques similar to the anodization process [133]. In the PEO process, both electrodes are submerged in a specific electrolyte bath. The counter electrode is usually in the form of a cylindrical mesh, while the working electrode is placed at the centre of the electrolyte bath (**Figure 2.9)** [133]. Here, electrolyte selection plays a crucial role in the PEO process and the characteristic properties of the final coating. PEO process is performed in a very high current (~1-2 A) over valve metals such as —Ti, Al, Mg, Zr and Ta [138]. The protective oxide layer is formed initially over the surface. By increasing the oxide layer thickness, the cell voltage also increases. At a particular point known as “dielectric breakdown voltage”, micro-discharges in the form of micro-arcs are generating in the system, which is usually accompanied by acoustic and optical emission [139, 140]. Various modes of micro-arcs may occur over the surface and in different depth of the oxide layer. This electron avalanche bombards the surface and increases the local temperature to more than 4500 K, which leads to the meltdown of metallic material near the electron discharge [139, 140]. Subsequently, the molten material is resolidified due to the presence of surrounding cold electrolyte and form a different variety of crystalline and amorphous phases, which eventually improve the hardness and corrosion and wear resistance of the oxide layer [141]. PEO treated samples exhibits superior adhesion of

the coating to the substrate due to diffusion and interaction of oxygen species in different levels in the protective oxide layer with the metallic-based substrate [141].

In this process, vigorous formation and release of bubbles and gases on the working electrode, along with the effect of micro arcs generation on the surface, lead to the formation of a unique micro-nano porous structure [142]. Moreover, with the correct choice of electrolyte and parameters, it is possible to incorporate micro-nano materials and elements into the coating and therefore engineer the surface for different application [143]. Remarkably, the incorporation of plasma during the PEO process and the ability to add additional elements to the oxide layer are among distinguishable differences between the PEO process and the typical anodization process [144, 145].

In the biomedical field, PEO is widely used for the fabrication and development of Ti bone implants [146]. Apart from mechanical and physiochemical improvements that this technique provides, it can form a unique hierarchical micro-nano morphology on the surface, which studies show can extensively improve the contact area between bone cells and implant surface [147-149]. This increase in the contact area along with the particular form of pores can significantly improve bone implant bonding and build a

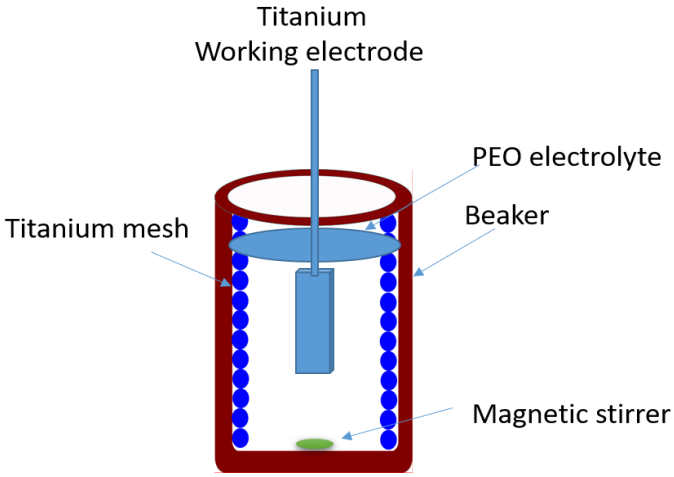

Figure 2.9. Schematic image of electrochemical cell used for the PEO process

suitable microenvironment for differentiation and proliferation of cells, which eventually results in osseointegration improvement [147-149]. Although PEO treatment exhibited a great potential to address osseointegration problems of implants, the problem with implant failure due to the infection still remains unsolved.

2.7.2. Electrophoretic deposition (EPD)

Electrophoretic deposition (EPD) is a well-known colloidal deposition process that provides fast and straightforward deposition ability for ceramic materials. It has been discovered around 1808, but the actual application as we know it today starts from 1933 with the fabrication of emitter for electron tube [150]. In this technique, initially, charged particles, either in the form of dispersion or suspension in the solution, are attracted to the electrode with opposite charge driven by DC electric field, which is called electrophoresis [151]. Then these particles are gradually deposited on the surface of a conductive sample, known as the deposition stage. With the correct choice of apparatus and adjusting of deposition parameters, morphology and thickness of the deposited film can be easily controlled [151].

There are different factors involved in the EPD process, which control yields, thickness, morphology and quality of coated layers on the surface that can be categorized into two main groups [150]:

1- Parameters in regard to the suspension such as particle size, dielectric constant of solution, conductivity, zeta potential and stability of suspension.
2- Parameters in regard to the treatment such as deposition duration, cell voltage, concentration of particles in the solution and conductivity of electrode.

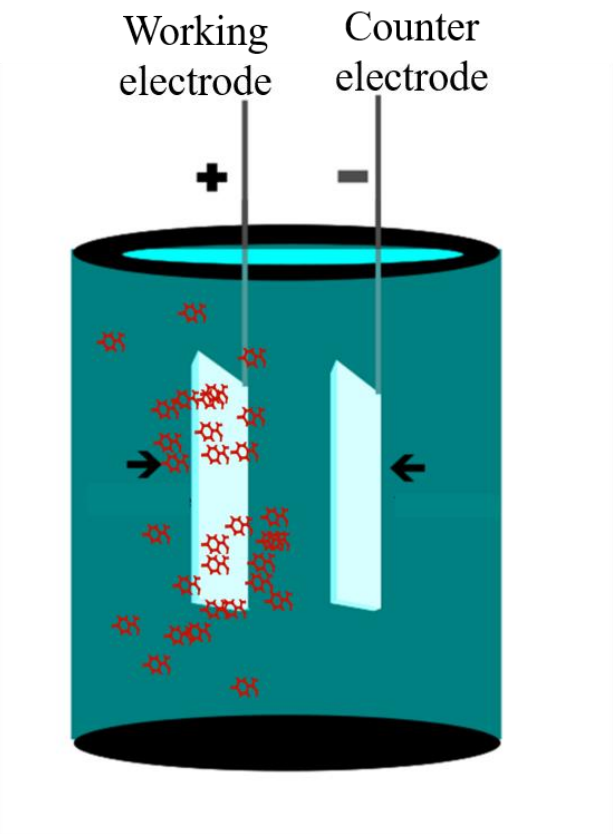

Figure 2.10. Schematic image of the EPD process

In the biomedical field and other industries, EPD has been used for the deposition of advanced material such as GO and Mxene, etc., on Ti and Ti-based materials as well as Mg and stainless steel [152-156]. The schematic picture of the EPD process is shown in **Figure 2.10.**

2.7.3. Hydrothermal treatment (HT)

HT is a simple and low-cost surface modification technique that is widely used in biomedical application to improve the osteoconductivity of metallic implants. This technique typically utilizes heat and pressure to modify the implant's surface by introducing nanostructures, nanowrinkle or hydroxyapatite (HAP) to the surface, which enhances bone cell–titanium implant contact area and eventually improves the bioactivity

biocompatibility of the implant [157-159]. Different types of HT solution have been investigated to develop titanium implants such as NaOH, H_2O_2, KOH, $CaOH_2$, $CaCl_2$ etc. [157, 160, 161]. Previous studies also show HT can improve the attachment of epithelial-like cells and integration of soft tissue in the early stage of implantation [162]. In addition, the hydrothermal modification of the titanium surface has revealed a great potential to improve the attachment of gingival epithelial-like cells and fibroblast to the surface. Further in vivo studies also highlight HT's ability to enhance peri-implant soft tissue bonding [161, 163, 164].

2.8. Mechano-bactericidal surface

In the traditional chemical-based approaches, in order to fight against bacteria and avoid biofilm formation on Ti and Ti alloy implant, different strategies such as binding of antibiotics, antimicrobial peptides to the implant surface are investigated [165, 166]. In this approach, antibacterial agents are engineered to get released in a suitable time and concentration to trigger the undesirable metabolic targets, while in the real application, the agents contaminate the surrounding environment, and due to uncontrolled diffusion, it affects and jeopardizes healthy body cells [167]. Moreover, in this approach, after a period of time, the system lost its effectiveness, which eventually requires replenishing or replacement [167]. On the other side, the excessive application of antibacterial agents is connected to the emergence of multidrug resistance pathogens worldwide, which means alternative solutions should be investigated to address the infection problem of implants [167].

In recent years, more innovative methods have been introduced to target bacterial infection based on defensive mechanisms observed in nature, which are known as

"mechano-bactericidal techniques" [165]. In the "mechano-bactericidal" approach, bacteria are killed after direct contact with the nanostructured surface via different mechanisms such as piercing and rupture (**Figure 2.11**) [168]. In comparison to the chemical-based approach, mechano-bactericidal techniques are considered sustainable killing methods as they obviate the necessity for replenishing antibacterial agents [169]. Moreover, this technique can address the previous issues regarding undesirable antibacterial agent diffusion and the development of resistant pathogens [169]. In nature, the mechano-bactericidal effect first was observed on P. claripennis Cicada wing. Ivanova et al. have further investigated the bactericidal efficacy of nanopillar structure on cicada wing to inhibit biofilm formation [169]. Hasan et al. observed that the nanopillar morphology over the cicada wing is mainly efficient against gram-negative bacteria such as *E.coli* with thinner peptidoglycan layers rather than gram-positive bacteria such as *S. aureus* bacteria [170]. Therefore they concluded that bacteria cell size, wall thickness and outer membrane significantly affect the bactericidal efficiency of the nanostructured surface [170]. They also suggested a new approach regarding the bactericidal effect of nanostructured surface based on deformation of the bacterial cell to a critical level which results in physical damage and killing of bacteria adhered to the surface known as "rupture mechanism" [170]. There is no consensus among experts over the optimal spacing between nano-spikes involved in the bacteria-killing process. However, literature data suggest the increasing aspect ratio of fabricated nanostructures (by increasing its height and sharpness) can notably improve the antibacterial efficiency [167, 171].

Several techniques have been proposed to fabricate mechano-bactericidal surface over titanium substrates, such as thermal oxidation [172], laser ablation [173], hydrothermal etching [174] and sputter deposition [175], which can lead to the formation of nano-wires, nano-spikes and nano-pillars morphologies over the surface. However, research in this area is still naive, and there is plenty of room for practical innovation, fabrication and development of the mechano-bactericidal concept [173, 176].

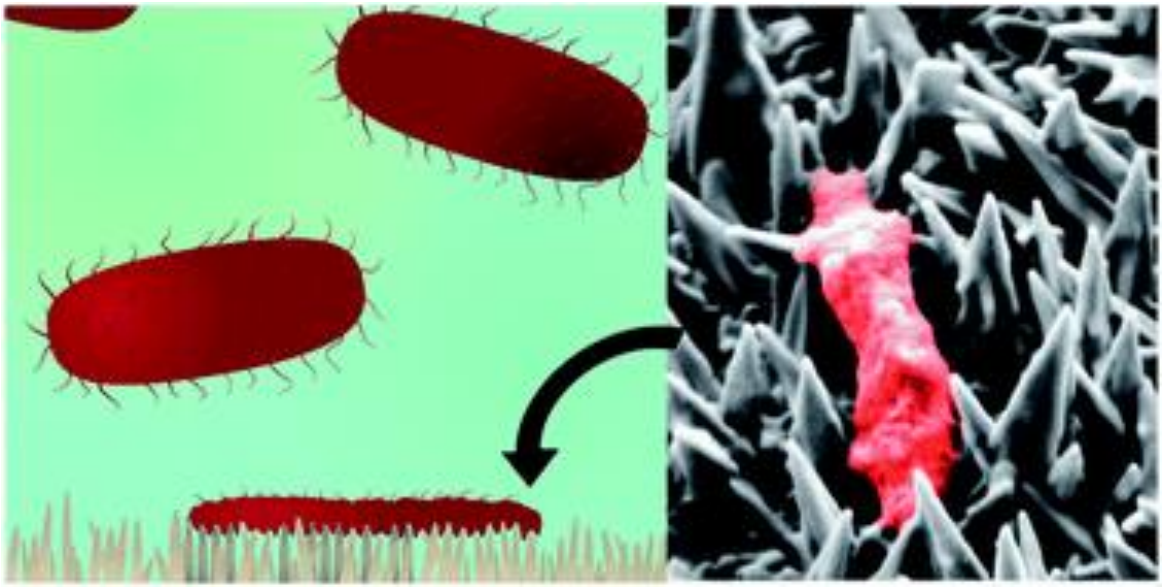

Figure 2.11.Schematic figure and SEM image of bacteria killed via mechano-bactericidal surface (Reproduced with permission [167]).

2.9. Identified knowledge gaps and unsolved problems to be addressed

As described earlier, PEO treated surface demonstrates excellent potential for osteoconductivity improvement of titanium implants [177]. However, it requires subsequent development to address the infection issue, which results in implant failure. Most of the research in this field focuses mainly on either osseointegration improvement or antibacterial enhancement. Here, it was introduced three different post-treatment

methods for PEO substrate, which can effectively address both osseointegration and antimicrobial issues simultaneously and therefore enhance the life span of titanium bone implants:

1- Decoration of graphene oxide flakes on the PEO substrate with PEO-EPD technique to improve antimicrobial and osseointegration properties (PEO-EPD).
2- Fabrication and engineering of novel titania nanostructures with mechano-bactericidal properties on PEO titanium substrate with HT method (PEO+HT).
3- Improvement of antibacterial activity of PEO coatings via the addition of 2D antimicrobial materials through simple drop-casting method (PEO+2D drop-casting).

2.10. Improving PEO method with subsequent surface modification to address infection and poor osseointegration problems

2.10.1. High voltage EPD (PEO-EPD)

As discussed earlier, the PEO treatment of titanium has proved to be an effective strategy for enhancing osseointegration properties [177]. However, typical PEO treatment has failed to show antimicrobial activity. In order to improve the antibacterial properties of fabricated PEO surface, different approaches such as the addition of silver and copper nanoparticles during the PEO process [178-180], deposition of antibacterial agents after the PEO process [181] or subsequent surface treatment of PEO matrix [182] have been investigated. Among various strategies to enhance the antimicrobial activity of implants, the application of 2D materials due to their inherent antibacterial activity and high aspect ratios have received a great deal of attention [67]. Moreover, they may act better in commercial application as many other nanomaterials such as silver

nanoparticles are frequently getting agglomerated in reality and lose their antimicrobial properties [183].

Recently, several studies explored the possible incorporation of GO to the metal matrix of Ti and Al with the PEO process in order to favour interfacial performance and functionality [184-186]. However, the presence of GO over the formed coating is not clear. Moreover, in other cases, only a few random deposition sites are detectable on the substrate, which might be developed due to the interaction of GO in the electrolyte with roughened PEO substrate and not the PEO process itself [184, 186]. Other studies suggest that the generation of vigorous gases in the form of micro-nano bubbles at electrodes during PEO treatment may interfere with the deposition process and impede the attachment of GO particles to the sample [150, 153].

Post-treatment of PEO treated sample with EPD technique appears to be an attractive alternative solution for deposition of GO over the PEO sample. However, there are several challenges, which need to be addressed appropriately. The typical low voltage EPD technique suffers weakened adhesion between the coating and the substrate [187]. Particularly, the presence of a thick oxide layer on the PEO substrate affects the conductivity of the substrate and limits the deposition yield with the common EPD technique [150]. As a potential solution for this problem, Nie et al. proposed a novel hybrid technique by the combination of PEO and EPD known as the PEO-EPD process [188]. In this method, EPD is performed in a relatively high voltage similar to the PEO condition, which leads to the generation of plasma in the system, while by the engineering of EPD parameters, it is possible to deposit particles on the substrate successfully. This combined method has demonstrated outstanding ability to address poor adhesion

problems of bio-ceramics on Ti-based substrate via exploiting electrolytic plasma in the process, which eventually enhances the bonding and integration of coating with the substrate [187, 189]. This method demonstrates great potential for deposition of GO on PEO substrate. However, its application for the fabrication of Ti-based implants with antibacterial activity has not been explored yet.

The other challenge with the EPD system is the formation of continuous coating film on the substrate. Although this matter is considered advantageous in many applications, in the bone-implant application, the presence of a micro-nano porous structure made by PEO treatment is vital for osseointegration [181, 190]. This hierarchical structure guarantees successful bioactivity of the surface and enhances the osseointegration ability of the implant. Therefore, the aim to deposit GO on the PEO surface partially instead of in a continuous form. It was proposed that this partial GO deposition pattern is crucial to have a mixture of two types of surfaces, one to improve osseointegration (produced by PEO porous structure) and second to eliminate bacteria (by introducing GO patches on the PEO treated sample).

2.10.2. Engineering of novel titania nanostructures with mechano- bactericidal properties on PEO titanium substrate with subsequent HT process (PEO+HT).

Post-treatment of PEO sample via HT is one of the most common methods for bioactivity improvement of PEO treated surface. This can be done through the high-temperature application of chemical etchant with or without pressure, which results in the formation of wrinkle and nanostructures on the surface, increasing the surface area and chemical activity of substrate [182, 191-193]. However, this technique was mainly

used to introduce or facilitate the fabrication of HAP layers on the PEO surface, therefore targets the bioactivity and corrosion resistance improvement of the implant surface [193, 194].

Although HAP formation is considered advantageous for the facilitation of bone-implant integration, it also includes Ca–P layers, which are infamous for their high brittleness and poor adhesion properties to Ti substrate [195, 196]. Moreover, common HAP does not show strong antimicrobial properties, which limits its further application. Therefore, it is usually required to be combined with different antibacterial agents such as silver or copper nanoparticles to address its low antibacterial activity issue [197, 198]. For these reasons, recent studies are shifting toward different approaches to tackle infection problems of implants.

As mentioned earlier, the mechano-biocidal approach has shown great potential in our fight against different pathogens. HT, as a straightforward and economical method widely, has been utilised to fabricate nanostructures on Ti and Ti-alloys with the ability to kill bacteria [199]. However, the application of this method on the PEO substrate for the fabrication of titania nanostructure with killing ability has not been thoroughly investigated [200].

One of the main reasons for this matter is the formation of HAP on the PEO surface either before or during HT, limiting the growth of tunable titania nanostructures [194]. As a potential solution, with the substitute of Ca-based solution in PEO and HT systems by a more simple, Ca-free electrolytes, we propose a new approach for the engineering of titania nanostructures on PEO substrate with dual applications: first osseointegration improvements and second antimicrobial activity enhancement. It is worth mentioning

that nanostructured titania fabricated via HT are not only effective against a different type of bacteria but also can favour different mammalian cell adhesion and proliferation [201, 202]. In fact, various studies show that these nanostructures are acting as guiding points for cells proliferation and control the growth orientation and direction of cells [201, 202].

2.10.3. Improvement of antibacterial activity of PEO coatings via the addition of 2D antimicrobial materials through simple drop-casting method (PEO+2D drop-casting)

Drop-casting is a fundamental casting technique compared to similar coating strategies such as doctor blading, spin coating, etc., which is straightforward, more accessible and affordable [203-208]. The schematic image of the drop-casting method is provided in **Figure 2.12**. This deposition method is working based on the dropping of the solution followed by subsequent evaporation of the solvent, which minimizes waste of material [99, 209]. The drop-casting method has already been widely employed in biomedical and industrial fields due to its simplicity, reproducibility and very low material waste[203-207]. Nevertheless, this method can not provide a very uniform thickness and topography, leading to the partial deposition of deposited materials on the substrate[205]. Although this drawback can limit the application of this technique in some fields, it can be beneficial for the fabrication of dual-purpose coatings and heterostructures, which requires partial coverage of coating instead of continuous films formation over the substrate[210]. Previous studies showed the successful combination of 2D antibacterial materials with PEO substrate in the elimination of bacteria. For instance, the partial deposition of GO on PEO surface with EPD technique led to the

formation of mixed structures comprising first, PEO surface with the ability to improve osteoconductivity and second, GO deposited flakes with superior antimicrobial activity against gram-positive and gram-negative bacteria . Motivated by this study, possible decoration of PEO substrate with other 2D antimicrobial particles such as Mxene, hBN, and GO via other techniques appears to be a promising strategy to address both low antibacterial and poor osseointegration properties of titanium-based implants. Therefore, the potential application of the drop-casting process as a simple and fast method for the deposition of antibacterial particles in a partial manner on PEO substrate is worthy of investigation.

Different parameters are involved in the drop-casting process, such as the wetting nature between the substrate and drop-casting solution (Surface tension), concentration, velocities and particles size in the solution, droplet size, etc. [211]. Moreover, in terms of antibacterial activity associated with deposited antimicrobial particles, other factors such as chemical composition, size, shape, surface charge and dose, exposure time and deposition pattern, the nature of bacteria, wettability and conductivity etc., are playing important roles, which are required to be further investigated [212, 213].

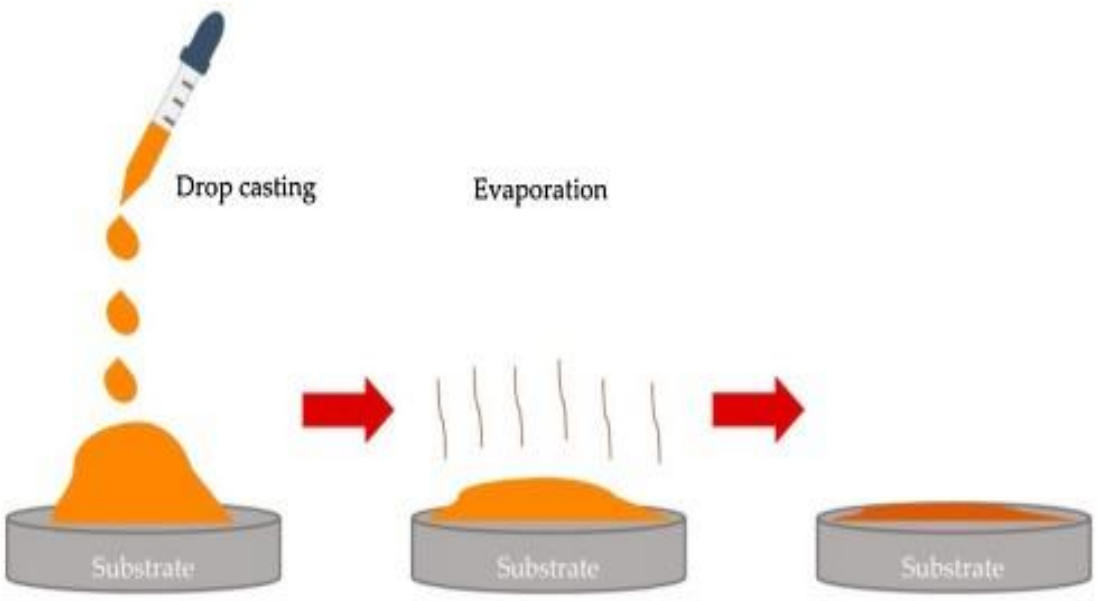

Figure 2.12. The schematic figure is demonstrating the drop-casting method [59].

2.11. References

1. Zimmerli, W. and P. Sendi, *Orthopaedic biofilm infections.* 2017. **125**(4): p. 353-364.
2. Abraham, C.M., *A brief historical perspective on dental implants, their surface coatings and treatments.* The open dentistry journal, 2014. **8**: p. 50-55.
3. Forshaw, R.J., *The practice of dentistry in ancient Egypt.* British Dental Journal, 2009. **206**(9): p. 481-486.
4. Lister, J., *On the Antiseptic Principle in the Practice of Surgery.* British medical journal, 1867. **2**(351): p. 246-248.
5. Pasqualini, U. and M.J.C.C.A. Pasqualini, *Treatise of Implant Dentistry.* 2009.
6. Kulinets, I., *Biomaterials and their applications in medicine*, in *Regulatory affairs for biomaterials and medical devices*. 2015, Elsevier. p. 1-10.
7. Ratner, B.D., *Biomaterials science: an interdisciplinary endeavor*, in *Biomaterials science*. 1996, Elsevier. p. 1-8.
8. Saini, M., et al., *Implant biomaterials: A comprehensive review.* World journal of clinical cases, 2015. **3**(1): p. 52-57.
9. Minetto, M.A., et al., *Common Musculoskeletal Disorders in the Elderly: The Star Triad.* Journal of clinical medicine, 2020. **9**(4): p. 1216.
10. Narayan, R.J.M.P.A.I., *ASM Handbook, Volume 23, Materials for Medical Devices.* 2012.
11. Lutz, W., W. Sanderson, and S.J.N. Scherbov, *The coming acceleration of global population ageing.* 2008. **451**(7179): p. 716-719.
12. Stevens, M.M.J.M.t., *Biomaterials for bone tissue engineering.* 2008. **11**(5): p. 18-25.
13. O'Brien, F.J., *Biomaterials & scaffolds for tissue engineering.* Materials Today, 2011. **14**(3): p. 88-95.
14. Shamsoddin, E., B. Houshmand, and M. Golabgiran, *Biomaterial selection for bone augmentation in implant dentistry: A systematic review.* 2019. **10**(2): p. 46-50.
15. (ARC), A.R.a.C. *Metal Implants and Medical Alloys Market (By Type: Titanium, Stainless Steel, Cobalt Chrome, Others; By Application: Orthopedic Implants, Cardiovascular Implants, Dental Application, Craniomaxillofacial Impnats, Neurological Implants) – Global Industry Analysis, Market Size, Opportunities and Forecast, 2019 - 20*. 2019; 190]. Available from: https://www.acumenresearchandconsulting.com/table-of-content/metal-implants-and-medical-alloys-market.
16. Heimann, R.B.J.M.f.M.A., *Appendix B Current world market situation of biomaterials and biomedical devices.* p. 503.
17. Chen, Q. and G.A. Thouas, *Metallic implant biomaterials.* Materials Science and Engineering: R: Reports, 2015. **87**: p. 1-57.
18. Hogan, L., *Research and Development in Titanium: Implications for a Titanium Metal Industry in Australia*. 2008: ABARE.
19. Geetha, M., et al., *Ti based biomaterials, the ultimate choice for orthopaedic implants–a review.* Progress in materials science, 2009. **54**(3): p. 397-425.

20. Brunette, D.M., et al., *Titanium in medicine: material science, surface science, engineering, biological responses and medical applications*. 2012: Springer Science & Business Media.
21. Geetha, M., et al., *Ti based biomaterials, the ultimate choice for orthopaedic implants–a review.* 2009. **54**(3): p. 397-425.
22. Niinomi, M.J.M.t., *Biologically and mechanically biocompatible titanium alloys.* 2008. **49**(10): p. 2170-2178.
23. Biesiekierski, A., et al., *A new look at biomedical Ti-based shape memory alloys.* Acta Biomaterialia, 2012. **8**(5): p. 1661-1669.
24. Textor, M., et al., *Properties and biological significance of natural oxide films on titanium and its alloys*, in *Titanium in medicine*. 2001, Springer. p. 171-230.
25. Vörös, J., et al., *Characterization of titanium surfaces*, in *Titanium in medicine*. 2001, Springer. p. 87-144.
26. Dambournet, D., I. Belharouak, and K. Amine, *Tailored Preparation Methods of TiO2 Anatase, Rutile, Brookite: Mechanism of Formation and Electrochemical Properties.* Chemistry of Materials, 2010. **22**(3): p. 1173-1179.
27. Hanaor, D.A.H. and C.C. Sorrell, *Review of the anatase to rutile phase transformation.* Journal of Materials Science, 2011. **46**(4): p. 855-874.
28. Sungur, Ş., *Titanium Dioxide Nanoparticles*, in *Handbook of Nanomaterials and Nanocomposites for Energy and Environmental Applications*, O.V. Kharissova, L.M.T. Martínez, and B.I. Kharisov, Editors. 2020, Springer International Publishing: Cham. p. 1-18.
29. Elias, C.N. and L. Meirelles, *Improving osseointegration of dental implants.* Expert Review of Medical Devices, 2010. **7**(2): p. 241-256.
30. McKibbin, B.J.T.J.o.b. and j.s.B. volume, *The biology of fracture healing in long bones.* 1978. **60**(2): p. 150-162.
31. Claes, L.E., et al., *Effects of Mechanical Factors on the Fracture Healing Process.* Clinical Orthopaedics and Related Research®, 1998. **355**.
32. Hanawa, T.J.F.i.b. and biotechnology, *Titanium–tissue interface reaction and its control with surface treatment.* 2019. **7**: p. 170.
33. Palma Carrió, C., et al., *Risk factors associated with early failure of dental implants. A literature review.* 2011.
34. Chandorkar, Y., R. K, and B. Basu, *The Foreign Body Response Demystified.* ACS Biomaterials Science & Engineering, 2019. **5**(1): p. 19-44.
35. Anderson, J.M., A. Rodriguez, and D.T. Chang. *Foreign body reaction to biomaterials*. in *Seminars in immunology*. 2008. Elsevier.
36. Shemtov-Yona, K. and D. Rittel, *An Overview of the Mechanical Integrity of Dental Implants.* BioMed research international, 2015. **2015**: p. 547384-547384.
37. Huiskes, R., et al., *The relationship between stress shielding and bone resorption around total hip stems and the effects of flexible materials.* 1992: p. 124-134.
38. MI, Z.R., et al., *Problem of Stress Shielding and Improvement to the Hip Implat Designs: A Review.* 2007. **7**(3): p. 460-467.
39. Guglielmotti, M.B., D.G. Olmedo, and R.L. Cabrini, *Research on implants and osseointegration.* 2019. **79**(1): p. 178-189.
40. Cunha, A., *Multiscale femtosecond laser surface texturing of titanium and titanium alloys for dental and orthopaedic implants*. 2015, Bordeaux.

41. Ren, B., et al., *Improved osseointegration of 3D printed Ti-6Al-4V implant with a hierarchical micro/nano surface topography: An in vitro and in vivo study.* Materials Science and Engineering: C, 2021. **118**: p. 111505.
42. Branemark, P.-I.J.J.p.D., *Osseointegration and its experimental background.* 1983. **50**: p. 399-410.
43. Deng, Y., et al., *Effect of surface roughness on osteogenesis in vitro and osseointegration in vivo of carbon fiber-reinforced polyetheretherketone–nanohydroxyapatite composite.* 2015. **10**: p. 1425.
44. Sykaras, N., et al., *Implant materials, designs, and surface topographies: their effect on osseointegration. A literature review.* 2000. **15**(5).
45. Guglielmotti, M.-B., et al., *A histomorphometric study of tissue interface by laminar implant test in rats.* 1999. **14**(4): p. 565-570.
46. Nover, A.B., et al., *Porous titanium bases for osteochondral tissue engineering.* 2015. **27**: p. 286-293.
47. Camps-Font, O., et al., *Postoperative Infections After Dental Implant Placement: Prevalence, Clinical Features, and Treatment.* Implant Dent, 2015. **24**(6): p. 713-9.
48. Ribeiro, M., F.J. Monteiro, and M.P. Ferraz, *Infection of orthopedic implants with emphasis on bacterial adhesion process and techniques used in studying bacterial-material interactions.* Biomatter, 2012. **2**(4): p. 176-194.
49. Bayliss, L.E., et al., *The effect of patient age at intervention on risk of implant revision after total replacement of the hip or knee: a population-based cohort study.* The Lancet, 2017. **389**(10077): p. 1424-1430.
50. De Nardo, L., et al., *Electrochemical surface modifications of titanium and titanium alloys for biomedical applications.* Coatings for Biomedical Applications: Woodhead Publishing, 2012: p. 106-42.
51. Elias, C.N., et al., *Biomedical applications of titanium and its alloys.* JOM, 2008. **60**(3): p. 46-49.
52. Maher, S., et al., *Engineered titanium implants for localized drug delivery: recent advances and perspectives of Titania nanotubes arrays.* Expert Opinion on Drug Delivery, 2018. **15**(10): p. 1021-1037.
53. Kim, S.I., *Bacterial infection after liver transplantation.* World journal of gastroenterology, 2014. **20**(20): p. 6211-6220.
54. Nazhat, S.N., A.M. Young, and J. Pratten, *Sterility and infection*, in *Biomedical Materials*. 2009, Springer. p. 239-260.
55. Khatoon, Z., et al., *Bacterial biofilm formation on implantable devices and approaches to its treatment and prevention.* Heliyon, 2018. **4**(12): p. e01067-e01067.
56. Nandakumar, V., et al., *Characteristics of bacterial biofilm associated with implant material in clinical practice.* Polymer Journal, 2013. **45**(2): p. 137-152.
57. Ivanova, E.P., et al., *The multi-faceted mechano-bactericidal mechanism of nanostructured surfaces.* 2020. **117**(23): p. 12598-12605.
58. Amin Yavari, S., et al., *Combating Implant Infections: Shifting Focus from Bacteria to Host.* 2020. **32**(43): p. 2002962.
59. Adlhart, C., et al., *Surface modifications for antimicrobial effects in the healthcare setting: a critical overview.* Journal of Hospital Infection, 2018. **99**(3): p. 239-249.

60. Cochis, A., et al., *The effect of silver or gallium doped titanium against the multidrug resistant Acinetobacter baumannii.* Biomaterials, 2016. **80**(Supplement C): p. 80-95.
61. Della Valle, C., et al., *A novel antibacterial modification treatment of titanium capable to improve osseointegration.* International Journal of Artificial Organs, 2012. **35**(10): p. 864-875.
62. Noimark, S., E. Allan, and I.P. Parkin, *Light-activated antimicrobial surfaces with enhanced efficacy induced by a dark-activated mechanism.* Chemical Science, 2014. **5**(6): p. 2216-2223.
63. Liao, C., Y. Li, and S.C. Tjong, *Visible-Light Active Titanium Dioxide Nanomaterials with Bactericidal Properties.* Nanomaterials (Basel, Switzerland), 2020. **10**(1): p. 124.
64. Chauret, C.P., *Sanitization*, in *Encyclopedia of Food Microbiology (Second Edition)*, C.A. Batt and M.L. Tortorello, Editors. 2014, Academic Press: Oxford. p. 360-364.
65. Adetayo, A. and D.J.O.j.o.c.m. Runsewe, *Synthesis and fabrication of graphene and graphene oxide: a review.* 2019. **9**(02): p. 207.
66. Losic, D., *Advancing of titanium medical implants by surface engineering: recent progress and challenges.* Expert Opinion on Drug Delivery, 2021: p. 1-24.
67. Sun, W. and F.G. Wu, *Two-Dimensional Materials for Antimicrobial Applications: Graphene Materials and Beyond.* Chem Asian J, 2018. **13**(22): p. 3378-3410.
68. Sturala, J., et al., *Frontispiece: Chemistry of Graphene Derivatives: Synthesis, Applications, and Perspectives.* 2018. **24**(23).
69. Liu, S., et al., *Antibacterial Activity of Graphite, Graphite Oxide, Graphene Oxide, and Reduced Graphene Oxide: Membrane and Oxidative Stress.* ACS Nano, 2011. **5**(9): p. 6971-6980.
70. Ma, Y., et al., *GO-modified double-walled polyurea microcapsules/epoxy composites for marine anticorrosive self-healing coating.* Materials & Design, 2020. **189**: p. 108547.
71. Zeng, Y., et al., *Graphene oxide/hydroxyapatite composite coatings fabricated by electrochemical deposition.* 2016. **286**: p. 72-79.
72. Nishida, E., et al., *Graphene oxide scaffold accelerates cellular proliferative response and alveolar bone healing of tooth extraction socket.* International journal of nanomedicine, 2016. **11**: p. 2265-2277.
73. Dubey, N., et al., *Graphene: a versatile carbon-based material for bone tissue engineering.* 2015. **2015**.
74. Perreault, F., et al., *Antimicrobial properties of graphene oxide nanosheets: why size matters.* 2015. **9**(7): p. 7226-7236.
75. Yadav, N., et al., *Graphene oxide-coated surface: inhibition of bacterial biofilm formation due to specific surface–interface interactions.* 2017. **2**(7): p. 3070-3082.
76. Salas, E.C., et al., *Reduction of Graphene Oxide via Bacterial Respiration.* ACS Nano, 2010. **4**(8): p. 4852-4856.

77. Mohammed, H., et al., *Antimicrobial Mechanisms and Effectiveness of Graphene and Graphene-Functionalized Biomaterials. A Scope Review.* 2020. **8**(465).
78. Daneshmandi, L., et al., *Graphene-Based Biomaterials for Bone Regenerative Engineering: A Comprehensive Review of the Field and Considerations Regarding Biocompatibility and Biodegradation.* 2021. **10**(1): p. 2001414.
79. Liao, C., Y. Li, and S.C. Tjong, *Graphene Nanomaterials: Synthesis, Biocompatibility, and Cytotoxicity.* International journal of molecular sciences, 2018. **19**(11): p. 3564.
80. Wu, X., et al., *A review on the biocompatibility and potential applications of graphene in inducing cell differentiation and tissue regeneration.* Journal of Materials Chemistry B, 2017. **5**(17): p. 3084-3102.
81. Adabi, M., et al., *Biocompatibility and nanostructured materials: applications in nanomedicine.* Artificial Cells, Nanomedicine, and Biotechnology, 2017. **45**(4): p. 833-842.
82. Lalwani, G., et al., *Toxicology of graphene-based nanomaterials.* Advanced drug delivery reviews, 2016. **105**(Pt B): p. 109-144.
83. Mei, L., et al., *Two-dimensional nanomaterials beyond graphene for antibacterial applications: current progress and future perspectives.* Theranostics, 2020. **10**(2): p. 757-781.
84. Ikram, M., et al., *Bactericidal behavior of chemically exfoliated boron nitride nanosheets doped with zirconium.* Applied Nanoscience, 2020. **10**(7): p. 2339-2349.
85. Rasool, K., et al., *Efficient Antibacterial Membrane based on Two-Dimensional Ti3C2Tx (MXene) Nanosheets.* Scientific Reports, 2017. **7**(1): p. 1598.
86. Li, M., L. Li, and S. Lin, *Efficient antimicrobial properties of layered double hydroxide assembled with transition metals via a facile preparation method.* Chinese Chemical Letters, 2020. **31**(6): p. 1511-1515.
87. Kim, T.I., et al., *Chemically exfoliated 1T-phase transition metal dichalcogenide nanosheets for transparent antibacterial applications.* 2019. **6**(2): p. 025025.
88. Tan, C., et al., *Recent Advances in Ultrathin Two-Dimensional Nanomaterials.* Chemical Reviews, 2017. **117**(9): p. 6225-6331.
89. Rastin, H., et al., *3D bioprinting of cell-laden electroconductive MXene nanocomposite bioinks.* Nanoscale, 2020. **12**(30): p. 16069-16080.
90. Anasori, B. and Û.G. Gogotsi, *2D metal carbides and nitrides (MXenes)*. 2019: Springer.
91. Gogotsi, Y. and B. Anasori, *The Rise of MXenes.* ACS Nano, 2019. **13**(8): p. 8491-8494.
92. Cheng, L., et al., *2D Nanomaterials for Cancer Theranostic Applications.* 2020. **32**(13): p. 1902333.
93. Ren, C.E., et al., *Charge- and Size-Selective Ion Sieving Through Ti3C2Tx MXene Membranes.* The Journal of Physical Chemistry Letters, 2015. **6**(20): p. 4026-4031.
94. Xie, Y., et al., *Role of Surface Structure on Li-Ion Energy Storage Capacity of Two-Dimensional Transition-Metal Carbides.* Journal of the American Chemical Society, 2014. **136**(17): p. 6385-6394.

95. Kim, H., Z. Wang, and H.N. Alshareef, *MXetronics: Electronic and photonic applications of MXenes.* Nano Energy, 2019. **60**: p. 179-197.
96. Naguib, M., et al., *25th Anniversary Article: MXenes: A New Family of Two-Dimensional Materials.* 2014. **26**(7): p. 992-1005.
97. Mayerberger, E.A., et al., *Antibacterial properties of electrospun Ti3C2Tz (MXene)/chitosan nanofibers.* RSC Advances, 2018. **8**(62): p. 35386-35394.
98. Maleski, K., V.N. Mochalin, and Y.J.C.o.M. Gogotsi, *Dispersions of two-dimensional titanium carbide MXene in organic solvents.* 2017. **29**(4): p. 1632-1640.
99. Lipton, J., et al., *Scalable, Highly Conductive, and Micropatternable MXene Films for Enhanced Electromagnetic Interference Shielding.* 2020. **3**(2): p. 546-557.
100. Kıvanç, M., et al., *Effects of hexagonal boron nitride nanoparticles on antimicrobial and antibiofilm activities, cell viability.* Materials Science and Engineering: C, 2018. **91**: p. 115-124.
101. Raddaha, N.S., et al., *Electrophoretic Deposition of Chitosan/h-BN and Chitosan/h-BN/TiO_2 Composite Coatings on Stainless Steel (316L) Substrates.* Materials (Basel, Switzerland), 2014. **7**(3): p. 1814-1829.
102. Lipp, A., K.A. Schwetz, and K. Hunold, *Hexagonal boron nitride: Fabrication, properties and applications.* Journal of the European Ceramic Society, 1989. **5**(1): p. 3-9.
103. Gao, G., et al., *Designing nanoscaled hybrids from atomic layered boron nitride with silver nanoparticle deposition.* Journal of Materials Chemistry A, 2014. **2**(9): p. 3148-3154.
104. Pandit, S., et al., *Antibacterial effect of boron nitride flakes with controlled orientation in polymer composites.* RSC Advances, 2019. **9**(57): p. 33454-33459.
105. Kumar, A., et al., *Bluish emission of economical phosphor h-BN nanoparticle fabricated via mixing annealing route using non-toxic precursor.* Journal of Solid State Chemistry, 2020. **288**: p. 121430.
106. Boccaccini, A., et al., *Electrophoretic deposition of biomaterials.* 2010. **7**(suppl_5): p. S581-S613.
107. Barjaktarević, D., et al., *Anodization of Ti-based materials for biomedical applications: A review.* 2016. **22**(3): p. 121-143.
108. Zhang, Z., et al., *Quantitative Analysis of Oxide Growth During Ti Galvanostatic Anodization.* 2020. **167**(11): p. 113501.
109. Edwards, J.J.L. and A. International, *Coating and Surface Treatment Systems for Metals, Finishing Pub.* 1997.
110. Brohede, U., et al., *Multifunctional implant coatings providing possibilities for fast antibiotics loading with subsequent slow release.* 2009. **20**(9): p. 1859-1867.
111. Piszczek, P., et al., *CVD of TiO2 and TiO2/Ag antimicrobial layers: Deposition from the hexanuclear μ-oxo Ti (IV) complex as a precursor, and the characterization.* 2013. **222**: p. 38-43.
112. Zahran, R., et al., *Effect of hydrofluoric acid etching time on titanium topography, chemistry, wettability, and cell adhesion.* 2016. **11**(11): p. e0165296.

113. Zhang, X., et al., *The fabrication of Ag-containing hierarchical micro/nano-structure on titanium and its antibacterial activity.* 2017. **193**: p. 97-100.
114. Rajesh, P., et al., *Pulsed laser deposition of hydroxyapatite on nanostructured titanium towards drug eluting implants.* 2013. **33**(5): p. 2899-2904.
115. Hassanin, H., et al., *Tailoring selective laser melting process for titanium drug-delivering implants with releasing micro-channels.* 2018. **20**: p. 144-155.
116. Wang, T., et al., *Controlled release and biocompatibility of polymer/titania nanotube array system on titanium implants.* 2017. **2**(1): p. 44-50.
117. Abdal-Hay, A., et al., *A novel simple one-step air jet spinning approach for deposition of poly (vinyl acetate)/hydroxyapatite composite nanofibers on Ti implants.* 2015. **49**: p. 681-690.
118. Smeets, R., et al., *Impact of dental implant surface modifications on osseointegration.* 2016. **2016**.
119. Gallardo-Moreno, A.M., et al., *In vitro biocompatibility and bacterial adhesion of physico-chemically modified Ti6Al4V surface by means of UV irradiation.* 2009. **5**(1): p. 181-192.
120. Al-Radha, A.S.D., et al., *Surface properties of titanium and zirconia dental implant materials and their effect on bacterial adhesion.* 2012. **40**(2): p. 146-153.
121. He, W., et al., *Enhancing osseointegration of titanium implants through large-grit sandblasting combined with micro-arc oxidation surface modification.* J Mater Sci Mater Med, 2019. **30**(6): p. 73.
122. Bonfante, E.A., et al., *Biomechanical testing of microblasted, acid-etched/microblasted, anodized, and discrete crystalline deposition surfaces: an experimental study in beagle dogs.* 2013. **28**(1).
123. Radin, S. and P.J.B. Ducheyne, *Controlled release of vancomycin from thin sol–gel films on titanium alloy fracture plate material.* 2007. **28**(9): p. 1721-1729.
124. Liu, Z., et al., *Construction of poly (vinyl alcohol)/poly (lactide-glycolide acid)/vancomycin nanoparticles on titanium for enhancing the surface self-antibacterial activity and cytocompatibility.* 2017. **151**: p. 165-177.
125. Roy, M., et al., *Mechanical, in vitro antimicrobial, and biological properties of plasma-sprayed silver-doped hydroxyapatite coating.* 2012. **4**(3): p. 1341-1349.
126. Szcześ, A., et al., *Synthesis of hydroxyapatite for biomedical applications.* 2017. **249**: p. 321-330.
127. Le Guéhennec, L., et al., *Surface treatments of titanium dental implants for rapid osseointegration.* 2007. **23**(7): p. 844-854.
128. Jain, P., et al., *Electrophoretic deposition of nanocrystalline hydroxyapatite on Ti6Al4V/TiO 2 substrate.* 2013. **10**(2): p. 263-275.
129. Patel, K.D., et al., *Tailoring solubility and drug release from electrophoretic deposited chitosan–gelatin films on titanium.* 2014. **242**: p. 232-236.
130. Gulati, K., et al., *Titania nanotubes for local drug delivery from implant surfaces*, in *Electrochemically Engineered Nanoporous Materials*. 2015, Springer. p. 307-355.
131. Liu, X., et al., *Antibacterial abilities and biocompatibilities of Ti–Ag alloys with nanotubular coatings.* 2016. **11**: p. 5743.
132. Campos, E.M., et al., *Albumin loaded PEO coatings on Ti—potential as drug eluting systems.* 2015. **283**: p. 44-51.

133. Marin, E., et al., *Effect of etching on the composition and structure of anodic spark deposition films on titanium.* 2016. **108**: p. 77-85.
134. Geißler, S., et al., *Effect of cathodic polarization on coating doxycycline on titanium surfaces.* 2016. **63**: p. 359-366.
135. He, X., et al., *Titanium-based implant comprising a porous microstructure assembled with nanoleaves and controllable silicon-ion release for enhanced osseointegration.* Journal of Materials Chemistry B, 2018. **6**(31): p. 5100-5114.
136. Zhang, L., et al., *Cytocompatibility and antibacterial activity of nanostructured H2Ti5O11·H2O outlayered Zn-doped TiO2 coatings on Ti for percutaneous implants.* Scientific Reports, 2017. **7**(1): p. 13951.
137. Ivanova, E.P., et al., *Natural Bactericidal Surfaces: Mechanical Rupture of Pseudomonas aeruginosa Cells by Cicada Wings.* 2012. **8**(16): p. 2489-2494.
138. Aliasghari, S., P. Skeldon, and G.E. Thompson, *Plasma electrolytic oxidation of titanium in a phosphate/silicate electrolyte and tribological performance of the coatings.* Applied Surface Science, 2014. **316**: p. 463-476.
139. Matykina, E., et al., *Incorporation of zirconia nanoparticles into coatings formed on aluminium by AC plasma electrolytic oxidation.* 2008. **38**(10): p. 1375-1383.
140. Malinovschi, V., et al., *Obtaining and characterization of PEO layers prepared on CP-Ti in sodium dihydrogen phosphate dihydrate acidic electrolyte solution.* 2019. **375**: p. 621-636.
141. Tsai, D.-S. and C.-C.J.M. Chou, *Review of the soft sparking issues in plasma electrolytic oxidation.* 2018. **8**(2): p. 105.
142. Snizhko, L., et al., *Excessive oxygen evolution during plasma electrolytic oxidation of aluminium.* 2007. **516**(2-4): p. 460-464.
143. Zhang, X., et al., *Growth mechanism of titania on titanium substrate during the early stage of plasma electrolytic oxidation.* Surface and Coatings Technology, 2020. **400**: p. 126202.
144. Ebrahimi, S., et al., *Improving optoelectrical properties of photoactive anatase TiO2 coating using rGO incorporation during plasma electrolytic oxidation.* 2019. **45**(2): p. 1746-1754.
145. Simchen, F., et al., *Introduction to Plasma Electrolytic Oxidation—An Overview of the Process and Applications.* 2020. **10**(7): p. 628.
146. Marin, E., et al., *Effect of etching on the composition and structure of anodic spark deposition films on titanium.* Materials & Design, 2016. **108**(Supplement C): p. 77-85.
147. Akin, F.A., et al., *Preparation and analysis of macroporous TiO2 films on Ti surfaces for bone–tissue implants.* 2001. **57**(4): p. 588-596.
148. Hanawa, T., *Titanium–Tissue Interface Reaction and Its Control With Surface Treatment.* Frontiers in Bioengineering and Biotechnology, 2019. **7**(170).
149. Echeverry-Rendón, M., et al., *Osseointegration improvement by plasma electrolytic oxidation of modified titanium alloys surfaces.* 2015. **26**(2): p. 72.
150. Besra, L. and M. Liu, *A review on fundamentals and applications of electrophoretic deposition (EPD).* Progress in Materials Science, 2007. **52**(1): p. 1-61.
151. Sarkar, P. and P.S. Nicholson, *Electrophoretic Deposition (EPD): Mechanisms, Kinetics, and Application to Ceramics.* 1996. **79**(8): p. 1987-2002.

152. Weng, G.-M., et al., *MXene Films, Coatings, and Bulk Processing*, in *2D Metal Carbides and Nitrides (MXenes): Structure, Properties and Applications*, B. Anasori and Y. Gogotsi, Editors. 2019, Springer International Publishing: Cham. p. 197-219.
153. Chavez-Valdez, A., M.S.P. Shaffer, and A.R. Boccaccini, *Applications of Graphene Electrophoretic Deposition. A Review.* The Journal of Physical Chemistry B, 2013. **117**(6): p. 1502-1515.
154. Besra, L. and M.J.P.i.m.s. Liu, *A review on fundamentals and applications of electrophoretic deposition (EPD).* 2007. **52**(1): p. 1-61.
155. Jiang, Y., Y. Bao, and K. Yang, *Composite Coatings Combining PEO layer and EPD Layer on Magnesium Alloy*, in *Magnesium Technology 2011*. 2011, John Wiley & Sons, Inc. p. 543-546.
156. Hwang, M.-J., et al., *Cathodic electrophoretic deposition (EPD) of phenylenediamine-modified graphene oxide (GO) for anti-corrosion protection of metal surfaces.* 2019. **142**: p. 68-77.
157. Sultana, R., et al., *Surface Modification of Titanium with Hydrothermal Treatment at High Pressure.* Dental Materials Journal, 2006. **25**(3): p. 470-479.
158. Yang, S., et al., *Hydrothermal treatment of Ti surface to enhance the formation of low crystalline hydroxyl carbonate apatite.* Biomaterials research, 2015. **19**: p. 4-4.
159. Ishak, I., et al., *Protruding Nanostructured Surfaces for Antimicrobial and Osteogenic Titanium Implants.* Coatings, 2020. **10**: p. 756.
160. Kim, C., et al., *Comparison of titanium soaked in 5 M NaOH or 5 M KOH solutions.* Materials science & engineering. C, Materials for biological applications, 2013. **33**(1): p. 327-339.
161. Haraguchi, T., et al., *Effect of Calcium Chloride Hydrothermal Treatment of Titanium on Protein, Cellular, and Bacterial Adhesion Properties.* 2020. **9**(8): p. 2627.
162. Oshiro, W., et al., *Effects of CaCl2 hydrothermal treatment of titanium implant surfaces on early epithelial sealing.* Colloids and Surfaces B: Biointerfaces, 2015. **131**: p. 141-147.
163. Ayukawa, Y., et al., *Long term retention of gingival sealing around titanium implants with CaCl2 hydrothermal treatment: A rodent study.* 2019. **8**(10): p. 1560.
164. Sakamoto, Y., et al., *Effect of hydrothermal treatment with distilled water on titanium alloy for epithelial cellular attachment.* 2019. **12**(17): p. 2748.
165. Lin, N., et al., *Nanodarts, nanoblades, and nanospikes: Mechano-bactericidal nanostructures and where to find them.* 2018. **252**: p. 55-68.
166. Hickok, N.J. and I.M.J.A.d.d.r. Shapiro, *Immobilized antibiotics to prevent orthopaedic implant infections.* 2012. **64**(12): p. 1165-1176.
167. Lin, N., et al., *Nanodarts, nanoblades, and nanospikes: Mechano-bactericidal nanostructures and where to find them.* Advances in Colloid and Interface Science, 2018. **252**: p. 55-68.
168. Linklater, D.P., et al., *Mechano-bactericidal actions of nanostructured surfaces.* 2020: p. 1-15.
169. Elbourne, A., et al., *Nano-structured antimicrobial surfaces: From nature to synthetic analogues.* 2017. **508**: p. 603-616.

170. Ivanova, E.P., et al., *Natural bactericidal surfaces: mechanical rupture of Pseudomonas aeruginosa cells by cicada wings.* 2012. **8**(16): p. 2489-2494.
171. Ivanova, E.P., et al., *Bactericidal activity of black silicon.* 2013. **4**(1): p. 1-7.
172. Sjöström, T., A.H. Nobbs, and B.J.M.L. Su, *Bactericidal nanospike surfaces via thermal oxidation of Ti alloy substrates.* 2016. **167**: p. 22-26.
173. Linklater, D.P., et al., *Mechano-bactericidal actions of nanostructured surfaces.* Nature Reviews Microbiology, 2021. **19**(1): p. 8-22.
174. Bhadra, C.M., et al., *Antibacterial titanium nano-patterned arrays inspired by dragonfly wings.* 2015. **5**(1): p. 1-12.
175. Sengstock, C., et al., *Structure-related antibacterial activity of a titanium nanostructured surface fabricated by glancing angle sputter deposition.* 2014. **25**(19): p. 195101.
176. Tripathy, A., et al., *Natural and bioinspired nanostructured bactericidal surfaces.* Advances in Colloid and Interface Science, 2017. **248**: p. 85-104.
177. Wei, Y., et al., *Construction of Zn-incorporated Micro/Nano Hierarchical Structure Coatings on Tantalum.* Journal of Bionic Engineering, 2020. **17**(6): p. 1186-1195.
178. Necula, B.S., et al., *In vitro antibacterial activity of porous TiO2–Ag composite layers against methicillin-resistant Staphylococcus aureus.* 2009. **5**(9): p. 3573-3580.
179. Yao, X., et al., *Microstructure and antibacterial properties of Cu-doped TiO2 coating on titanium by micro-arc oxidation.* 2014. **292**: p. 944-947.
180. Cochis, A., et al., *The effect of silver or gallium doped titanium against the multidrug resistant Acinetobacter baumannii.* Biomaterials, 2016. **80**: p. 80-95.
181. Sun, N., et al., *Graphene oxide-coated porous titanium for pulp sealing: an antibacterial and dentino-inductive restorative material.* Journal of Materials Chemistry B, 2020. **8**(26): p. 5606-5619.
182. Marin, E., et al., *Effect of etching on the composition and structure of anodic spark deposition films on titanium.* Materials & Design, 2016. **108**: p. 77-85.
183. Wong, K.K. and X.J.M. Liu, *Silver nanoparticles—the real "silver bullet" in clinical medicine?* 2010. **1**(2): p. 125-131.
184. Zuo, Y., et al., *Effect of graphene oxide additive on tribocorrosion behavior of MAO coatings prepared on Ti6Al4V alloy.* Applied Surface Science, 2019. **480**: p. 26-34.
185. Gao, Y., et al., *Microstructure and Properties of Graphene Oxide-doped TiO2 Coating on Titanium by Micro Arc Oxidation.* Journal of Wuhan University of Technology-Mater. Sci. Ed., 2018. **33**(6): p. 1524-1529.
186. Yang, W., et al., *Preparation of MAO coatings doped with graphene oxide.* Surface Engineering, 2017. **33**(10): p. 739-743.
187. Ulasevich, S.A., et al., *Deposition of hydroxyapatite–incorporated TiO 2 coating on titanium using plasma electrolytic oxidation coupled with electrophoretic deposition.* 2016. **6**(67): p. 62540-62544.
188. Nie, X., A. Leyland, and A. Matthews, *Deposition of layered bioceramic hydroxyapatite/TiO2 coatings on titanium alloys using a hybrid technique of micro-arc oxidation and electrophoresis.* Surface and Coatings Technology, 2000. **125**(1): p. 407-414.

189. Nie, X., et al., *Deposition of layered bioceramic hydroxyapatite/TiO2 coatings on titanium alloys using a hybrid technique of micro-arc oxidation and electrophoresis.* 2000. **125**(1-3): p. 407-414.
190. González Castillo, E.I., et al., *Nanocomposite coatings obtained by electrophoretic co-deposition of poly(etheretherketone)/graphene oxide suspensions.* Journal of Materials Science, 2020. **55**.
191. Strzała, A., W. Simka, and M.J.A.P.P.A. Marszałek, *Hydrothermal synthesis of hydroxyapatite on titanium after anodic oxidation.* 2012. **121**(2): p. 561-564.
192. Fazel, M., et al., *Influence of hydrothermal treatment on the surface characteristics and electrochemical behavior of Ti-6Al-4V bio-functionalized through plasma electrolytic oxidation.* Surface and Coatings Technology, 2019. **374**: p. 222-231.
193. Sun, J., Y. Han, and K. Cui, *Microstructure and apatite-forming ability of the MAO-treated porous titanium.* Surface and Coatings Technology, 2008. **202**(17): p. 4248-4256.
194. Zhang, P., et al., *Effect of Ti-OH groups on microstructure and bioactivity of TiO2 coating prepared by micro-arc oxidation.* Applied Surface Science, 2013. **268**: p. 381-386.
195. Parcharoen, Y., P. Termsuksawad, and S. Sirivisoot, *Improved Bonding Strength of Hydroxyapatite on Titanium Dioxide Nanotube Arrays following Alkaline Pretreatment for Orthopedic Implants.* Journal of Nanomaterials, 2016. **2016**: p. 9143969.
196. Mishra, A., et al., *Study of Mechanical and Tribological Properties of Nanomica Dispersed Hydroxyapatite Based Composites for Biomedical Applications.* Advances in Materials Science and Engineering, 2017. **2017**: p. 9814624.
197. Costescu, A., et al., *Fabrication, Characterization, and Antimicrobial Activity, Evaluation of Low Silver Concentrations in Silver-Doped Hydroxyapatite Nanoparticles.* Journal of Nanomaterials, 2013. **2013**: p. 194854.
198. Kolmas, J., E. Groszyk, and D. Kwiatkowska-Różycka, *Substituted Hydroxyapatites with Antibacterial Properties.* BioMed Research International, 2014. **2014**: p. 178123.
199. Tsimbouri, P., et al., *Osteogenic and bactericidal surfaces from hydrothermal titania nanowires on titanium substrates.* 2016. **6**(1): p. 1-12.
200. Qadir, M., et al., *Calcium Phosphate-Based Composite Coating by Micro-Arc Oxidation (MAO) for Biomedical Application: A Review.* Critical Reviews in Solid State and Materials Sciences, 2018. **43**(5): p. 392-416.
201. Diu, T., et al., *Cicada-inspired cell-instructive nanopatterned arrays.* Scientific Reports, 2014. **4**(1): p. 7122.
202. Bhadra, C.M., et al., *Antibacterial titanium nano-patterned arrays inspired by dragonfly wings.* Scientific Reports, 2015. **5**(1): p. 16817.
203. Brum, R.S., et al., *Polymer coatings based on sulfonated-poly-ether-ether-ketone films for implant dentistry applications.* Journal of Materials Science: Materials in Medicine, 2018. **29**(8): p. 132.
204. Dugasani, S.R., et al., *Optoelectronic properties of DNA thin films implanted with titania nanoparticle-coated multiwalled carbon nanotubes.* 2019. **9**(1): p. 015011.

205. A, K.S., et al., *Super-hydrophobicity: Mechanism, fabrication and its application in medical implants to prevent biomaterial associated infections.* Journal of Industrial and Engineering Chemistry, 2020. **92**: p. 1-17.
206. Decandia, G., et al., *Initiated Chemical Vapor Deposition of Crosslinked Organic Coatings for Controlling Gentamicin Delivery.* Pharmaceutics, 2020. **12**(3): p. 213.
207. Zarghami, V., et al., *Prolongation of bactericidal efficiency of chitosan — Bioactive glass coating by drug controlled release.* Progress in Organic Coatings, 2020. **139**: p. 105440.
208. Eslamian, M. and F. Zabihi, *Ultrasonic Substrate Vibration-Assisted Drop Casting (SVADC) for the Fabrication of Photovoltaic Solar Cell Arrays and Thin-Film Devices.* Nanoscale Research Letters, 2015. **10**(1): p. 462.
209. Aslan, F., H. Esen, and F. Yakuphanoglu, *The effect of coumarin addition on the electrical characteristics of Al/Coumarin:CdO/p-Si/Al photodiode prepared by drop casting technique.* Optik, 2019. **197**: p. 163203.
210. Huang, Z., et al., *Tunable excitonic properties in two-dimensional heterostructures based on solution-processed PbI2 flakes.* Journal of Materials Science, 2020. **55**(24): p. 10656-10667.
211. Brian, D. and M.J.R.o.S.I. Eslamian, *Design and development of a coating device: Multiple-droplet drop-casting (MDDC-Alpha).* 2020. **91**(3): p. 033902.
212. Li, Z. and K. Aik Khor, *Preparation and Properties of Coatings and Thin Films on Metal Implants*, in *Encyclopedia of Biomedical Engineering*, R. Narayan, Editor. 2019, Elsevier: Oxford. p. 203-212.
213. Begum, S., et al., *2D and Heterostructure Nanomaterial Based Strategies for Combating Drug-Resistant Bacteria.* ACS omega, 2020. **5**(7): p. 3116-3130.

Chapter 3

Research methodology

In this chapter, research methodology and essential material preparation procedures are provided. In line with core research objectives, the initial PEO setup was designed and described in this section. The post PEO treatments such as PEO-EPD, HT and drop-casting processes were explained later. Moreover, different 2D materials preparation technique and fundamental antibacterial and biomineralisation procedures were discussed in this chapter. Other procedures not included here are described in research papers presented in chapters 4, 5, 6 and 7.

3.1. Introduction

One of the essential steps in developing any new bone implants is selecting suitable materials and the fabrication process. The utilized technology should be accessible, scalable and economical to successfully transform the newly proposed concept to the current orthopaedic product market.

One of the well-known fabrication processes in the orthopaedic industries is plasma electrolytic oxidation (also known as PEO). As discussed earlier, this surface treatment method modifies the inert Ti substrate into a remarkable bioactive surface, therefore, address the osseointegration problems of Ti-based implants. Nevertheless, the PEO process usually requires additional post-treatment to address the infection problems. This chapter presents the methodology regarding the design, fabrication and optimization of the PEO setup and process, following by post-treatment strategies to further develop the surface with hydrothermal treatment (HT), high voltage electrophoretic deposition (PEO-EPD) and drop-casting method. This chapter also describes the characterization methodology to investigate the physicochemical properties of the fabricated samples and in-vitro antibacterial and bioactivity studies to evaluate the effectiveness of the final products.

3.2. PEO setup and optimization process for the fabrication of porous oxide layer substrate

Before the PEO process, initial Ti-sheets with 99.9% purity and 1 mm thickness was provided by Nilaco (Japan). Samples with a width of 1.5 cm and different length were obtained by cutting the Ti-sheet and cleaned by dipping in acetone in a sonication bath for 10 min followed by rinsing with DI water to remove any surface contamination.

All samples were dried in the electric oven for 3 h at 50 °C. The programmable DC power supply (N5752A, Agilent Technologies, USA) was used for the anodization process, while voltage-time data were collected by coupled LabVIEW software. A single step PEO process was performed under the galvanostatic condition based on the length of each titanium strips to guarantee a current density of 50 mA/cm^2 were received during 1 min of the PEO process. The upper portion of each Ti-strips was electrically isolated to reduce the burn out of the section where not placed inside the electrolyte. The working electrode (Ti- strip) was connected to the positive pole and placed in the middle of the setup, while cylindrical titanium mesh as a counter electrode was connected to the negative pole (**Figure 3.1**). The distance between the working electrode and counter electrode was adjusted at 4.5 cm. the acidic PEO treatment was performed in the acidic electrolyte containing 1.4 M H_3PO_4, and the Ti-samples which underwent the acidic treatment were labelled as the "acidic PEO" samples, while the basic PEO treatment was conducted in the basic solution containing sodium metasilicate pentahydrate (10.5 g l^{-1}), phosphoric acid (2 ml l^{-1}) and potassium hydroxide (2.8 g l^{-1}) in Millipore water [1]. The pH of acidic and basic electrolytes was 1 and 12, respectively. Finally, the treated sample rinsed in DI water and dried in the electric oven at 50 °C.

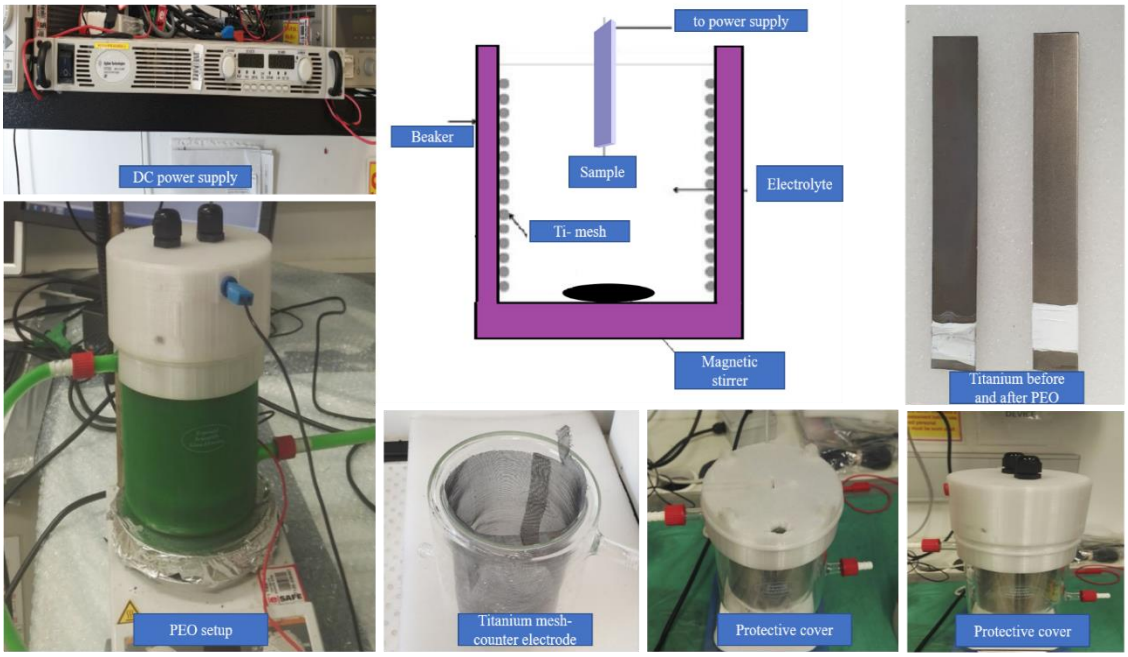

Figure 3.1.The experimental setup for PEO treatment of titanium strips.

3.3. The formation of titania nanostructure on PEO substrates by HT

HT treatment was conducted on both acidic and basic PEO samples. The HT process involved the application of a 100 ml reactor filled with 1 M NaOH solution. A few ml on top of the reactor remained unfilled to decrease the chance of reactor explosion during high-temperature operation. The rectangular-shaped PEO treated samples with the average size of (1 cm ×1.5 cm) were cut from the original fabricated PEO substrate and were placed in the bottom of the reactor. The hydrothermal treatment carried out for different durations of 1, 2, 4, 6, 8, 12 and 24 h at ~150 °C via an electric furnace. After finishing each HT session, the hot reactors were placed in the cold water bath for at least 20 min to cool down. Afterwards, the samples were carefully removed from the reactor with a special tweezer and placed in new containers filled with DI water for 24 h to remove the residual impurities from the treated samples. Finally, samples were dried in

the electric oven at 50 °C for 2h. Several stages of the process have been schematically depicted in (**Figure 0.2**).

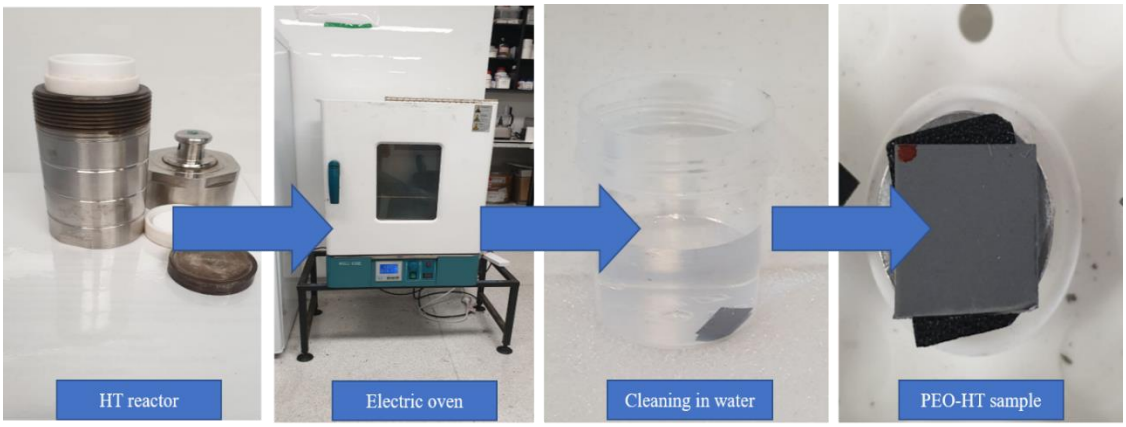

Figure 3.2. The hydrothermal process for the fabrication of nanostructures on PEO substrates.

3.4. Graphene oxide (GO) preparation

GO paste was generated via modified Hummer's method and through chemical oxidation of graphite powder. The original graphite flakes were supplied by Eyre Peninsula mine, South Australia and sieved to obtain the average diameter size of 250 µm. A mixture of H_2SO_4 (27 ml)and H_3PO_4 (3 ml) with a volume ratio of 9:1 was prepared and placed in the fridge for few hours to cool down. Then, 3 g of graphite flakes with 18 gr potassium permanganate (KMnO4) was combined and slowly added to the acidic mixture [2]. The final solution was kept stirring at 50 °C for 13 h. After reaching the ambient temperature, 1 ml of H_2O_2 was slowly added to the solution, which altered the solution to a brownish mixture. In order to wash the produced GO, 10 ml of hydrochloric acid (HCl 35%) and 30 ml of deionized water were added, and the solution then centrifuged at 4200 rpm for 2 h with 35% HCl and distilled water, respectively. Then, the supernatant was disposed of, and the residuals went through rewash, which continued for 4 times.

3.5. MXene preparation

A ternary layered carbide MAX phase material Ti_3AlC_2 (Carbon Ukraine) was used to prepare MXene materials. Lithium fluoride (LiF) and hydrochloric acid (HCl, 32%) were purchased from SIGMA –Aldrich (Australia) and used to prepare in-situ HF. The synthesis steps of MXene materials mainly followed a literature guideline [3]. It is a relatively low-risk and stable MXene synthesis scheme. In brief, MAX phase material was crushed into small pieces and was ground and sieved to the size range of 25 μm. Then LiF was carefully added to HCl. Afterwards, Ti_3AlC_2 powder was gradually added to the mixture and placed in an ice bath. The reaction vessel was stirred for 1 h. In the next stage, the mixture was stirred and kept at 35°C for 24 h. The final solution then centrifuged with DI water at 3,500 rpm for 30 minutes with the Eppendorf Centrifuge device at least 5 times.

3.6. hBN preparation

The exfoliation of bulk hexagonal boron nitride (hBN) flakes was performed by following the process demonstrated by Nine et al. [4]. In brief, the bulk hBN was soaked in an alkaline (2 M NaOH) aqueous solution (10 mg/ml) followed by the mechanical exfoliation using a planetary ball-milling (PM200, Retsch, Germany) [4]. The milling was performed in a zirconia pot partially filled with 3 mm zirconia balls 6 h with an interval of 20 min every 30 min. The exfoliated and agglomerated hBN sheets were further ultrasonicated (Branson Digital Sonifier 450) for an hour before washing with DI water using an Eppendorf Centrifuge to obtain a neutral suspension of hBN [4]. The final suspension of hBN was prepared in ethanol.

3.7. The decoration of PEO substrate with GO patches via PEO-EPD technique

The high voltage electrophoretic deposition technique, also known as PEO-EPD was utilized for the partial deposition of GO flakes over the basic PEO surface. PEO-EPD setup has been demonstrated in **Figure 3.3**. It comprises of two-electrodes cell arrangement with working electrodes distance of 13 mm. PEO treated sample was used as cathode and connected to the positive pole, while rectangular titanium sheet with a thickness of 1 mm was used as anode and attached to the negative pole. GO in the form of concentrated suspension was added to the mixture of ethylene glycol 94:5 wt%,

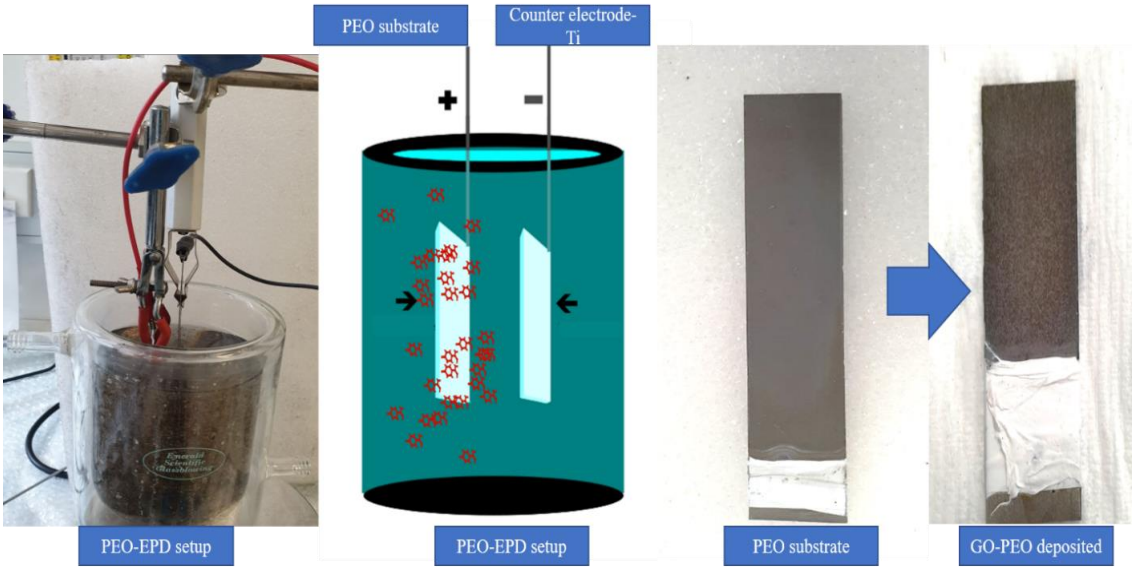

Figure 3.3. The experimental setup for PEO-EPD treatment and GO decoration on PEO samples.

deionized water 5 wt% and KF 0.5 wt% to reach the final concentration of 1 mg/l [5]. The GO flakes in the electrolyte then dispersed by an ultrasonic probe agitator for 20 min before poured into the PEO-EPD setup. Programmable DC power supply (N5752A, Agilent Technologies, USA) was utilized for the deposition process, while voltage-time data were collected by coupled LabVIEW software.

3.8. Partial deposition of 2D multi-layered flakes on PEO substrate via drop-casting method

Bulk GO, MXene and hBN in the form of a concentrated paste with different concentrations were diluted in ethanol to reach the concentration of 0.5 and 0.05 mg/ml. Diluted 2D materials solutions then were sonicated in an ultrasonication bath for 30 min. In the next step, 40 µl of each solution utilizing micropipette were cast onto the cleaned and dried PEO substrates (15 mm × 10 mm) and left in the electric oven overnight to dry at 50 °C [6]. The schematic figure of the process is provided in **Figure 3.4**.

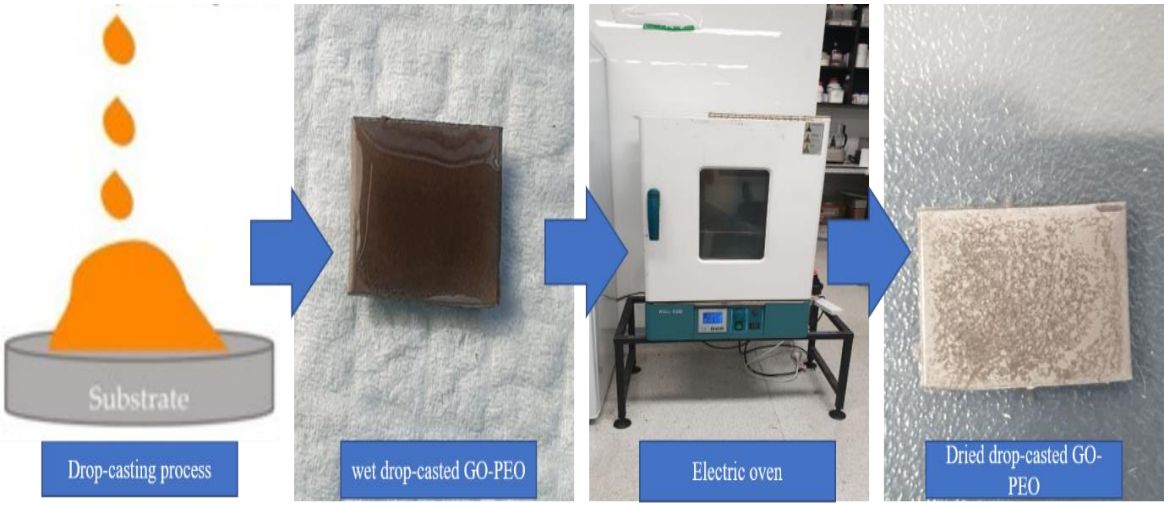

Figure 3.4. The drop-casting process and its example with deposition of GO flakes over PEO substrate.

3.9. Antibacterial activity assessment of mechano-bactericidal surface

The antibacterial test was carried out based on ISO 22916:2011 against *E. coli* (Gram-negative, DSM 3423) and *S. aureus* (Gram-positive, DSM 346) bacteria. Initially, bacteria streaked over the agar plate and incubated at 37°C overnight to form colonies.

Then a single colony from streaked strain was collected and transferred to the 5 ml TSB growth medium. The solution remained in the shaker for 2 to 3 h. cultured bacteria diluted

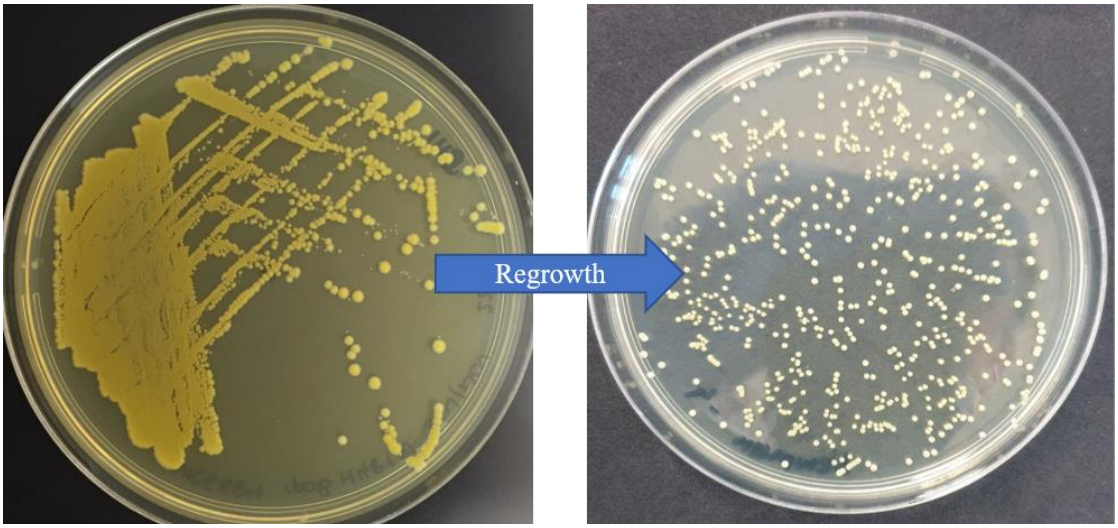

Figure 3.5. The process of streaking bacteria to collect a single colony for bacteria culture (*S. aureus*).

to the concentration of 6 x 10^5 Colony Forming Unit (CFU)/mL. UV lamp in the biosafety cabinet was used to disinfect titanium-based samples (each side 20 min). Then 12.6 µL of cultured bacteria were placed on the surface of samples and covered with polypropylene coverslips (8 mm in diameter) to obtain a homogeneous layer of bacteria. Samples in direct contact with bacteria were incubated at 37 °C for 24 h in an incubator. Bacteria then removed from samples by addition of 1 ml PSB and application of sonication bath. Afterwards, bacteria were diluted and placed on the agar plate and incubated overnight at 37 °C. CFUs were counted, and results were compared with control titanium samples. The images of *S. aureus* colonies during streaking and after regrowth stages are presented in **Figure 3.5.**

3.10. SBF mineralization test

The bio-mineralization test, also known as the Simulated body fluid (SBF) test, is a universal in-vitro technique, an alternative to the in-vivo studies for predicting surface

bioactivity by mimicking the body environment similar to the blood plasma [7]. SBF solution was produced based on the protocol provided by Kokubo et al. [8]. It contains different salts and chemicals usually present in the body fluid. **Table 3.1** demonstrates the chemicals used to produce 1 L SBF solution with (pH 7.40):

Table 3.1. Regents used for the preparation of SBF solution [8]

Order	**Reagent**	**Amount**
1	NaCl	7.996 g
2	$NaHCO_3$	0.350 g
3	KCl	0.224 g
4	$K_2HPO_4 \cdot 3H_2O$	0.228 g
5	$MgCl_2 \cdot 6H_2O$	0.305 g
6	1M-HCl	40 mL
(About 90 % of total amount of HCl to be added)		
7	$CaCl_2$	0.278 g
8	Na_2SO_4	0.071 g
9	$(CH_2OH)_3CNH_2$	6.057 g

Produced solution maintained in the refrigerator in Polyethylene containers. For the SBF test, dried and clean samples were placed in the bottom of a 50 ml polyethylene container filled with SBF solution and maintained in an electric oven for three weeks at 37 °C (**Figure 3.6 a**). In order to provide a suitable ion concentration of SBF for mineralization, the solution was refreshed every day (**Figure 3.6 a**). Finally, after 21 days, samples were removed from containers, rinsed and dried at ambient temperature overnight. A typical SEM image of the sample after a successful SBF mineralisation is provided in **Figure 3.6 b.**

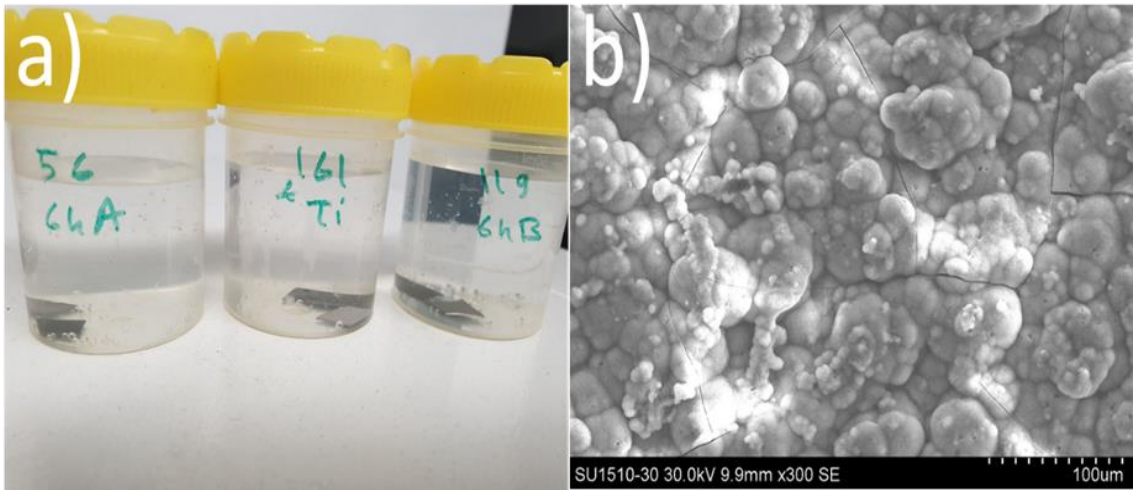

Figure 3.6. **a)** Samples during SBF mineralization test, **b)** Typical SEM image of the surface after mineralization process for 21 days.

3.11. Materials and chemicals

Different essential chemicals used in this research are described in **Table 3.2.**

Table 3.2. Different types of materials and compounds used.

Chemical/Material	**Formula**	**Grade**	**Source**
Ti sheets	Ti	99.9%	Nilaco (Japan)
MAX	Ti_3AlC_2	99.0%	Carbon Ukraine

Ethanol	C_2H_5OH	99.0%	Sigma-Aldrich
Potassium fluoride	KF	99.0%	Sigma-Aldrich
Phosphoric acid	H_3PO_4	86%	Chem Supply
Hydrochloric acid	HCl	32%	Chem Supply
Lithium fluoride	LiF	99.0%	Sigma-Aldrich
Potassium permanganate	KMnO4	99.0%	Chem Supply
Sodium Chloride	NaCl	99.7%	Chem Supply
Sodium bicarbonate	$NaHCO_3$	99.7 %	Chem Supply
Potassium Chloride	KCl	99.0%	UNIVAR
di-Potassium Hydrogen Ortho Phosphate	$K_2HPO_4 \cdot 3H_2O$	98.0%	Chem Supply
Magnesium chloride hexahydrate	$MgCl_2 \cdot 6H_2O$	99.0	Merck
Calcium chloride	$CaCl_2$	>98 %	Merck
Sodium sulphate	Na_2SO_4	≥99.0%	Sigma-Aldrich
TRIS (hydroxylmethyl) methylamine	$(CH_2OH)_3CNH_2$	≥99.0%	Sigma-Aldrich

Sodium metasilicate pentahydrate	Na_2SiO_3	≥95.0%	Sigma-Aldrich
Potassium hydroxide	KOH	85.0%	Chem Supply
Sodium hydroxide	NaOH	97.0%	Chem Supply

3.12. References:

1. Srinivasan, V., et al., *Review on Plasma Electrolytic Oxidation of Titanium Coatings.* 2016. **2**(1): p. 29-34.
2. Akhavan, O. and E. Ghaderi, *Toxicity of Graphene and Graphene Oxide Nanowalls Against Bacteria.* ACS Nano, 2010. **4**(10): p. 5731-5736.
3. Alhabeb, M., et al., *Guidelines for Synthesis and Processing of Two-Dimensional Titanium Carbide (Ti3C2Tx MXene).* Chemistry of Materials, 2017. **29**(18): p. 7633-7644.
4. Nine, M.J., et al., *Cross-overlapped flat-silver/hexagonal boron nitride for translucent heat-reflective coatings.* Applied Materials Today, 2020. **20**: p. 100764.
5. Mazinani, A., et al., *Graphene oxide (GO) decorated on multi-structured porous titania fabricated by plasma electrolytic oxidation (PEO) for enhanced antibacterial performance.* Materials & Design, 2021. **200**: p. 109443.
6. Lim, H.N., N.M. Huang, and C.H. Loo, *Facile preparation of graphene-based chitosan films: Enhanced thermal, mechanical and antibacterial properties.* Journal of Non-Crystalline Solids, 2012. **358**(3): p. 525-530.
7. Liu, X., C. Ding, and Z. Wang, *Apatite formed on the surface of plasma-sprayed wollastonite coating immersed in simulated body fluid.* Biomaterials, 2001. **22**(14): p. 2007-2012.
8. Kokubo, T., et al., *Solutions able to reproduce in vivo surface-structure changes in bioactive glass-ceramic A-W3.* 1990. **24**(6): p. 721-734.

Chapter 4

Engineering of nanostructured titania surfaces with tunable and mixed topography

This chapter discusses the potential application of novel PEO electrolyte combined with post hydrothermal treatment to form tuneable titania nanostructures on porous PEO treated surface. The obtained hierarchical micro-nano mixed morphologies consist of arrays of vertically aligned titania nano blades/nano spikes structures randomly distributed over anodized titania surface. The developed surface demonstrated exceptional bioactivity and wettability after the biomineralisation test, evident from the formation of hydroxyapatite particles covering the surface area. These results highlight the potential application of the fabricated titania nanostructures with this technique in the development of the next generation of titanium medical implants.

This chapter has been provided in the manuscript style under a Confidentiality Agreement

Arash Mazinani, Hadi Rastin, MD Julker Nine, Diana Tran, Tran Tung, Dusan Losic

Engineering of nanostructured titania surfaces with tunable and mixed topography by combined plasma electrolytic oxidation (PEO) and hydrothermal process.

Statement of Authorship

Title of Paper	Engineering of nanostructured titania surfaces with tunable and mixed topography by combined plasma electrolytic oxidation (PEO) and hydrothermal process
Publication Status	☐ Published ☐ Accepted for Publication ☐ Submitted for Publication ☑ Unpublished and Unsubmitted work written in manuscript style
Publication Details	Arash Mazinani, Hadi Rastin, MD Julker Nine, Diana Tran, Tran Thanh Tung, Dusan Losic

Principal Author

Name of Principal Author (Candidate)	Arash Mazinani
Contribution to the Paper	Conceptualization,Structure of Manuscript,Original draft
Overall percentage (%)	70
Certification:	This paper reports on original research I conducted during the period of my Higher Degree by Research candidature and is not subject to any obligations or contractual agreements with a third party that would constrain its inclusion in this thesis. I am the primary author of this paper.
Signature	Date: 24.05.2021

Co-Author Contributions

By signing the Statement of Authorship, each author certifies that:

i. the candidate's stated contribution to the publication is accurate (as detailed above);

ii. permission is granted for the candidate in include the publication in the thesis; and

iii. the sum of all co-author contributions is equal to 100% less the candidate's stated contribution.

Name of Co-Author	Prof Dusan Losic
Contribution to the Paper	Conceptualization,resources, funding acquization,review, editing, supervision, submission
Signature	Date: 24 May 2021

Name of Co-Author	Dr Md Julker Nine
Contribution to the Paper	selected investigation, editing and review, supervision
Signature	Date: 24/05/21

Please cut and paste additional co-author panels here as required.

Name of Co-Author	Dr Tran Thanh Tung		
Contribution to the Paper	selected investigation, editing and review		
Signature		Date	24/5/2021

Name of Co-Author	Hadi Rastin		
Contribution to the Paper	selected investigation, editing and review		
Signature		Date	25/05/2021

Name of Co-Author	Dr Diana Tran		
Contribution to the Paper	selected investigation, editing and review		
Signature		Date	26/05/2021

Engineering of nanostructured titania surfaces with tuneable and mixed topography by combined plasma electrolytic oxidation (PEO) and hydrothermal process

Arash Mazinani[1,2], Hadi Rastin[1,2], MD Julker Nine[1,2], Diana Tran[1,2], Tran Tung[1,2], Dusan Losic[1,2]*

1-School of Chemical Engineering and Advanced Materials, The University of Adelaide, Adelaide, SA 5005, Australia

2-ARC Hub for Graphene Enabled Industry Transformation, The University of Adelaide, Adelaide, SA 5005, Australia

*Corresponding Author: Prof. Dusan Losic
School of Chemical Engineering and Advanced Materials, The University of Adelaide, Adelaide, SA 5005, Australia; email: dusan.losic@adelaide.edu.au

Abstract:

This study presents the engineering of titania multi-structured surfaces with mixed morphologies containing randomly distributed micro-nano porous structure fabricated by plasma electrolytic oxidation (PEO) using an acidic electrolyte and array of vertically aligned titania nanoblade structures fabricated by post hydrothermal treatment (HT) using NaOH electrolyte. A typical titania nanoblade structure showed its characteristic 2D geometry with an average height of about 700 nm, a width of around 100 nm at the bottom base side, with sharp and slightly rendered edges that end to a sharp tip with approximately 10 nm width. By increasing the duration of HT, it was found that the shape of these 2D nanostructures can be transformed into 1D (nanoneedle) structures, confirming the application of this approach to create a unique hierarchical surface morphology with a combination of micro-nano pores and 2D to 1D nanostructures. Furthermore, the fabricated multi-structured surface exhibited super-hydrophilic properties with excellent apatite formation ability, highly desirable for biomedical applications. This engineering strategy of Ti surface by a combination of two processing technologies is scalable and very promising for the engineering of

advanced titanium-based materials for broad industrial applications, including new smart orthopaedic implants.

Keywords: Titanium; Plasma Electrolytic Oxidation (PEO); hydrothermal process, Titania nanostructures, Bioactive surface

1. Introduction

Titanium-based materials are widely used for broad industrial, domestic, architectural, defence and biomedical applications thanks to their excellent properties, such as mechanical strength, low weight, chemical and corrosion resistance, non-toxicity and biocompatibility[1-3]. Since Ti and its alloys were introduced and clinically proved as biomedical implants sixty years ago, a broad range of surface modification treatments have been developed and clinically implemented to enhance the osseointegration properties of Ti implants [4, 5]. In the last three decades, the surface modifications of Ti were dominated by micro-structuring processes with the aim to create rough surfaces that were aligned with studies showing their advantages for bone cells adhesion and osseointegration improvement [3]. However, recent studies indicated the importance of nanoscale dimensions and nanostructured Ti surface that attracted research toward exploring more advanced surface engineering approaches using nanotechnologies [6, 7]. These new technologies will provide new opportunities to significantly improve some limitations and existing properties of titanium implants by developing new surface characteristics, including novel engineered topographies with nanoscale and surface chemistry modification to enhance their osseointegration properties, corrosion resistance and also to prevent biofilm formation [6-9]. Currently, a new trend in the development of advanced biomedical implants is emerging, called “smart medical implants” with multifunctional properties for application in sensing, drug delivery and antibacterial protection[10]. These smart implants require new surface and nanoengineering technologies to develop novel surface with synergetic combinations of unique micro-nano topographies and surface chemistries. Several surface

engineering processes, including chemical etching, anodic oxidation, plasma electrolytic oxidation (PEO), plasma deposition, electrophoretic deposition, laser ablation and hydrothermal process were explored toward nanostructuring of titanium surface, showing ability to generate these types of nanostructures with broad range of morphologies possessing different shapes, dimensions and interfacial properties [9, 11-14].

Among several electrochemically based techniques that were proved for efficient surface engineering of Ti, one promising technique is the plasma electrolytic oxidation (PEO) technique, also known as micro arc oxidation (MAO). This unique method is founded on the application of a high electric field (several hundred V) on Ti, used as an electrode in an electrolytic solution that leads to the formation of electron avalanche, which is hitting the metal surface in the shape of micro arcs with a localised arc temperature of around 2000 °C [15, 16]. These micro arcs melt the surface locally and form a molten oxide. This molten oxide eventually resolidifies due to the presence of cold electrolytic solution and form a protective oxide film with a unique porous morphology and extremely hard surface [17]. The PEO surface modification technique is commercially used to advance Ti-based materials for industrial and defence applications. It is considered a promising technique to improve the properties of titanium implants for dental and orthopaedic applications.

The hydrothermal treatment (HT) is another common method that is extensively applied for surface engineering and structural modification of titanium to generate a broad range of titania and titanate nanostructures, including nanorods, nanowires, nanoribbons, nanopillars used in many applications such as solar cells, photocatalysis, supercapacitors and biomedical implants [18-23]. Previous studies showed that the morphology and dimension of these created nanostructures on the Ti surface could be tailored using HT conditions, including the selection of electrolytes (KOH, NaOH, NH4OH, HF, etc.), the reaction time, concentration, temperature, pressure and stirring [24-26]. It was reported that KOH electrolyte specifically promotes horizontal growth and formation of nanowires, nanobelts and nanoribbon. In contrast, NaOH promotes the growth of vertically aligned nanostructure in the form of spikes, pillars, rods and flakes [27-31]. Significant achievement on utilising HT process to form nanostructures was demonstrated by Ivanova

et al. to demonstrate biocidal surface with mixed nanoribbons and nanospikes morphologies that exhibited excellent antimicrobial properties against several bacteria providing the mechanical mode of action to kill bacteria by disrupting their cell membrane [32].

On the other hand, the latest trend in advancing performances of Ti medical implants in terms of improved bone cells attachment is the generation of the surface with combined micro and nano scale structures or hierarchical micro-nano structures (HMN) that include a broad range of different 1D and 2D morphologies. These types of mixed morphologies are expected not only to promote bone cells adhesion and increase interface area, which is needed to improve osseointegration, but also to significantly improve their antibacterial properties that is still an unsolved problem in typical medical implants [33-35]. Regarding the osseointegration ability of HMN structures, Gongadze et al. demonstrated that nanostructures with a sharp edge and spike-like morphology could augment surface charge density and strengthen the electric field required for the improvement of osteoblast-titanium bounding and finally enhance the osseointegration characteristics of the surface [36]. With previous studies showing strong antibacterial performance of heterostructures, engineering of mixed micro and nano morphologies appears to be a very promising strategy to design a new generation of smart biomedical implants[37].

To fabricate Ti surface with the mixed nano to micro topographies in our previous work, we demonstrated a scalable and straightforward method that combines electrochemical anodisation and laser sintering of Ti (3D printing) able to create a unique surface with nanotubular and microparticles structures [32-33]. The fibroblasts cell adhesion revealed their great tendency to adhere to these micro-nano structured implant surface compared with control surfaces (flat Ti) [38]. This work prompted to explore the combination of other methods for surface engineering of Ti surface by combination of PEO treatment with post HT process, which still demonstrates plenty of room to explore. Earlier studies conducted in the complex electrolytes containing calcium and phosphorous ions notably resulted in the formation of thick appetite layers after post HT process, instead of the nanostructured titania over the surface [39-45]. Therefore, the ability to engineer Ti-based nanostructures with adjustable size over the PEO surface was

limited that initiated more research to address this problem [46-49]. The learning point was that although common PEO+HT processes enable the formation of hydroxyapatite (that is beneficial for bio integration improvement), however, it also prevents the fabrication of nanostructured titania arrays, which are highly effective against bacterial biofilm formation [21, 50]. Moreover, studies suggest that the formed Ca–P layers in the hydroxyapatite suffer high brittleness and demonstrate insufficient adhesion to the substrate[51, 52].

To address these limitations, in this paper, we present a new fabrication strategy to create Ti surface with mixed nano and micro topographies by combining PEO and HT, using specific conditions that prevent the formation of apatite layers. We proposed to apply the PEO method in a Ca-free electrolyte that will create titania oxide film with an array of micro and nano pores. The subsequent HT process on the PEO surface fabricates additional arrays of new titanate nanostructures that can be tuned to various forms such as nanoribbons, nanorods, nanospikes, nanopillars etc. depends on the electrolyte and HT conditions. It was critical that the initial PEO micro to nanoporous layer is preserved and new 2D nanostructures created on the top of the PEO layer. To prove the proposed concept, among many controlling parameters explored in this work, we present the influence of HT time on the morphology of created nanostructures, chemical composition, crystal structures, wettability, mechanical strength and biomineralisation ability. This material with mixed and hierarchical topography will provide many unique multifunctional properties not only related to biomedical implants but also many other applications, including supercapacitors, photocatalytic, tribological, electron transfer and sensing that worth exploring.

2. Experimental Section

2.1. Materials

Titanium (99.99 %) foil (thickness 1 mm) were supplied by Nilaco (Japan); orthophosphoric acid 85 wt%, sodium hydroxide pellets were obtained from Chem Supply (South Australia), used as received

without any further purification. High pure Milli-Q water also used whenever needed during the experiment. The SBF solution was produced according to Kokubo and Takadama research[53] with reagent-grade chemicals, buffered at pH 7.4 with tris-hydroxymethyl-aminomethane and HCl at 36.5°C.

2.2. Fabrication of PEO surface on Titanium

In order to fabricate the porous oxide layer over Ti foil, a modified single-step PEO anodisation process in an acidic solution at 25 °C was adopted [54]. Rectangular shape commercially pure titanium foils (3cm x 1cm) with the average thickness of 1 mm were cut from titanium sheet. All the samples were cleaned by sonication in acetone for 10 min. In the next step, specimens were rinsed in Millipore water for another 10 min to ensure removal of surface contamination produced during manufacturing and handling. Eventually, all samples were dried in a thermostatic oven for 2 h at 50 °C. The PEO treatments for titanium foil was conducted by utilising a programmable DC power supply (N5752A, Agilent Technologies, Everett, WA, USA) coupled with LabVIEW software under the galvanostatic condition by modifying previous research protocol carried out by Kuromoto et al. [54, 55]. Specimens were treated in a single PEO step at a current density of 50 mA/cm^2, using a magnetic stirrer at 250 rpm for 1min. The electrolyte used in this experiment was containing 1.4 M H_3PO_4 (with pH 1.1), which resulted in the formation of the coating that, for simplicity, is called the "PEO sample". After PEO treatment, samples were removed instantly from electrolytic solution, rinsed in an ultrasonic bath with Millipore water for 6 minutes and then dried in cool air.

2.3. Fabrication of nanostructured surface on the PEO films by hydrothermal treatment

PEO treated samples in the acidic solutions were washed in the ultrasonic bath in ethanol/water solution 50/50 (v/v %) for 6 min and then dried in a thermostatic oven at 50 °C for 2 hours. Hydrothermal treatment (HT) carried out with 1M NaOH solution in 100 ml reactor (autoclave) with Teflon liner for different time intervals from 1 to 8 hours and at 150 °C as described by Anitha et al. and Jaggessar [56, 57]. Afterwards,

samples were carefully removed from the reactor, cleaned by soaking and rinsing in Millipore water and dried in the oven at 50 °C.

2.4. Labelling system of samples based HT conditions

Table 1 presents the labelling system and HT conditions such as reaction time and temperature of HT for each sample.

Table 1. PEO treatment and hydrothermal treatment conditions.

Sample name	PEO electrolyte	HT Reaction time (Hrs)	HT Reaction temperature (°C)
A-PEO	Acidic Solution	0	-
A-HT_{1h}	Acidic Solution	1	150
A-HT_{2h}	Acidic Solution	2	150
A-HT_{3h}	Acidic Solution	3	150
A-HT_{4h}	Acidic Solution	4	150
A-HT_{5h}	Acidic Solution	5	150
A-HT_{6h}	Acidic Solution	6	150
A-HT_{8h}	Acidic Solution	8	150

2.5. Characterisations

Structural characterisation of the porous structure after PEO treatment was performed using SEM Quanta 450 (field emission scanning electron microscope, Eindhoven) coupled with an EDS analysis device. Structural characterisation after (PEO+HT) carried out by high resolution focussed ion beam (FIB) with FEI Helios Nanolab 600 instrument. Samples were placed and fixed on an SEM sample holder using carbon tape, and then 3 nm platinum was coated over them. SEM images were taken on samples from the top view and also at 52 degrees, while cross-sections and EDS spectra were used to collect data from

different spots over the samples. Raman spectroscopy (WITEC Alpha300) was utilised to confirm the presence of anatase or rutile phases over the (PEO+HT) surface in the range of 0-1000 cm^{-1} wavelength with a 532 nm laser. XRD analysis was performed using Rigaku MiniFlex 600, Japan, with the operating condition of (40 kV and 15 mA, 2θ = 20–80 and scan rate of 2.5 °/min). Contact angle measurement was carried out by optical-tensiometers model (T301 – ATA scientific pty ltd) with a small droplet size of 2.2 ± 0.1 µl. The microhardness test was performed using the LM700 microhardness tester with a predefined condition of 100 g force and a dwell time of 10 s over PEO surfaces. Finally, a biomineralisation test was carried out on samples by immersing samples in 50 ml SBF solution for 21 days. The SBF solution was made according to Kokubo and Takadama research [53], then was poured into a polyethylene beaker and refreshed every day to keep the required ion concentration at a suitable level for the mineralisation process, similar to the human blood condition. After 21 days, samples were removed from the solution and dried in the air. All samples were measured at least three times, and reported data are average values with standard deviation.

3. Results and Discussion

3.1. Voltage–time dependencies for galvanostatic PEO process

Based on our preliminary investigation and literature reports exploring a range of applied current densities and time, in this work, a galvanostatic mode with 50 mA/cm2 and 1 min were chosen as the optimal condition for the fabrication of multi porous PEO surface on Ti [14, 54, 55]. Typical voltage-time dependencies during PEO treatment in the acidic electrolytes at 50 mA/cm^2 is presented in **Fig.1a**. Recorded values for cell voltage exhibited an increasing trend in the first few seconds of the process, which finally were stabilised at values ~200 V. Our result showed a breakdown voltage of around 170 V after 10 s of the PEO process, evident from the formation of arcs over the substrate accompanied with acoustic emission. These results are in agreement with previous reports for PEO treatment in a similar acidic solution [55].

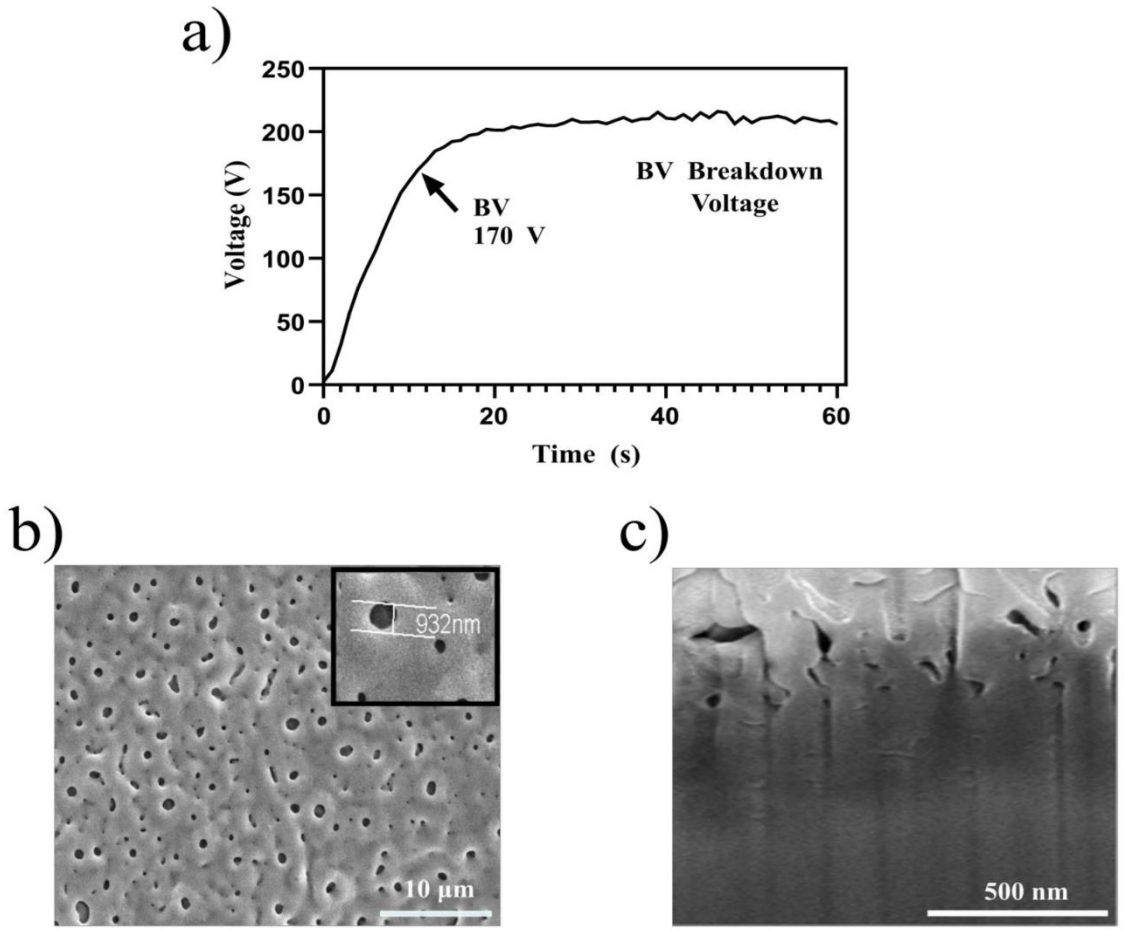

Figure 1. a) V-Time curve during PEO treatment after 1 min, b) SEM image of Ti surface after PEO process, c) Cross-section image of the PEO treated sample after 1 min in the acidic electrolyte.

SEM characterisations of fabricated PEO titania oxide substrates are presented in **Fig. 1b** and **c**. SEM images show a typical PEO porous topography with randomly dispersed pores across the surface. The pores diameters are in the range of 120 nm to ~1 µm with an average inter-distance of 1.6 microns. A typical high-resolution image of a single pore is exhibited in the inset of **Fig 1b**. This pore morphology is similar to the previous reports from Kuromoto et al. and Kawashita et al. obtained on the Ti via potensio-static

PEO treatment at 180 V using a higher concentration of phosphoric acid [54, 58]. The PEO condition in our experiment led to the formation of a porous oxide layer with an average thickness of 510 nm during a short period of 60 s (**Fig.1c**). The measured thickness is slightly higher than 330 nm oxide layer thickness, reported by previous studies carried out in a similar condition via a potensio-static condition of 200 V [44]. It is worth mentioning that fabricated porous micro-nano morphology on PEO surface plays a crucial role in bone bonding and ingrowth of bone cells with titanium implants[59].

3.2.Characterisation of PEO-HT fabricated surface

The Fib-SEM images presented in **Fig. 2** are showing topography of nanostructures created over PEO sample after HT process at different time intervals between 1 to 8 h. During first hour of HT (sample A-HT_{1h}), very tiny nanostructures were formed (**Fig. 1a**). FIB image from cross section of these nanostructures showed that the average height of these nanostructures was around ~100 nm (**Fig. 2b**). Following images clearly demonstrated the formation of titanate nanostructures with different shapes and dimensions that started to be strongly appearing on the surface after 2 h of HT process for sample A-HT_{2h} (**Fig. 2c**). These characteristic arrays of vertical nanostructures, which we describe as "nanoblades" morphology, has distinctive 2D geometry with large width on the bottom and with thin, blade-like spires and sharp ends on the top. After 4 h of HT(sample A-HT_{2h}), no notable change in the morphology of nanostructures was observed (**Fig. 2d**) and formed nanoblades continued to grow by increasing HT duration. A typical single nanoblade structure with an average width of around 100 nm at the bottom base side and with sharp edges that are slightly rendered to build a sharp tip with approximately 10 nm width and height about 700 nm is demonstrated on the inset of **Fig. 2e**.

By increasing the HT time to 6 h, sample A-HT_{6h} (**Fig. 2e**), very thin and sharp nanoneedles were also observed within dominant nanoblade structures. This observation indicated the possibility of tuning the nanostructure morphology by changing the duration of the HT process from mainly nanoblade to mixed nanoblade/nanoneedles. By continuing HT to 8 h, sample A-HT_{8h} (**Fig. 2f**), the surface was predominantly

covered with twisted nanoneedles forming a grass-like structure with only a few nanoblade structures observable over the surface. It signifies that 6 h is the maximum duration of HT to fabricate relatively upright mixed nanoblade/nanoneedle structures over the PEO surface. Moreover, 4 h demonstrated the optimum duration of HT to create dominant upright nanoblades morphology. Therefore further surface characterizations were mainly focused on the candidate A-HT_{4h} and A-HT_{6h} samples.

The dimensions of the fabricated nanostructures with HT were highly influenced by the duration of HT process, which were showing an increasing trend in their height from around 100 nm (A-HT_{1h}) to about 1000 nm (nanoneedle) after 6 h of HT process (A-HT_{6h}). The size analysis, including height and inter-distance between nanostructures fabricated by different HT duration, is summarised in **Fig. 3a**. This analysis was taken from at least 20 nanostructures formed at each time intervals with "ImageJ" software. This graph shows an average spacing up to 400 nm for large nanostructures formed on A-HT_{6h}, while in shorter HT duration, nanoblade formed with lower height and shorter interspacing. A typical low-resolution SEM image taken from A-H_{4h} (**Fig. 3b**) shows the presence of micro-nano pores related to the initial PEO process confirming mixed micro-nano morphology on Ti surface obtained by the combination of PEO and HT process. To evaluate the elemental composition of these nanoblade structures created by the HT process, the EDS analysis carried out on the A-HT_{4h}, and the results are presented in **Fig. 3c.** The EDS graph clearly highlighted the presence of Ti, O and particularly Na as a result of HT in NaOH solution over the surface.

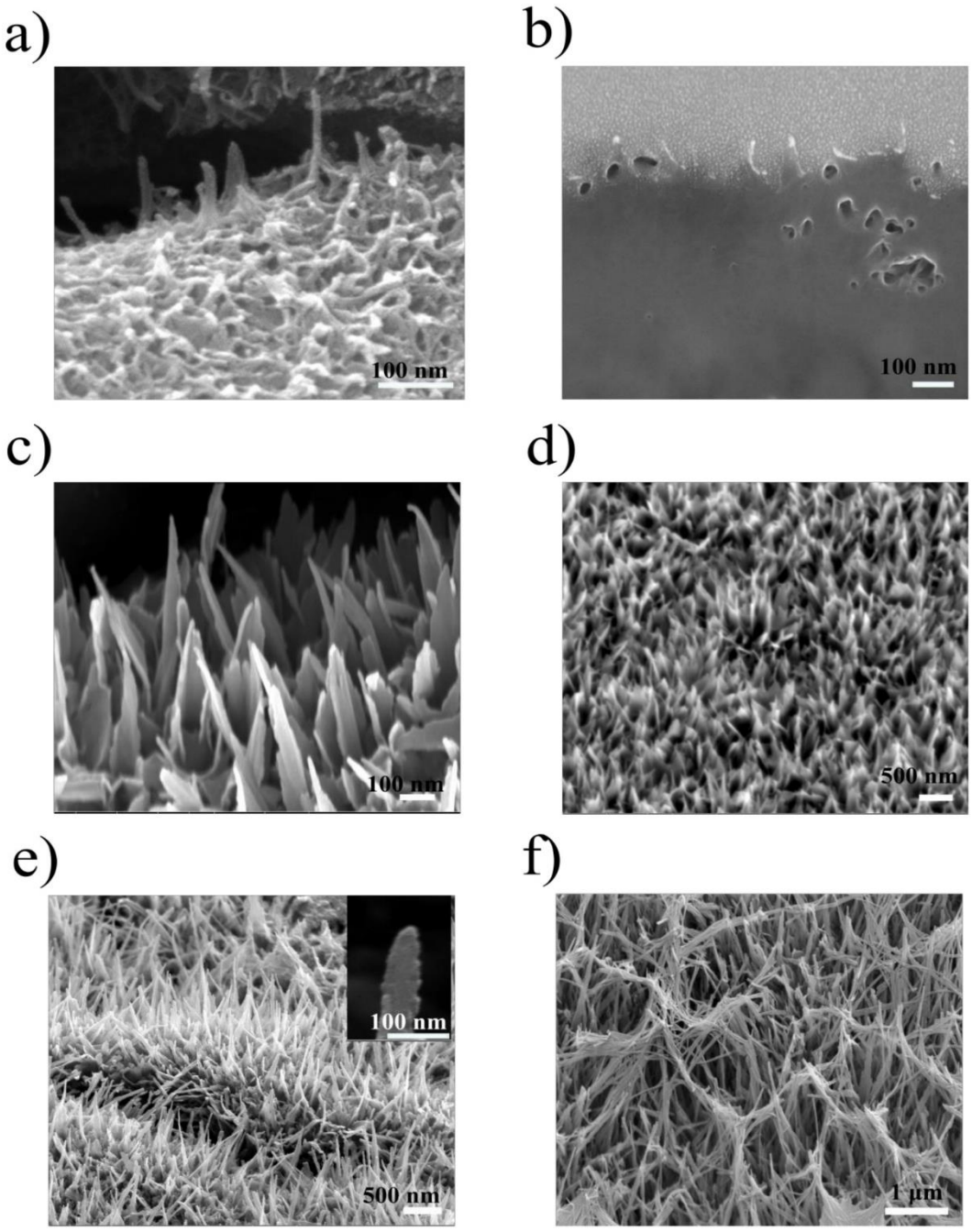

12

Figure 2. High-resolution FIB-SEM images showing topography with nanostructures obtained after HT (a) A-HT_{1h}, (b) A-HT_{1h} cross section view, (c) A-HT_{2h}, (d) A-HT_{4h}, (e) A-HT_{6h}, (f) A-HT_{8h}.

It is worth noting that different but mainly 1D morphologies of titania such as nanopillars [60], nanowires[29], nanospikes[61] have been reported using HT with NaOH solution. However, 2D morphology as nanoblades fabricated on the PEO titanium oxide layer presented in this work has not been reported before. In a recent study on the untreated Ti substrate by using similar HT condition and duration ranging between 2 to 4 h, nanopillars formation was reported [57]. Therefore, it is evident that underlying PEO substrate is playing a fundamental role in the formation of observed nanoblades in our samples.

This is the first demonstration of a successful combination of PEO and HT process for fabrication of HMN structure with titania nanoblade morphology as a new approach for nanoengineering of unique and mixed nanostructures on Ti surface. Moreover, unlike most customary fabricated titania nanostructures that only exhibit sharp tips in their structure, our novel nanoblade structure also demonstrates 2D morphology on side edges, along with micro-nano PEO pores that may contribute to the antibacterial and osteointegration enhancement of the sample.

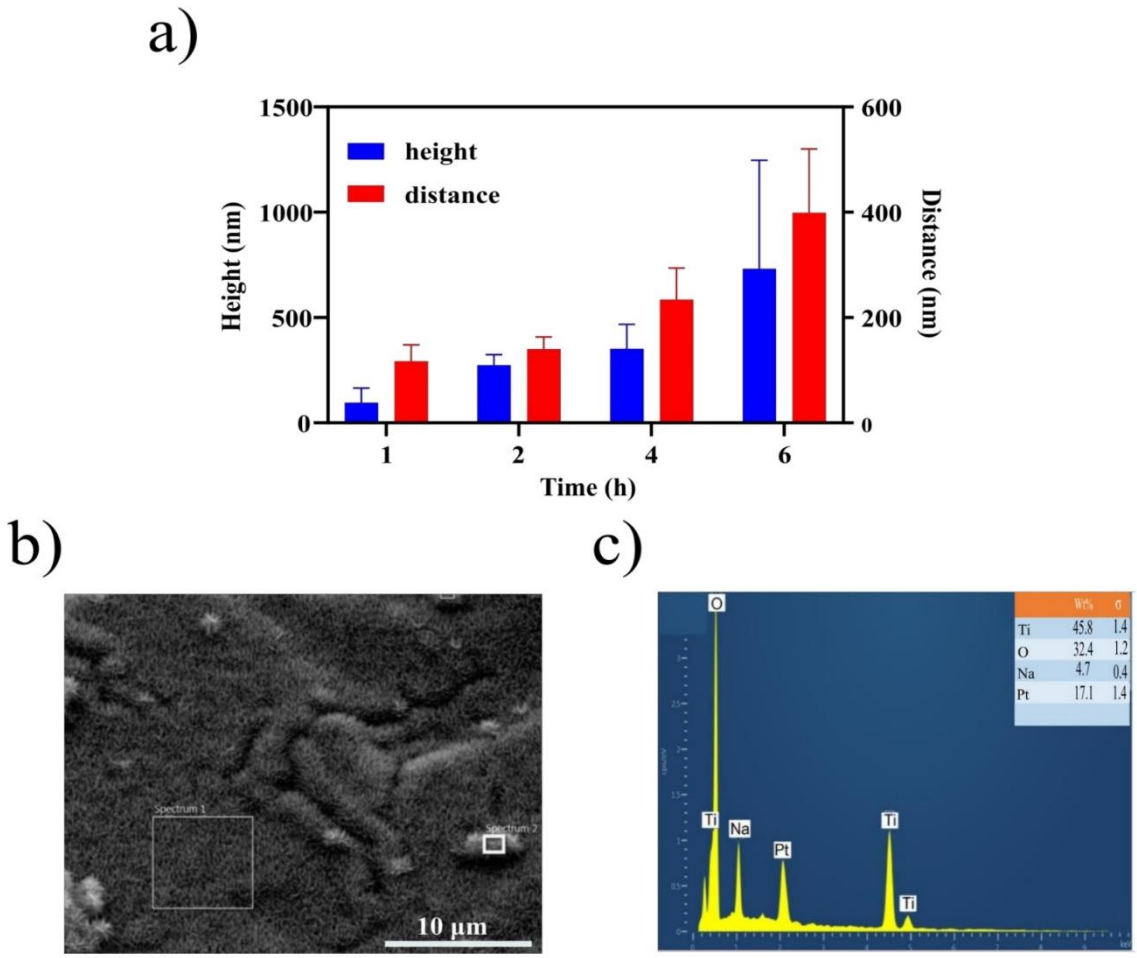

Figure 3. a) Correlation of dimensions of fabricated nanostructures (the height and inter-spacing) for different samples HT treated for 1 to 6 h (average data are presented), b) low magnification SEM image of A-HT_{4h}, c) corresponding EDS result for A-HT_{4h} sample.

3.3. Physicochemical characterisation of titania nanostructures

The XRD spectra for PEO treated and PEO+HT treatment after 4 h (A-HT_{4h}), and 6 h HT (A-HT_{6h}) are presented in **Fig. 4a**. Comparison of obtained peaks with standard JCPDS card, no. 65-3362 and standard anatase phase (JCPDS card No. 21-1272) revealed the formation of anatase, which is evident from the presence of peaks at 2θ values of 25.8° and 48.5° corresponding to (101) and (200) planes after HT. Particularly, the peak at 48.5° was intensified after HT treatment indicating the improvement of the oxide layer crystallinity during HT. Previous studies highlight the positive impact of the anatase phase in the development of HAP sites and eventually better bone-implant integration[62].

Raman study showed no peak observable for the control sample (as received titanium foil), but after the PEO process, several peaks of anatase phase appeared on the Raman spectra of samples (**Fig. 4b**). Based on the previous studies, in order to obtain the best fitting for Raman spectra, Lorentzian curve fitting by five different Raman bands was utilised [63]. Therefore, four peaks were obtained at about 146, 404, 473 and 631 cm^{-1} confirming the formation of the anatase phase. HT process leads to the formation of sodium titanate on the PEO surface that alter the Raman spectra. The associated peaks at around 270 and 699 cm^{-1} were weak at first and then intensified by increasing the time of the HT process. Our results confirm previous works indicating the hydrothermal treatment of PEO surface in NaOH can improve the preferential formation of Na_2TiO_3 over other possible complex titanates formation such as $Na_2Ti_6O_{13}$ and $Na_2Ti_3O_7$ [63]. Therefore, the presence of different percentage of Ti ions and variation in oxygen vacancies can lead to a non-stoichiometric condition in the oxide layer and finally lead to the formation of reactive oxygen species (ROS), which are known to provide strong antimicrobial activities[63]. This is an additional advantage that is important for designing advanced Ti-based implants for antimicrobial protection with multiple modes of action involving ROS and the mechanical killing of bacteria with sharp nanostructures.

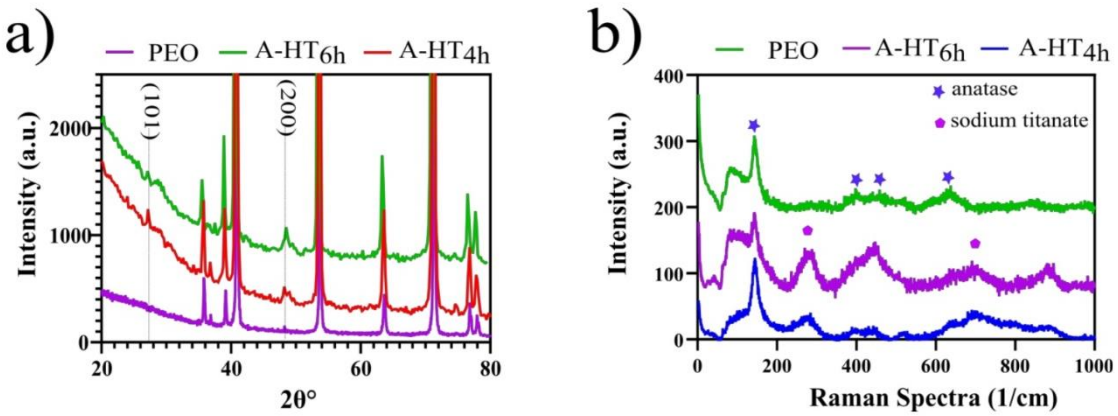

Figure 4. a) XRD spectra of a PEO sample, A-HT$_{4h}$ and A-HT$_{6h}$, b) corresponding Raman spectra.

In the next stage, contact angle measurement is carried out on different samples, presented in **Fig. 5a**. As-received Ti sample showed contact angle values around 75°. PEO treatment showed a slight increase in hydrophilicity to around 60°**.** This increase in hydrophilicity is mainly attributed to introducing new chemical composition to the surface (titania vs Ti) and partially influenced by the generation of micro-nano morphology and the increase in the surface roughness. Previous studies on the interplay between surface energy and structure on interfacial properties of PEO titania suggest that hydrophilicity of PEO oxide layer is primarily influenced by the modification of chemical composition through anodisation rather than the introduction of micro-nano structure [64]. Moreover, all HT treated samples showed a significant increase in the hydrophilicity evident by a decrease in CA values to less than 5°, making these surfaces super-hydrophilic, therefore very favourable for cell adhesion and growth. Other research also emphasises the role of NaOH alkaline HT in increasing the surface energy of titanate nanostructures, resulting in the enhancement of wettability and bioactivity of coating [65, 66].

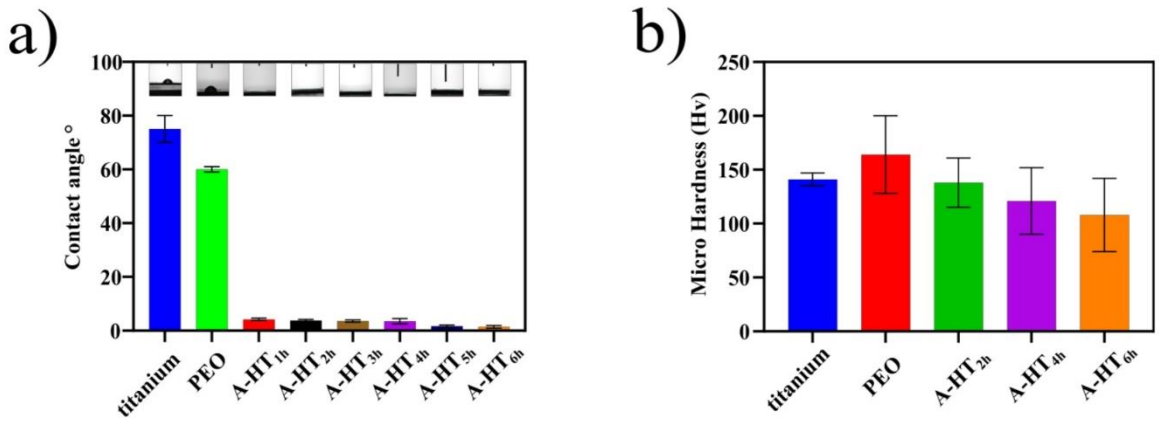

Figure 5. a) Contact angle (CA) measurement for different samples before and after HT, b) Vickers hardness measurement for candidate samples.

Vickers micro-hardness characterisation (Hv) results are presented in **Fig. 5b**. The obtained results demonstrate a considerable increase in the hardness of PEO treated Surfaces (164 Hv) compared to untreated Ti control (141 Hv). It is important to note that no vulnerability to brittle fracture was noticed in the PEO fabricated substrates showing strong robustness and mechanical resistance. Based on previous studies, continuing the PEO treatment would further develop the oxide layer on the surface. However, in the current study, the focus is on the role of initial PEO substrate for the generation of micro-nano pores and its combination with titania nanoblade structure for osseointegration enhancement, not the mechanical improvement of the surface. Therefore, a relatively shorter duration for PEO treatment was chosen. Samples after hydrothermal treatment showed slightly lower hardness values, suggesting a negative mechanical impact of hydrothermal treatment. This decrease in the mechanical stability of the PEO coating after HT was also reported by Lin et al. [49]. By increasing the duration of HT, hardness values dropped to 138 Hv for sample A-HT_{2h} and to the low value of 121 Hv and 108 Hv for A-HT_{4h} and A-HT_{6h}, respectively.

3.8 Bio mineralisation test

Finally, the biomineralisation test was accomplished by 21 days immersion of samples in the SBF solution. Results summarised in **Fig. 6** show SEM, EDS and XRD results of the A-HT_{6h} sample along with control samples (titanium and PEO samples) after immersing in SBF. The bare Ti sample did not demonstrate any potential for mineralisation (images not included). SEM image and EDS result of PEO sample after SBF test in **Fig. 6b** and **d** (PEO/SBF) revealed the presence of tiny particles, which were randomly formed over the surface containing Ca and P with the ratio of Ca/P ~ 2.1. SEM micrographs of the A-HT_{6h} after SBF test (A-HT_{6h}/SBF) demonstrated spherical grains ~53 μm in size with smaller particles on top of them, which completely covered the surface (**Fig. 6c**). A higher concentration of Ca and P ions with a Ca/P ratio of ~ 2.26 was observed on HT treated surface after SBF (**Fig. 6e)**.

XRD spectra analysis of different samples before and after HT revealed the successful formation of HAP layers on the surface for both PEO and PEO+HT samples, evident from the existence of HAP characteristic peaks in agreement with (100), (200), (002), (102), (112), (300), (301), (312) and (213) standard planes ICDD 9–432 HAp standard peaks[67].

Our result showed the notable ability of HT to improve the mineralisation potential of PEO samples by introducing Ti–OH groups to the surface, which is in agreement with previous reports [68]. The subsequent reactions between sodium titanate and SBF solution and the exchange of Na+ ions with H_3O+ ions can lead to the formation of the appetite layer on the surface. Meanwhile, other factors such as tailoring and increasing nanostructures can also improve the hydrophilicity of the surface and promote apatite formation on HT treated PEO surface [41, 69].

18

\

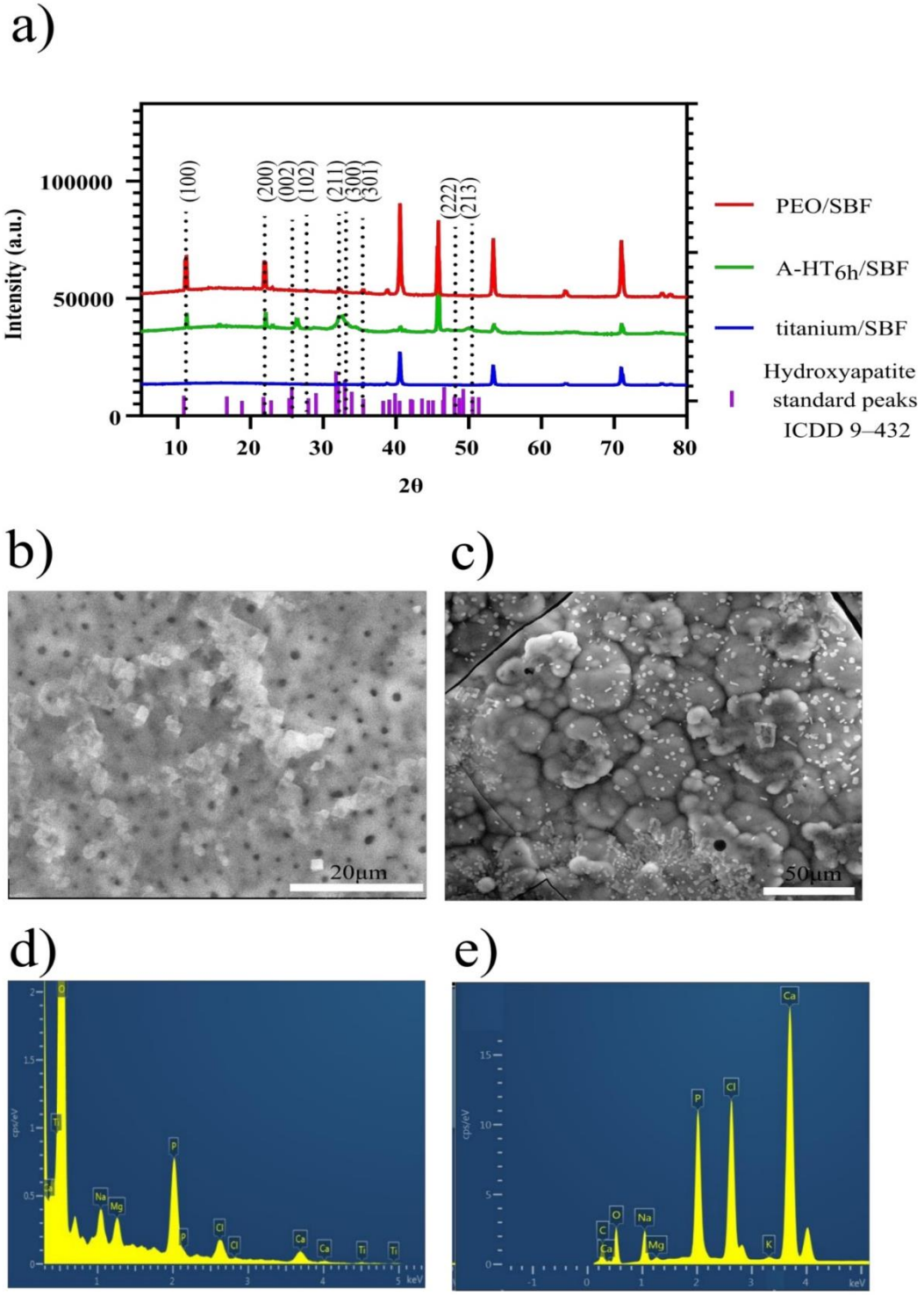
a)
Intensity (a.u.)
100000
50000
0
10
20
30
40
50
60
70
80
2θ
(100)
(200)
(002)
(102)
(211)
(300)
(301)
(222)
(213)
PEO/SBF
A-HT6h/SBF
titanium/SBF
Hydroxyapatite
standard peaks
ICDD 9–432
b)
20μm
c)
50μm
d)
e)

Figure 6. a) XRD spectra of samples after SBF mineralization test for different samples, SEM images of samples after mineralization test for b) PEO/SBF, c) A-HT_{6h}/SBF, EDS spectrum of the corresponding samples for d) PEO/SBF, e) A-HT_{6h}/SBF.

4. Conclusion and future studies

In summary, we demonstrated the engineering of new titania nanostructured surfaces with a unique mixed morphology containing randomly distributed micro-nano porous structure fabricated by PEO process using H_3PO_4 electrolyte and array of characteristic titania nanoblades and nanoneedle structures fabricated by a subsequent hydrothermal process using NaOH electrolyte. Our results showed that the shape and dimensions (the height and their inter-distance) of fabricated titania nanostructures could be controlled by the time of the HT process. The maximum size of nanostructures on the surface increased from ~100 nm (for A-HT_{1h}) to ~1000 nm after 6 h of HT process (A-HT_{6h}), while possessing a typical 2D geometry, with a width of around 100 nm at the bottom base side and sharp tip with about 10 nm width. The mixed morphologies of nanoblades and nanoneedles were successfully fabricated after 6 h of HT (A-HT_{6h}). Further increasing HT time to 8 h (A-HT_{8h}) led to the fabrication of twisted nanoneedles or nanograss morphology. These significant results are indicating the great potential of this process to tune titania nanostructures with different shapes and dimensions and, therefore, potentially tailor biological performance, which eventually may affect osseointegration and antimicrobial properties. The contact angle (CA) measurements showed a significant increase in the hydrophilicity of hydrothermally treated samples (to less than 5°) which is also highly beneficial for bone cells adhesion. The microhardness test revealed relatively acceptable mechanical properties for HT samples with a slightly decreasing trend after nanostructuring via the HT process. Finally, a significant mineralisation potential after 6 h HT was demonstrated, showing another great benefit of this fabrication process to improve the bioactivity of Ti-PEO treated implants. This new engineering approach for the fabrication of nanostructured surface with

tunable and mixed topography with hard and bioactive surfaces opens tremendous opportunities for creating advanced materials for industrial applications and particularly for developing new smart orthopaedic implants. Particularly, fabricated sharp nanostructures on the surface of titanium implants may demonstrate antimicrobial activity against various types of bacteria. Therefore, further biological and antibacterial studies are required to evaluate the successful application of these novel nanoblade structures in the orthopaedic field.

Acknowledgement:

The authors acknowledge the support from the University of Adelaide and the School of Chemical engineering and advanced materials. AM acknowledge the support from ARC grant-funded supplementary scholarship (ARC IH 150100003) and acknowledge the assistance of Dr Mohammadreza Barati and Dr Animesh Basak, and Dr Reza Ghomashchi for imaging and assistance during the fabrication and analysing process. Writers acknowledge in-kind support from IM CRC Australia.

References:

1. Kaur, M. and K. Singh, *Review on titanium and titanium based alloys as biomaterials for orthopaedic applications.* Materials Science and Engineering: C, 2019. **102**: p. 844-862.
2. Konstantinov, A.S., et al., *Ti-B-based composite materials: Properties, basic fabrication methods, and fields of application (review).* Composites Part A: Applied Science and Manufacturing, 2018. **108**: p. 79-88.
3. Rastin, H., et al., *3D bioprinting of cell-laden electroconductive MXene nanocomposite bioinks.* Nanoscale, 2020. **12**(30): p. 16069-16080.
4. Albrektsson, T. and A. Wennerberg, *The impact of oral implants-past and future, 1966-2042.* J Can Dent Assoc, 2005. **71**(5): p. 327.
5. Geetha, M., et al., *Ti based biomaterials, the ultimate choice for orthopaedic implants–a review.* Progress in materials science, 2009. **54**(3): p. 397-425.
6. Chen, Q. and G.A. Thouas, *Metallic implant biomaterials.* Materials Science and Engineering: R: Reports, 2015. **87**: p. 1-57.
7. Walsh, F., et al., *Plasma electrolytic oxidation (PEO) for production of anodised coatings on lightweight metal (Al, Mg, Ti) alloys.* Transactions of the IMF, 2009. **87**(3): p. 122-135.
8. Diamanti, M.V., B. Del Curto, and M. Pedeferri, *Anodic oxidation of titanium: from technical aspects to biomedical applications.* Journal of Applied Biomaterials and Biomechanics, 2011. **9**(1): p. 55-69.

9. Maher, S., et al., *Engineered titanium implants for localised drug delivery: recent advances and perspectives of Titania nanotubes arrays.* Expert opinion on drug delivery, 2018. **15**(10): p. 1021-1037.
10. Ledet, E.H., et al., *Smart implants in orthopedic surgery, improving patient outcomes: a review.* Innovation and entrepreneurship in health, 2018. **5**: p. 41-51.
11. Weszl, M., et al., *Investigation of the mechanical and chemical characteristics of nanotubular and nano-pitted anodic films on grade 2 titanium dental implant materials.* Materials Science and Engineering: C, 2017. **78**: p. 69-78.
12. Rupp, F., et al., *Enhancing surface free energy and hydrophilicity through chemical modification of microstructured titanium implant surfaces.* Journal of Biomedical Materials Research Part A: An Official Journal of The Society for Biomaterials, The Japanese Society for Biomaterials, and The Australian Society for Biomaterials and the Korean Society for Biomaterials, 2006. **76**(2): p. 323-334.
13. Sul, Y.-T., et al., *Characteristics of the surface oxides on turned and electrochemically oxidised pure titanium implants up to dielectric breakdown:: the oxide thickness, micropore configurations, surface roughness, crystal structure and chemical composition.* Biomaterials, 2002. **23**(2): p. 491-501.
14. Mazinani, A., et al., *Graphene oxide (GO) decorated on multi-structured porous titania fabricated by plasma electrolytic oxidation (PEO) for enhanced antibacterial performance.* Materials & Design, 2020: p. 109443.
15. Mu, W. and Y. Han, *Characterisation and properties of the MgF2/ZrO2 composite coatings on magnesium prepared by micro-arc oxidation.* Surface and Coatings Technology, 2008. **202**(17): p. 4278-4284.
16. Snizhko, L., et al., *Anodic processes in plasma electrolytic oxidation of aluminium in alkaline solutions.* Electrochimica Acta, 2004. **49**(13): p. 2085-2095.
17. Cochis, A., et al., *The effect of silver or gallium doped titanium against the multidrug resistant Acinetobacter baumannii.* Biomaterials, 2016. **80**(Supplement C): p. 80-95.
18. Yang, S., et al., *Hydrothermal treatment of Ti surface to enhance the formation of low crystalline hydroxyl carbonate apatite.* Biomaterials research, 2015. **19**: p. 4-4.
19. Abothu, I.R., et al. *Low-cost embedded capacitor technology with hydrothermal and sol-gel processes.* in *9th International Symposium on Advanced Packaging Materials: Processes, Properties and Interfaces (IEEE Cat. No.04TH8742). 2004 Proceedings.* 2004.
20. Zhang, Y., et al., *Effect of hydrothermal treatment on catalytic properties of PtSnNa/ZSM-5 catalyst for propane dehydrogenation.* Microporous and Mesoporous Materials, 2006. **96**(1): p. 245-254.
21. Tripathy, A., et al., *Natural and bioinspired nanostructured bactericidal surfaces.* Advances in Colloid and Interface Science, 2017. **248**: p. 85-104.
22. Abothu, I.R., et al. *Low-cost embedded capacitor technology with hydrothermal and sol-gel processes.* in *Advanced Packaging Materials: Processes, Properties and Interfaces, 2004. Proceedings. 9th International Symposium on*. 2004. IEEE.
23. Wong, C.L., Y.N. Tan, and A.R. Mohamed, *A review on the formation of titania nanotube photocatalysts by hydrothermal treatment.* Journal of Environmental Management, 2011. **92**(7): p. 1669-1680.
24. Yuan, Z.-Y. and B.-L. Su, *Titanium oxide nanotubes, nanofibers and nanowires.* Colloids and Surfaces A: Physicochemical and Engineering Aspects, 2004. **241**(1): p. 173-183.
25. Yuan, Z.-Y., W. Zhou, and B.-L. Su, *Hierarchical interlinked structure of titanium oxide nanofibers.* Chemical Communications, 2002(11): p. 1202-1203.
26. Yuan, X., et al., *Micro/nano hierarchical structured titanium treated by NH4OH/H2O2 for enhancing cell response.* PloS one, 2018. **13**(5): p. e0196366-e0196366.

27. Kim, C., et al., *Comparison of titanium soaked in 5 M NaOH or 5 M KOH solutions.* Materials science & engineering. C, Materials for biological applications, 2013. **33**(1): p. 327-339.
28. Hsu, H.-C., et al., *Surface modification of commercially pure ti treated with aqueous naoh treatment and ethyl alcohol aging.* J. Med. Biol. Eng, 2013. **33**: p. 331-336.
29. Tsimbouri, P.M., et al., *Osteogenic and bactericidal surfaces from hydrothermal titania nanowires on titanium substrates.* Scientific Reports, 2016. **6**: p. 36857.
30. Zhao, G.-l., et al., *Effect of alkali treatments on apatite formation of microarc-oxidized coating on titanium alloy surface.* Transactions of Nonferrous Metals Society of China, 2015. **25**(4): p. 1151-1157.
31. Wei, D., et al., *Characteristic and in vitro bioactivity of a microarc-oxidized TiO2-based coating after chemical treatment.* Acta Biomaterialia, 2007. **3**(5): p. 817-827.
32. Bhadra, C.M., et al., *Antibacterial titanium nano-patterned arrays inspired by dragonfly wings.* Scientific Reports, 2015. **5**: p. 16817.
33. Gittens, R.A., et al., *The effects of combined micron-/submicron-scale surface roughness and nanoscale features on cell proliferation and differentiation.* Biomaterials, 2011. **32**(13): p. 3395-3403.
34. Gao, Y., et al., *Effects of microrough and hierarchical hybrid micro/nanorough surface implants on osseointegration in ovariectomised rats: A longitudinal in vivo microcomputed tomography evaluation.* Journal of Biomedical Materials Research Part A, 2012. **100A**(8): p. 2159-2167.
35. Xie, Y., et al., *Enhanced cellular responses to titanium coating with hierarchical hybrid structure.* Materials Science and Engineering: C, 2014. **38**(Supplement C): p. 272-277.
36. Gongadze, E., et al., *Adhesion of osteoblasts to a nanorough titanium implant surface.* International Journal of Nanomedicine, 2011. **6**: p. 1801-1816.
37. Yeo, I.-S.L., *Modifications of Dental Implant Surfaces at the Micro- and Nano-Level for Enhanced Osseointegration.* 2020. **13**(1): p. 89.
38. Maher, S., et al., *Engineering of Micro- to Nanostructured 3D-Printed Drug-Releasing Titanium Implants for Enhanced Osseointegration and Localized Delivery of Anticancer Drugs.* ACS Applied Materials & Interfaces, 2017. **9**(35): p. 29562-29570.
39. Xiu, P., et al., *Hierarchical Micropore/Nanorod Apatite Hybrids In-Situ Grown from 3-D Printed Macroporous Ti6Al4V Implants with Improved Bioactivity and Osseointegration.* Journal of Materials Science & Technology, 2017. **33**(2): p. 179-186.
40. Huang, Q., et al., *A novel titania/calcium silicate hydrate hierarchical coating on titanium.* Colloids and Surfaces B: Biointerfaces, 2015. **134**: p. 169-177.
41. Song, H.-J., et al., *Fabrication of hydroxyapatite and TiO2 nanorods on microarc-oxidized titanium surface using hydrothermal treatment.* Applied Surface Science, 2010. **256**(23): p. 7056-7061.
42. Lugovskoy, A. and S. Lugovskoy, *Production of hydroxyapatite layers on the plasma electrolytically oxidised surface of titanium alloys.* Materials Science and Engineering: C, 2014. **43**: p. 527-532.
43. Ko, S.-H., et al., *Characterisations of Ca- and Mg-incorporating micro/nanostructured surfaces on titanium fabricated by microarc oxidation and hydrothermal treatments.* Journal of Physics and Chemistry of Solids, 2015. **87**: p. 147-152.
44. Du, Q., et al., *The hydrothermal treated Zn-incorporated titania based microarc oxidation coating: Surface characteristics, apatite-inducing ability and antibacterial ability.* Surface and Coatings Technology, 2018. **352**: p. 489-500.
45. Ma, F.C., et al., *Various Morphologies Hydroxyapatite Crystals on Ti MAO Film Prepared by Hydrothermal Treatment.* Physics Procedia, 2013. **50**: p. 442-448.
46. Suchanek, K., et al., *Ammonium Hydroxide Mediated Hydrothermal Crystallization of Hydroxyapatite Coatings on Titanium Substrate.* Ceramics, 2019. **2**(1): p. 180-189.

47. Parcharoen, Y., P. Termsuksawad, and S. Sirivisoot, *Improved Bonding Strength of Hydroxyapatite on Titanium Dioxide Nanotube Arrays following Alkaline Pretreatment for Orthopedic Implants.* Journal of Nanomaterials, 2016. **2016**: p. 13.
48. Duan, Y., et al., *The effect of adhesive strength of hydroxyapatite coating on the stability of hydroxyapatite-coated prostheses in vivo at the early stage of implantation.* Archives of medical science : AMS, 2012. **8**(2): p. 199-208.
49. Lin, D.-J., et al., *Rapid nanoscale surface modification on micro-arc oxidation coated titanium by microwave-assisted hydrothermal process.* Materials Science and Engineering: C, 2019. **95**: p. 236-247.
50. Diu, T., et al., *Cicada-inspired cell-instructive nanopatterned arrays.* Scientific reports, 2014. **4**: p. 7122.
51. Mishra, A., et al., *Study of Mechanical and Tribological Properties of Nanomica Dispersed Hydroxyapatite Based Composites for Biomedical Applications.* Advances in Materials Science and Engineering, 2017. **2017**: p. 9814624.
52. Dong, M., L. Liu, and S. Zhang, *Nanostructural Biomaterials and Applications.* Journal of Nanomaterials, 2016. **2016**: p. 5903201.
53. Kokubo, T. and H. Takadama, *How useful is SBF in predicting in vivo bone bioactivity?* Biomaterials, 2006. **27**(15): p. 2907-15.
54. Kuromoto, N.K., R.A. Simão, and G.A. Soares, *Titanium oxide films produced on commercially pure titanium by anodic oxidation with different voltages.* Materials Characterisation, 2007. **58**(2): p. 114-121.
55. Galvis, O.A., et al., *Formation of grooved and porous coatings on titanium by plasma electrolytic oxidation in H2SO4/H3PO4 electrolytes and effects of coating morphology on adhesive bonding.* Surface and Coatings Technology, 2015. **269**: p. 238-249.
56. Anitha, V., et al., *Morphology-dependent low macroscopic field emission properties of titania/titanate nanorods synthesised by alkali-controlled hydrothermal treatment of a metallic Ti surface.* Nanotechnology, 2015. **26**(35): p. 355705.
57. Jaggessar, A. and P.K.D.V. Yarlagadda, *Modelling the growth of hydrothermally synthesised bactericidal nanostructures, as a function of processing conditions.* Materials Science and Engineering: C, 2020. **108**: p. 110434.
58. Kawashita, M., et al., *Bonelike Apatite Formation on Anodically Oxidized Titanium Metal in Simulated Body Fluid*, in *Key Engineering Materials*. 2004. p. 459-462.
59. Polo, T.O.B., et al., *Plasma Electrolytic Oxidation as a Feasible Surface Treatment for Biomedical Applications: an in vivo study.* Scientific Reports, 2020. **10**(1): p. 10000.
60. Hasan, J., S. Jain, and K. Chatterjee, *Nanoscale Topography on Black Titanium Imparts Multi-biofunctional Properties for Orthopedic Applications.* Scientific Reports, 2017. **7**: p. 41118.
61. Sjöström, T., A.H. Nobbs, and B. Su, *Bactericidal nanospike surfaces via thermal oxidation of Ti alloy substrates.* Materials Letters, 2016. **167**: p. 22-26.
62. Uchida, M., et al., *Structural dependence of apatite formation on titania gels in a simulated body fluid.* Journal of Biomedical Materials Research Part A: An Official Journal of The Society for Biomaterials, The Japanese Society for Biomaterials, and The Australian Society for Biomaterials and the Korean Society for Biomaterials, 2003. **64**(1): p. 164-170.
63. Marin, E., et al., *Effect of etching on the composition and structure of anodic spark deposition films on titanium.* Materials & Design, 2016. **108**(Supplement C): p. 77-85.
64. Rupp, F., et al., *Enhancing surface free energy and hydrophilicity through chemical modification of microstructured titanium implant surfaces.* J Biomed Mater Res A, 2006. **76**(2): p. 323-34.
65. Hook, A.L., et al., *Combinatorial discovery of polymers resistant to bacterial attachment.* Nat Biotechnol, 2012. **30**(9): p. 868-875.
66. Merian, T. and J.M. Goddard, *Advances in nonfouling materials: perspectives for the food industry.* J Agric Food Chem, 2012. **60**(12): p. 2943-57.

67. haghbin nazarpak, M., et al., *Effect of Gamma Irradiation on Structural and Biological Properties of a PLGA-PEG-Hydroxyapatite Composite.* The Scientific World Journal, 2014. **2014**.
68. Nahum, E. and S. Lugovskoy, *A Comparative Study of Hydroxyapatite Coating Produced with Plasma Electrolytic Oxidation and Hydrothermal Treatment on Titanium Alloys: Ti6Al4V and Ti6Al7Nb for Dental Implants.* 2018.
69. Zhao, G.L., et al., *Structure and apatite induction of a microarc-oxidized coating on a biomedical titanium alloy.* Applied Surface Science, 2010. **257**(5): p. 1762-1768.

Chapter 5

Towards optimal fabrication of antibacterial titania nanostructures: A combined approach of plasma electrolytic oxidation and hydrothermal treatment (HT)

In this chapter, the potential application of two generic (acidic and basic Ca-free) PEO electrolytes on the formation of antibacterial titania nanostructures with post HT were investigated. The nanostructures formed on the acidic PEO substrates after HT showed faster nucleation and growth compared to the basic PEO treated samples. Fabricated nanostructures in both acidic and basic groups demonstrated high antibacterial activity against E.coli bacteria. The candidate group (acidic PEO group) also showed exceptional antibacterial activity with 99% efficiency against S. aureus, making the proposed approach favourable for the fabrication of the next generation of titanium antibacterial implants.

This chapter has been provided in the manuscript style under a Confidentiality Agreement .

Arash Mazinani, Md Julker Nine, Hadi Rastin, Roberto Chiesa, Gabriele Candiani, Paolo Tarsini, Dusan Losic, Towards optimal fabrication of antibacterial titania nanostructures: A combined approach of plasma electrolytic oxidation and hydrothermal treatment.

Statement of Authorship

Title of Paper	Towards optimal fabrication of antibacterial titania nanostructures via advanced mechano- bactericidal PEO surface
Publication Status	☐ Published ☐ Accepted for Publication ☐ Submitted for Publication ☑ Unpublished and Unsubmitted work written in manuscript style
Publication Details	Arash Mazinani, Md Julker Nine, Hadi Rastin, Roberto Chiesa, Gabriele Candiani, Paolo Tarsini, Dusan Losic.

Principal Author

Name of Principal Author (Candidate)	Arash Mazinani
Contribution to the Paper	Conceptualization,Structure of Manuscript,Original draft
Overall percentage (%)	70
Certification:	This paper reports on original research I conducted during the period of my Higher Degree by Research candidature and is not subject to any obligations or contractual agreements with a third party that would constrain its inclusion in this thesis. I am the primary author of this paper.
Signature	Date 24.05.2021

Co-Author Contributions

By signing the Statement of Authorship, each author certifies that:

i. the candidate's stated contribution to the publication is accurate (as detailed above);
ii. permission is granted for the candidate in include the publication in the thesis; and
iii. the sum of all co-author contributions is equal to 100% less the candidate's stated contribution.

Name of Co-Author	Prof Dusan Losic
Contribution to the Paper	Conceptualization,resources, funding acquization,review, editing, supervision, submission
Signature	Date 24 May 2021

Name of Co-Author	Dr Md Julker Nine
Contribution to the Paper	selected investigation, editing and review, supervision
Signature	Date 24/05/2021

Please cut and paste additional co-author panels here as required.

Name of Co-Author	Hadi Rastin		
Contribution to the Paper	selected investigation, editing and review		
Signature		Date	25/05/2021

Name of Co-Author	Roberto Chiesa		
Contribution to the Paper	selected investigation, editing and review		
Signature		Date	18/05/2021

Name of Co-Author	Gabriele Candiani		
Contribution to the Paper	selected investigation, editing and review		
Signature		Date	18/05/2021

Please cut and paste additional co-author panels here as required.

Name of Co-Author	Paolo Tarsini		
Contribution to the Paper	selected investigation, editing and review		
Signature		Date	18.05.2021

Towards optimal fabrication of antibacterial titania nanostructures: A combined approach of plasma electrolytic oxidation and hydrothermal treatment

Arash Mazinani[1,2], Md Julker Nine[1,2], Hadi Rastin[1,2], Roberto Chiesa[3], Gabriele Candiani[3], Paolo Tarsini[3], Dusan Losic[1,2]*

[1]School of Chemical Engineering and Advanced Materials, The University of Adelaide, Adelaide, SA 5005, Australia

[2]ARC Hub for Graphene Enabled Industry Transformation, The University of Adelaide, Adelaide, SA 5005, Australia

[3]Department of Chemistry, Materials and Chemical Engineering "G. Natta", Politecnico di Milano, Via Mancinelli 7, 20131 Milano, Italy

*Corresponding Author: Prof. Dusan Losic,
email: dusan.losic@adelaide.edu.au

Abstract:

The plasma electrolytic oxidation (PEO) technique is a well-established electrochemical method to make highly durable and biocompatible titania layers that can be used for surface modifications of medical metal implants for improving their cellular adhesion and viability. Implants. However, the effect of PEO electrolytes on the formation and growth of nanostructures with mechano-bactericidal properties has not been thoroughly investigated. The work reports the successful fabrication of tuneable titania nanostructures on titanium PEO surface treated by the combination of PEO and hydrothermal (HT) process. Two generic PEO electrolytes (i.e. acidic and basic) have been explored to determine their impact on the formation of nanostructures with different morphologies and dimensions. Interestingly, the elimination of calcium from the PEO electrolyte during the PEO process led to the formation of sodium titanate nanostructures in the forms of nano-blades, nano-needles, and micro-nano belts by HT process using different times. While the HT process on the PEO surfaces fabricated in the acidic electrolyte created nanostructures with similar morphologies but with a significantly faster formation and growth rate compared to the basic electrolyte. All HT treated PEO samples demonstrated very high mineralisation ability. Moreover, the nanostructures created using HT on the acidic PEO process showed better antimicrobial activity with 88% decrease in the number of *E.coli* colonies compared to 68% prepared using PEO basic electrolyte. Therefore, further antibacterial analysis carried out on the nanostructures formed

on the acidic group as a candidate sample which revealed superior antibacterial activity against *S. aureus* with ~ 99% colonies reduction after 24 h incubation. These findings on the effect of acidic and basic electrolyte in nanostructure formation and their antibacterial efficiency will provide a valuable contribution to using PEO technology to fabricate the next generation of medical implants with advanced antimicrobial and bio integration abilities.

Keywords: Titanium implants**,** Antibacterial surfaces, Plasma electrolytic oxidation, Titania nanostructures, Hydrothermal treatment, Mechanobactericidal.

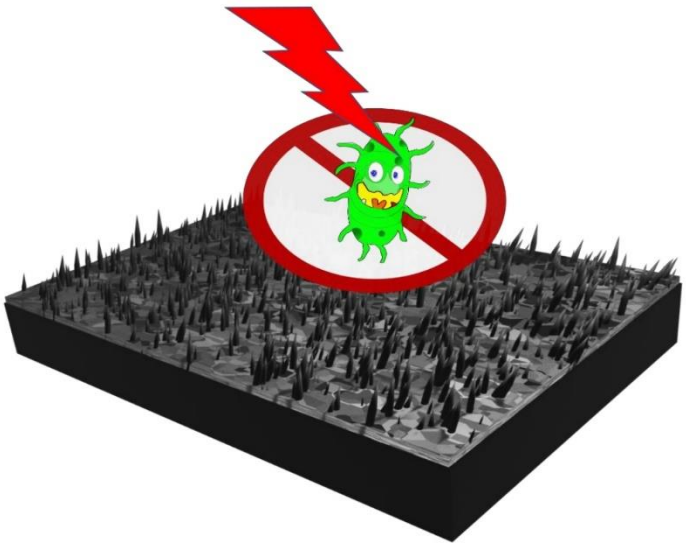

Introduction

Titanium is one of the most popular metals for the fabrication of biomedical implants worldwide. This valve metal is known for its excellent biocompatibility, corrosion resistance and low specific weight compared with other available metals (such as CrCo, Stainless steel etc.) in the biomedical field[1]. Nevertheless, it does not show any antibacterial properties itself and fail to resolve the poor integration problem of implants with bone tissue, which may increase the chance of aseptic loosening and eventually lead to implant failure [2]. It is worth mentioning that implant failure usually requires revision surgery, which would create substantial health and economic burden with distressing impact on patients [3-6]. In order to improve the integration ability of biomedical surface, different methods such as roughening with grit blasting, machining or acid etching, plasma spray coating with hydroxyapatite (HAP), ion implantation, etc., have been introduced [7-9]. One of the popular techniques for the surface modification of titanium materials providing extremely hard and durable porous titania surface is called plasma electrolytic oxidation (PEO), also known as the micro arc oxidation (MAO) technique, initially established in the industry as the advanced anodic oxidation techniques. This method involves the application of high voltage for the generation of micro arcs and the subsequent local meltdown of titanium samples in the specific electrolytes, resulting in the formation of thousands of micro nanopores on the metallic surface with the ability to improve bone-cell integration through the ingrowth of bone tissue [10-13]. The advantages of the PEO process are recognised for medical titanium implants application, with many studies showing that PEO surfaces exhibited notable improvement in implants' osseointegration ability[14-16].

To improve PEO-modified implants' performance, the PEO technique is successfully combined with other surface modification methods such as hydrothermal treatment (HT) to generate hydroxyapatite (HAP), improve the bioactivity and corrosion resistance of the final surface[17, 18]. Although HAP formation has been considered essential for bone-implant integration, it contains Ca–P layers, which are infamous for high brittleness and low adhesion to Ti substrate [19, 20]. Moreover, common HAP does not show high antimicrobial activity, which limits its further application. Therefore, it is usually required to be combined with different antibacterial agents such as silver or copper nanoparticles to address its low antibacterial activity issue [21, 22]. This may add to the complication due to the biosafety and cytotoxicity problems associated with nanoparticles released in the body [23-26].

For these reasons, recent studies are shifting toward different approaches to tackle infection problems of Ti medical implants and simultaneously advance both their antibacterial and bio integration performance. The formation of tunable nanostructures on the implant surface is one of the novel approaches, targeting multidrug resistance pathogens infection, which has become one of the critical subjects for global public health [27-30]. This so-called mechano-bactericidal approach is associated with the nano-structured surface killing efficacy through direct contact with bacteria. Bacterial elimination can occur through various mechanisms such as piercing, rupture and elastic pillar deformations[31]. The mechano-bactericidal approach, compared to the usual chemical-based tactics, is highly sustainable, acts locally with minimised damage to the surrounding tissues and doesn't require replenishing of antibacterial agents [31, 32]. In nature, the mechano-bactericidal effect first observed on P. claripennis Cicada wing. Ivanova et al. [32] have further investigated the bactericidal efficacy of nano-pillar structures on cicada wing on the inhibition of biofilm formation. Hasan et al. [33] observed that the nano-pillar morphology over the cicada wing is mainly efficient against gram-negative bacteria such as *E.coli* with thinner peptidoglycan layers rather than gram-positive ones such as *S. aureus.* Therefore, they concluded that bacteria cell size and membrane wall thickness might affect the bactericidal efficiency of the nano-structured surface.

Recent studies have shown the possible formation of titania nanostructures with nano-wires, nano-spikes and nano-pillars morphologies over Ti and Ti-based alloys by different techniques such as hydrothermal etching, anodisation, thermal oxidation, etc.[34]. Particularly, HT as a simple and inexpensive fabrication method has been widely used to form and develop nanostructures on Ti-based material with the ability to kill bacteria [35, 36]. Although significant attention has been paid to titanium alloys as a substrate for titania nanostructures growth in the HT system, the PEO treated Ti surface (which intrinsically has shown great potential for osseointegration improvement) has not been thoroughly investigated. Our preliminary studies showed the successful possibility of engineering titania nanostructures on PEO substrate through the HT treatment process. In the proposed method, by eliminating Ca from the PEO electrolyte, the formation of HAP on the surface was inhibited. Alternatively, this technique opened a door for constructing titania nanostructures with high controllability, which is hypostasized to simultaneously address both osseointegration and antibacterial properties.

In the present work, the critical parameters such as the initial PEO electrolyte chemical composition (acid and basic) and HT Time (1 to 24 hours) on the formation and growth of the

nanostructures are investigated. The fabricated structures by the combined PEO-HT method using different conditions were characterised using several techniques, including SEM, FIB, Raman spectroscopy, XRD spectroscopy and wettability test to explore their morphology, shape, chemical composition and other physicochemical properties. Finally, their bioactivity and antimicrobial properties against several bacterial strains such as (*E. coli* and *S. aureus)* were evaluated to provide more insight on the impact of shape and size of these nanostructures on their antibacterial performance. These findings are showing the effect of acidic and basic PEO electrolytes on nanostructure formation and their antibacterial efficiency, which provide a valuable contribution toward the development of the next generation of medical implants with antimicrobial and bio-integration properties.

2. EXPERIMENTAL SECTION

2.1. Materials

Ti-sheets with 1 mm thickness and 99.9 % purity were obtained from Nilaco (Japan); 85 wt% orthophosphoric acid (H_3PO_4), potassium hydroxide (KOH) pellet and sodium hydroxide (NaOH) pellets were obtained from Chem Supply (South Australia), used as received without any further purification, Sodium metasilicate pentahydrate $Na_2SiO_3 \cdot 5H_2O$ was obtained from Sigma-Aldrich Pty Ltd., pure Milli-Q water (EMD Millipore Corporation, Billerica machine) with 18.2 MΩcm resistivity was used wherever applicable.

2.1. Plasma electrolytic oxidation (PEO) treatments of Ti-strips

Ti sheets were cut to a specific size of 2 cm × 1.5 cm. Then were cleaned by soaking in acetone in a sonication bath for 10 min followed by washing with DI water. Cleaned samples were kept in the electric oven for three h at 50 °C. The programmable DC power supply (N5752A, Agilent Technologies, USA) was employed for the PEO treatment. The corresponding voltage-time response was recorded by LabVIEW software, connected to the anodisation set-up. A single step PEO process was carried out based on previous research protocols described by Kuromoto [37] under the galvanostatic condition with a fixed current density of 50 mA/cm^2 for 1 min. The distance between the working electrode (Ti-strip) and

counter electrode (Ti cylindrical mesh) was 4.5 cm. For the acidic PEO treatment, an acidic electrolyte [37] containing 1.4 M H_3PO_4 was used. The Ti-samples were treated in the acidic solution were donated as "acidic PEO" samples. In contrast, the basic PEO treatment was conducted in the basic solution containing potassium hydroxide, sodium metasilicate pentahydrate and orthophosphoric acid, according to a protocol described by Aliasghari et al.[38]. The recorded pH for acidic and basic solutions were 1.1 and 12, respectively. The final PEO treated samples in the basic solution were denoted as "basic PEO" samples. Finally, samples were washed in DI water and dried in the electric oven at 50 °C.

2.2. Hydrothermal treatment of PEO treated samples

In the next stage, both acidic and basic PEO samples underwent hydrothermal treatment (HT) for different durations of 1, 2, 4, 6, 8, 12 and 24 h in a 100 ml reactor filled with 1 M NaOH solution at ~150 °C, as described by Jaggessar et al. [35] and Anitha et al.[39]. HT treated samples then were soaked in DI water to remove any residual impurities from their surfaces. Afterwards, samples were dried in the electric oven at 50 °C for 2 h.

2.3. Labelling system of samples based on PEO types and HT conditions

Table 1 presents the labelling system based on the PEO types and HT conditions of each sample.

6

Table 1. PEO treatment and hydrothermal treatment conditions.

Sample name	PEO type	HT Reaction time (Hrs)	HT Reaction temperature (°C)
A-PEO	Acidic	0	-
A-HT_{1h}	Acidic	1	150
A-HT_{2h}	Acidic	2	150
A-HT_{4h}	Acidic	4	150
A-HT_{6h}	Acidic	6	150
A-HT_{8h}	Acidic	8	150
A-HT_{12h}	Acidic	12	150
A-HT_{24h}	Acidic	24	150
B-PEO	Basic	0	-
B-HT_{1h}	Basic	1	150
B-HT_{2h}	Basic	2	150
B-HT_{4h}	Basic	4	150
B-HT_{6h}	Basic	6	150
B-HT_{8h}	Basic	8	150
B-HT_{12h}	Basic	12	150
B-HT_{24h}	Basic	24	150

2.4. The procedure of the Bio-mineralization test

The biomineralisation test was conducted by immersion of samples in 50 ml of SBF solution for 21 days. The SBF solution was produced according to Kokubo and Takadama provided protocol [40]. Polyethylene containers filled with SBF solution refreshed every day to keep ion concentration at a suitable level sufficient for biomineralisation. After 21 days, samples were removed from containers and dried at ambient temperature for one day.

2.5. Antibacterial assay

The antibacterial assay was performed according to ISO 22916:2011 against *E. coli* (gram-negative, DSM 3423) and *S. aureus* (gram-positive, DSM 346) bacteria. Briefly, cultured bacteria diluted to the 6 x 105 Colony Forming Unit (CFU)/mL concentration. In the next step, samples were disinfected via UV exposure for 20 min per side and inoculated with 12.6 µL of cultured bacteria. Polypropylene coverslips (8 mm in diameter) were placed on the top of the test inoculum to achieve a homogeneous bacteria layer. Samples in direct contact with bacteria were incubated at 37°C for 24 h in an incubator. Bacteria then removed from samples diluted and placed on an agar plate and incubated overnight in an incubator at 37°C. CFUs were counted, and results were compared with control titanium samples.

3. Characterisations

Morphological characterisation of the PEO treated Ti substrates carried out via SEM Quanta 450 (Eindhoven) equipped with EDS analysis, while for high-resolution imaging and investigation of nanostructure formation, FIB-SEM (Focused Ion Beam Scanning Electron Microscope FEI Helios Nanolab 600, USA) was utilised after HT process. Raman measurements were performed by (WITEC Alpha300) at room temperature with the wavelength in the range of 0-2000 cm^{-1} and a 532 nm laser beam as the excitation source to analyse the oxide layer before and after HT. XRD spectra analysis was carried out using Rigaku MiniFlex 600, with the standard operating condition of (40 kV, $2\theta = 3–80$ with a scan rate of 2.5) to analyse the oxide layer structural evolutions. Contact angles of water drops over the fabricated samples were calculated using the sessile drop method via optical-tensiometers model T301 – ATA scientific pty ltd with a droplet size of 2.2 ± 0.1 µL.

3.1. Statistical analysis

Samples were tested at least three times, and corresponding generated data were given means standard deviations. Moreover, samples were analysed utilising GraphPad version 6 software (GraphPad Software, La Jolla, CA). Statistical comparison among groups was carried out via one-way analysis of variance (ANOVA) (multiple comparisons) with post hoc Tukey's test to indicate significant differences between experimental groups. Differences were considered statistically significant when $P < 0.05$.

4. Results and discussions

4.1. Morphological characterisation of PEO surfaces using acidic and basic electrolytes

Our previous studies revealed that a single step PEO treatment for 1 min at 50 mA/cm^2 is the optimised time and current density to fabricate the desired morphology of micro-nano pores, which can entirely cover the Ti surface and improve the osseointegration. Therefore, similar conditions were applied in the current study [13]. Typical voltage-time graph during PEO treatments in the acidic and basic electrolytes generated by LabVIEW software are presented in **figure 1**. Cell voltage values during the acidic PEO treatment was following an increasing trend initially and then reached a stable value at ~ 200 V. Breakdown voltage of ~ 170 V was recorded after 10 seconds of the acidic PEO process, evident from the generation of sparks starting from the edge of the sample and covered the surface after few seconds. Unlike acidic PEO, the basic PEO process followed an increasing trend for the whole period of the anodisation process and reached the final cell voltage of ~ 400 V after 1min. Here, the breakdown voltage of 310 V was recorded after 40 sec following the generation of arcs and acoustic emission. In general, the observed arcs during the basic PEO process were brighter than the acidic PEO treatment, which can be attributed to the discharge at a higher final voltage during basic PEO treatment.

The SEM images of samples after 1 min PEO treatment using acidic and basic electrolyte are shown in **Figures 1b** and **1c**. The appearance of the oxide layer for the acidic PEO treatment (**Fig. 1b**) was comparatively flat, and the oxide mainly consisted of pores with size ranging from 120 nm to around 1 µm and few worm-like morphologies with an average spacing of 1.60 µm (between bigger pores), which were homogeneously distributed along with the oxide layer. This observed morphology is similar to the previous reports by Kuromoto et al.[37] and Kawashita et al.[41] conducted through potensiostatic PEO process at 180 V. Pores density of 3 per 1 µm^2 of area for acidic PEO sample was calculated using Image J software.

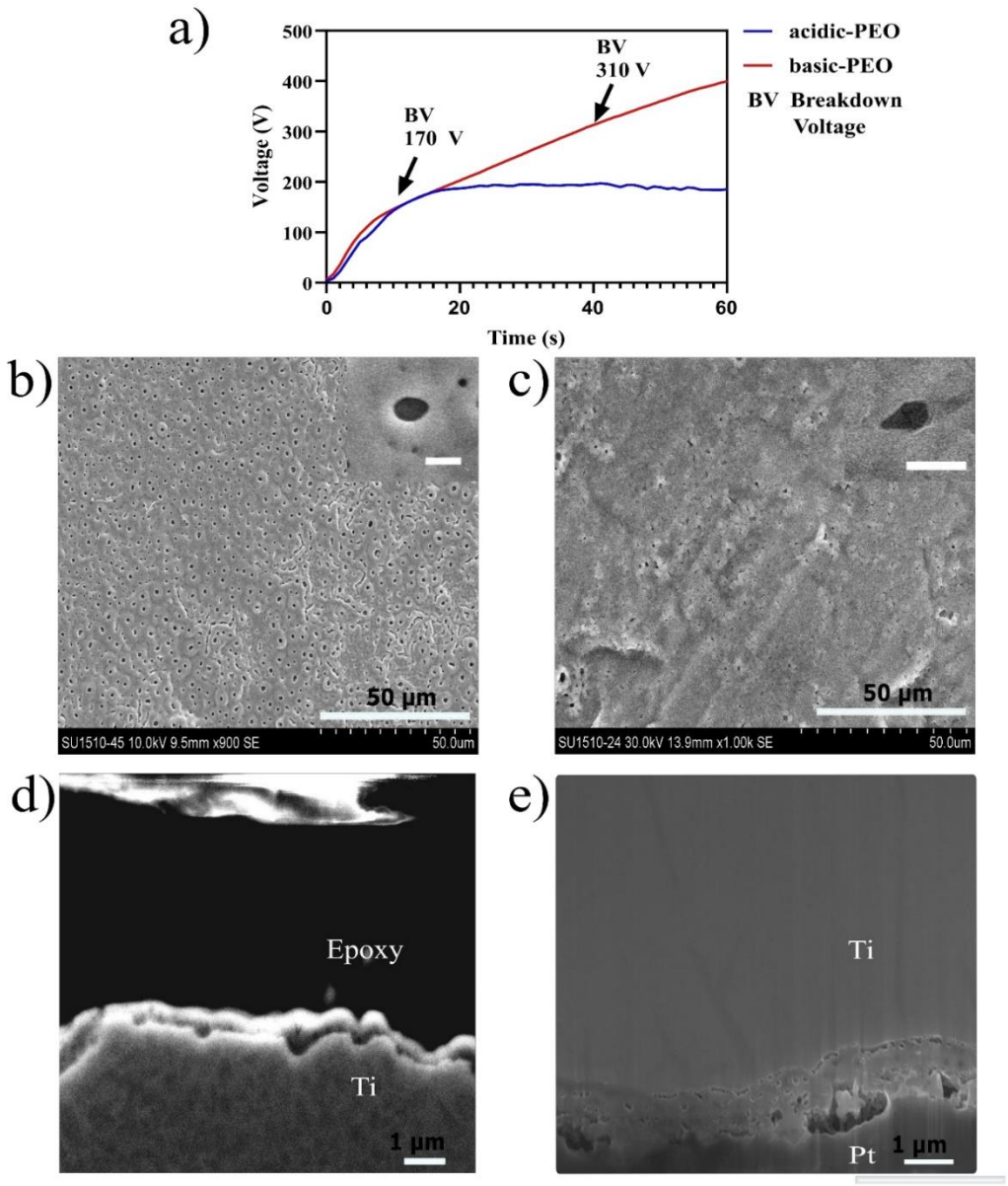

Figure 1. a) Voltage-Time graph generated during acidic and basic PEO processes, b) SEM image of PEO titania surface after 1 min in the acidic solution (inset, scale bars: 1 µm), c) SEM image of PEO titania surface after 1 min in the basic solution (inset, scale bars: 1 µm), d) cross-section image of acidic PEO, e) cross-section image of basic PEO.

10

On the contrary, the basic PEO treatment didn't demonstrate high flatness compared with acidic PEO surface; it showed the similar pores morphology with pore size ranging from 100 nm to 1 µm with an average spacing of 1.62 µm (between bigger pores). There were a few crater-like morphologies found homogeneously distributed along the surface. An average pore density of 4 per 1 μm^2 area was calculated for the basic PEO surface. Cross-section analysis presented in **Figures 1d** and **1e** showed the average oxide thickness of around 800 nm for basic PEO surface and approximately 530 nm for acidic PEO substrate after 1 min PEO treatment.

4.2. Characterisation of formed nanostructures on PEO surfaces using hydrothermal process (HT)

The FIB-SEM images of nanostructures generated on the acidic PEO and basic PEO surfaces by HT are depicted in **Fig. 2.** The process started with the formation of tiny nanostructures over the PEO substrate. These nanostructures then merged to form nano roots (with less than 100 nm height) during the first hour of HT (A-HT_{1h}). These nanoroots then grew vertically to form nanoblade structures, strongly evident after 2 h (A-HT_{2h}) with 200 nm height. The nanoblade structures continued to grow to more than 1000 nm after 6 h of HT (A-HT_{6h}). Moreover, some nano-needle type structures were simultaneously present on HT treated acidic PEO surface after 6 h, growing up to more than 800 nm. After increasing the HT duration to 8 h (A-HT_{8h}), most nano-blade structures are transformed to nano-blade/nano-belts type morphologies while getting bent and entangled. This nano-belt length can reach up to 3 microns after 24 h (A-HT_{24h}) while getting merged to form a grass-like morphology.

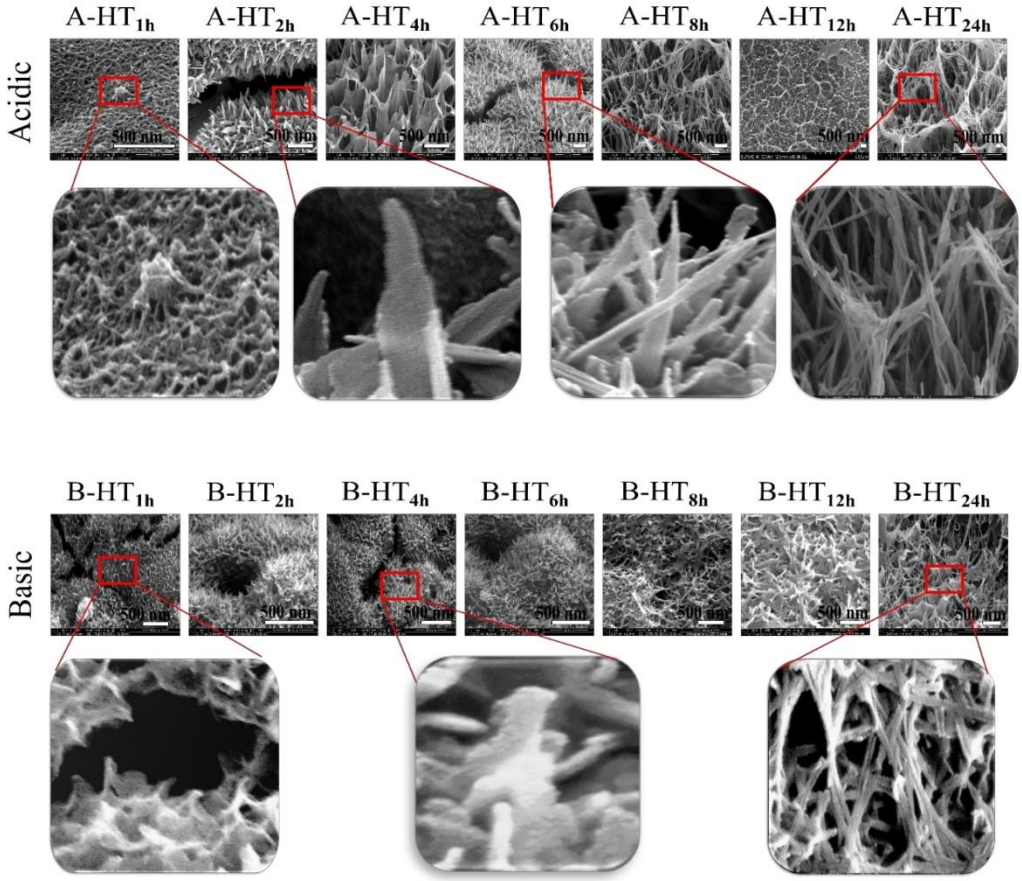

Figure 2. A summary of typical morphology of generated nanostructures on PEO surface (acidic and basic electrolyte) using HT process in NaOH 1 M for 1 to 24 hours.

For the basic PEO samples, the nano-root formation process starts within the first hour of HT (B-HT_{1h}), while the nano-roots' height can reach 60 nm. Nano-blades structures were evident after 2 h of HT (B-HT_{2h}), which continue to grow to 180 nm by 6 h HT (B-HT_{6h}). After 8 h (B-HT_{8h}), entangled nano-belts were the dominant morphology over the surface (with around 1550 nm length). Further HT to 24 h (B-HT_{24h}) led to the formation of disordered micro-nano structures, while the surface is still predominantly covered with elongated nano-belts with length up to 600 nm. **Fig. 3** summarises the average nanostructure height/length in each HT

duration stage for acidic and basic PEO samples, measured by Image J software from at least 15 tallest nanostructures. A lower growth speed of titania nanostructures on basic PEO surface was also reported in a previous study[42], which used a Ca-based solution for the PEO process. However, the different HT and PEO solutions selection led to the formation of smaller nano-needle and nano-leaves structures instead of titania nano-blade in their experiments.

As it is evident from the SEM-FIB images, 4 h and 6 h hydrothermally treated samples on both acidic and basic PEO substrates demonstrate the tallest upright-oriented nanostructures, which are assumed to damage bacteria membrane and eventually kill bacteria mechanically. Therefore, further investigation was mainly focused on these optimised durations. In a recent research conducted to evaluate HT's effect on the growth of nanostructures on Ti alloy, a similar average length of 260 nm has been reported after 3 h HT at 145 °C [35]. However, observed nanostructures are mainly in the form of nano-pillars, which are different from nano-blade structures obtained in this work for a similar HT duration applied on acidic PEO substrates (A-HT_{2h} and A-HT_{4h}). Moreover, the basic PEO surface that underwent HT treatment demonstrated much lower nanostructures growth speed than Ti alloy substrate. More importantly, many of the micropores generated by the PEO process were still observable even after 6 h of HT on the acidic PEO substrate (A-HT_{6h}) and after 12 h (B-HT_{12h}) on the basic PEO substrate (supplementary section **Fig. S1**), which can significantly contribute to the osseointegration improvement.

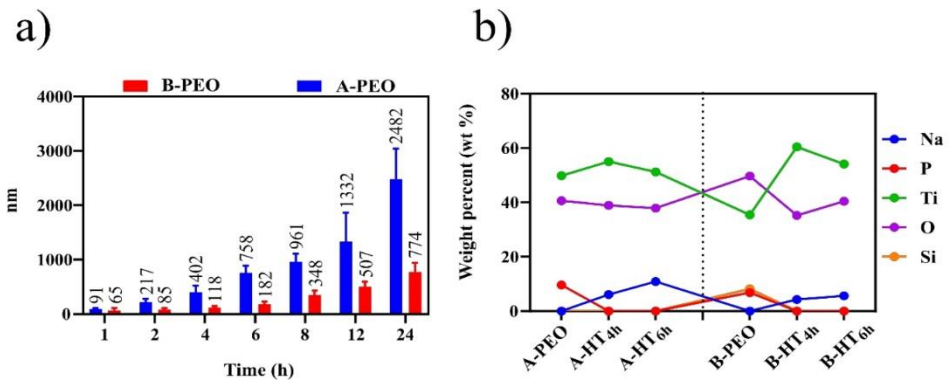

Figure 3. a) Comparative average height of titania nanostructures formed on acidic and basic PEO substrates at different HT durations, b) Corresponding EDS results b of samples at different HT durations.

The size analysis comparison of nanostructures height at different HT interval is presented in **Fig. 3a**. For the optimised samples of A-HT_{4h} and A-HT_{6h} on acidic PEO surface, the average height of ~ 402nm and ~ 758nm were achievable, respectively, whereas for the optimised samples of B-HT_{4h} and B-HT_{6h} on basic PEO surface measured average heights were ~118 nm and ~182 nm correspondingly.

The chemical composition (in weight percentage, wt.%) of optimised samples at different HT duration is depicted in **Fig. 3b**. The initial acidic PEO oxide layer contains Ti and O with the addition of P, while Si in the basic PEO oxide layer is also evident. Therefore, less Ti is available on the basic PEO oxide layer compared to the acidic PEO surface. After HT treatments, titania nanostructures are formed on both acidic and basic PEO substrates. EDS analysis shows these nanostructures are comprised of Ti, O and Na. By continuing the HT treatment to 6 h, more level of Na is added to the nanostructures for both acidic and basic samples, while the level of Na in nanostructures formed on acidic PEO surface is almost 2 times higher than the basic PEO surface after 6 h HT. As previously mentioned, the growth rate of nanostructures on the acidic PEO surface is much quicker than basic PEO ones, particularly at optimised HT duration of 4 h and 6 h can be around 4 times faster. The observed growth behaviour can be justified by the presence of more Ti in the acidic PEO surface compared to the basic PEO surface that undergoes localised etching in NaOH and dissolved in HT solution. It is assumed that the released Ti on the HT solution is then added to the nucleation sites and leads to the formation and growth of different nanostructures.

XRD spectra of acidic and basic PEO substrates before and after HT for 4 h and 6 h are provided in **Fig. 4a**. For all specimen, titanium peaks were in accordance with the standard JCPDS card, no. 65-3362, while the presence of anatase phase was evident by the formation of diffraction peaks at 2θ values of 25.8° and 48.5°, belong to the reflection of the (101) and (200) planes of the standard anatase phase (JCPDS card No. 21-1272). The anatase peaks for both acidic and basic samples were intensified after HT. Moreover, the intensity of the anatase peaks increased with the increase in HT time, indicating that HT improved the crystallinity of anatase in the PEO oxide layer. These results are in agreement with previous findings reported previously[43]. A slight shift toward the left side of the XRD pattern was observed after HT

for basic PEO substrate, which possibly is linked with the expansion of TiO_2 lattice during HT [44]. Due to the sudden discharges of micro arcs during the general PEO process, the temperature increases to more than 4500 K locally, leading to the melting of Ti nearby the arcs. In the next stage, these melted Ti are resolidified instantly in the cold electrolyte, favouring the formation of the anatase phase [45, 46]. The intensified anatase peaks after HT highlight the development of anatase in the oxide layer, promoting the nucleation of HAP on the samples and eventually enhancing the surface's osseointegration properties [47].

Raman Spectroscopy results for acidic and basic PEO surfaces before and after HT at optimised duration (4 h and 6 h) are shown in **Fig. 4b**. While no peak was evident for the bare titanium control sample (not included), five characteristics peaks associated with the formation of anatase phase at 146, 199, 404, 473 and 631 cm^{-1} confirmed the presence of anatase after HT for both acidic and basic PEO surfaces. In general, observed peaks for the basic PEO sample after HT were sharper, while more broadened peaks for HT treated acidic PEO sample were observable [48].

Moreover, the presence of peaks at 279 cm^{-1} and 671 cm^{-1} are associated with the formation of sodium titanate as well as more complex sodium titanates such as $Na_2Ti_6O_{13}$ [41] and $Na_2Ti_3O_7$ [42] due to the interaction of sodium titanates and sodium hydrogen titanates with variant stoichiometry in the HT system. These peaks are intensified by increasing the HT duration. The observed non-stoichiometric condition in the oxide film means Ti and O are present in variant concentrations in the oxide layer that eventually may lead to the generation of reactive oxygen species (ROS) in the presence of body fluid[48]. Apart from the mechanical killing mechanism associated with nanostructures formation, ROS formation may also play an important role in the antimicrobial improvement of titania nanostructures.

In the next stage, static contact angle measurement was utilised to quantify the wettability of different samples. Contact angle values (CA) for the titanium control sample, as well as acidic and basic PEO substrates before and after HT, are demonstrated in **Fig. 4c**. Ti substrate showed the CA values of ~ 74°. It has been commonly accepted that a CA greater than 65° is considered to be a hydrophobic surface [44]. Therefore, the Ti control sample in this experiment showed a hydrophobic nature. PEO treatment in both acidic and basic solution resulted in the formation of an oxide layer comprised of micro-nano pores, which improved the wettability of coating by decreasing the CA values to ~ 60°. The formation of titania

nanostructures after HT drastically reduce the CA values and make the surface super hydrophilic. Measured CA values for the A-HT_{4h} and A-HT_{6h} were 4° and 2°, respectively.

In contrast, these values for basic group of B-HT_{4h} and B-HT_{6h} were 15° and 7°, respectively. As it can be seen, formed nanostructures on the acidic PEO surface (A-HT_{4h} and A-HT_{6h}) demonstrate higher hydrophilicity after HT, compared to the basic PEO substrates (B-HT_{4h} and B-HT_{6h}). These results confirm the importance of electrolyte composition on the nanostructure growth after HT, which eventually affect the wettability properties of the implant. It is worthwhile to mention that wettability is playing a critical role in bone-implant interaction by affecting the initial proteins adsorption. In general, hydrophilic surfaces can improve cell adhesion and proliferation, promoting bio-mineralisation and osseointegration properties [43].

16

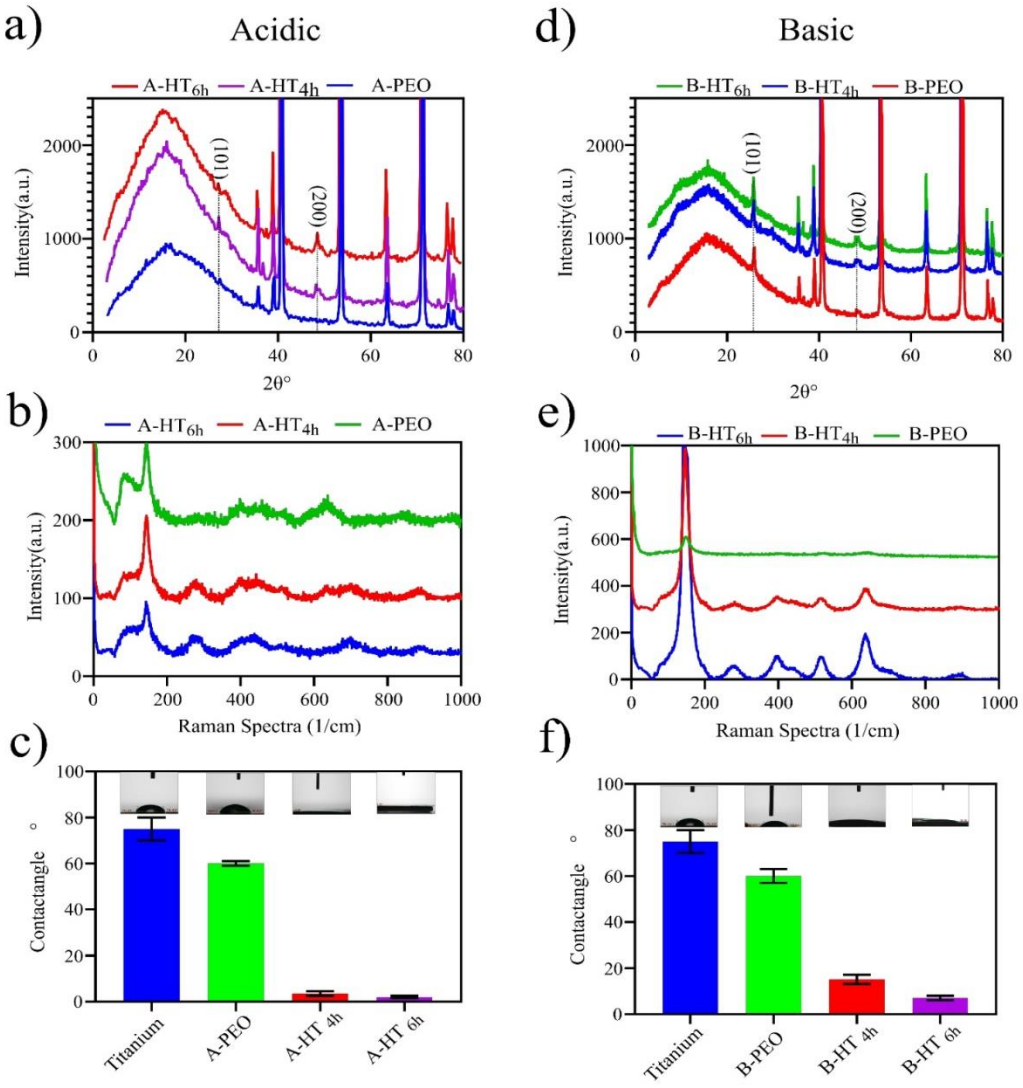

Figure 4. Comparative chemical and surface analysis of PEO controls (A-PEO and B-PEO) and HT treated PEO substrates after 4 h and 6 h: a) XRD patterns for the acidic group, b) Raman spectra for the acidic group, c) Contact angle measurement (wettability test) for the acidic group, d) XRD patterns for the basic group, e) Raman spectra for the basic group, f) Contact angle measurement (wettability test) for the basic group.

17

4.3. Bio-mineralization assessment of the PEO-HT nano-structured substrates

The bio-mineralisation test is a common in vitro technique, which has proven effective in predicting surface bioactivity by mimicking the environment similar to the human blood plasma [49]. In Figure 5, the comparative analysis of different samples after 21 days of SBF immersion has been provided. For both acidic and basic PEO surfaces, the formation of small-sized particles (up to 1.4 μm) over the surface was observable. Moreover, these particles were not covering the whole surfaces area. On the other side, both HT treated PEO surfaces demonstrated a higher degree of deposition, evident from the formation of much bigger sized particles (10-40 μm) covering the specimens' whole surface area. After the SBF test for all samples, EDS analysis showed the Ca/P ratio greater than 2, highlighting the formation of a biphasic mixture containing calcium hydroxide and calcium phosphate apatite [50].

XRD spectra comparison for different samples after the mineralisation process demonstrated the presence of hydroxyapatite characteristic peaks corresponding to (100), (200), (002), (102), (112), (300), (301), (312) and (213) planes (according to ICDD 9–432 HAp standard peaks[51]) for both acidic and basic PEO substrates, before and after HT. Moreover, some of the HAP peaks at 2θ of 26° and 32° were intensified after SBF mineralisation, emphasising the higher level of HAp deposition for hydrothermally treated PEO samples. In conclusion, the result of SEM, EDS and XRD are confirming better bioactivity of hydrothermally treated PEO substrates in comparison to untreated PEO substrates. Therefore, titania nano-structured PEO substrates fabricated via hydrothermal treatment are expected to improve the osseointegration properties of Ti-based implant highly. These results are in accordance with previously reported mineralisation results for nano-structured PEO substrates[52].

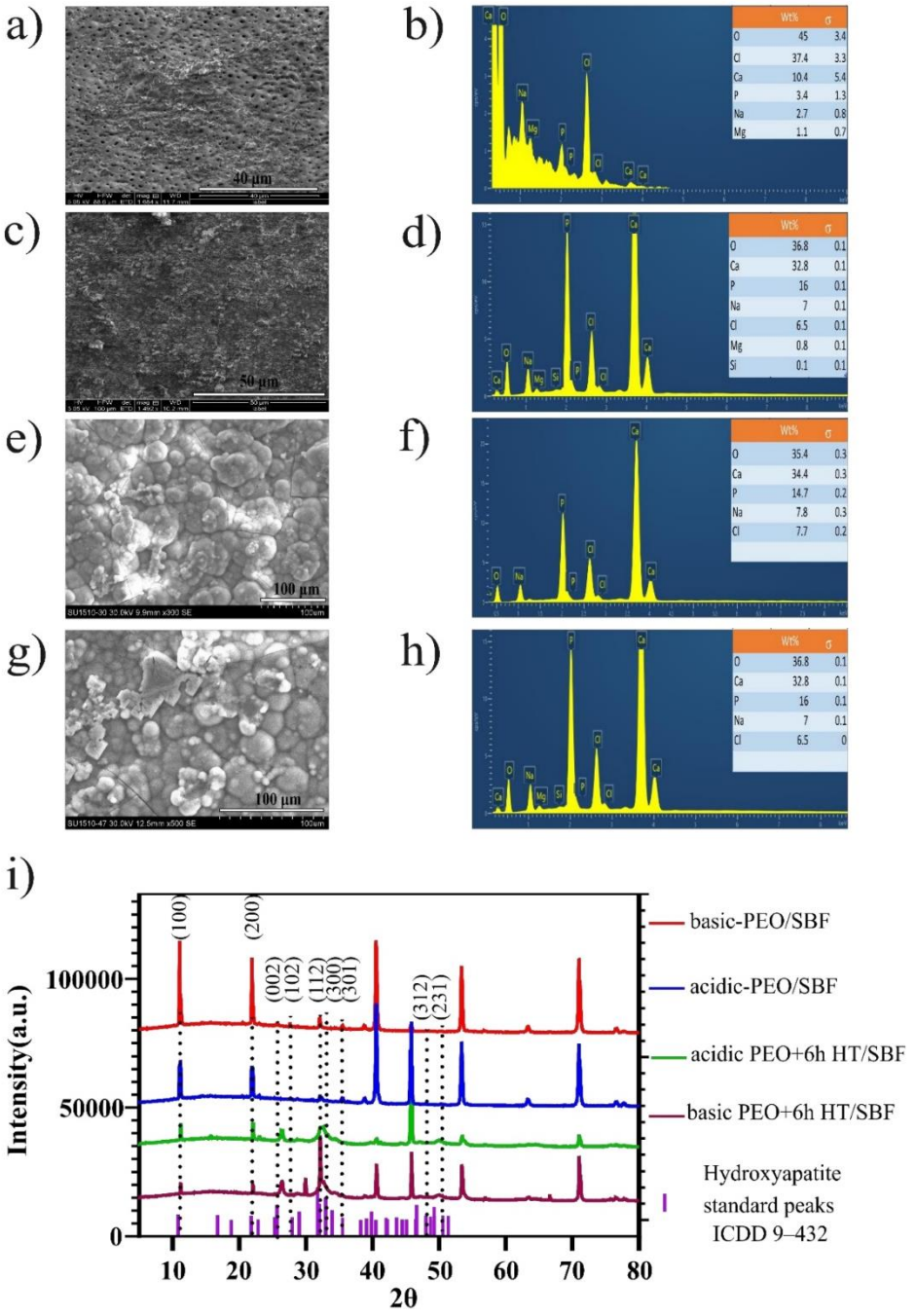

Figure 5. Comparative SEM and EDS , XRD results after 21 days SBF immersion for: a) SEM for A-PEO/SBF, b) Corresponding EDS for A-PEO/SBF, c) SEM for B-

PEO/SBF, d) Corresponding EDS for B-PEO/SBF, e) SEM for A-HT_{6h}/SBF), f) Corresponding EDS for A-HT_{6h}/SBF, g) SEM for B-HT_{6h}/SBF, h) Corresponding EDS for B-HT_{6h}/SBF, i) Corresponding XRD pattern after SBF test for different samples.

4.4. Characterisation of Antibacterial properties of the PEO-HT nano-structured substrates

The result of antibacterial activity against *E. coli* and *S. aureus* bacteria, along with corresponding photographs of recultured colonies, have been presented in Figure 6. As demonstrated in **Fig. 6a,** acidic and basic PEO groups behaved differently after incubation with *E. coli.* The result showed a 56 % decrease in the number of bacteria colonies compared to titanium control for the acidic PEO surface, while no decrease in the number of bacteria observed for the basic PEO sample. It is worth mentioning that other studies also reported a similar result confirming that different PEO treated surfaces may act differently against one particular type of bacteria [53]. In fact, several physical and chemical factors such as chemical composition, roughness, wettability, etc., can directly affect samples' antibacterial activity [54-56]. On the other side, all HT treated acidic PEO samples showed higher antibacterial activity against E. coli, with an 88% and 60% decrease in the number of colonies for A-HT_{4h} and A-HT_{6h}, respectively. These reduction in numbers for the basic group of B-HT_{4h} and B-HT_{6h} were 68% and 63%, respectively. These results outline the higher antibacterial activity of nanostructures on the acidic PEO samples after HT, compared with basic PEO group. This observation can be justified by quicker formation and development of titania nanostructures on the acidic PEO substrates during HT, which, along with these acidic PEO samples' natural antibacterial activity, leads to super antimicrobial activity against *E.coli.* Therefore, the acidic PEO treated samples were selected as candidate samples for further antibacterial studies.

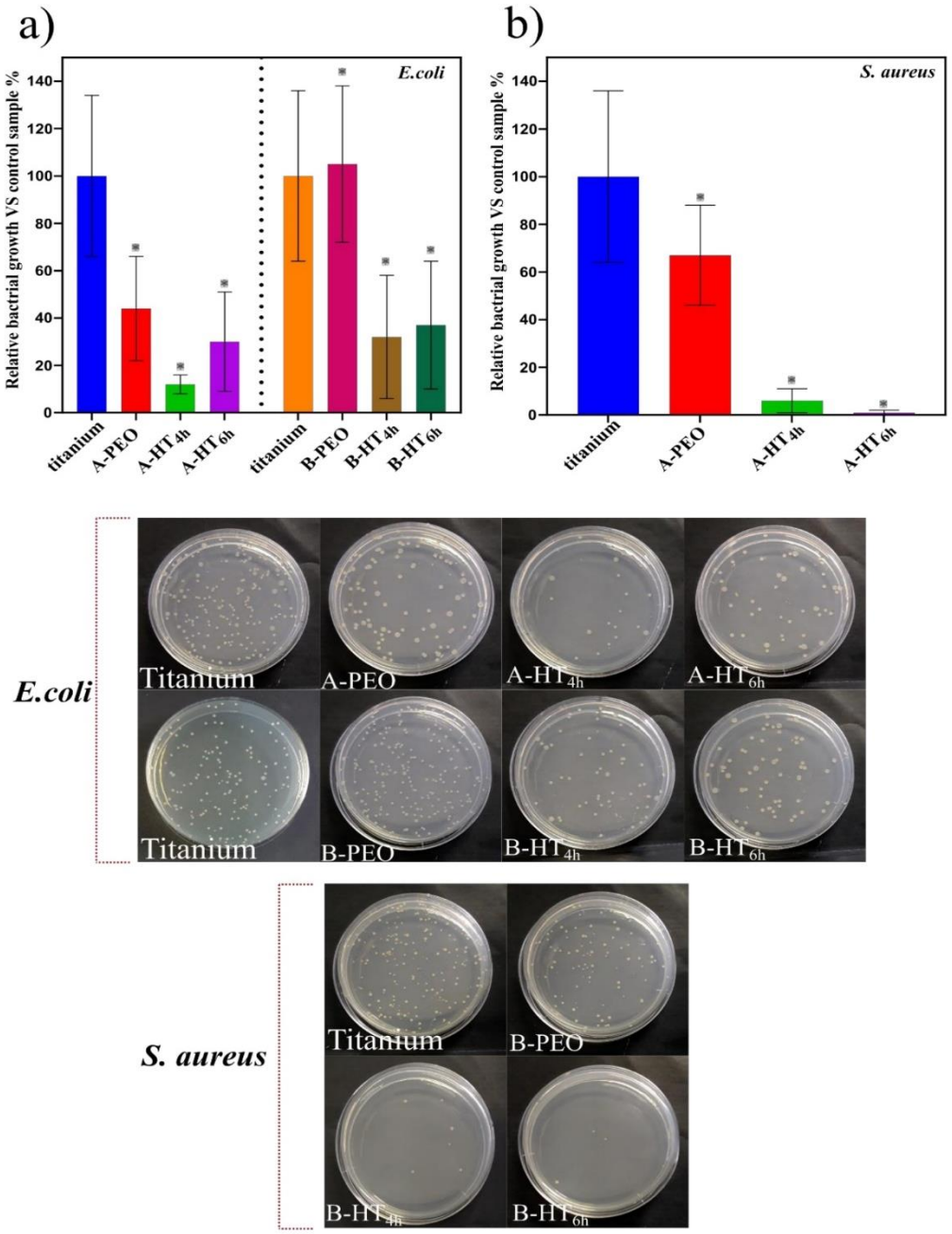

Figure 6. Relative bacterial growth in contact with different samples against a) *E. coli*, b) *S. aureus* with corresponding photographs of colonies, *p < 0.05.

21

In the next stage, candidate samples' antimicrobial activity (the acidic PEO modified group) against *S. aureus* were analysed. As it can be seen in **Fig. 6b,** the acidic PEO sample demonstrated some extent of antibacterial activity with a 33% decrease in the number of colonies, while both A-HT_{4h} and A-HT_{6h} samples demonstrated a superior antimicrobial activity with 94% and 99% reduction in the number of colonies, respectively. Unlike *E.coli,* the *S. aureus* bacteria are more vulnerable to mechanical interaction, as they are not protected by a resilient outer membrane. That explains the higher sensitivity of gram-positive bacteria to mechanical damage by piercing, shearing and deformation compared to gram-negative bacteria[57].

Moreover, a similar study carried out by Jaggessar et al.[35] on textured titanium alloy reported a maximum reduction of *S. aureus* colonies for around 86% on nanostructures with a height of ~ 4602 nm. However, in the current research, we showed the antibacterial activity of ~ 99% is achievable by the fabrication of much smaller nanostructures ~ 750 nm for A-HT_{6h}. Another factor, which must be taken into account is the aspect ratio of nanostructured surfaces. It has been reported that biomimetic nano-textured surfaces with high aspect ratio and shorter and sharp nanostructures can significantly kill bacteria via cell lysis [32]. It is assumed that apart from the mechanical damage, other killing mechanisms such as the formation of sodium titanate (which has been reported previously in some type of PEO system) can contribute to HT treated PEO samples' antibacterial efficiency via increasing radical species formation [48]. This finding is significant, as eliminating gram-positive bacteria such as *S. aureus* on biocidal surfaces has been reported to be more challenging [32, 58].

5. Conclusion

In summary, the impact of Ca-free acidic (pH 1.1) and basic (pH 12) electrolytes used for the PEO process on titania nanostructure formation and growth by hydrothermal process and their bioactivity and antibacterial activity were explored. Break down voltage for basic solution recorded at higher voltage values of 310 V compared to 170 V for the acidic PEO sample. Both surfaces demonstrated generic PEO porous structures, while pores with slightly higher density were recorded for the basic electrolyte. An average oxide layer thickness of around 800 nm was measured for the basic PEO surface. In contrast, a thinner oxide layer with about 530 nm thickness was observed for substrates prepared in the acidic electrolyte during very short 1 min PEO treatment. During the HT process in NaOH for different durations, various titania

nanostructure morphologies with different growth rate and steps were created on the PEO surface. Initially, on the acidic PEO substrates, nano-roots were formed. These nano-roots then changed to create upright nano-blades and nano-needles structures (with the height of 800-1000 nm) in the next HT hours up to 6 h. Further HT to 24 h led to entangled micro-nano belts' formation with a reachable length of 3000 nm. Fabricated nanostructures were comprised of sodium titanate in the form of complex $Na_2Ti_6O_{13}$ and $Na_2Ti_3O_7$, identified by Raman spectroscopy. Contact angle (CA) measurements showed super hydrophilicity of HT treated PEO substrates with CA below 5° for 4 h and 6 h HT treatment of acidic PEO substate, while CA values of 15° and 7° for 4 h and 6 h basic PEO HT treated samples were recorded, respectively. SBF mineralisation test demonstrated excellent bioactivity of both acidic and basic PEO substrates before and after HT. However, full coverage of the surface with hydroxyapatite only observed for HT treated PEO substrates with big sized particles (10-40 μm) enriched with Ca and P. Finally, the antibacterial test revealed a superior antibacterial activity against *E. coli,* with 88% and 60% decrease in the number of colonies for 4 h and 6 h HT treated acidic PEO samples, respectively. While these bacterial reduction for basic PEO samples after 4 h and 6 h HT were 68% and 63%, respectively. As titania nanostructures over the acidic PEO substrates demonstrated a higher growth rate with better antibacterial activity, further antimicrobial test against gram-positive bacteria (*S. aureus*) was conducted for this candidate sample only. Results showed an outstanding antimicrobial activity of 4 h and 6 h HT acidic PEO substrates with 94% and 99% reduction in the number of colonies compared with control samples, respectively. The presented results confirm the successful application of the PEO process in Ca-free electrolytes with acidic and basic compositions combined with HT to fabricate titania nanostructures with a broad range of morphologies and dimensions with tunable and superior antibacterial properties. This combined method can be elegantly used for advancing performances of existing medical implants

Conflicts of interest

There are no conflicts to declare.

Acknowledgements

The authors acknowledge the funding by the ARC Research Hub for Graphene Enabled Industry Transformation, (IH150100003). The authors thank the University of Adelaide, school of chemical engineering and advanced materials and department of chemistry, materials

and chemical engineering "G. Natta", Polytechnic University of Milan and Dr Mohammadreza Barati for their support in this project.

Supplementary information :

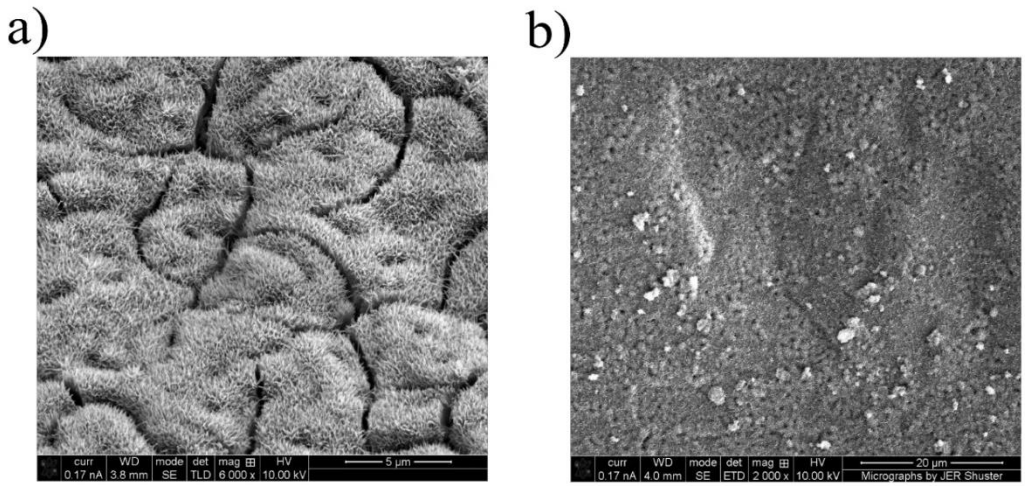

Figure S1. Low magnification SEM images of samples: a) A-HT_{6h} and b) B-HT_{12h}

References:

1. Hermawan, H., D. Ramdan, and J.R.J.B.e.-f.t.t.a. Djuansjah, *Metals for biomedical applications.* 2011. **1**: p. 411-430.
2. Nine, M.J., et al., *Wear Debris Characterization and Corresponding Biological Response: Artificial Hip and Knee Joints.* Materials, 2014. **7**(2): p. 980-1016.
3. Bayliss, L.E., et al., *The effect of patient age at intervention on risk of implant revision after total replacement of the hip or knee: a population-based cohort study.* The Lancet, 2017. **389**(10077): p. 1424-1430.
4. De Nardo, L., et al., *Electrochemical surface modifications of titanium and titanium alloys for biomedical applications.* Coatings for Biomedical Applications: Woodhead Publishing, 2012: p. 106-42.
5. Elias, C.N., et al., *Biomedical applications of titanium and its alloys.* JOM, 2008. **60**(3): p. 46-49.
6. Maher, S., et al., *Engineered titanium implants for localised drug delivery: recent advances and perspectives of Titania nanotubes arrays.* Expert Opinion on Drug Delivery, 2018. **15**(10): p. 1021-1037.
7. Jemat, A., et al., *Surface Modifications and Their Effects on Titanium Dental Implants.* BioMed Research International, 2015. **2015**: p. 791725.
8. Ching, H.A., et al., *Effects of surface coating on reducing friction and wear of orthopaedic implants.* Science and Technology of Advanced Materials, 2014. **15**(1): p. 014402.
9. Rastin, H., et al., *3D bioprinting of a cell-laden antibacterial polysaccharide hydrogel composite.* Carbohydrate Polymers, 2021. **264**: p. 117989.
10. Mu, W. and Y. Han, *Characterisation and properties of the MgF2/ZrO2 composite coatings on magnesium prepared by micro-arc oxidation.* Surface and Coatings Technology, 2008. **202**(17): p. 4278-4284.
11. Snizhko, L., et al., *Anodic processes in plasma electrolytic oxidation of aluminium in alkaline solutions.* Electrochimica Acta, 2004. **49**(13): p. 2085-2095.
12. Hanawa, T., *Titanium–Tissue Interface Reaction and Its Control With Surface Treatment.* Frontiers in Bioengineering and Biotechnology, 2019. **7**(170).
13. Mazinani, A., et al., *Graphene oxide (GO) decorated on multi-structured porous titania fabricated by plasma electrolytic oxidation (PEO) for enhanced antibacterial performance.* Materials & Design, 2021. **200**: p. 109443.
14. Richiez-Nieves, P., et al., *A Sheep Model for the Osseointegration of PEO-treated Gamma Titanium Aluminide.* 2020. **1**(3).
15. Santos-Coquillat, A., et al., *In vitro and in vivo evaluation of PEO-modified titanium for bone implant applications.* 2018. **347**: p. 358-368.
16. Fini, M., et al., *In vitro and in vivo behaviour of Ca-and P-enriched anodised titanium.* 1999. **20**(17): p. 1587-1594.
17. Tian, P., et al., *In vitro degradation behavior and cytocompatibility of biodegradable AZ31 alloy with PEO/HT composite coating.* 2015. **128**: p. 44-54.
18. Kossenko, A., et al., *Effect of time on the formation of hydroxyapatite in PEO process with hydrothermal treatment of the Ti-6Al-4V alloy.* Glass Physics and Chemistry, 2013. **39**(6): p. 639-642.
19. Parcharoen, Y., P. Termsuksawad, and S. Sirivisoot, *Improved Bonding Strength of Hydroxyapatite on Titanium Dioxide Nanotube Arrays following Alkaline Pretreatment for Orthopedic Implants.* Journal of Nanomaterials, 2016. **2016**: p. 9143969.
20. Mishra, A., et al., *Study of Mechanical and Tribological Properties of Nanomica Dispersed Hydroxyapatite Based Composites for Biomedical Applications.* Advances in Materials Science and Engineering, 2017. **2017**: p. 9814624.

21. Costescu, A., et al., *Fabrication, Characterisation, and Antimicrobial Activity, Evaluation of Low Silver Concentrations in Silver-Doped Hydroxyapatite Nanoparticles.* Journal of Nanomaterials, 2013. **2013**: p. 194854.
22. Kolmas, J., E. Groszyk, and D. Kwiatkowska-Różycka, *Substituted Hydroxyapatites with Antibacterial Properties.* BioMed Research International, 2014. **2014**: p. 178123.
23. Martínez-Gracida, N.O., et al., *Synergism in novel silver-copper/hydroxyapatite composites for increased antibacterial activity and biocompatibility.* Ceramics International, 2020. **46**(12): p. 20215-20225.
24. Salaie, R.N., et al., *The biocompatibility of silver and nanohydroxyapatite coatings on titanium dental implants with human primary osteoblast cells.* Materials Science and Engineering: C, 2020. **107**: p. 110210.
25. Ferdous, Z. and A. Nemmar, *Health Impact of Silver Nanoparticles: A Review of the Biodistribution and Toxicity Following Various Routes of Exposure.* International journal of molecular sciences, 2020. **21**(7): p. 2375.
26. Rastin, H., et al., *3D bioprinting of cell-laden electroconductive MXene nanocomposite bioinks.* Nanoscale, 2020. **12**(30): p. 16069-16080.
27. Szunerits, S. and R. Boukherroub, *Antibacterial activity of graphene-based materials.* Journal of Materials Chemistry B, 2016. **4**(43): p. 6892-6912.
28. Gao, Q., et al., *Antibacterial and hydroxyapatite-forming coating for biomedical implants based on polypeptide-functionalised titania nanospikes.* Biomaterials Science, 2020. **8**(1): p. 278-289.
29. Sjöström, T., A.H. Nobbs, and B. Su, *Bactericidal nanospike surfaces via thermal oxidation of Ti alloy substrates.* Materials Letters, 2016. **167**: p. 22-26.
30. Ivanova, E.P., et al., *Bactericidal activity of black silicon.* Nature Communications, 2013. **4**: p. 2838.
31. Ivanova, E.P., et al., *The multi-faceted mechano-bactericidal mechanism of nano-structured surfaces.* Proceedings of the National Academy of Sciences, 2020. **117**(23): p. 12598-12605.
32. Elbourne, A., R.J. Crawford, and E.P. Ivanova, *Nano-structured antimicrobial surfaces: From nature to synthetic analogues.* Journal of Colloid and Interface Science, 2017. **508**: p. 603-616.
33. Ivanova, E.P., et al., *Natural Bactericidal Surfaces: Mechanical Rupture of Pseudomonas aeruginosa Cells by Cicada Wings.* Small, 2012. **8**(16): p. 2489-2494.
34. Tripathy, A., et al., *Natural and bioinspired nano-structured bactericidal surfaces.* Advances in Colloid and Interface Science, 2017. **248**: p. 85-104.
35. Jaggessar, A. and P.K.D.V. Yarlagadda, *Modelling the growth of hydrothermally synthesised bactericidal nanostructures, as a function of processing conditions.* Materials Science and Engineering: C, 2020. **108**: p. 110434.
36. Guo, Z., et al., *Surface bioactivation through the nano-structured layer on titanium modified by facile HPT treatment.* Scientific Reports, 2017. **7**(1): p. 4155.
37. Kuromoto, N.K., R.A. Simão, and G.A. Soares, *Titanium oxide films produced on commercially pure titanium by anodic oxidation with different voltages.* Materials Characterisation, 2007. **58**(2): p. 114-121.
38. Aliasghari, S., P. Skeldon, and G.E. Thompson, *Plasma electrolytic oxidation of titanium in a phosphate/silicate electrolyte and tribological performance of the coatings.* Applied Surface Science, 2014. **316**: p. 463-476.
39. Anitha, V., et al., *Morphology-dependent low macroscopic field emission properties of titania/titanate nanorods synthesised by alkali-controlled hydrothermal treatment of a metallic Ti surface.* Nanotechnology, 2015. **26**(35): p. 355705.
40. Kokubo, T. and H. Takadama, *How useful is SBF in predicting in vivo bone bioactivity?* Biomaterials, 2006. **27**(15): p. 2907-15.

41. Kawashita, M., et al., *Bonelike Apatite Formation on Anodically Oxidized Titanium Metal in Simulated Body Fluid*, in *Key Engineering Materials*. 2004. p. 459-462.
42. He, X., et al., *Titanium-based implant comprising a porous microstructure assembled with nanoleaves and controllable silicon-ion release for enhanced osseointegration.* Journal of Materials Chemistry B, 2018. **6**(31): p. 5100-5114.
43. Lin, D.-J., et al., *Rapid nano-scale surface modification on micro-arc oxidation coated titanium by microwave-assisted hydrothermal process.* Materials Science and Engineering: C, 2019. **95**: p. 236-247.
44. Shalini, S., et al., *Effect of Na doping on structure, morphology and properties of hydrothermally grown one dimensional TiO2 nanorod structures.* Journal of Materials Science: Materials in Electronics, 2017. **28**(4): p. 3500-3508.
45. Hussein, R.O., et al., 2010: p. 105203-105216.
46. Malinovschi, V., et al., *Obtaining and characterisation of PEO layers prepared on CP-Ti in sodium dihydrogen phosphate dihydrate acidic electrolyte solution.* Surface and Coatings Technology, 2019. **375**: p. 621-636.
47. Uchida, M., et al., *Structural dependence of apatite formation on titania gels in a simulated body fluid.* Journal of Biomedical Materials Research Part A: An Official Journal of The Society for Biomaterials, The Japanese Society for Biomaterials, and The Australian Society for Biomaterials and the Korean Society for Biomaterials, 2003. **64**(1): p. 164-170.
48. Marin, E., et al., *Effect of etching on the composition and structure of anodic spark deposition films on titanium.* Materials & Design, 2016. **108**: p. 77-85.
49. Liu, X., C. Ding, and Z. Wang, *Apatite formed on the surface of plasma-sprayed wollastonite coating immersed in simulated body fluid.* Biomaterials, 2001. **22**(14): p. 2007-2012.
50. Raynaud, S., et al., *Calcium phosphate apatites with variable Ca/P atomic ratio I. Synthesis, characterisation and thermal stability of powders.* Biomaterials, 2002. **23**(4): p. 1065-1072.
51. haghbin nazarpak, M., et al., *Effect of Gamma Irradiation on Structural and Biological Properties of a PLGA-PEG-Hydroxyapatite Composite.* The Scientific World Journal, 2014. **2014**.
52. Huang, Q., et al., *Preparation and characterisation of TiO2/silicate hierarchical coating on titanium surface for biomedical applications.* Materials Science and Engineering: C, 2016. **60**: p. 308-316.
53. Ponomarev, V.A., et al., *Ag(Pt) nanoparticles-decorated bioactive yet antibacterial Ca- and P-doped TiO2 coatings produced by plasma electrolytic oxidation and ion implantation.* Applied Surface Science, 2020. **516**: p. 146068.
54. Wu, S., et al., *Role of the Surface Nanoscale Roughness of Stainless Steel on Bacterial Adhesion and Microcolony Formation.* ACS omega, 2018. **3**(6): p. 6456-6464.
55. Kramer, A. and O. Assadian, *Survival of Microorganisms on Inanimate Surfaces.* Use of Biocidal Surfaces for Reduction of Healthcare Acquired Infections, 2014: p. 7-26.
56. Yuan, Y., et al., *Surface characteristics influencing bacterial adhesion to polymeric substrates.* RSC Advances, 2017. **7**(23): p. 14254-14261.
57. Akhavan, O. and E. Ghaderi, *Toxicity of Graphene and Graphene Oxide Nanowalls Against Bacteria.* ACS Nano, 2010. **4**(10): p. 5731-5736.
58. Hasan, J., et al., *Selective bactericidal activity of nanopatterned superhydrophobic cicada Psaltoda claripennis wing surfaces.* Applied Microbiology and Biotechnology, 2013. **97**(20): p. 9257-9262.

Chapter 6

Antibacterial development of titania PEO surface with PEO-EPD technique

This chapter explains a novel approach in antibacterial improvement of titania PEO porous structure via partial deposition of graphene oxide patched (GO) on the surface through high voltage electrophoretic deposition technique (PEO-EPD). The mixed morphology of surfaces obtained with this new technique ensures antibacterial and osseointegration improvement of the fabricated samples simultaneously. The results showed exceptional antibacterial activity toward gram-positive (*Staphylococcus aureus*) and gram-negative (*E.coli*) bacteria with an antibacterial efficiency of ~80% and ~100%.

This chapter has been published as:

Arash Mazinani, Md Julker Nine, Roberto Chiesa, Gabriele Candiani, Paolo Tarsini, Tran Tung, Dusan Losic. Graphene oxide (GO) decorated on multi-structured porous titania fabricated by Plasma Electrolytic Oxidation (PEO) for enhanced antibacterial performance, Material and Design. 2021; Volume 200; 109443. doi.org/10.1016/j.matdes.2020.109443.

Statement of Authorship

Title of Paper	Graphene oxide (GO) decorated on multi-structured porous titania fabricated by Plasma Electrolytic Oxidation (PEO) for enhanced antibacterial performance
Publication Status	☑ Published ☐ Accepted for Publication ☐ Submitted for Publication ☐ Unpublished and Unsubmitted work written in manuscript style
Publication Details	Arash Mazinani, Md Julker Nine, Roberto Chiesa, Gabriele Candiani, Paolo Tarsini, Tran Tung, Dusan Losic. Graphene oxide (GO) decorated on multi-structured porous titania fabricated by Plasma Electrolytic Oxidation (PEO) for enhanced antibacterial performance, Material and design journal. published

Principal Author

Name of Principal Author (Candidate)	Arash Mazinani
Contribution to the Paper	Conceptualization,Structure of Manuscript,Original draft
Overall percentage (%)	70
Certification:	This paper reports on original research I conducted during the period of my Higher Degree by Research candidature and is not subject to any obligations or contractual agreements with a third party that would constrain its inclusion in this thesis. I am the primary author of this paper.
Signature	Date: 24.05.2021

Co-Author Contributions

By signing the Statement of Authorship, each author certifies that:

i. the candidate's stated contribution to the publication is accurate (as detailed above);
ii. permission is granted for the candidate in include the publication in the thesis; and
iii. the sum of all co-author contributions is equal to 100% less the candidate's stated contribution.

Name of Co-Author	Prof Dusan Losic
Contribution to the Paper	Conceptualization,resources, funding acquization,review, editing, supervision, submission
Signature	Date: 24 May 2021

Name of Co-Author	Dr Md Julker Nine
Contribution to the Paper	selected investigation, editing and review, supervision
Signature	Date: 24/05/2021

Please cut and paste additional co-author panels here as required.

Name of Co-Author	Tran Thanh Tung		
Contribution to the Paper	selected investigation, editing and review		
Signature		Date	24/5/2021

Name of Co-Author	Roberto Chiesa		
Contribution to the Paper	selected investigation, editing and review		
Signature		Date	18/05/2021

Name of Co-Author	Gabriele Candiani		
Contribution to the Paper	selected investigation, editing and review		
Signature		Date	18/05/2021

Name of Co-Author	Paolo Tarsini		
Contribution to the Paper	selected investigation, editing and review		
Signature		Date	18.05.2021

Contents lists available at ScienceDirect

Materials and Design

journal homepage: www.elsevier.com/locate/matdes

Graphene oxide (GO) decorated on multi-structured porous titania fabricated by plasma electrolytic oxidation (PEO) for enhanced antibacterial performance

Arash Mazinani [a,b], Md Julker Nine [a,b], Roberto Chiesa [c], Gabriele Candiani [c], Paolo Tarsini [c], Tran Thanh Tung [a,b], Dusan Losic [a,b,*]

[a] School of Chemical Engineering and Advanced Materials, The University of Adelaide, Adelaide, SA 5005, Australia
[b] ARC Hub for Graphene Enabled Industry Transformation, The University of Adelaide, Adelaide, SA 5005, Australia
[c] Department of Chemistry, Materials and Chemical Engineering "G. Natta", Politecnico di Milano, Via Mancinelli 7, Milano 20131, Italy

HIGHLIGHTS

- Plasma Electrolytic Oxidation (PEO) and Electrophoretic Deposition (ED) are combined for Graphene Oxide deposition (GO).
- Partial deposition of (GO) sheets on PEO anodized titanium as new antibacterial surface is demonstrated.
- The optimized deposition with 60% GO surface coverage is found as the best performing.
- Antibacterial activity ~80% against *E.coli* and ~100% against *S. aureus* bacteria is achieved.

GRAPHICAL ABSTRACT

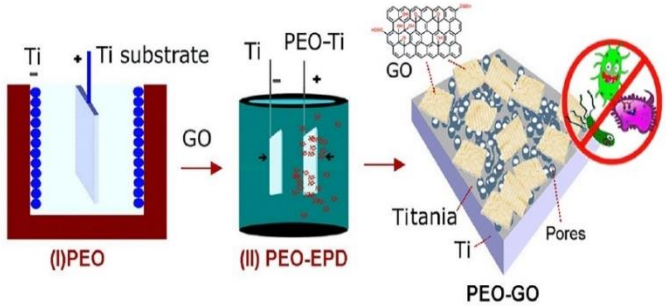

ARTICLE INFO

Article history:
Received 4 July 2020
Received in revised form 23 December 2020
Accepted 28 December 2020
Available online 31 December 2020

Keywords:
Antibacterial surfaces
Plasma electrolytic oxidation
Electrophoretic deposition
Graphene oxide

ABSTRACT

Plasma electrolytic oxidation (PEO) is proven as a scalable method for surface treatment of titanium (Ti) providing a thick oxide layer with porous micro-nano morphology. Despite the lack of antibacterial performance, this modification has potential to improve the osseointegration properties of Ti-based implant. To address this limitation, we demonstrated a new concept, showing that partial incorporation of graphene oxide (GO) to porous-PEO Ti-surface can significantly improve its antibacterial performance. Our idea for partial coating compared with a full surface coverage of GO was motivated to create a mixed surface with porous PEO and GO to improve antibacterial ability, while maintaining the osseointegration properties. To achieve these goals, we combined PEO and electrophoretic deposition process (EPD) to deposit GO sheets over the titanium PEO-treated substrate. The SEM, EDS, optical profilometry, XRD and Raman spectroscopy confirmed the growth of unique multi-structured porous PEO structures decorated with GO patches. The bio-mineralization test provided the evidence of hydroxyapatite formation over the PEO-GO surface, indicating its good bioactivity. Finally, PEO-GO samples demonstrated a superior antibacterial rate of ~80% against *E.coli* and ~100% against *S. aureus*. These results indicate that PEO-GO modified titanium substrates are very promising for the development of advanced biomedical implants.

1. Introduction

Over the years, titanium (Ti) and Ti-alloys have replaced many other common metals such as magnesium (Mg) alloy and stainless steel used

* Corresponding author at: School of Chemical Engineering and Advanced Materials, The University of Adelaide, Adelaide, SA 5005, Australia.
E-mail address: dusan.losic@adelaide.edu.au (D. Losic).

https://doi.org/10.1016/j.matdes.2020.109443

in the bio-implants production. Nowadays, Ti is considered as the first choice for a number of biomedical applications such as dental implants, bone implants and localized drug delivery systems due to its excellent durability, corrosion resistance, mechanical strength, low specific weight and biocompatibility [1–3]. Despite being a "valve metal" with suitable biocompatible property, the rejection of Ti-based implants as a result of poor bio-integration and bacterial infection are concerning. Additionally, it is causing significant healthcare costs and devastating impact on patients [4–6]. The osseointegration property of Ti-implant has a crucial role in bone bonding and improving the implant lifetime, which is mainly influenced by Ti-implant composition and the applied surface treatment [7,8]. To improve osseointegration properties, the surface of commercial implants is usually modified by different methods such as hydroxyapatite coating (HAp), micro-roughening by chemical etching, grit-blasting, laser micro-machining and powder coating [9–12]. Moreover, many other micro and nano fabrication methods (including electrochemical anodization, Plasma Electrolytic Oxidation (PEO) also known as Micro Arc Oxidation (MAO), hydrothermal process, polymer coatings, etc.) were explored to improve the bioactivity of implants [13–16]. Among them, PEO surface modification of Ti-alloy is demonstrated to be a very successful scalable process, which was introduced in dental and orthopaedic fields, showing excellent outcome in the osseointegration improvement [8,17]. The PEO roughened surface with a unique combination of micro-nano pores provides suitable sites for ingrowth of bone tissue, which can accelerate bone-implant bonding and improves mechanical anchoring of implants [7]. This unique method is working based on the generation of micro arcs, resulted from the application of high electric field in an electrolytic solution, that bombards the valve metals surface locally and forms a protective oxide layer dominated with micro-nano structure morphology [18–21]. However, apart from the improved osseointegration properties of PEO treated Ti-implant, the problem with low antibacterial protection remains unsolved [22].

Graphene derivatives (e.g. graphene, graphene oxide (GO), reduced graphene oxide (rGO), doped and other functionalized graphene) with a variety of extraordinary mechanical, and physiochemical properties opened their way into the versatile applications such as multifunctional-coating [23], photocatalysts [24], composites [25,26], supercapacitors [27] and environmental application [28]. Among many graphene derivatives, GO and rGO have recently drawn a significant attention in the biomedical and antimicrobial fields after revealing their potential to be efficient antimicrobial nanomaterials [29,30]. Antibacterial studies using different types of graphene-based materials against *Escherichia coli (E.coli)* showed that GO has the highest antimicrobial properties, followed by rGO, graphite, and graphite oxide [31]. Research has been carried out to understand the mechanisms behind the antibacterial activity of graphene-based materials towards gram-negative and gram-positive bacteria. The proposed mechanisms are still the subject of great interest for researchers, which are principally based on the formation of reactive oxygen species (ROS), and oxidative stress along with possessing sharp edges identified to be effective in the antimicrobial activity of GO and rGO. Additional parameters such as hydrophobicity and surface roughness along with the mode of contact between the basal plane of graphene derivatives and bacteria were found to be effective on the antimicrobial properties of these materials [32,33]. Meanwhile, It has been shown that GO has a potential to promote mechanical stability of coatings by decreasing the number of microcracks and also has an ability to enhance the bioactivity via improving the adhesion and proliferation of bone cell unites so-called osteoblasts [34–36]. Based on these promising results, efforts have been made to form and implement graphene-based composite to tackle microbial Multidrug Resistance (MDR), such as *Klebsiella pneumonia*, and to improve the antibacterial activity of Ti-implants [33,37]. In order to deposit graphene derivatives on the metallic implants, different methods such as dip-coating, plasma coating, spray-coating, electrophoretic deposition (EPD), anodization-EPD, anodization-hydrothermal, etc. have been explored [38–41].

Recently, several studies were carried out to incorporate GO to the PEO matrix of light metals such as Al and Ti [42–44], to improve their interfacial performance and functionality. However, the presence of GO over the coating is not evident, while only a few random deposition sites are differentiable over the substrate [42,44]. Other studies suggest that the generation of micro-nano bubbles during the PEO process at electrodes may impede the attachment of GO flakes to the substrate [45,46]. Other researchers also investigated new approaches to immobilize GO sheets over the PEO surface, such as application of APTE to fabricate GO thin film on the surface. Their results demonstrated the great potential of GO continuous film on the PEO surface for killing gram-positive bacteria such as *S. mutans* [22].

The EPD is a fast and straightforward process that allows deposition of GO over the metallic surface [45,46]. To date, several studies conducted to deposit GO-based continuous films over biomaterials such as Ti and Mg utilizing EPD technique [47,48]. Unfortunately, the low voltage EPD technique suffers weakened adhesion between the coating and the substrate [49]. Notably, the presence of a thick oxide layer on PEO substrate limits the deposition yield of GO with common EPD techniques. As a potential solution for this problem, Nie et al. [50] suggested a hybrid technique by the combination of PEO and EPD known as PEO-EPD process. This combined method has shown a great potential to tackle poor adhesion problem of bioceramics on valve metals such as Ti-surface through utilizing electrolytic plasma during EPD process and finally improve adhesion properties of coatings [49–51]. Nevertheless, researches were mainly focusing on the deposition of continuous GO film on the PEO matrix, which totally cover the micro-nano pores. These approaches may devalue the initial benefit of the PEO porous structure, which is required to be present for bone-implant integration [22,48].

Motivated by these studies, we come up with a new concept to improve osseointegration and antibacterial properties of titania surfaces simultaneously by combining micro-nano porous PEO surface partially covered with GO, which is presented in this paper. To achieve this goal, a new fabrication strategy is introduced, which consists of two steps: initial fabrication of PEO titania substrate followed by its partial coverage with GO through PEO-EPD technique. We proposed that the partial GO deposition is critical to have a mixture of two types of surfaces, first- to improve osseointegration and secondly- to prevent bacterial adhesion and colonization. In this study, the effect of deposition time for the PEO-EPD process was explored to achieve the desired GO deposition pattern with partial surface coverage. The morphological, physiochemical, mineralization potential and antimicrobial characteristics of the deposited titania surfaces with optimized conditions are presented to evaluate their performances as a potential new surface engineering technology for biomedical implants.

2. Experimental section

2.1. Materials

Ti-foils with 99.9% purity and thickness of 1 mm provided by Nilaco (Japan); orthophosphoric acid (H_3PO_4), 85 wt%, potassium hydroxide (KOH) pellet, 30 wt% hydrogen peroxide (H_2O_2), sulphuric acid (H_2SO_4), 35 wt% hydrochloric acid (HCl) and ethylene glycol were obtained from Chem Supply (South Australia). Sodium metasilicate pentahydrate and potassium permanganate ($KMnO_4$) were supplied from Sigma-Aldrich Pty Ltd. and potassium fluoride (KF) from Ajax Sigma–Aldrich. Graphite powder with an average diameter of 250 μm was collected from Eyre Peninsula mining site, South Australia. Pure Milli-Q water was used with the resistivity of 18.2 MΩcm refined by EMD Millipore Corporation, Billerica machine.

2.2. Graphene oxide (GO) preparation

GO was prepared by chemical oxidation of graphite powder using modified Hummer's method [52]. In short, a 9:1 mixture of H_2SO_4 and H_3PO_4 was prepared and placed in a refrigerator to cool down to 3 °C. Then the acidic solution slowly added to the mixture of $KMnO_4$ (18 g) and graphite powder (3 g), while was stirred and heated up to 50 °C for about 13 h. After reaching the ambient temperature, 1 ml of H_2O_2 was gently added to the solution resulted in the formation of the brownish mixture. The solution was then centrifuged at 4200 rpm for 2 h with 35% HCl and distilled water, respectively.

2.3. Modification of titanium surface with plasma electrolytic oxidation (PEO) method

Samples with a specific size (2 cm × 1.5 cm) obtained from Ti-foils were cleaned by acetone in a sonication bath for 10 min followed by rinsing with DI water to remove any surface contamination. All samples were dried in the oven for 3 h at 50 °C. The programmable DC power supply (N5752A, Agilent Technologies, USA) was utilized for the anodization process, while voltage-time data were collected by coupled LabVIEW software. The PEO treatment was performed in a single step, under the galvano-static condition with a fixed current density of 50 mA/cm^2 and stirring speed of 250 rpm for 1 min by modifying previous research protocols carried out by Kuromoto et al. [53] and a similar basic electrolyte reported by Aliasghari et al. [53–55]. Briefly, the PEO electrolyte was comprised of sodium silicate, phosphoric acid as well as potassium hydroxide dissolved in deionized water. After PEO anodization treatment, samples were washed in an ultrasonic bath with Millipore water for 10 min and then dried in the oven for 2 h at 50 °C. The resulting coating was denoted as PEO sample.

2.4. Combined plasma electrolytic oxidation and electrophoretic deposition (PEO-EPD) for GO deposition

For the preparation of the GO solutions, 0.5 mg GO in the form of concentrated suspension was added to the 500 ml electrolyte containing ethylene glycol 94:5 wt%, deionized water 5 wt% and KF 0.5 wt% based on the modified research protocol by Ali et al. [56]. Prior to the PEO-EPD process, GO sheets in the electrolyte were dispersed by ultrasonic agitator for 20 min. The pH of solution and zeta potential of added GO were 12 and −29 mV, respectively. The PEO-EPD process was carried out in different deposition time (7, 15, 30 and 60 s) without electrolyte agitation under the constant current mode of 100 mA/cm^2 using two-electrodes cell arrangement with working electrodes distance of 13 mm. The working electrode was PEO substrate and the counter electrode was a Ti-plate which situated parallel facing each other. The coated samples were removed from the cell and dried in an electric oven for 2 h at 50 °C.

3. Characterizations

Structural characterization of the porous structure obtained from PEO treatment and GO-enhanced morphology were investigated by SEM Quanta 450 (field emission scanning electron microscope, Eindhoven) coupled with EDS analysis as well as FIB-SEM (Focused Ion Beam Scanning Electron Microscope FEI Helios Nanolab 600, USA). The Zeta potential measurement of the electrolyte containing GO was carried out utilizing Malvern Zetasizer Nano Series (NS) before the deposition process. Surface topography of samples and surface roughness analysis were performed using a benchtop 3D optical profiler (Bruker ContourGT-K1). The vertical scanning interferometry (VSI) mode with a 20× objective was utilized for profilometry analysis. Raman spectroscopy instrument (WITEC Alpha300) was exploited to analyze the oxide layer after PEO process and to confirm the presence of GO after deposition process (PEO-EPD) with the range of 0–2000 cm^{-1} wavelength with a 532 nm laser beam. XRD analysis was carried out employing Rigaku MiniFlex 600, with the operating condition of (40 kV, 2θ = 3–80 with a scan rate of 2.5). Contact angle measurement was performed using optical-tensiometers model T301 – ATA scientific pty ltd and sessile drop method with droplet size of, 2.2 ± 0.1 μl. Microhardness test was also performed using a microhardness tester (ECO LM700, USA) with the predefined condition of 100 g force and dwell time of 10 s, which was applied over the surface of samples. The biomineralization test was performed according to the literature reported by Kokubo et al. [57]. In brief, samples were immersed in 50 ml simulated body fluid (SBF) solution for 21 days, while the solution was being replaced every two days to maintain the level of ion concentrations adequate for mineralization process. The antibacterial test was conducted according to ISO 22916:2011 against *E. coli* (Gram-negative, DSM 3423) and *S. aureus* (Gram-positive, DSM 346) bacteria. Briefly, bacteria were grown overnight and next diluted to a final concentration of 6×10^5 Colony Forming Unit (CFU)/ml to be inoculated (12.6 μl) on the surface of UV-disinfected (20 min per side) test specimens of about 10 mm × 10 mm. In order to obtain a homogeneous layer of bacteria, polypropylene coverslips (8 mm in diameter) were placed on the top of test inoculum, and the samples were incubated for 24 h at 37 °C in a humidified atmosphere. Bacteria were then eluted, serially diluted, and plated on Petri dishes containing agar growth medium and cultured for another 24 h at 37 °C. CFUs were finally counted and the antibacterial activity was calculated according to the following:

$$I\,(\%) = \frac{B_{CTRL} - B_{test}}{B_{test}} * 100$$

Where I (%) is the percentage of bacterial inhibition, B_{CTRL} is the viable bacteria recovered from control samples (untreated Ti), B_{test} is the viable bacteria recovered from specific samples. Samples were tested at least in triplicate, and related data were stated as the mean ± standard deviation and were analysed using GraphPad version 6 software (GraphPad Software, La Jolla, CA). Statistical comparison among groups was performed via one-way analysis of variance (ANOVA) (multiple comparisons) with post hoc Tukey's test to indicate significant differences between experimental groups. Differences were considered statistically significant when $P < 0.05$.

4. Results and discussions

4.1. Voltage–time response of PEO process and morphological characteristics of fabricated PEO titania structures

The basic solution for the PEO process is selected in this work, as it is more effective than the acidic electrolyte for the fabrication of protective and robust oxide layers [53,55]. Moreover, our previous research showed that 1 min PEO treatment is the optimized duration to achieve a suitable voltage for the fabrication of micro-nano structured pores, which can cover the entire surface with the desired morphology. Further PEO treatment would only increase the oxide layer thickness and does not affect the overall morphology required for the osseointegration improvement. Typical voltage–time (V-t) response curve for the PEO treatment in the basic electrolyte was generated by LabVIEW software, using single-step anodization at 50 mA/cm^2 and provided in Fig. 1a. The result showed an increasing trend in the cell voltage values with a breakdown voltage of ~310 V after 40 s, which was evident by the formation of arcs starting from the edge of the sample. Moreover, at around 60 s, voltage reached to ~380 V, arcs became brighter and spread all over the working electrode. Finally, the PEO process led to the formation of a generic porous micro-nano structure on Ti sample similar to the PEO surface morphology reported by Aliasghari et al. [55]. Fig. 1b shows the SEM image of the substrate after the PEO process. The formed oxide layer was enriched with silicon and titanium (supplementary Fig. S1), comprised of pores ranging from 200 nm to 1 μm with an

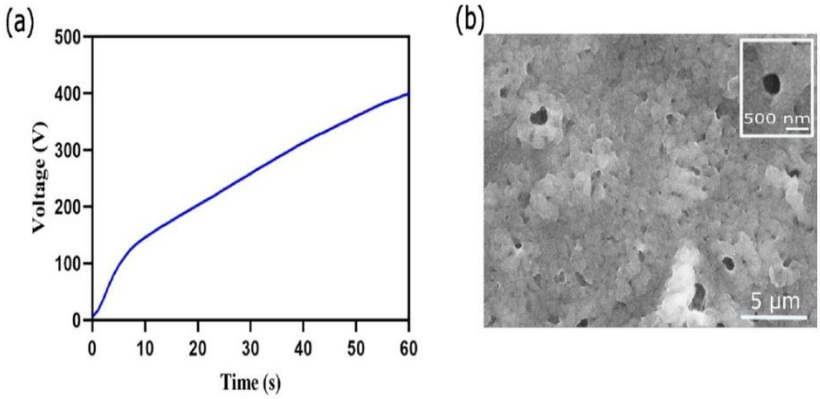

Fig. 1. a) Voltage-Time plot for the PEO process, b) SEM image of fabricated PEO titania surface with PEO technique in the basic solution at 50 mA/cm^2 after 1 min.

average spacing of 1.62 µm (between bigger pores) and few crater-like morphologies, which were distributed along the flat oxide layer surface. This analysis was taken from at least 15 spots with "Image J" software. A typical single pore morphology after PEO process is presented on the inset of Fig. 1b.

Overall, these results confirm the successful formation of PEO porous micro-nano morphology over the Ti substrate. Similar researches have shown the ability of these modified surfaces to promote osseointegration via increasing the surface area and attachments sites between bone cells and the implant surface [58,59].

4.2. Voltage–time response of PEO-EPD process for GO deposition and morphological characteristics of PEO-GO surface

Deposition of GO on PEO surface was performed in the next step using PEO-EPD process. Fig. 2 summarizes the voltage–time response and optical microscopy images of the generated PEO-GO surface after deposition at different durations. Fig. 2a shows a sudden increase of voltage to 455 V followed by a sharp decrease to ~320 V and a subsequent gradual decrease to reach a stable value of ~230 V for 1 min of the deposition process. It is important to note that, the proposed GO

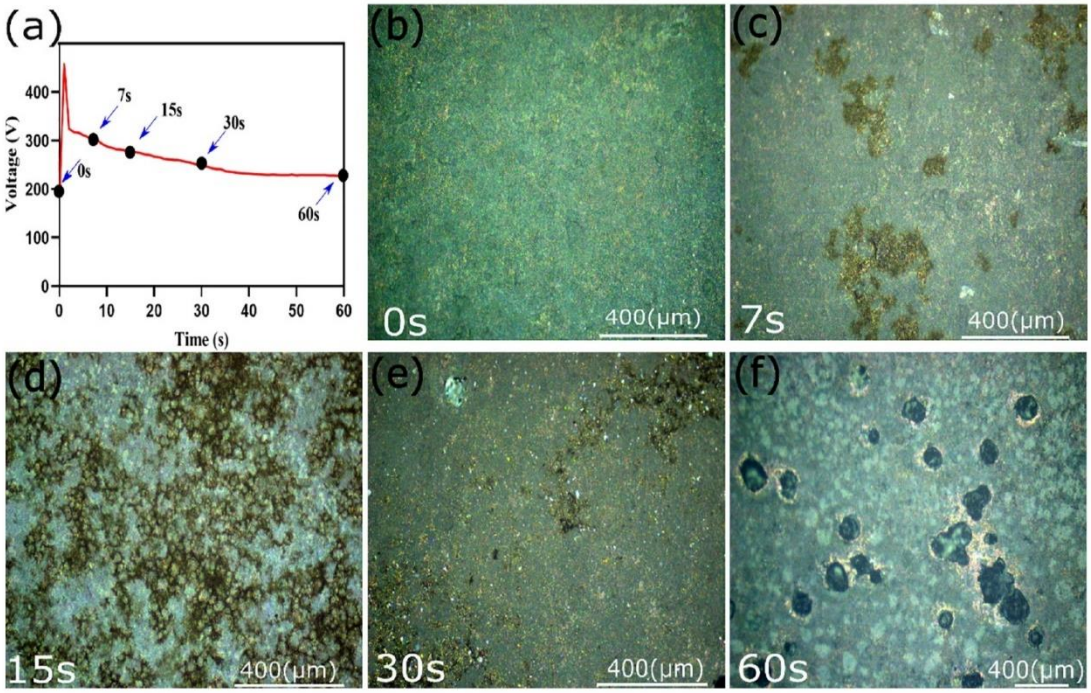

Fig. 2. a) Voltage-time plot during PEO-EPD process for deposition of GO on PEO surface. Optical images of PEO-GO surface obtained by PEO-EPD process during the different time: b) 0 s (PEO control), c) 7 s (EPD-7), d) 15 s (EPD-15), e) 30 s (EPD-30) and f) 60 s (EPD-60) showing the different density of GO patches on PEO titania surface.

deposition method with PEO-EPD technique in this study, doesn't follow the typical EPD kinetics described by Hamaker's law [46]. This deviation from linearity is mainly attributed to the generation of gases, secondary PEO arcs and thickening of GO insulating layers at high voltage EPD process (PEO-EPD) [60]. Fig. 2 represents the optical images of GO deposition pattern with PEO-EPD process at 0, 7, 15, 30 and 60 s, which are denoted as EPD-0 (PEO control sample), EPD-7, EPD-15, EPD-30 and EPD-60, respectively.

Organic electrolyte (ethylene glycol) is known to help to reduce the gas formation during high voltage EPD process. However, a small addition of water is added to the electrolyte to generate micron-sized bubbles through hydrolysis at electrodes. These formed bubbles along with the secondary arc generation during high voltage EPD process would provide better control for deposition of GO patches with the desired coverage [60]. During PEO-EPD process, negatively charged GO flakes in the electrolyte were attracted to the PEO substrate (positive pole) driven by the electric force. Then, the deposition took place on the working electrode gradually. Fig. 2b shows the PEO control surface before GO deposition (EPD-0), while the deposition pattern after 7 s (EPD-7) is presented in Fig. 2c. By increasing the deposition time to 15 s, the formation of small bubbles partially impedes the attachment of GO flakes, while deposition continues to take place in the other zones. The most uniform pattern of GO deposition is presented in Fig. 2d, achievable within 15 s of the deposition process (EPD-15) that is accepted as optimal surface and condition. As previously mentioned, another factor involves in the current PEO-EPD process is "the secondary arc generation". Due to the sudden jump of cell voltage to over 400 V, as a result of alternative PEO process, secondary arcs were generated, which bombarded the surface and gradually disrupted the uniform deposition process. Here, after 30 s of PEO-EPD process, the formation of secondary arcs and gases, known as "high voltage EPD side reactions" [60] were intensified and resulted in the disruption of GO deposition process and formation of large-sized pores (Fig. 2e). Finally, after 1 min of PEO-EPD process, strong arcs and intensive gas formation completely ruined the coating and they left the surface with very large-sized holes (>200 μm diameter, evident in Fig. 2f).

To further reveal surface morphology and chemical composition of optimized PEO-GO substrate prepared by 15 s of PEO-EPD process, series of SEM and EDS images are presented in Fig. 3. Fig. 3a and b clearly show the presence of GO flakes on the blurry and dim zones of the image that partially are covering the PEO porous structure. Moreover, many open pores are still detectable in the image. Fig. 3c represents the FIB-SEM cross-section image of the sample from a random site with GO presence. As can be seen, the average PEO thickness is around 800 nm (EDS mapping of the cross-section also has been provided in the supplementary Fig. S4). EDS analysis confirmed the presence of C with more than 28 wt% in the cross-section (Fig. 3d). SEM images showed the presence of PEO pores ranging from 50 nm to 1 μm with an average spacing of 1.02 μm between the bigger pores. Moreover, the result of Raman intensity mapping of GO for 100 μm ×100 μm area of PEO-GO sample with steps of 10 μm (Fig. 3e) showed GO sheets covered around 66% of the PEO substrate (also supplementary Fig. S2). Further pixel analysis of PEO-GO optical image with Image J software in Fig. 3f confirmed more than 57% of the surface was covered with GO (supplementary Fig. S3 and Table S1 for the pixel density calculation).

The results of surface topography and comparative surface profile analysis are presented in Fig. 4. Both 2 D and 3 D images for PEO surface before GO deposition (EPD-0) demonstrated the inhomogeneous presence of pores along the surface (Fig. 4a), while after GO deposition for 15 s (PEO-GO) many of these pores were covered with GO layers and a reduced number of pores was observable (Fig. 4b). On the other side, analysis of topography profile of surfaces in Fig. 4a and b revealed a significant increase of profile height both in X and Y directions as a result of further PEO treatment during PEO-EPD process. Moreover, the profile of the PEO surface was characterized by the arithmetic mean of profile roughness (Ra), root-mean square of profile roughness (Rq), and total height roughness (Rt) of 0.65, 0.83 and 4.82 μm, respectively. Whereas, for coated GO samples, these numbers were remarkably increased to 0.85, 1.05 and 6.69 μm correspondingly.

4.3. Compositional and mechanical characterization of fabricated PEO substrate decorated with GO (PEO-GO)

The XRD spectra for PEO (control) and PEO-GO after GO deposition for 15 s with PEO-EPD process (EPD-15) is depicted in Fig. 5a. Comparison between XRD patterns of standard peaks for anatase phase (JCPDS card No. 21–1272) and titanium standard (reproduced by JCPDS card, no. 65–3362) is confirming the formation of anatase on both PEO and PEO-GO samples. Particularly, diffraction peaks at 2θ values of 25.8°, 39.1° and 48.5° can be indexed to the (101), (112), and (200) planes of the anatase phase. These results are also consistent with the previous PEO surface XRD spectra analysis reported by Malinovschi et al. [61]. Moreover, a small shift towards the left side of the XRD spectra noticed after PEO-EPD process. Based on the literature, the observed shift towards lower 2θ values in the XRD spectra is associated with the expansion of TiO_2 lattice, which probably occurs during the high voltage PEO-EPD process [62].

It is worth mentioning that when the cell voltage during PEO treatment exceeds the breakdown voltage of the oxide layer, thousands of micro arcs are formed and hit the titanium surface.

These micro-arc discharges can increase the temperate to more than 4500 K and lead to local melting of the Ti outer surface [63]. The presence of electrolyte in the system would result in the rapid cooling of the surface in a very short period and favours the development of anatase and rutile phases [61]. Different studies suggested that the anatase phase is more beneficial for nucleation of HAp on Ti surface when it is compared to rutile phase [64]. As a result, it is expected that both PEO and PEO-EPD samples, which demonstrated anatase peaks in their XRD spectra would have suitable osseointegration properties.

On the other side, XRD spectroscopy is considered as a bulk analysis technique. Consequently, it is not able to reveal the corresponding feature peak for GO at 11° on the surface of the GO coated PEO substrate [65]. Therefore, other spectroscopy techniques such as Raman Spectroscopy is required to confirm the presence of GO over the surface.

To identify the presence of GO, Raman spectroscopy was utilized before and after GO deposition process (Fig. 5b). PEO substrate before PEO-EPD process is characterized with 4 peaks obtained at ~146, 390, 514 and 628 cm^{-1}, which were associated with the formation of the anatase phase over the oxide layer. The Raman spectrum of the PEO-GO confirmed the presence of two distinguished peaks at 1341 cm^{-1} and 1590 cm^{-1}, known as D and G bands for GO, respectively [66]. These peaks exhibit the successful introduction of GO to the PEO surface. The I_D/I_G value is known as "Intensity ratio" calculated after GO deposition is around 1.04, which is in the range of reported values in other similar experiments [67]. In general, G band is associated with phonon scattering from sp^2 C atoms that lays in range of ~1500–1600 cm^{-1}, while D peak confirms the presence of defects, impurities and disorientation in sp^3 bonded C atoms that change in the range of ~1200–1500 cm^{-1} [68]. Meanwhile, no peak was observable for Ti strip sample before the PEO process.

Measured contact angle (CA) values for pure titanium control sample as well as PEO and PEO-GO (EPD-15) are presented in Fig. 5c. In this experiment, Ti sample showedCA ~74°, while PEO control demonstrated better hydrophilicity as a result of engineered micro-nano structure introduced to the surface via PEO process (CA~ 63°). Moreover, After GO deposition, due to the presence of GO and the formation of bigger pores during PEO-EPD process, CA value dropped drastically to around 16°. The measured CA values for PEO (CA~63°) and PEO-GO (CA~16°) samples in this work are consistent with previous results for PEO (with CA~ 60°) and PEO covered with GO thin film (with CA~ 19°) reported in the similar study [22]. It is worth mentioning that high wettability of implant surface, plays an essential role in bone

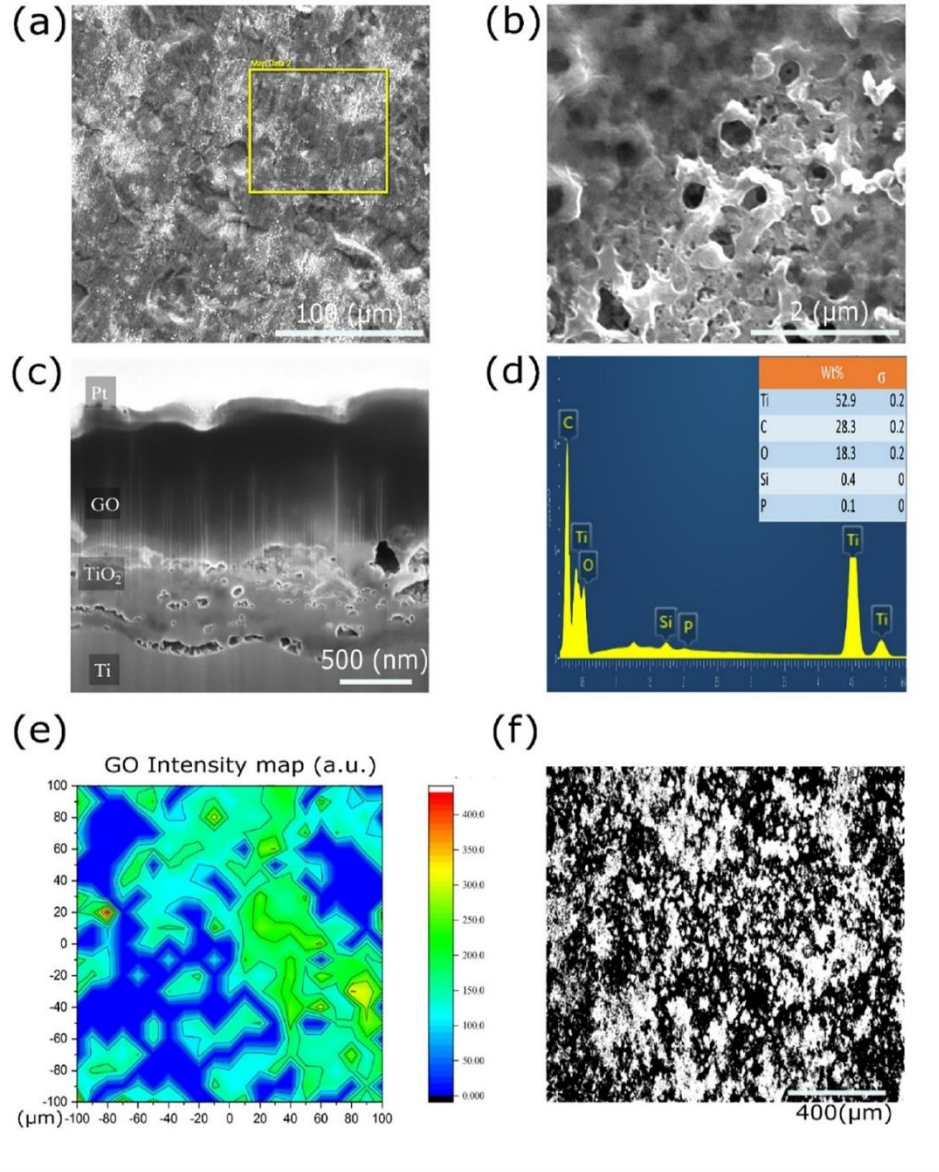

Fig. 3. SEM image of optimized PEO-GO sample (EPD-15) at a) low magnification, b) high magnification, c) PEO-GO sample cross-section, d) EDS results from PEO-GO cross-section, e) Raman GO intensity mapping of PEO-GO for 100 µm × 100 µm area, f) Converted PEO-GO (EPD-15) optical image to black-white colour for GO concentration calculation with Image J.

bonding and bioactivity of titanium bone implants [69,70]. Similar research conducted on a PEO sample covered with GO thin film with low CA values reported a dramatic increase in the proliferation and osseointegration abilities of the surface. Therefore, the fabricated PEO-GO samples in the current work with relatively high wettability are also expected to promote cell adhesion and proliferation [22].

The results obtained by Vickers micro-hardness test from PEO and PEO-GO substrates have been presented in Fig. 5d. The microhardness values for untreated Ti sample also have been provided for comparison. It is evident that PEO modification has improved the mechanical hardness of the Ti sample from 141 Hv to 154 Hv. The formation of anatase during PEO treatment can justify this outcome, wherein the presence of the oxide layer has been confirmed by XRD and Raman spectroscopy. Previous research reports also suggested that the formation of anatase can improve the micro-hardness of the PEO coatings [40,71]. After PEO-EPD treatment and GO deposition (EPD-15), hardness value depicts a further increase to ~171 Hv. A possible explanation for the observed results would be the generation of the secondary arcs during PEO-EPD process, which gives extra mechanical strength to the oxide layer [50,72]. It's well known that the increase in the PEO treatment duration results in the thickening of the oxide layer. As a result, the mechanical hardness of the coating is improved [73]. However, the lower

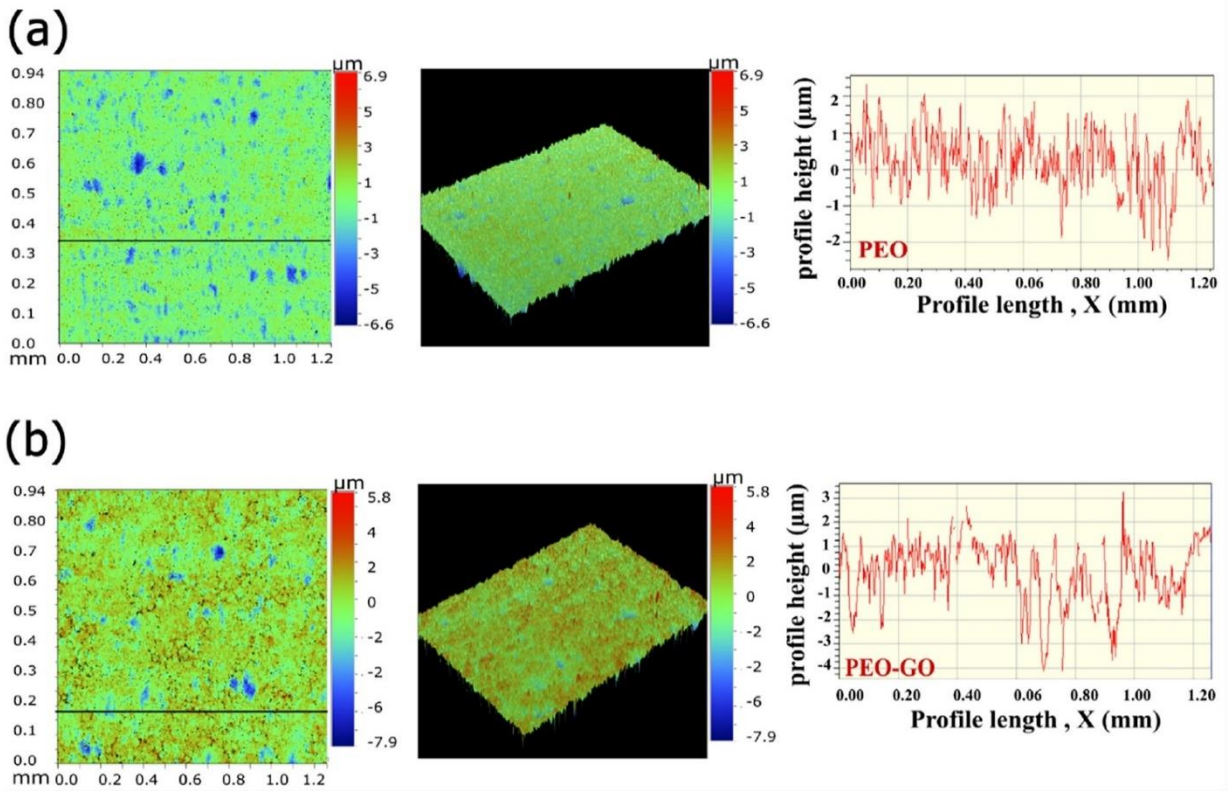

Fig. 4. Comparative image of 2D and 3D images and cross-sectional surface profile graphs of PEO and PEO-GO surface obtained by optical profilometry: a) Surface morphology of PEO sample (EPD-0), b) Surface morphology of PEO-GO sample (EPD-15).

electrical conductivity of the oxide layer on the PEO substrate would interfere with the successful deposition of GO sheets on the PEO substrate in the subsequent PEO-EPD process. For that reason, the initial PEO process in this research only performed for one 1 min to form a thin oxide layer with around 800 nm thickness. This PEO duration guaranteed the total coverage of Ti-surface with the desired micro-nano morphology required for the osseointegration improvement. The thinner PEO oxide layer thickness on our samples explains the observed lower microhardness values for the fabricated samples compared to the previous studies [61,74]. Finally, no vulnerability to brittle fracture observed over both treated samples which signifies strong bonding between the oxide layer and Ti substrate.

4.4. Bio-mineralization test

SEM, XRD and EDS analysis of PEO control (EPD-0) and GO modified sample, PEO-GO, after 21 days immersion in SBF solution are presented in Fig. 6. The SEM result showed the formation of small particles around 1.4 μm over the PEO-GO/SBF surface. The PEO control surface after SBF immersion (PEO/SBF) also showed smaller particles, which were deposited over the surface. XRD spectra of both PEO and PEO-GO samples after immersion showed some of the main characteristic peaks of hydroxyapatite corresponding to (100), (200), (002), (102), (112), (300), (301), (312) and (231) planes (based on ICDD 9–432 [75]), which are confirming the presence of HAp along with other salts on both PEO and PEO-GO samples after SBF immersion. Magnified XRD pattern of samples after mineralization are presented in the supplementary section, Fig. S5.

EDS analyses are also performed and their results confirmed the presence of Ca and P on both PEO and PEO-GO samples (with Ca/P molar ratio more than 2) after biomineralization test (Fig. 6d and e). Based on previous research, when Ca/P ratio is greater than 1.667, the mineralized materials form a biphasic mixture comprised of calcium phosphate apatite and $Ca(OH)_2$ [76]. It is worth mentioning that while appetite formation was evident on both treated samples after SBF test, no mineralization observed for Ti sample. The SBF is comprised of chemicals similar to the human plasma and the SBF mineralization test is considered as a powerful method to predict the in-vivo bioactivity of implant surface [77]. Therefore, the growth of apatite on both PEO and PEO-GO samples after immersion in SBF demonstrates their possible ability to improve osseointegration through the formation of interfacial bonds between bone cells and implant surface after implantation [78].

4.5. Antibacterial activity characterizations

The optical images of bacterial colonies on Petri dishes after recovery from PEO and PEO-GO substrates and further cultivation are presented in Figs. 7a–f. From photographs, it is apparent that the number of colonies for both *E. coli* and *S. aureus* bacteria is substantially decreased after direct contact with GO-deposited substrates (EPD-15). Particularly *S. aureus* cell growth was completely inhibited on PEO-GO surface, which implies that the substrate displays a high antibacterial activity

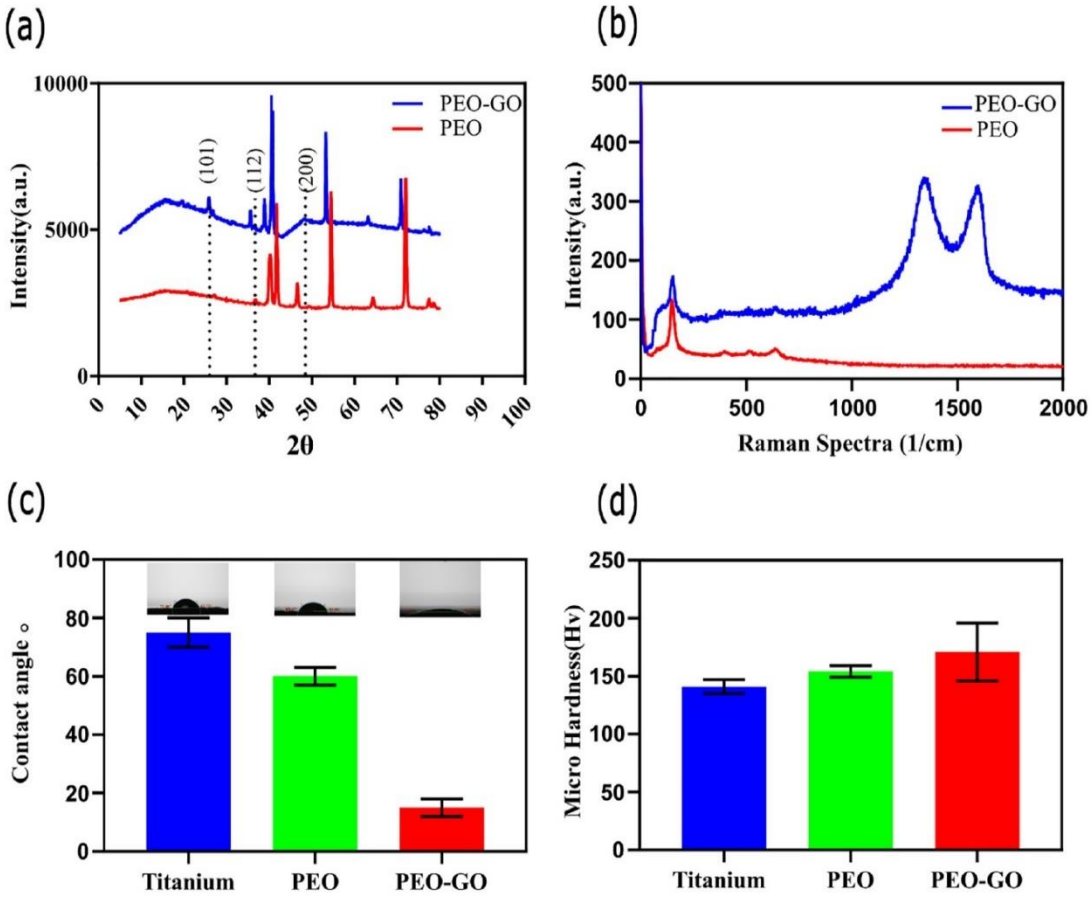

Fig. 5. Comparative chemical, mechanical, interfacial, and surface analysis of PEO control (EPD-0) and PEO-GO (EPD-15) after GO deposition: a) XRD graphs, b) Raman graphs, c) Contact angle measurement, d) Micro hardness test.

against this bacterium. A relative bacteria cell viability over different samples are reported in Fig. 7g and h. These results showed no notable antimicrobial activity for CTRL samples (Ti), while PEO-GO substrates did inactivate 79(±11)% of *E. coli* bacteria ($p<0.01$). Moreover, as mentioned above, no viable *S. aureus* was eluted from PEO-GO ($p<0.01$), which demonstrates a high vulnerability of *S. aureus* bacteria to the GO deposited substrate. On the other hand, PEO substrate showed some extent of antibacterial activity against *S. aureus* (I (%) = 52(± 17)%, $p<0.05$), while no effect was found against *E. coli*. Similar studies on the antibacterial assessment of modified PEO samples also point out that the modified PEO samples may only show the antibacterial activity against a particular type of bacteria, while they can be ineffective against other types of bacteria [79]. Moreover, the higher sensitivity of gram-positive bacteria such as *S. aureus* to the GO coated surface compared with *E. coli* bacterium was also reported by Akhavan et al. [80]. The plausible explanation for higher resistance of *E. coli* bacteria against mechanical damage induced by GO sheets could be attributed to the presence of a protective outer membrane in gram-negative *E. coli* bacteria. This membrane is instead absent in gram-positive *S. aureus* bacteria. This could make gram-positive bacteria more vulnerable to direct contact interaction with GO sheets [80]. Based on the literature data, GO sheets demonstrate high antibacterial ability against different types of bacteria such as *E. coli, S. aureus and P. aeruginosa* [81,82]. Recently, Sun et al. [22] reported a similar antibacterial activity for GO coated PEO samples against *S. mutans* with a high antibacterial ratio of 90.81%. This finding also highlights the superior antibacterial ability of GO/PEO mixture against gram-positive bacteria. Among different proposed mechanisms associated with the antimicrobial ability of GO, mechanical damage of bacteria membrane via direct contact with GO sharp edges and the generation of reactive oxygen species triggered by GO oxidative stress and charge transfer are more plausible scenarios [83,84]. Overall, the fabricated PEO-GO samples in this work demonstrated a very high antibacterial activity against *E. coli* and *S. aureus* bacteria, which makes the PEO-EPD process a suitable approach for fabrication of the next generation of antimicrobial GO-coated implants.

5. Conclusion

In summary, the fabrication of PEO titania surface with partially decorated GO sheets was achieved by combined PEO-EPD process. The optimization of PEO-EPD process was carried out in different time interval between 0 s to 1 min, showing the most desirable coverage of GO at 15 s (sample EPD-15), which was confirmed with optical microscopy and optical profilometry. Raman spectroscopy showed the presence of D and G bands, confirming the deposition of GO over the PEO matrix. XRD analysis demonstrated the formation of anatase titania phase

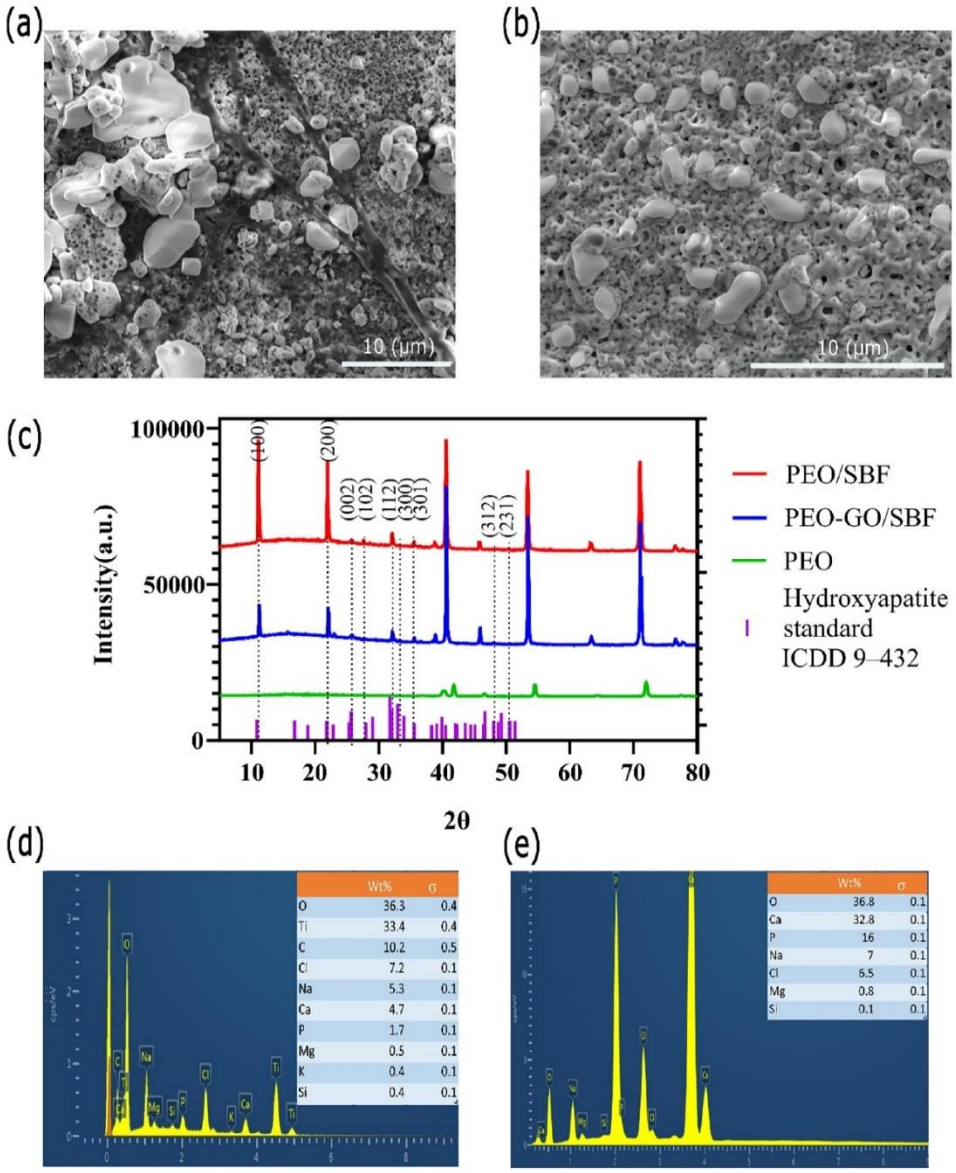

Fig. 6. SEM image of samples after SBF test: a) PEO-GO, b) PEO), c) XRD spectra of different samples before and after SBF mineralization test, d) corresponding EDS analysis for PEO-GO/SBF, e) corresponding EDS analysis for PEO/SBF.

after the PEO treatment. Vickers hardness test showed an improvement in hardness of the coating after PEO and a further increase of hardness values after PEO-EPD treatment with 154 Hv and 171 Hv, respectively. The calculated hardness values for bare titanium surface was around ~141 Hv. Moreover, CA measurements showed a notable decrease in values to ~16° after PEO-EPD treatment. SBF mineralization test carried out and confirmed the presence of HAp on both PEO and GO coated PEO samples. The antibacterial study showed significant antibacterial activity of GO decorated PEO surface for both bacteria compared to control, with the antibacterial rate of ~80% for *E.coli* and ~100% for *S.aureus*. In short, PEO-EPD process showed a significant potential for fabrication of controllable GO coating on the PEO titania substrate. This can address both osseointegration and antimicrobial performance of the titanium implants and open a new door in the application of graphene derivatives in bone-implant industries.

Author statement

Arash Mazinani: most investigation, methodology data processing, writing first draft

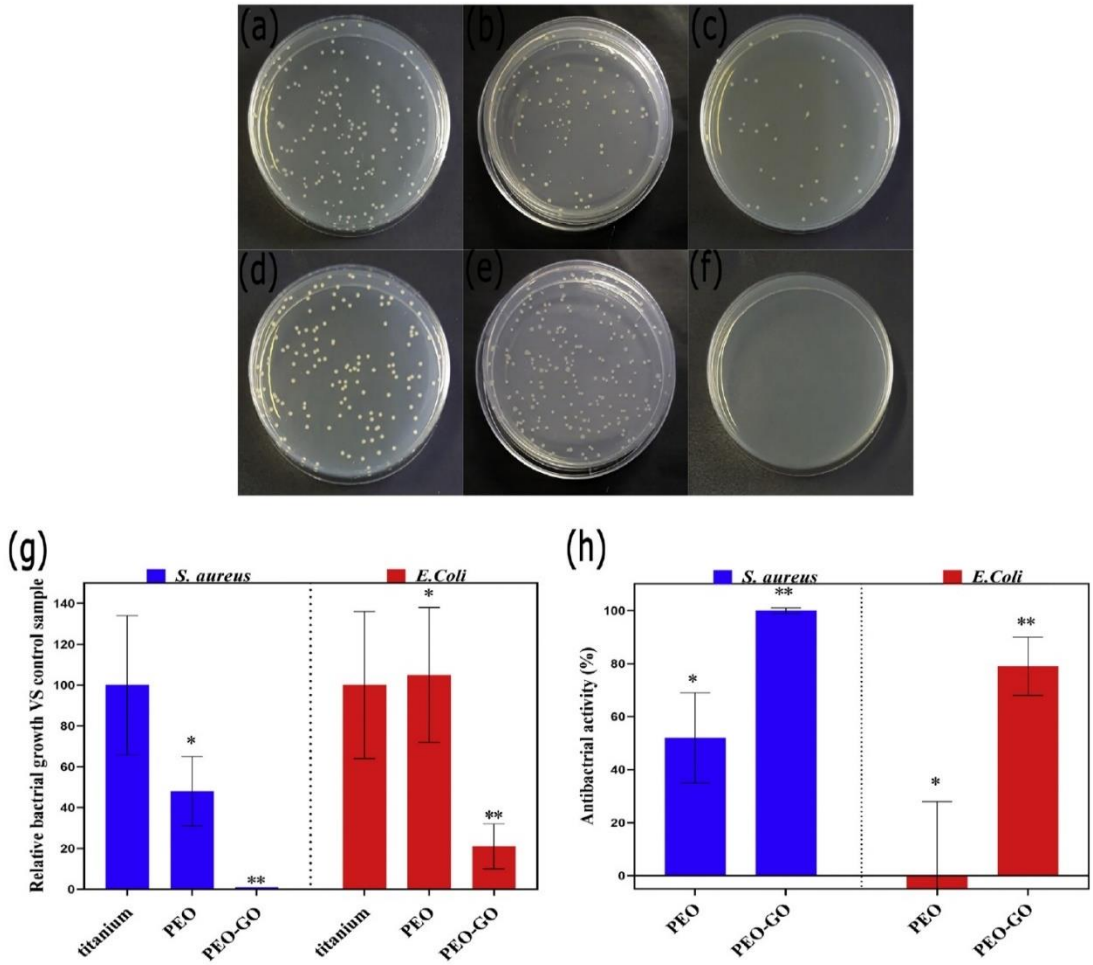

Fig. 7. Analysis of bacterial viability on control, PEO and PEO-GO (EPD-15) substrates. Photographs of *E. coli* colonies on agar Petri dishes after elution from: a) CTRL (Titanium) sample, b) PEO, c) PEO-GO substrate; photographs of *S. aureus* colonies after elution from d) CTRL (Ti) sample, e) PEO, f) PEO-GO substrate; g) relative bacterial growth in contact with different samples; h) corresponding antibacterial activity of different samples. $^{*}p < 0.05$; $^{**}p < 0.01$ vs. control.

Md Julker Nine: co-supervisor, methodology, some data processing, Review & Editing
Roberto Chiesa: bacterial study, Review & Editing
Gabriele Candiani: bacterial study, Review & Editing
Paolo Tarsini: bacterial study, Review & Editing
Tran Thanh Tung: some data processing, Review & Editing
Dusan Losic: principal supervisor, Review & Editing, Resources, Submission

Declaration of Competing Interest

There are no conflicts to declare.

Acknowledgements

The authors acknowledge the funding by the ARC Research Hub for Graphene Enabled Industry Transformation, (IH150100003). The authors thank the University of Adelaide, school of chemical engineering and advanced materials and department of chemistry, materials and chemical engineering "G. Natta", Polytechnic University of Milan and Professor Reza Ghomashchi for their support in this project.

Appendix A. Supplementary data

Supplementary data to this article can be found online at https://doi.org/10.1016/j.matdes.2020.109443.

References

[1] L. De Nardo, et al., Electrochemical surface modifications of titanium and titanium alloys for biomedical applications. Coatings for Biomedical Applications, Woodhead Publishing, 2012 106–142.
[2] C.N. Elias, et al., Biomedical applications of titanium and its alloys, JOM 60 (3) (2008) 46–49.
[3] S. Maher, et al., Engineered titanium implants for localized drug delivery: recent advances and perspectives of Titania nanotubes arrays, Expert Opinion on Drug Delivery 15 (10) (2018) 1021–1037.
[4] V.D. Bui, et al., Antibacterial coating of Ti-6Al-4V surfaces using silver nano-powder mixed electrical discharge machining, Surf. Coat. Technol. 383 (2020), 125254.
[5] T. Albrektsson, et al., Osseointegrated titanium implants. Requirements for ensuring a long-lasting, direct bone-to-implant anchorage in man, Acta Orthop. Scand. 52 (2) (1981) 155–170.
[6] B. Klinge, et al., Peri-implant diseases, Eur. J. Oral Sci. 126 (S1) (2018) 88–94.
[7] T. Hanawa, Titanium–Tissue Interface Reaction and Its Control With Surface Treatment, Front. Bioeng. Biotechnol. 7 (170) (2019).
[8] E. Marin, et al., Effect of etching on the composition and structure of anodic spark deposition films on titanium, Mater. Des. 108 (2016) 77–85.
[9] E. Farber, et al., Development of the titanium meshes by selective laser melting and chemical etching for using as medical implants, Materials Today: Proceedings 30 (2020) 746–751.
[10] J.C.M. Souza, et al., Nano-scale modification of titanium implant surfaces to enhance osseointegration, Acta Biomater. 94 (2019) 112–131.
[11] C. Hallgren, et al., An in vivo study of bone response to implants topographically modified by laser micromachining, Biomaterials 24 (5) (2003) 701–710.
[12] D. Losic, et al., Titania nanotube arrays for local drug delivery: recent advances and perspectives, Expert Opin. Drug Delivery 12 (1) (2015) 103–127.
[13] E. Al-Hassani, F. Al-Hassani, M. Najim, Effect of polymer coating on the osseointegration of CP-Ti dental implant, 1968, 2018 030022 1.
[14] M. Montazeri, et al., Investigation of the voltage and time effects on the formation of hydroxyapatite-containing titania prepared by plasma electrolytic oxidation on Ti–6Al–4V alloy and its corrosion behavior, Appl. Surf. Sci. 257 (16) (2011) 7268–7275.
[15] I.d.S.V. Marques, et al., Biomimetic coatings enhance tribocorrosion behavior and cell responses of commercially pure titanium surfaces, Biointerphases 11 (3) (2016), 031008.
[16] S. Yang, et al., Hydrothermal treatment of Ti surface to enhance the formation of low crystalline hydroxyl carbonate apatite, Biomater. Res. 19 (2015) 4–6.
[17] E. Sandrini, et al., In vitro assessment of the osteointegrative potential of a novel multiphase anodic spark deposition coating for orthopaedic and dental implants, J. Biomed. Mater. Res. B Appl. Biomater. 73 (2) (2005) 392–399.
[18] W. Mu, Y. Han, Characterization and properties of the MgF2/ZrO2 composite coatings on magnesium prepared by micro-arc oxidation, Surf. Coat. Technol. 202 (17) (2008) 4278–4284.
[19] L. Snizhko, et al., Anodic processes in plasma electrolytic oxidation of aluminium in alkaline solutions, Electrochim. Acta 49 (13) (2004) 2085–2095.
[20] D.V. Mashtalyar, et al., Hard wearproof PEO-coatings formed on Mg alloy using TiN nanoparticles, Appl. Surf. Sci. 503 (2020), 144062.
[21] S.V. Gnedenkov, et al., Formation and properties of composite coatings on aluminum alloys, Russ. J. Inorg. Chem. 62 (1) (2017) 1–11.
[22] N. Sun, et al., Graphene oxide-coated porous titanium for pulp sealing: an antibacterial and dentino-inductive restorative material, J. Mater. Chem. B 8 (26) (2020) 5606–5619.
[23] M.J. Nine, et al., Graphene: a multipurpose material for protective coatings, J. Mater. Chem. A 3 (24) (2015) 12580–12602.
[24] S.X. Nguyen, et al., Heterojunction of graphene and titanium dioxide nanotube composites for enhancing photocatalytic activity, J. Phys. D. Appl. Phys. 51 (26) (2018), 265304.
[25] V. Singh, et al., Graphene based materials: Past, present and future, Prog. Mater. Sci. 56 (8) (2011) 1178–1271.
[26] D. Losic, D. Tran, S. Kabiri, Composite graphene-based material, 2018 Google Patents.
[27] Z.Q. Wen, et al., Morphology-controlled MnO2–graphene oxide–diatomaceous earth 3-dimensional (3D) composites for high-performance supercapacitors, Dalton Trans. 45 (3) (2016) 936–942.
[28] P. Akshay, et al., Portable and efficient graphene-oxide based multistage filtration unit for water purification, Materials Today: Proceedings 26 (2020) 2344–2350.
[29] X. Wu, et al., Graphene oxide as an efficient antimicrobial nanomaterial for eradicating multi-drug resistant bacteria in vitro and in vivo, Colloids Surf. B: Biointerfaces 157 (2017) 1–9.
[30] M.J. Nine, et al., Interlayer growth of borates for highly adhesive graphene coatings with enhanced abrasion resistance, fire-retardant and antibacterial ability, Carbon 117 (2017) 252–262.
[31] S. Liu, et al., Antibacterial Activity of Graphite, Graphite Oxide, Graphene Oxide, and Reduced Graphene Oxide: Membrane and Oxidative Stress, ACS Nano 5 (9) (2011) 6971–6980.
[32] O. Akhavan, E. Ghaderi, A. Esfandiar, Wrapping Bacteria by Graphene Nanosheets for Isolation from Environment, Reactivation by Sonication, and Inactivation by Near-Infrared Irradiation, J. Phys. Chem. B 115 (19) (2011) 6279–6288.
[33] S. Szunerits, R. Boukherroub, Antibacterial activity of graphene-based materials, J. Mater. Chem. B 4 (43) (2016) 6892–6912.
[34] N. Dubey, et al., Graphene: A Versatile Carbon-Based Material for Bone Tissue Engineering, Stem Cells Int. 2015 (2015) 12.
[35] M. Diba, et al., Electrophoretic deposition of graphene-related materials: A review of the fundamentals, Prog. Mater. Sci. 82 (Supplement C) (2016) 83–117.
[36] Y. Zeng, et al., Graphene oxide/hydroxyapatite composite coatings fabricated by electrochemical deposition, Surf. Coat. Technol. 286 (Supplement C) (2016) 72–79.
[37] H. Ji, H. Sun, X. Qu, Antibacterial applications of graphene-based nanomaterials: Recent achievements and challenges, Adv. Drug Deliv. Rev. 105 (Part B) (2016) 176–189.
[38] Z. Changhong, et al., The promising application of graphene oxide as coating materials in orthopedic implants: preparation, characterization and cell behavior, Biomed. Mater. 10 (1) (2015), 015019.
[39] V.C. Anitha, et al., Enhanced electrochemical performance of morphology-controlled titania-reduced graphene oxide nanostructures fabricated via a combined anodization-hydrothermal process, RSC Adv. 6 (15) (2016) 12571–12583.
[40] W. Liu, et al., Effects of graphene nanosheets on the ceramic coatings formed on Ti6Al4V alloy drill pipe by plasma electrolytic oxidation, J. Alloys Compd. 789 (2019) 996–1007.
[41] S. Singh, et al., Corrosion behaviour of plasma sprayed graphene nanoplatelets reinforced hydroxyapatite composite coatings in simulated body fluid, Ceram. Int. 46 (2020) 13539–13548.
[42] Y. Zuo, et al., Effect of graphene oxide additive on tribocorrosion behavior of MAO coatings prepared on Ti6Al4V alloy, Appl. Surf. Sci. 480 (2019) 26–34.
[43] Y. Gao, et al., Microstructure and Properties of Graphene Oxide-doped TiO2 Coating on Titanium by Micro Arc Oxidation, J. Wuhan Univ. Technol. 33 (6) (2018) 1524–1529.
[44] W. Yang, et al., Preparation of MAO coatings doped with graphene oxide, Surf. Eng. 33 (10) (2017) 739–743.
[45] A. Chavez-Valdez, M.S.P. Shaffer, A.R. Boccaccini, Applications of Graphene Electrophoretic Deposition. A Review, J. Phys. Chem. B 117 (6) (2013) 1502–1515.
[46] L. Besra, M. Liu, A review on fundamentals and applications of electrophoretic deposition (EPD), Prog. Mater. Sci. 52 (1) (2007) 1–61.
[47] X. Chen, et al., Electrochemical behaviour of EPD synthesized graphene coating on titanium alloys for orthopedic implant application, Procedia CIRP 71 (2018) 322–328.
[48] A. Bordbar Khiabani, et al., Electrophoretic deposition of graphene oxide on plasma electrolytic oxidized-magnesium implants for bone tissue engineering applications, Materials Today: Proceedings 5 (7, Part 3) (2018) 15603–15612.
[49] S.A. Ulasevich, et al., Deposition of hydroxyapatite–incorporated TiO2 coating on titanium using plasma electrolytic oxidation coupled with electrophoretic deposition, RSC Adv. 6 (67) (2016) 62540–62544.
[50] X. Nie, A. Leyland, A. Matthews, Deposition of layered bioceramic hydroxyapatite/TiO2 coatings on titanium alloys using a hybrid technique of micro-arc oxidation and electrophoresis, Surf. Coat. Technol. 125 (1) (2000) 407–414.
[51] A. S, et al., The effect of graphite particle size on the corrosion and wear behaviour of the PEO-EPD coating fabricated on commercially pure zirconium, Surf. Coat. Technol. 363 (2019) 301–313.
[52] D.C. Marcano, et al., Improved synthesis of graphene oxide, ACS Nano 4 (8) (2010) 4806–4814.
[53] N.K. Kuromoto, R.A. Simão, G.A. Soares, Titanium oxide films produced on commercially pure titanium by anodic oxidation with different voltages, Mater. Charact. 58 (2) (2007) 114–121.
[54] O.A. Galvis, et al., Formation of grooved and porous coatings on titanium by plasma electrolytic oxidation in H2SO4/H3PO4 electrolytes and effects of coating morphology on adhesive bonding, Surf. Coat. Technol. 269 (2015) 238–249.
[55] S. Aliasghari, P. Skeldon, G.E. Thompson, Plasma electrolytic oxidation of titanium in a phosphate/silicate electrolyte and tribological performance of the coatings, Appl. Surf. Sci. 316 (2014) 463–476.
[56] I. Ali, et al., One-step electrochemical synthesis of graphene oxide-TiO2 nanotubes for improved visible light activity, Opt. Mater. Express 7 (5) (2017) 1535–1546.
[57] T. Kokubo, H. Takadama, How useful is SBF in predicting in vivo bone bioactivity? Biomaterials 27 (15) (2006) 2907–2915.
[58] P. Richiez-Nieves, et al., A Sheep Model for the Osseointegration of PEO-treated Gamma Titanium Aluminide, Eur. J. Dental Oral Health 1 (2020).
[59] M. Echeverry-Rendón, et al., Osseointegration improvement by plasma electrolytic oxidation of modified titanium alloys surfaces, J. Mater. Sci. Mater. Med. 26 (2) (2015) 72.
[60] M. Diba, et al., Electrophoretic deposition of graphene-related materials: A review of the fundamentals, Prog. Mater. Sci. 82 (2016) 83–117.
[61] V. Malinovschi, et al., Obtaining and characterization of PEO layers prepared on CP-Ti in sodium dihydrogen phosphate dihydrate acidic electrolyte solution, Surf. Coat. Technol. 375 (2019) 621–636.
[62] S. Shalini, et al., Effect of Na doping on structure, morphology and properties of hydrothermally grown one dimensional TiO2 nanorod structures, J. Mater. Sci. Mater. Electron. 28 (4) (2017) 3500–3508.
[63] Hussein, R.O., et al., 2010: p. 105203-105216.
[64] M. Uchida, et al., Structural dependence of apatite formation on titania gels in a simulated body fluid, J. Biomed. Mater. Res. Part A 64 (1) (2003) 164–170.
[65] J. Qiu, et al., Combination types between graphene oxide and substrate affect the antibacterial activity, Bioactive Materials 3 (3) (2018) 341–346.
[66] Q. Zhou, et al., Bioactivity of periodontal ligament stem cells on sodium titanate coated with graphene oxide, Sci. Rep. 6 (2016) 19343.
[67] U. Kiran, et al., Graphene Coating on Copper by Electrophoretic Deposition for Corrosion Prevention, Coatings 7 (2017).
[68] A. Janković, et al., Graphene-based antibacterial composite coatings electrodeposited on titanium for biomedical applications, Prog. Org. Coat. 83 (2015) 1–10.
[69] A.L. Hook, et al., Combinatorial discovery of polymers resistant to bacterial attachment, Nat. Biotechnol. 30 (9) (2012) 868–875.
[70] T. Merian, J.M. Goddard, Advances in nonfouling materials: perspectives for the food industry, J. Agric. Food Chem. 60 (12) (2012) 2943–2957.

[71] L. Fang, et al., Effects of oxidation time on microstructure and corrosion resistance of micro-arc oxidation film on aluminum alloy, Fenmo Yejin Cailiao Kexue yu Gongcheng/Materials Science and Engineering of Powder Metallurgy 23 (5) (2018) 503–510.
[72] Y. Jiang, Y. Bao, K. Yang, Composite Coatings Combining PEO Layer and EPD Layer on Magnesium Alloy, Magnesium Technology, Springer 2011, pp. 543–546.
[73] X. Ma, et al., A model describing the growth of a PEO coating on AM50 Mg alloy under constant voltage mode, Electrochim. Acta 251 (2017) 461–474.
[74] E. Matykina, et al., In vitro corrosion performance of PEO coated Ti and Ti6Al4V used for dental and orthopaedic implants, Surf. Coat. Technol. 307 (2016) 1255–1264.
[75] M. haghbin nazarpak, et al., Effect of Gamma Irradiation on Structural and Biological Properties of a PLGA-PEG-Hydroxyapatite Composite, Sci. World J. 2014 (2014).
[76] S. Raynaud, et al., Calcium phosphate apatites with variable Ca/P atomic ratio I. Synthesis, characterisation and thermal stability of powders, Biomaterials 23 (4) (2002) 1065–1072.
[77] X. Liu, C. Ding, Z. Wang, Apatite formed on the surface of plasma-sprayed wollastonite coating immersed in simulated body fluid, Biomaterials 22 (14) (2001) 2007–2012.
[78] M. Mehrali, et al., Electrophoretic deposition of calcium silicate–reduced graphene oxide composites on titanium substrate, J. Eur. Ceram. Soc. 36 (2) (2016) 319–332.
[79] V.A. Ponomarev, et al., Ag(Pt) nanoparticles-decorated bioactive yet antibacterial Ca- and P-doped TiO2 coatings produced by plasma electrolytic oxidation and ion implantation, Appl. Surf. Sci. 516 (2020), 146068.
[80] O. Akhavan, E. Ghaderi, Toxicity of Graphene and Graphene Oxide Nanowalls Against Bacteria, ACS Nano 4 (10) (2010) 5731–5736.
[81] R. Silva-Leyton, et al., Polyethylene/graphene oxide composites toward multifunctional active packaging films, Compos. Sci. Technol. 184 (2019), 107888.
[82] H. Ji, H. Sun, X. Qu, Antibacterial applications of graphene-based nanomaterials: Recent achievements and challenges, Adv. Drug Deliv. Rev. 105 (2016) 176–189.
[83] F. Perreault, et al., Antimicrobial Properties of Graphene Oxide Nanosheets: Why Size Matters, ACS Nano 9 (7) (2015) 7226–7236.
[84] N. Yadav, et al., Graphene Oxide-Coated Surface: Inhibition of Bacterial Biofilm Formation due to Specific Surface–Interface Interactions, ACS Omega 2 (7) (2017) 3070–3082.

Supplementary Information

Figure S1. PEO control sample EDS analysis.

Figure S2. Raman Intensity mapping of GO for PEO-GO sample (EPD-15) with analysis area of 100 µm * 100 µm and steps of 10 µm and corresponding GO coverage percentage.

Figure S3. Converted PEO-GO (EPD-15) image to black-white colour.

Figure S4. EDS mapping of sample PEO-GO (EPD-15) cross section: a) SEM real image, b) corresponding maps for Carbon, c) corresponding maps for Platinum coating, d) corresponding maps for Oxygen, e) corresponding maps for Titanium, f) corresponding maps for Silicon, g) FIB-SEM cross section images showing both coated and non-coated sites of PEO-GO sample.

Figure S5. XRD Spectra of samples after SBF mineralization for: a) whole regions (2θ range from 2 to 80), b) magnified spectra for Region 1 (2θ range from 24 to 38), c) magnified spectra for Region 2 (2θ range from 45 to 51).

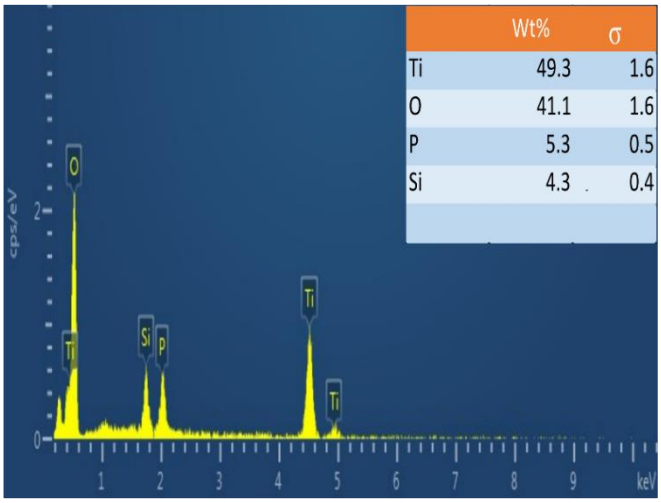

Figure S1. PEO control sample EDS analysis.

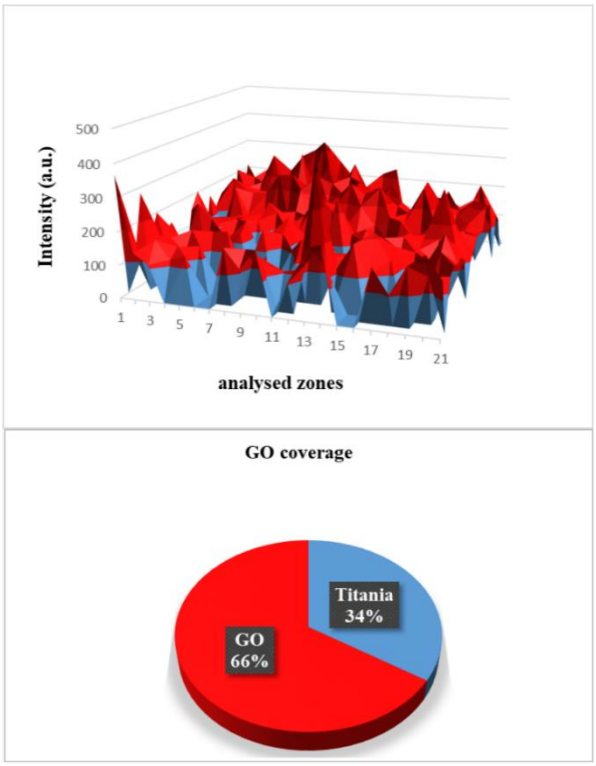

Figure S2. Raman Intensity mapping of GO for PEO-GO sample (EPD-15) with analysis area of 100 µm * 100 µm and steps of 10 µm and corresponding GO coverage percentage.

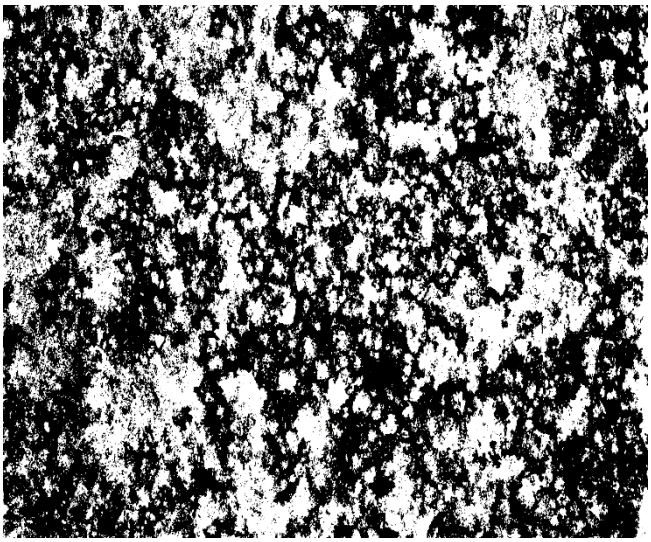

Figure S3. Converted PEO-GO (EPD-15) image to black-white colour.

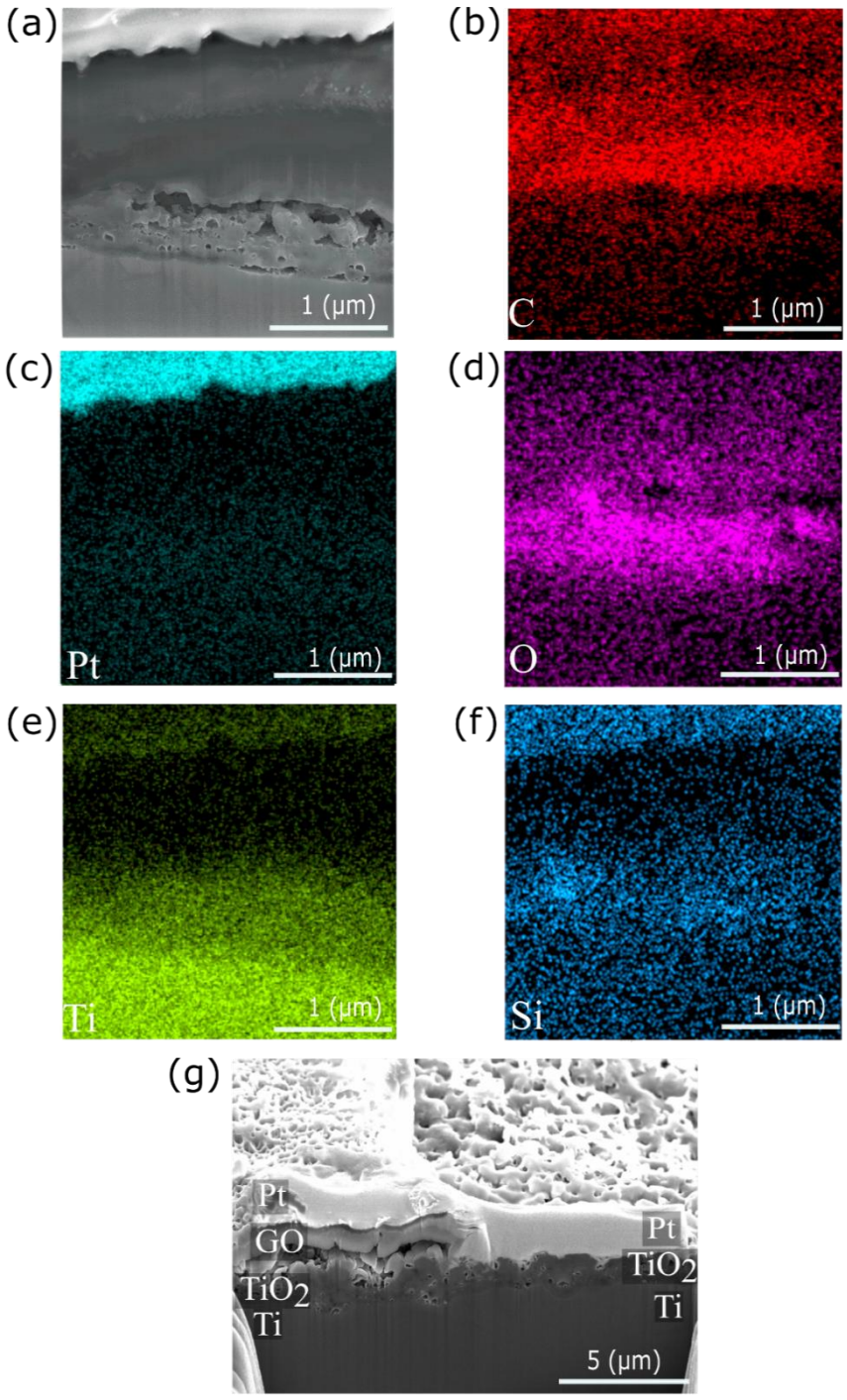

Figure S4. EDS mapping of sample PEO-GO (EPD-15) cross section: a) SEM real image, b) corresponding maps for Carbon, c) corresponding maps for Platinum coating, d) corresponding maps for Oxygen, e) corresponding maps for Titanium, f)

corresponding maps for Silicon, g) FIB-SEM cross section images showing both coated and non-coated sites of PEO-GO sample.

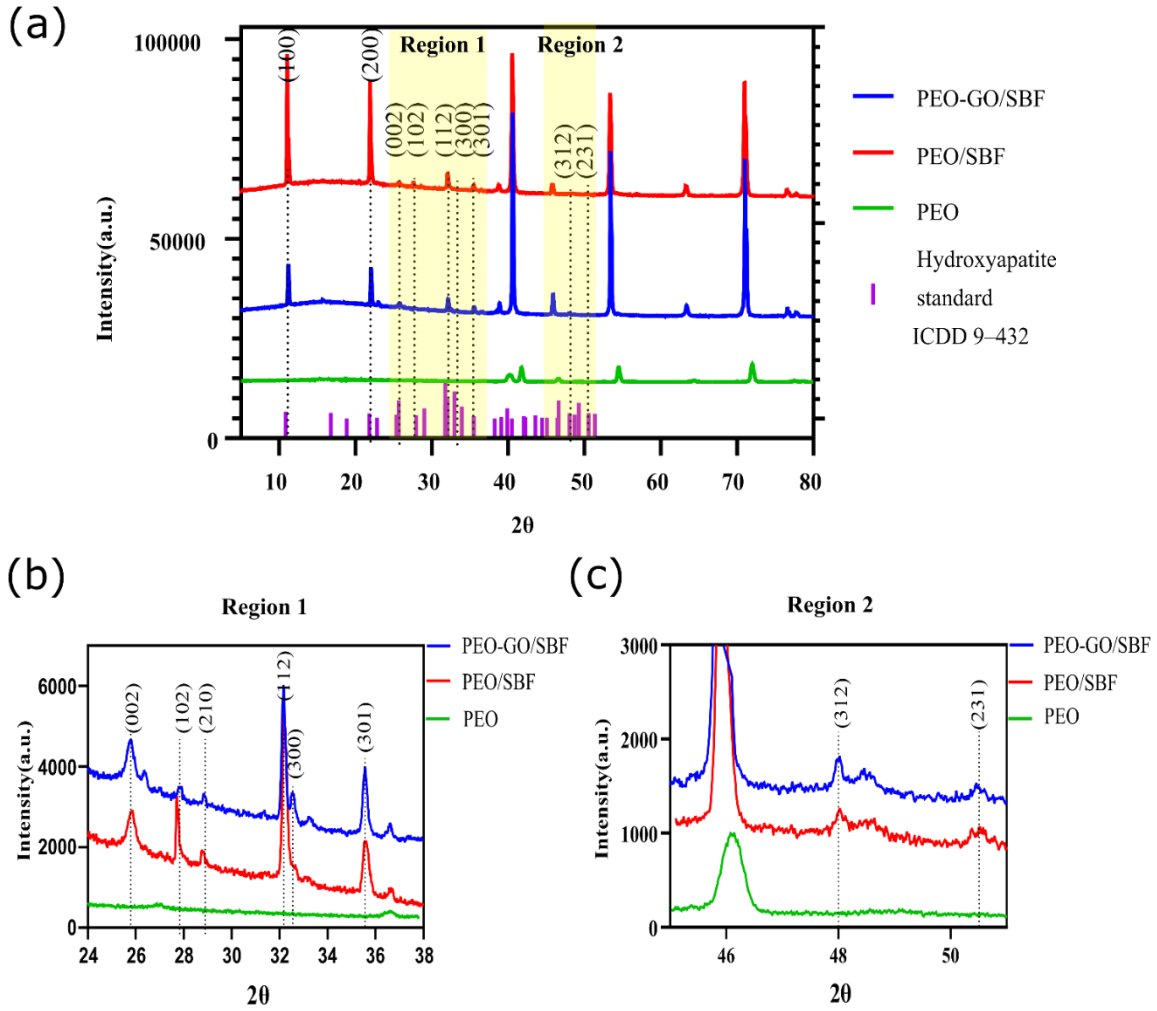

Figure S5. XRD Spectra of samples after SBF mineralization for: a) whole regions (2θ range from 2 to 80), b) magnified spectra for Region 1 (2θ range from 24 to 38), c) magnified spectra for Region 2 (2θ range from 45 to 51).

Table S1. Pixel analysis of PEO-GO deposition pattern and GO area density calculation with "Image J" software.

Materials and colour	Area (pixels) Total : 1,414,930	Area Density
Black colour (GO)	814603	57%
White colour (titania)	600327	43%

Chapter 7

Comparative antibacterial activity of 2D materials coated on the porous-titania

In this chapter, the potential application of 2D materials in the antibacterial development of titania PEO porous surface was investigated. Three well-known 2D flakes of hBN, GO, and MXene were deposited on PEO treated substrate in different concentrations. Partial deposition of flakes was essential to expose PEO porous structure required for bio integration improvement, which was achieved via the drop-casting process. The result demonstrated outstanding antibacterial activity of MXene deposited PEO surface against gram-positive bacteria (*S. aureus*) with around 95 % efficiency. While the fabricated samples were less effective against *E.coli* with maximum inactivation efficiency of around 18%, obtained for the hBN deposited PEO sample.

This chapter has been published as:

Arash Mazinani, Hadi Rastin, Md Julker Nine, James Lee, Alexandra Tikhomirova, Tran Thanh Tung, Reza Ghomashchi, Stephen Kidd, Sarah Vreugde, Dusan Losic.

(doi.org/10.1039/D1TB01122G)

Statement of Authorship

Title of Paper	Comparative antibacterial activity of 2D materials coated on the porous-titania
Publication Status	☑ Published ☐ Accepted for Publication ☐ Submitted for Publication ☐ Unpublished and Unsubmitted work written in manuscript style
Publication Details	Arash Mazinani, Md Julker Nine, James Lee, Alexandra Tikhomirova, Hadi Rastin, Tran Thanh Tung, Reza Ghomashchi, Stephen Kidd, Sarah Vreugde,Dusan Losic https://doi.org/10.1039/D1TB01122G

Name of Principal Author (Candidate)	Arash Mazinani		
Contribution to the Paper	Conceptualization,Structure of Manuscript,Original draft		
Overall percentage (%)	70%		
Certification:	This paper reports on original research I conducted during the period of my Higher Degree by Research candidature and is not subject to any obligations or contractual agreements with a third party that would constrain its inclusion in this thesis. I am the primary author of this paper.		
Signature		Date	21.05.2021

Co-Author Contributions

By signing the Statement of Authorship, each author certifies that:

i. the candidate's stated contribution to the publication is accurate (as detailed above);
ii. permission is granted for the candidate in include the publication in the thesis; and
iii. the sum of all co-author contributions is equal to 100% less the candidate's stated contribution.

Name of Co-Author	Prof Dusan Losic		
Contribution to the Paper	Conceptualization,resources, funding acquization,review, editing, supervision, submission		
Signature		Date	24 May 2021

Name of Co-Author	Dr Md Julker Nine		
Contribution to the Paper	selected investigation, editing and review, supervision		
Signature		Date	24/05/2021

Please cut and paste additional co-author panels here as required.

Name of Co-Author	Alexandra Tikhomirova
Contribution to the Paper	selected investigation, editing and review
Signature	Date: 24/5/2021

Please cut and paste additional co-author panels here as required.

Name of Co-Author	Hadi Rastin
Contribution to the Paper	selected investigation, editing and review
Signature	Date: 25/05/2021

Name of Co-Author	Dr Tran Thanh Tung
Contribution to the Paper	selected investigation, editing and review
Signature	Date: 24/5/2021

Name of Co-Author	Prof Reza Ghomashchi
Contribution to the Paper	selected investigation, editing and review
Signature	Date: 24-05-2021

Name of Co-Author	James Lee
Contribution to the Paper	selected investigation, editing and review
Signature	Date: 25/05/21

Name of Co-Author	Dr Stephen Kidd
Contribution to the Paper	selected investigation, editing and review
Signature	Date: 25 May 2021

Name of Co-Author	Sarah Vreugde
Contribution to the Paper	selected investigation, editing and review
Signature	Date: 01/07/2021

Journal of Materials Chemistry B

ROYAL SOCIETY OF CHEMISTRY

PAPER

View Article Online
View Journal | View Issue

Cite this: J. Mater. Chem. B, 2021, 9, 6412

Comparative antibacterial activity of 2D materials coated on porous-titania†

Arash Mazinani,[ab] Hadi Rastin,[ab] Md Julker Nine,[ab] James Lee,[c] Alexandra Tikhomirova,[c] Tran Thanh Tung,[ab] Reza Ghomashchi,[bd] Stephen Kidd,[c] Sarah Vreugde[e] and Dusan Losic *[ab]

Plasma electrolytic oxidation (PEO) is a well-established technique for the treatment of titanium-based materials. The formed titania-PEO surface can improve the osseointegration properties of titanium implants. Nevertheless, it can not address bacterial infection problems associated with bone implants. Recently, 2-dimensional (2D) materials such as graphene oxide (GO), MXene, and hexagonal boron nitride (hBN) have received considerable attention for surface modifications showing their antibacterial properties. In this paper, a comparative study on the effect of partial deposition of these three materials over PEO titania substrates on the antibacterial efficiency and bioactivity is presented. Their partial deposition through drop-casting instead of continuous film coating is propsed to simultaneously address both antibacterial and osseointegration abilities. Our results demonstrate the dose-dependent nature of the deposited antibacterial agent on the PEO substrate. GO–PEO and MXene–PEO samples showed the highest antibacterial activity with 70 (±2) % and 97 (±0.5) % inactivation of *S. aureus* colonies in the low concentration group, respectively. Furthermore, only samples in the higher concentration group were effective against *E. coli* bacteria with 18 (±2) % and 17 (±4) % decrease in numbers of colonies for hBN–PEO and GO–PEO samples, respectively. Moreover, all antibacterial samples demonstrated acceptable bioactivity and good biocompatibility, making them a considerable candidates for the next generation of antibacterial titanium implants.

Received 19th May 2021,
Accepted 19th July 2021

DOI: 10.1039/d1tb01122g

rsc.li/materials-b

1. Introduction

With the development of biomedical science, the need for the fabrication of bioactive implants with efficient antibacterial activity has become one of the most critical topics. Titanium and its alloys have been widely used for the fabrication of biomedical and dental implants worldwide.[1] This transition metal is well-known for its excellent biocompatibility, desirable mechanical strength, good corrosion resistance, and low specific weight.[2,3] Nonetheless, a considerable number of titanium-based implants are still failing to address infection challenges, and poor osseointegration remains problematic in many cases, which eventually leads to implant failure and increases the risk of implant revision.[4–8] The common practices employed to improve osseointegration properties of titanium surface in dental and orthopaedic fields are machining, etching, physical or chemical vapour deposition coating, hydrothermal treatment, thermal spray coating and plasma electrolytic oxidation (PEO).[7,9,10] PEO treatment is considered one of the popular electrochemical techniques similar to the anodisation process, which by means of plasma arc generation, can remarkably improve the mechanical and physicochemical properties of the treated surface, such as hardness, corrosion resistance and wear resistance.[11] However, the key feature that makes this technique so unique for the fabrication of biomedical implants is the formation of hierarchical micro–nano pores during the process.[12,13] The hierarchical surface morphology significantly increases the contact area between bone cell and implant required for bone–implant bonding and simultaneously offers a suitable micro-environment for differentiation and proliferation of cells.[12,13] Nevertheless, PEO treated samples still cannot properly address the infection challenge of the biomedical implants.[14] In order to improve the antibacterial properties of fabricated PEO and titania surface, different approaches such as the addition of silver and copper nanoparticles during the PEO/anodisation process,[15–18] deposition of antibacterial agents after the PEO process[14,19] or subsequent surface treatment of PEO

[a] School of Chemical Engineering and Advanced Materials, The University of Adelaide, Adelaide, SA 5005, Australia. E-mail: dusan.losic@adelaide.edu.au
[b] ARC Hub for Graphene Enabled Industry Transformation, The University of Adelaide, Adelaide, SA, Australia
[c] Department of Molecular and Biomedical Science, The University of Adelaide, Adelaide, SA, Australia
[d] School of Mechanical Engineering, The University of Adelaide, SA, Australia
[e] Department of Surgery-Otolaryngology Head and Neck Surgery, The University of Adelaide, Woodville South, Australia

† Electronic supplementary information (ESI) available: Fig. S1 provides the Raman mapping result of deposited 2D flakes. Fig. S2 presents the result of the MIC test for penicillin and gentamicin against *E. coli*. See DOI: 10.1039/d1tb01122g

View Article Online
Paper Journal of Materials Chemistry B

matrix[20] have been investigated. Among various strategies to enhance the antimicrobial activity of implants, the application of 2D materials (such as GO, MXene, *etc.*), due to their inherent antibacterial activity and high aspect ratios, have received a great deal of attention as antibacterial additives.[21] However, in the biomedical field, GO is considered the material of the current focus as it has demonstrated the highest antimicrobial activity against micro-organisms such as *Escherichia coli* (*E.coli*) compared with rGO, graphite, graphite oxide and graphene itself.[22] In addition to graphene, other 2D nanomaterials beyond graphene (2D NBG) such as transition metal carbides and carbonitrides (MXene), layered double hydroxides (LDHs), LAPONITE® (Lap), hexagonal boron nitride (hBN) and transition metal disulphide (TMD), *etc.* have been identified and explored, as a new solution for antibacterial coatings to combat drug-resistant bacteria for medical implants.[23–27] Inherent physical and chemical properties of the coatings govern the antibacterial potential of 2D materials. Parameters and factors such as shape, lateral size, orientation, concentration, number of layers, phase structure, exposure time, and cell type and surface functionalisation were found to control the antibacterial efficacy of 2D materials.[23,28] Nevertheless, the common mechanisms underlying the observed antimicrobial activity for these materials are physical and mechanical damaging, also known as "trapping" and "nano-knives" mechanisms, lipid extraction, oxidative stress-induced either by the formation of reactive oxygen species (ROS) or *via* direct electron and charge transfer.[28–30] Previous studies on the deposition of 2D materials over the PEO treated substrates were mainly paying attention into the formation of continuous film on the titania substrate. This method would devalue the advantage of porous PEO treated substrate by covering the substrate pores, which would be essential for osseointegration improvement.[31,32]

Herein, the antibacterial activity of three common types of 2D materials, including hBN, MXene, and GO, partially deposited on the porous PEO titania surface, are investigated. This study aims to understand and compare the antibacterial properties of the selected 2D materials (GO, hBN, MXene) at different low and high concentrations over PEO treated substrates.[33] Their concentrations are adjusted to provide partial deposition of their 2D sheets on the PEO surface and ensure some extent of PEO surface exposure for enhanced bone–implant integration, while the presence of 2D flakes would improve the antimicrobial activity of the substrate. Amongst different parameters associated with the antibacterial ability of 2D materials, this research focuses on the impact of different types and concentrations of 2D materials on their antimicrobial activity against *S. aureus* and *E. coli* strains. The results from this study provide valuable insights into the *in vitro* bioactivity, and antibacterial responses of these 2D materials to improve the performance of PEO modified Ti implants.

2. Experimental section

2.1. Materials

Ti-sheets with 99.9% purity were provided from Nilaco (Japan) with an average thickness of 1 mm; orthophosphoric acid (H_3PO_4), 85 wt% and potassium hydroxide (KOH) in pellet form was purchased from Chem Supply (South Australia), while sodium metasilicate pentahydrate $Na_2SiO_3{\cdot}5H_2O$ was obtained from Sigma-Aldrich Pty Ltd (Germany), pure Milli-Q water with 18.2 MΩ cm resistivities was purified by EMD Millipore Corporation, Billerica machine. Dulbecco's Modified Eagle Medium (DMEM) was supplied by Life Technologies Corporation (Grand Island, NY, USA). LIVE/DEAD cell viability kit containing ethidium homodimer-1 (EthD-1) and calcein AM and the AlamarBlue assays were obtained from Invitrogen (CA, USA).

2.2. Plasma electrolytic oxidation (PEO) treatments of Ti-sheets

Rectangular Ti-sheets (20 mm × 15 mm × 1 mm) were utilised in this experiment. Samples were placed inside a beaker containing acetone in a sonication bath for 10 min followed by washing with DI water. The electric oven was used to dry the sample after a cleansing process for 2 h at 50 °C. PEO process carried out *via* programmable DC power supply (N5752A, Agilent Technologies, and the USA) coupled with LabVIEW software to record voltage-time change during PEO treatment. The current density was set at 50 mA cm^{-2} for 1 min, adopted from previous research data provided by Kuromotoet *et al.*[34] The basic solution comprising of potassium hydroxide, sodium metasilicate pentahydrate and orthophosphoric acid was used as an electrolyte, while the distance of around 45 mm between the working electrode (Ti-sheets) and counter electrode (Ti cylindrical mesh) maintained during PEO treatment.[35] Later, the as-prepared PEO samples were washed and dried in the electric oven for 4 h at 50 °C.

2.3. Preparation of 2D materials

GO was generated by employing modified Hummers' method[36] *via* exfoliation of graphite oxide using a specific solvent. In summary, H_2SO_4 and H_3PO_4 were mixed (9 : 1) and cooled down in a fridge to reach 3 °C. In the next step, 3 g graphite powder was mixed with 18 g $KMnO_4$, and the acidic solvent was added to the mixture gently. The final mixture was stirred for 15 h at 50 °C. Afterwards, the mixture was left to cool down at ambient temperature, and around 1 mL of H_2O_2 was dropped gradually to eliminate the excess of $KMnO_4$, which led to the formation of a brownish mixture. In the final stage, the solution was mixed with hydrochloric acid (HCl) and Millipore water (1 : 3) and centrifuged at 4200 rpm with Eppendorf Centrifuge device for 2 h for at least 3 times.[37]

The exfoliation of bulk hexagonal boron nitride (hBN) flakes was performed by following the process demonstrated by Nine *et al.* previously.[38] In brief, the bulk hexagonal boron nitride (hBN) was soaked in an alkaline (2 M NaOH) aqueous solution (10 mg mL^{-1}) followed by the mechanical exfoliation using a planetary ball-milling (PM200, Retsch, Germany). The milling was performed in a zirconia pot partially filled with 3 mm zirconia balls 6 h with an interval of 20 min every 30 min. The exfoliated and agglomerated hBN sheets were further ultrasonicated (Branson Digital Sonifier 450) for an hour before washing with DI water using an Eppendorf Centrifuge to obtain

a neutral suspension of hBN. The final suspension of hBN was prepared in ethanol.

A ternary layered carbide MAX phase material Ti_3AlC_2 (Carbon Ukraine) was used to prepare MXene materials. Lithium fluoride (LiF) and hydrochloric acid (HCl, 32%) were purchased from SIGMA – Aldrich (Australia) and used to prepare *in situ* HF. The synthesis steps of MXene materials mainly followed a literature guideline.[39] It is a relatively low-risk and stable MXene synthesis scheme. In brief, MAX phase material was crushed into small pieces and was ground and sieved to the size range of <25 μm. Then, LiF was carefully added to 9M HCl to form an etching mixture. Afterwards, Ti_3AlC_2 powder was gradually added into the mixture and placed in an ice bath. The reaction vessel was stirred for 1 h. In the next stage, the mixture was stirred and kept at 35 °C for 24 h. The final solution then centrifuged with DI water at 3500 rpm for 30 minutes with the Eppendorf Centrifuge device, and repeating at least 5 times to remove all residuals.

2.4. Drop casting of 2D materials on the PEO substrates

The drop-casting method is an accessible and affordable deposition method, working based on the dropping of the solution followed with subsequent evaporation of the solvent, which minimises waste of material.[40,41] Bulk GO, MXene and hBN in the form of a concentrated paste with different concentrations were diluted in ethanol to reach the concentration of 0.5 mg mL^{-1} (for the high concentration group) and 0.05 mg mL^{-1} (for the low concentration group). Diluted 2D materials solutions were then sonicated in an ultrasonication bath for 30 min. In the next step, 40 μL of each solution was cast onto the cleaned and dried PEO substrates (15 mm × 10 mm) and left in the convection oven overnight to dry at 50 °C.[42]

3. Characterisations

Morphological and topographical characterisation of the samples was conducted by FIB-SEM (Focused Ion Beam Scanning Electron Microscope FEI Helios Nanolab 600, USA) as well as SEM Quanta 450 (Eindhoven) equipped with EDS analysis. WITEC Alpha300 Raman spectroscopy device was utilised in the range between 0 to 2000 cm^{-1} based on samples with 532 nm green laser beam. Crystallography analysis of samples was analysed with XRD Rigaku MiniFlex 600 device with an operating condition of 40 kV, $2\theta = 3$–80 degrees and a scan rate of 5 degrees per min. FEI Tecnai G2 Spirit TEM instrument (100 keV, SDD Detector) was used for TEM imaging. Wettability analysis of samples carried out by sessile drop method *via* optical-tensiometers model T301 – ATA scientific pty ltd, while water droplet size of 2.2 ± 0.1 μL was utilised during contact angle measurement. The zeta potential and average diameter of flakes were measured *via* Zetasizer Nano Series – Malvern at room temperature. The bioactivity test conducted according to Kokubo *et al.*,[43] by preparation of simulated body fluid (SBF) and immersion of samples in a 50 mL container filled with SBF solution for 3 weeks. SBF solutions were replaced every two days to provide a fresh solution for the biomineralisation process. The antibacterial test carried out according to ISO 22916:2011 against *S. aureus* Gram-positive strain Newman and a Gram-negative *E. coli* strain JLD24. Newman is a commonly used reference strain of *S. aureus* in various genetic and *in vivo* experiments, while JLD24 was isolated from the infected bone of a patient with a diabetic foot infection. Briefly, single bacterial colonies were resuspended in sterile tryptic soy broth (TSB) or up to 3 h to reach the OD_{600} of 0.2 for a concentration of $\sim 1 \times 10^8$ Colony Forming Unit (CFU) per mL. Each side of the sample's surface was disinfected using UV for 20 min and 20 μL of bacteria culture incubated in triplicate with the rectangular shape (10 mm × 15 mm) samples (placed in 6-well cell culture plates) for 24 h at 37 °C. Following 24 h incubation, 1 mL PBS solution was added to each well and placed in a sonication bath (170 W) for 6 min to ensure detachment of bacteria from the substrate. 100 μL of PBS-resuspended bacteria from each sample were then collected, serially diluted, and spread on tryptic soy agar plates and finally cultured for another 24 h at 37 °C. The relative numbers of viable bacterial cells, reported as CFUs were quantified and compared to the control titanium. In order to evaluate the minimum concentration of penicillin and gentamicin required for the inhibition of the clinically obtained *E. coli* strain (JLD24), a minimum inhibitory concentration (MIC) test *via* the broth microdilution method was also conducted. MIC tests were carried out in 96 flat-bottom microtiter plates. 20 μL of log-phase bacterial cultures ($\sim 8 \times 10^5$ CFUs) were added to a series of wells containing 180 μL of TSB serially diluted with the antibiotic penicillin or gentamicin at a dilution factor of 1/2. The MIC was defined as the lowest concentration of antibiotic, in which no growth was observed after 24 h of growth at 37 °C. Wells without bacterial culture were included as negative growth controls. For the *in vitro* biocompatibility test, initially, the human foreskin fibroblast cells were seeded in a T25 flask in Dulbecco's Modified Eagle Medium (DMEM) containing 10% (v/v) fetal bovine serum and 1% (v/v) penicillin/streptomycin and grown at 37 °C with 5% CO_2. At 80–90% confluence, cells were treated with 0.25% trypsin and resuspended in DMEM, the cells were centrifuged at 5000 rpm for 5 min to obtain cell pellets for further experiments. To examine whether the prepared samples with higher concentrations of nanomaterials are biocompatible, the samples were incubated in DMEM for 24 hours. Afterwards, the culture media was removed and collected. On the other hand, 2.5×10^4 fibroblasts were seeded into a 96-well plate and grown at 37 °C with 5% CO_2 for 24 hours. Next, the culture media was removed, and each well was then filled with 100 μL of collected DMEM media from samples. After a specified incubation time (2 h and 24 h), the culture media was removed and 100 μL of PBS with 10% v/v AlamarBlue solution (Invitrogen, CA, USA) were added, followed by incubation in the dark for 3 h at 37 °C. Next, 100 μL of incubated AlamarBlue medium in each well were transferred to a black 96-well plate and the optical density (OD) at 570 and 600 nm was determined with a FLUOstar OPTIMA plate reader (BMG Labtech, Ortenberg, Germany). In addition, the cells were stained using LIVE/DEAD cell viability kit containing ethidium homodimer-1 (EthD-1) and Calcein AM for 30 min and observed under an LSM700 Confocal Laser Scanning Microscope (Zeiss Microscopy, Oberkochen, Germany).

View Article Online
Paper Journal of Materials Chemistry B

3.1. Statistical analysis

Samples were tested in triplicate, and final data were provided as mean standard deviations. Furthermore, GraphPad version 8 software was utilised to carry out the statistical comparison among groups *via* a one-way analysis of variance (ANOVA) (multiple comparisons) test. In all cases, differences with $p < 0.05$ were considered significant.

4. Results and discussions

4.1. Characterisation of selected 2D flakes before drop-casting

The characterisation of MXene before drop-casting is provided in Fig. 1(a–c). TEM image of the MXene is provided in Fig. 1a, showing the sharp edge of MXene flakes. Raman spectrum of MXene is demonstrated in Fig. 1a. The initial sharp peak at around 150 cm^{-1} is related to the formation of oxidised Ti_3C_2 due to the application of high power laser beam during the Raman spectroscopy or can be related to the residual MAX phase.[44,45] The small sharp peak at ~200 cm^{-1} and broadened and merged peaks at ~400 cm^{-1} and ~630 cm^{-1} are related to the decrease in order of crystallinity and collapse of MAX phase and successful formation of Ti_3C_2 during the etching process, which is in agreement with previous literature data.[44,45] It is worth mentioning that reported MAX phase characteristic peaks at 267.8, and 360 cm^{-1} completely vanished after *in situ* HF treatment. The XRD spectrum graph of the generated MXene from the MAX phase is provided in Fig. 1c. Based on the literature data, the exfoliation of the MAX phase with *in situ* HF results in the appearance of a broadening peak at ~8°, which is associated with the structural expansion of (002) plane of MAX phase and successful generation of MXene. Moreover, another characteristic peak at 2θ value of 61.5° is corresponding to (110) plane of Ti_3C_2 MXene,[46] while peaks at 9.9°, 39.2° and 42° show the presence of residual Ti_3AlC_2 after etching.[47] During the etching, some impurities such as TiC are also introduced, which can be identified by the presence of peaks at 36° and 41.7° corresponding to TiC (111) and (200) planes, respectively.[48]

The characterisation of hBN before drop-casting is represented in Fig. 1(d–f). TEM image of the hBN flakes has presented in Fig. 1d, showing the multi-layered hBN flakes.[38] Raman spectrum of hBN is displayed in Fig. 1e. Similar to graphene, the hBN

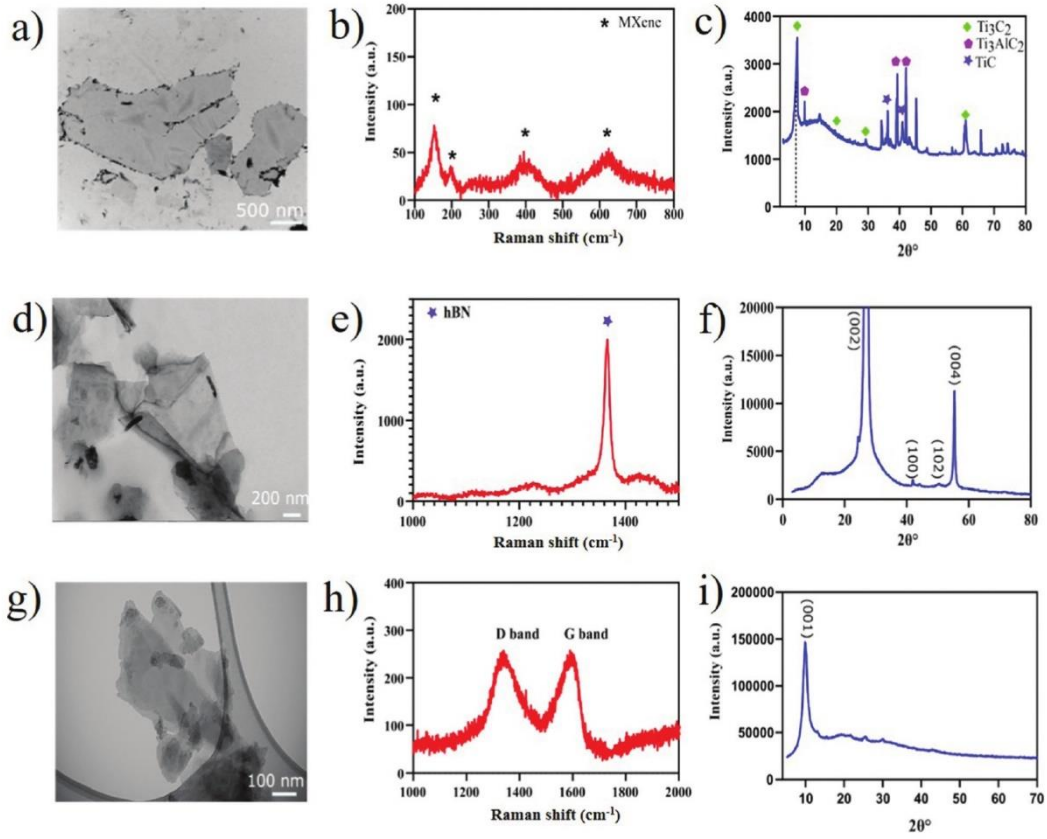

Fig. 1 Characterization of 2D flakes before drop-casting, (a) TEM image of MXene, (b) Raman spectroscopy of MXene, (c) XRD spectrum of MXene, (d) TEM image of hBN, (e) Raman spectroscopy of hBN, (f) XRD spectrum of hBN, (g) TEM image of GO, (h) Raman spectroscopy of GO, (i) XRD spectrum of GO.

spectrum possesses a characteristic G peak, which is associated with the E_{2g} phonon mode and is observable at 1366 cm^{-1}. The XRD patterns of hBN flakes are depicted in Fig. 1f. Four prominent characteristic peaks of the hBN phase (JCPDS PDF No:034-421) are evident in the spectrum related to (002), (100), (102) and (004) planes.

Morphological and physicochemical characterisation of GO is presented in Fig. 1(g–i). TEM image of the GO flakes has provided in Fig. 1g, showing the multi-layered GO flake structure. As shown in the Raman spectrum in Fig. 1h, two characteristic peaks of GO known as D and G bands are visible at 1341 cm^{-1} and 1590 cm^{-1}, respectively. The presence of G band is related to the graphitic structure and scattering of phonons in sp^2 C atoms occurring at around 1580 cm^{-1}. On the other side, D band is associated with structural defects and disorientation in GO sheets that lie in the range of ~1200–1500 cm^{-1}.[49] The calculated I_D/I_G value, which is also recognised as "Intensity ratio" was around 1.007 that gives an estimation about the defects in the sample and is in the range of previously reported values for GO.[50] XRD diffraction spectrum of GO in Fig. 1i reveals the characteristic sharp peak at around $2\theta = -10^\circ$ corresponding to the GO (001) plane.[51,52]

4.2. Physiochemical and morphological characterisation

The voltage–time curve during the PEO process, along with the morphological and physicochemical characterisation of the initial PEO treated titanium substrate, are exhibited in Fig. 2. During the PEO treatment in the basic electrolyte, voltage gradually increases. Based on the visual observation, break down voltage starts at around 310 V and after about 40 s after the onset of treatment, which is evident by the generation of small arcs accompanied with acoustic emission. These plasma arcs are formed initially around the edges and corners of the sample, and after few seconds, they are covering the whole surface of the specimen resulting in the formation of a porous surface layer (thousands of micro–nano pores) beneficial for

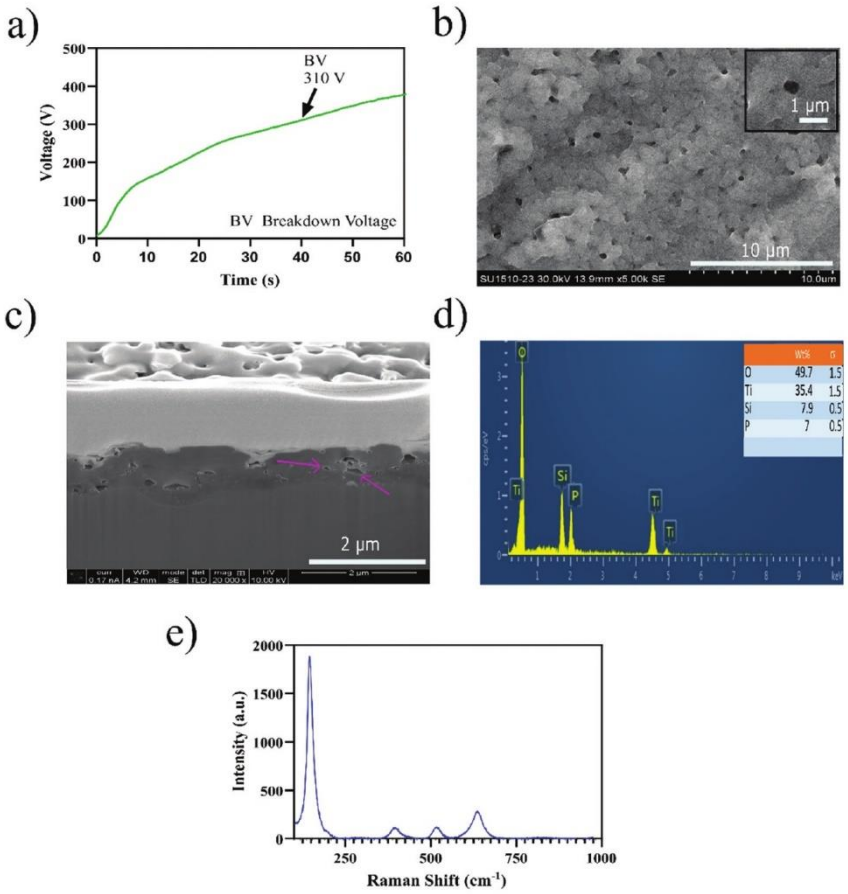

Fig. 2 (a) Voltage–time curve during basic PEO processes, (b) SEM image of PEO treated titania (inset, typical pore size and morphology, scale bars: 1 μm), (c) SEM image of the cross-section of PEO titania, (d) corresponding EDS analysis of PEO treated surface, (e) Raman spectrum of the oxide layer.

the osseointegration process. After 60 s, the final cell voltage of around 400 V was achieved. Our previous experiments showed that basic PEO electrolyte could generate a thicker protective oxide layer after 1 min titanium PEO treatment compared to the acidic electrolyte. SEM images of the PEO treated sample after 1 min PEO treatment and its corresponding cross-section are provided in Fig. 2b and c, which show the morphology of pores and relatively uniform thickness of the oxide layer. PEO sample displayed a relatively flat surface while fully covered with typical rough micro–nanopores ranging from 160 to 1300 nm with an average diameter of 504 nm. Some crater-like, as well as worm-like morphologies, were detectable over the substrate (Fig. 2c). The calculated average thickness of the PEO oxide layer was about 870 nm. The EDS analysis of the sample in Fig. 2d revealed the PEO film is enriched with Ti and O, while both P and Si were also detectable over the surface. These results are in agreement with previous results reported after PEO treatment in typical basic solutions.[19,35] Raman spectroscopy analysis confirmed the presence of anatase phase in the PEO oxide layers supported by characteristic peaks observed at ~145, 392, 514 and 635 cm^{-1} in the Raman spectrum (Fig. 2e). Based on previous works, the anatase phase is formed due to the significant increase in the temperature during the arc generation stage in the PEO system.[53] It is worth mentioning that the application of high voltage during the PEO process leads to the formation of microplasma in the electrolyte, which can increase the local temperature to around 4500 K.[53] Subsequently, a small fraction of titanium melts each time arcs hitting the surface, while the presence of a colder electrolyte surrounding the electrodes results in the sudden cooling of the system and the formation of anatase and rutile phases in the oxide layer. The anatase phase developed on PEO treated surface can favour mineralisation and improve osseointegration of treated Ti-based implants.[54] The zeta potential and Z-average diameter of 2D materials in the mixture of ethanol and water (1 : 1) are classified in Table 1. The zeta potential measurements, which works based on the surface charge of flakes in the system, can provide unique information regarding the stability of 2D flakes in suspension. In general, 2D flakes dispersed in a system with zeta-potential values near ±30 mV or greater than +30 mV or less than −30 mV are considered stable.[55] Our results show relatively good stability of GO and MXene flakes in the suspension (with ζ-potential of −34 and −27, respectively), while hBN flakes showed ζ-potential of around −10. Based on the literature data, flakes with ζ-potential between −10 to +10 mV are considered neutral.[56] Moreover, the table also demonstrates that 2D flakes are in a relatively similar size range of 2000–3000 (d nm).

Table 1 Average size and zeta potential of 2D material flakes in solution before drop-casting

Sample	Zeta potential (mW)	Z-Average (d μm)
GO	−34.7 ± 3.8	2.75 ± 1.04
MXene	−27.7 ± 2.3	2.67 ± 0.68
hBN	−9.9 ± 0.7	2.28 ± 0.43

4.3. Characterisation of engineered substrates

SEM images and EDS spectrum of different flakes deposited on the PEO substrate are demonstrated in Fig. 3. In Fig. 3a, SEM images of the substrate after deposition with MXene flakes in low (0.05 mg mL^{-1}) and high (0.5 mg mL^{-1}) concentrations confirmed the successful partial deposition of MXene over the porous PEO substrate, evident from the presence of open pores after drop-casting. Raman mapping of the sample after drop-casting at high concentration (0.5 mg mL^{-1}) also is provided in the supplementary section (Fig. S1c, ESI†). Furthermore, EDS analysis of the flakes on the surface in Fig. 3a(i) highlighted the presence of Ti, C in MXene and Ti, O and Si over the substrates. Similarly, SEM images of samples after deposition with hBN flakes in low and high concentrations, provided in Fig. 3b, showed the successful deposition of hBN flakes over the PEO substrate in a partial manner. The result of Raman mapping (Fig. S1b, ESI†) for this sample was also in agreement with SEM results, showing the presence of many open pores over the substrate after drop-casting with hBN flakes. The EDS result in Fig. 3b(i) indicated that deposited flakes are enriched with boron and nitride, and a small amount of Na impurities. Finally, SEM images and Raman mapping of deposited GO flakes on PEO substrate with different concentrations showed PEO pores were still open in both GO concentrations throughout the surface, which is beneficial for bone–implant integration (Fig. 3c and Fig. S1a, ESI†). The EDS analysis Fig. 3c(i) shows the high intensity of C atoms over the surface of GO deposited PEO samples.

4.4. Antimicrobial assessment

Staphylococcus bacteria are responsible for more than two-thirds of all infections in bone implants. Therefore, they have the highest relevance to infection of bone implants and are the focus of this work.[57] The antimicrobial activity of different drop-cast 2D materials on PEO substrates against Gram (+) *S. aureus* and Gram (−) *E. coli* bacteria was evaluated using the plate count method. Fig. 4 exhibits typical photographs of *S. aureus* bacteria colonies recultivated after direct contact with samples before and after drop-casting with different concentrations of 2D materials. As can be seen, the PEO substrate exhibited a slight antibacterial efficiency with a 17 (±6) % decrease in the number of colonies. For the first group of deposited 2D flakes in a low concentration of 0.05 mg mL^{-1} (MXn-low, GO-low, hBN-low), these photographs showed a significant decrease in the number of colonies for MXn-low, GO-low samples compared to the Ti control sample, while only a slight reduction of *S. aureus* colonies observed for hBN-low sample after the antibacterial test. On the other hand, for the second group of deposited 2D flakes in a high concentration of 0.5 mg mL^{-1} (MXn-high, GO-high, hBN-high), all the treated samples exhibited enhanced antibacterial activity. Particularly for the MXn-high sample, we noticed superior antibacterial activity compared to the control sample. A relative bacterial growth for each sample was compared to the titanium control, as presented in Fig. 4. The results revealed a remarkable

View Article Online
Journal of Materials Chemistry B Paper

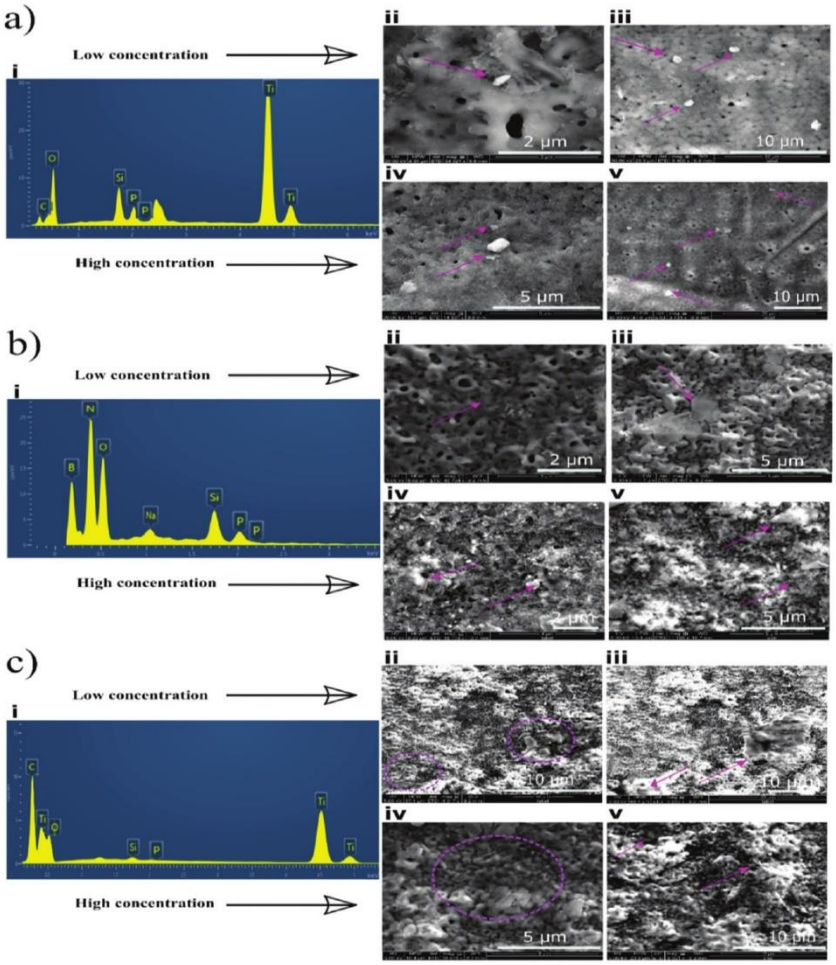

Fig. 3 SEM images and EDS results after deposition of 2D flaked over titania PEO substrate for (a) MXene, (b) hBN, (c) GO; In each group of selected deposited 2D flakes: (i) EDS result at high concentration, (ii) high magnification SEM image of sample deposited with low concentration of 2D flakes, (iii) low magnification SEM image of sample deposited with low concentration of 2D flakes, (iv) high magnification SEM image of sample deposited with high concentration of 2D flakes, (v) low magnification SEM image of sample deposited with high concentration of 2D flakes.

antibacterial activity for GO-low and MXn-low samples with inactivation of 70 (±2) % and 56 (±1) % of *S. aureus* bacteria, respectively. This number for the hBN-low sample was lower and at around 18 (±5) %. The increase in the concentration of 2D flakes further improved the antibacterial ability with 77 (±1.6) % and 97 (±0.5) % inactivation for GO-low and MXn-low samples.

Interestingly, the hBN-high sample was able to inactivate 64 (±1.3) % of bacteria after incubation. Previous studies also evaluated the antibacterial activity of 2D materials in the form of continuous film, membrane, or discrete patches.[14,19,21] However, in this work, we aimed to provide a realistic comparison between the antibacterial activity of these 2D materials with similar concentrations. The antibacterial result for hBN is in agreement with other studies, which demonstrated the hBN flakes had bacteriostatic/bactericidal activity only at a high concentration of 0.4 mg mL^{-1} against Gram-positive bacteria such as *Staphylococcus pasteuri*.[58] However, the bactericidal potential of hBN in the hBN-high sample against *S. aureus* was relatively high and beyond our expectations. This result is becoming more important when considering the much lower toxicity of hBN materials than carbon-based materials (such as graphene and CNTs).[59] Nevertheless, the exact mechanisms behind the antibacterial properties of hBN have not been fully understood.[59] Previous studies reported significant higher antimicrobial activity of MXene nanosheets compared with its initial MAX phase.[60] Moreover, much other research revealed the antibacterial activity of MXene against different bacteria such as *B. subtilis* in colloidal solutions or as a membrane.[61]

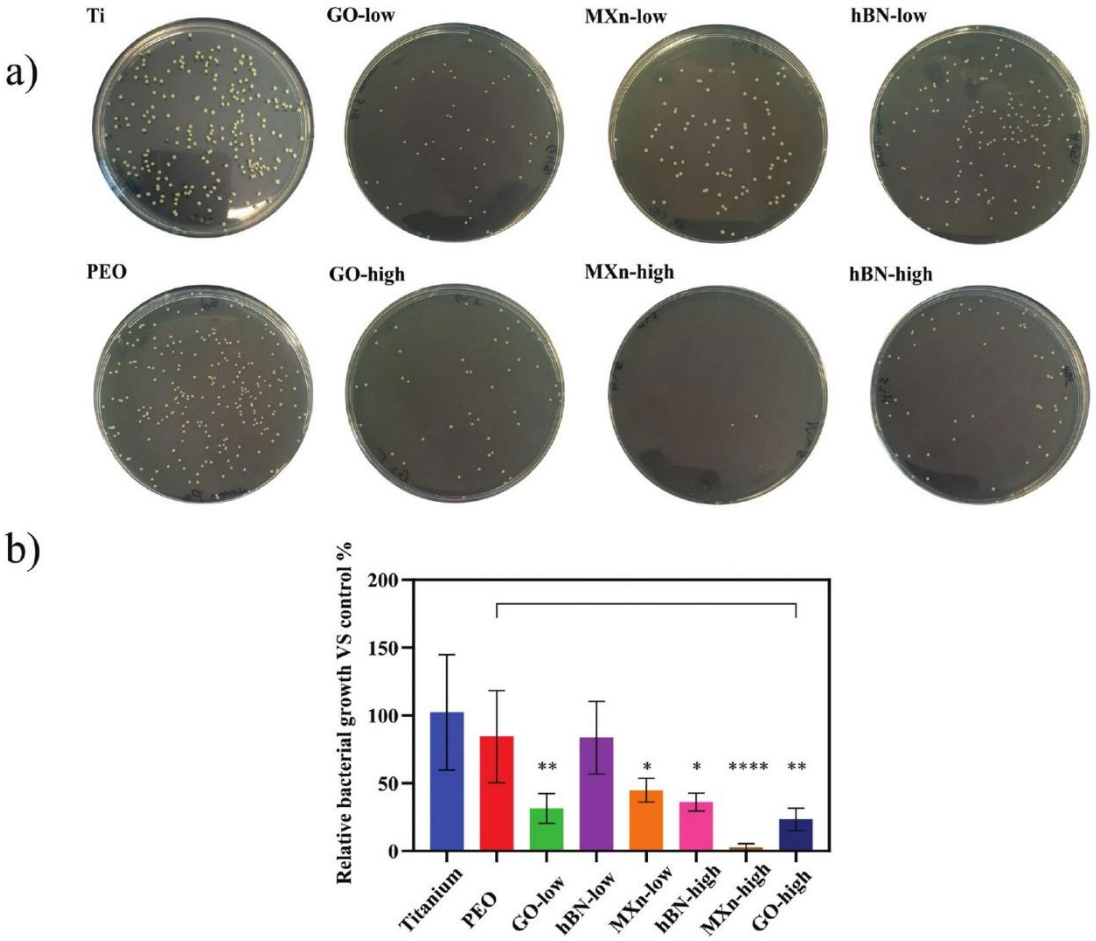

Fig. 4 (a) Surviving *S. aureus* colonies after contact with titanium control and deposited 2D materials flakes in low concentration of 0.05 mg mL^{-1} labelled as MXn-low, GO-low, hBN-low, while for high concentration of 0.5 mg mL^{-1} were labelled as MXn-high, GO-high, hBN-high, (b) relative bacterial growth of *S. aureus* compared to titanium control on different samples; $*p < 0.05$, $**P \leq 0.01$, $***P \leq 0.001$ and $****P \leq 0.0001$.

As discussed earlier, the common antibacterial mechanism of 2D materials is associated with physical and mechanical damage and generation of oxidative stress-induced either by the formation of reactive oxygen species (ROS) or *via* direct electron and charge transfer.[28–30] Moreover, all the deposited 2D materials on the PEO surface demonstrated negative zeta potential values (Table 1), which can decrease the attachment of bacteria to the PEO surface due to the electrostatic repulsion between bacteria membrane and coated surface.[62] Furthermore, other factors such as the role of functionalisation and surface termination groups (OH, O, F, *etc.*) induced during the production process should be further investigated.

The result of antibacterial studies against *E.coli* strain is provided in Fig. 5. As can be seen from photographs, the initial PEO samples showed a slight decrease in the number of colonies compared to Ti untreated samples. The deposition of 2D materials on PEO substrate in low concentration did not only improve the antibacterial properties, in some cases, but also resulted in a higher presence of bacteria colonies. On the other side, by deposition of a higher concentration of 2D flakes on the PEO surface, slightly higher antimicrobial activity was achieved. Particularly, the hBN-high and GO-high samples with ~18 (± 2) % and ~17 (± 4) % decrease in the number of *E. coli* colonies compared to the Ti control sample demonstrated the highest antimicrobial activity, while the MXn-high sample showed lower antibacterial activity with only ~7 (± 1) % decrease in the number of colonies. It is worth mentioning that the JLD24 *E. coli* strain used in this experiment was isolated from a patient with a monomicrobial infection who was on the penicillin augmentin. Therefore this bacteria strain can be regarded as a penicillin-resistant *E. coli* strain, which may be harder to kill. A MIC test reveals a strong resistance to penicillin with a MIC of 1000 μg mL^{-1}

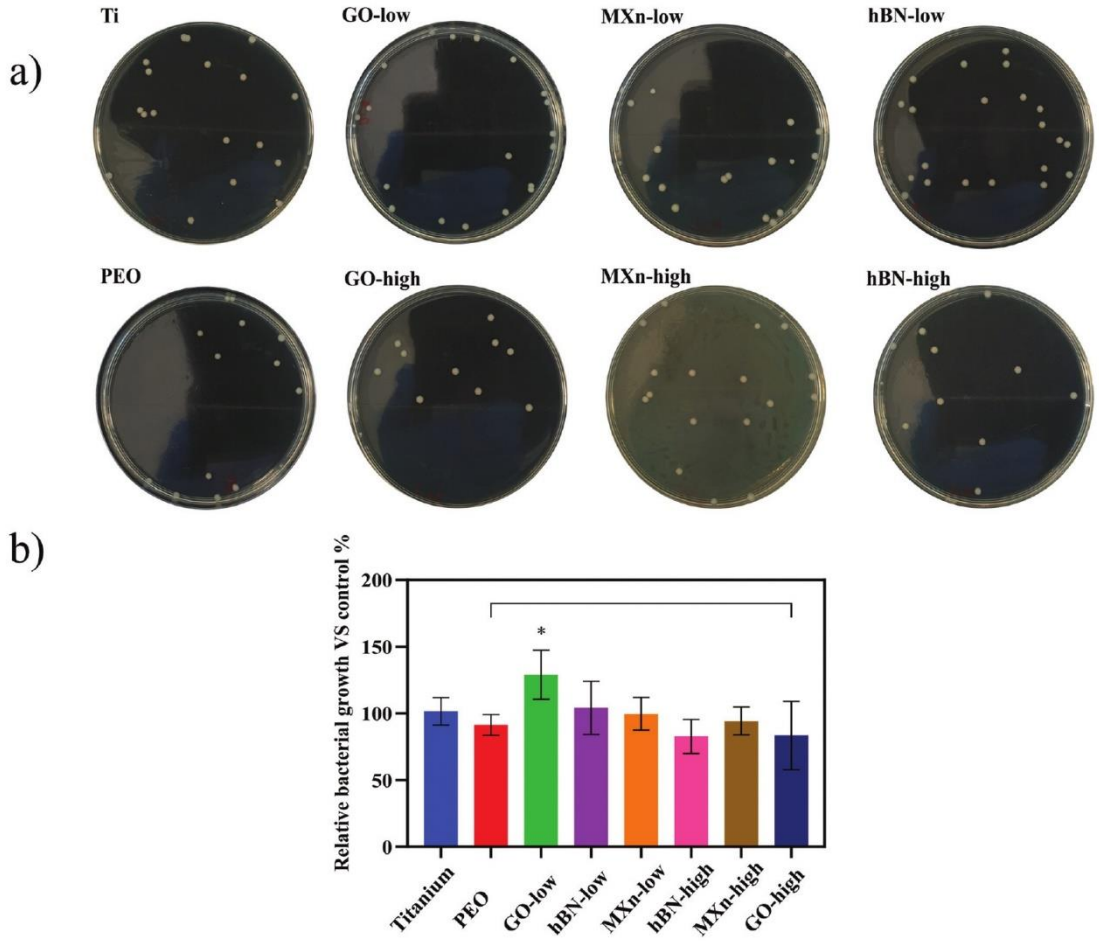

Fig. 5 (a) Surviving *E. coli* colonies after contact with titanium control and deposited 2D materials flakes in low concentration of 0.05 mg mL^{-1} labelled as MXn-low, GO-low, hBN-low, while for high concentration of 0.5 mg mL^{-1} were labelled as MXn-high, GO-high, hBN-high, (b) relative bacterial growth of *E. coli* compared to titanium control on different samples; $*p < 0.05$.

and intermediate resistance to gentamicin with a MIC of 7.91 μg mL^{-1}. (ESI,† Fig. S2).

Moreover, different studies have revealed *E. coli* bacteria present less sensitivity to mechanical damaging compared to Gram-positive bacteria such as *S. aureus*.[19,63] While Gram-positive species have a single outer membrane surrounded by a layer of peptidoglycan, Gram-negative species have an additional protective outer membrane not present in Gram-positive species, which could provide more effective protection against the mechano-bactericidal surface with sharp edges.[19,63] It can be conferred that deposited 2D materials in this study are specifically active against the Gram-positive cellular membranes.

4.5. Biomineralisation assessment

The result of biomineralisation and wettability tests for deposited samples at higher concentration of 2D flakes (0.5 mg mL^{-1}) are presented in Fig. 6. As can be seen in the SEM images, all samples demonstrated some extent of mineralisation ability evident from the formation of submicron particles over their surface. The formation of HAP on MXn-high, GO-high and hBN-high samples was confirmed from XRD spectrum analysis (Fig. 6) and through the presence of many HAP distinctive peaks corresponding to (100), (200), (002), (210), (112), (301), (221), (222), (312) planes (based on ICDD 9-432[64]). Moreover, several peaks related to the PEO treated Ti substrate are also observable in the XRD spectrum. Particularly characteristic peaks at around 38°, 42°, 44°, 65° and 79° belong to the Ti substrate (reproduced by JCPDS card, no. 65-3362) while peaks at around 24° and 39° can be indexed to the (101), (112) planes of the anatase phase generated through PEO process (JCPDS card no. 21-1272).[65] It is worth mentioning that as XRD spectroscopy is considered as a bulk analysis technique, therefore, it can not reveal all the peaks

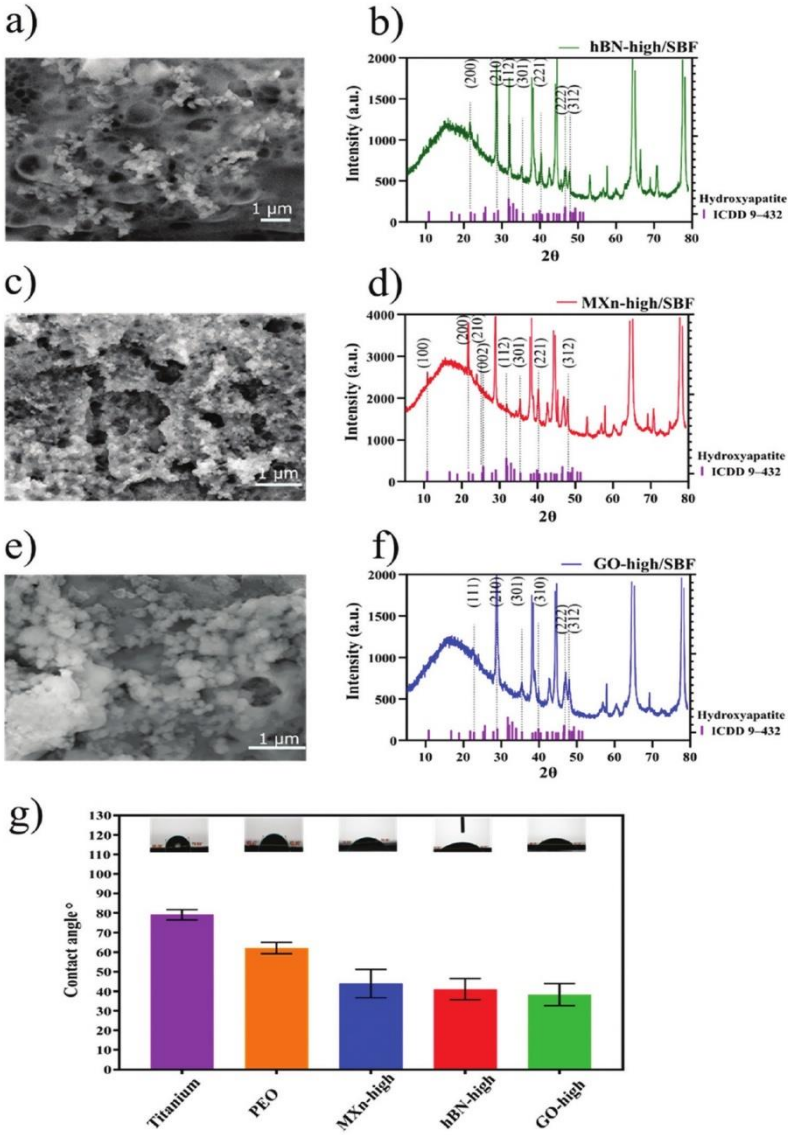

Fig. 6 Result of SBF biomineralization test for the 2D flakes deposited on PEO samples at high concentration 0.5 mg mL^{-1}. (a) SEM image of MXn-high after mineralization (MXn-high/SBF), (b) corresponding XRD spectrum for MXn-high/SBF, (c) SEM image for hBN-high sample after mineralization (hBN-high/SBF), (d) corresponding XRD spectrum for hBN-high/SBF, (e) SEM image for GO-low sample after mineralization (GO-high/SBF), (f) corresponding XRD spectrum for GO-high/SBF, (g) contact angle measurement for different samples.

related to the pure HAP nanoparticles and peaks associated with the substrate are affecting the final XRD patterns.

Based on the SEM images, it can be inferred that biomineralisation mainly occurs on available non-coated PEO sites. The previous studies also confirmed the inherent biomineralisation ability of the PEO surface, which treated in a similar basic electrolyte.[19] These results highlight the importance of a partial deposition pattern of 2D material flakes over the PEO substrate instead of a continuous film formation, which provides reasonable PEO open pores required for successful biomineralisation.

In the next stage, wettability analysis of candidate groups (MXn-high, GO-high, hBN-high) was evaluated by the sessile drop method (Fig. 6g). Our result demonstrated a contact angle value (CA) of ~79° for untreated Ti samples. After the initial PEO treatment, the CA values drop to 62°, due to the formation of a thicker oxide layer and the introduction of micro–nano

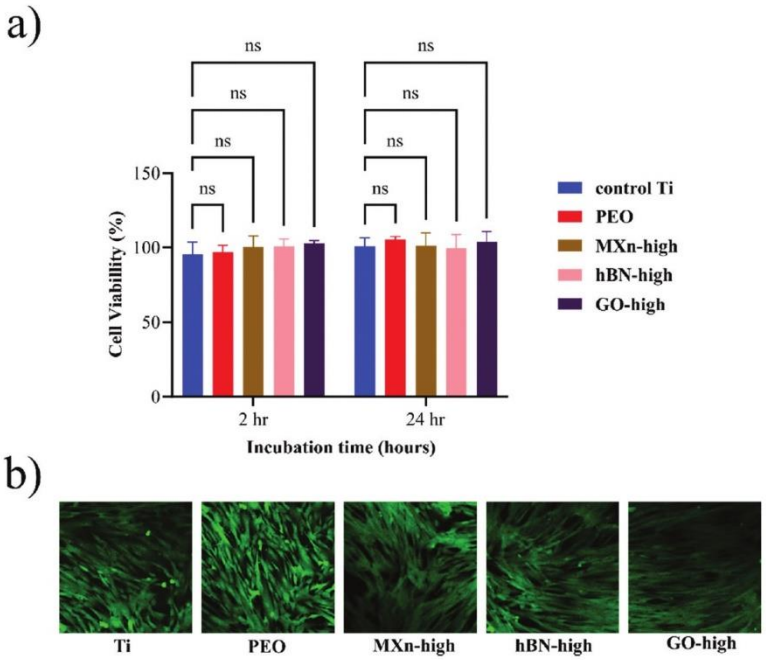

Fig. 7 *In vitro* biocompatibility of samples toward foreskin fibroblasts cells after 2 and 24 hours *via* (a) AlamarBlue assay, (b) LIVE/DEAD cell assay.

pores over the surface. Partial deposition of the PEO surface with 2D flakes significantly improved the overall hydrophilicity of MXn-high, hBN-high and GO-high samples to 43°, 41°and 38°, respectively. The enhancement in the hydrophilicity of the MXn-high sample is in agreement with previously reported data with 37° for Ti_3C_2Tx film. The recorded CA values for the GO-high sample is also in the range of reported values in the previous studies.[66] On the other side, previous studies demonstrated that hBN coating on flat TiO_2 substrate is hydrophobic,[67] although factors such as surface roughness and contact distance between the underlying substrate and hBN coating can affect the wettability.[68] Therefore, it is anticipated that the partial deposition of layered 2D materials on the titania nanostructures substrate would affect the overall resultant wettability.[68] For instance, the partial deposition of hydrophobic hBN instead of continuous film formation on the titania substrate would expose the edges of the hydrophilic nanostructures (as seen in SEM results in Fig. 3b), making them together amphiphilic by nature and more interactive with liquid. Hence, it results in an overall low CA (41°). This can also be explained by Wenzel model as following:

$$\cos\theta_\omega = r\cos\theta$$

where, θ_ω is the contact angle for roughened surface, θ is the contact angle for the initially smooth surface, and r is defined as the roughness ratio related to the real and projected liquid–solid contact area. Therefore, the hydrophilic surface can be more hydrophilic if the roughness is increased.[68]

In general, parameters such as surface energy, charge and hydrophobicity characteristics of the surface are involved in the bacterial adhesion and proliferation on the samples. *S. aureus* and *E. coli* are typically considered hydrophobic bacteria.[69,70] Hydrophobic bacteria tend to adhere to the hydrophobic surfaces.[71] Therefore, the decrease in the CA values would result in the reduction of the bacterial adhesion. However, it is not always the case with the 2D materials, as one of the fundamental killing mechanisms underlying their antibacterial ability is the mechanical damage *via* sharp edges. Therefore, some studies suggest that the effective attachment of bacteria to 2D materials may favour the inactivation of bacteria by direct contact and eventually lead to membrane damage and killing of bacteria.[60]

4.6. *In vitro* biocompatibility assessment

The *in vitro* biocompatibility of the prepared samples was assessed through an indirect contact method. As seen in Fig. 7a, the control samples and nanomaterial-treated surfaces do not differ in terms of cell viability. To further confirm the viability of cells exposed to the collected DMEM culture media, cells were stained with EthD-1 (red fluorescence, dead cells) and calcein AM (green fluorescence, live cells) and imaged under confocal microscopy (Fig. 7b). As seen, all fibroblasts remained viable without noticeable dead cells, indicating that the samples are biocompatible.

5. Conclusion

In summary, three well-known 2D materials (GO, MXene and hBN) were partially deposited on titania PEO substrate *via* a facile drop-casting technique to evaluate their antibacterial

performances. Amongst different parameters associated with the antimicrobial ability of the aforementioned flakes, the effect of concentration on the antimicrobial activity and bioactivity of deposited PEO substrates was investigated. The antibacterial studies revealed the concentration-dependent nature of deposited flakes on PEO substrate. The highest antibacterial activity against *S. aureus* in low concentration (0.05 mg mL^{-1}) was observed for GO deposited on PEO sample (GO–PEO) with 70 (±2) % inactivation of colonies, while in higher concentration (0.5 mg mL^{-1}), MXene–PEO showed the best antimicrobial performance with 97 (±0.5) % decrease in the number of CFUs. On the other side, none of the 2D flakes deposited on PEO samples was effective against *E. coli* bacteria at a low concentration. However, a minor decrease in the number of colonies (with ~18 (±2) % for hBN-PEO, ~17 (±4) % for GO–PEO and ~7 (±1) % for MXene–PEO samples) was observed for the high concentration group, demonstrating higher sensitivity of Gram-positive bacteria to the antibacterial 2D materials. The mineralisation ability of the deposited PEO samples at a higher concentration of flakes (candidate group) was further assessed through the SBF mineralisation test. Our results demonstrated the successful formation of HAP particles over the samples evident from SEM images and XRD patterns. Moreover, the *in vitro* biocompatibility test through AlamarBlue and LIVE/DEAD cell assays showed good biocompatibility of fabricated samples deposited at high concentration of flakes. Therefore, the combination of PEO substrate with 2D multilayered flakes *via* the drop-casting method can be a simple, effective and novel approach for the fabrication of antibacterial-bioactive titanium implants.

Conflicts of interest

There are no conflicts to declare.

Acknowledgements

The authors acknowledge the funding by the ARC Research Hub for Graphene Enabled Industry Transformation (IH150100003). The authors thank the University of Adelaide, the School of Chemical Engineering and Advanced Materials, the Department of Molecular and Biomedical Science, The Department of Otolaryngology, Head and Neck Surgery at The Queen Elizabeth Hospital and Dr Jacqui McRae for their support to this paper.

Notes and references

1 M. Saini, Y. Singh, P. Arora, V. Arora and K. Jain, *World J. Clin. Cases*, 2015, **3**, 52–57.
2 K. Gulati, S. Ramakrishnan, M. S. Aw, G. J. Atkins, D. M. Findlay and D. Losic, *Acta Biomater.*, 2012, **8**, 449–456.
3 M. Long and H. J. Rack, *Biomaterials*, 1998, **19**, 1621–1639.
4 L. E. Bayliss, D. Culliford, A. P. Monk, S. Glyn-Jones, D. Prieto-Alhambra, A. Judge, C. Cooper, A. J. Carr, N. K. Arden, D. J. Beard and A. J. Price, *Lancet*, 2017, **389**, 1424–1430.
5 L. De Nardo, L. Altomare, B. Del Curto, A. Cigada and L. Draghi, *Coatings for Biomedical Applications*, Woodhead Publishing, 2012, 106–142.
6 C. N. Elias, J. H. C. Lima, R. Valiev and M. A. Meyers, *JOM*, 2008, **60**, 46–49.
7 S. Maher, A. Mazinani, M. R. Barati and D. Losic, *Expert Opin. Drug Delivery*, 2018, **15**, 1021–1037.
8 M. J. Nine, D. Choudhury, A. C. Hee, R. Mootanah and N. A. A. Osman, *Materials*, 2014, **7**, 980–1016.
9 E. Marin, M. V. Diamanti, M. Boffelli, M. Sendoh, M. P. Pedeferri, A. Mazinani, M. Moscatelli, B. Del Curto, W. Zhu, G. Pezzotti and R. Chiesa, *Mater. Des.*, 2016, **108**, 77–85.
10 E. Sandrini, R. Chiesa, A. Cigada, G. Rondelli and M. Santin, *J. Appl. Biomater. Biomech.*, 2003, **1**, 33–42.
11 T. Hryniewicz, *Metals*, 2018, **8**, 1058.
12 F. A. Akin, H. Zreiqat, S. Jordan, M. B. J. Wijesundara and L. Hanley, *J. Biomed. Mater. Res.*, 2001, **57**, 588–596.
13 T. Hanawa, *Front. Bioeng. Biotechnol.*, 2019, **7**, 170.
14 N. Sun, S. Yin, Y. Lu, W. Zhang and X. Jiang, *J. Mater. Chem. B*, 2020, **8**, 5606–5619.
15 B. S. Necula, L. E. Fratila-Apachitei, S. A. Zaat, I. Apachitei and J. J. A. B. Duszczyk, *Acta Biomater.*, 2009, **5**, 3573–3580.
16 X. Yao, X. Zhang, H. Wu, L. Tian, Y. Ma and B. J. A. S. S. Tang, *Appl. Surf. Sci.*, 2014, **292**, 944–947.
17 A. Cochis, B. Azzimonti, C. Della Valle, E. De Giglio, N. Bloise, L. Visai, S. Cometa, L. Rimondini and R. Chiesa, *Biomaterials*, 2016, **80**, 80–95.
18 R. V. Chernozem, M. A. Surmeneva, B. Krause, T. Baumbach, V. P. Ignatov, O. Prymak, K. Loza, M. Epple, F. Ennen-Roth, A. Wittmar, M. Ulbricht, E. A. Chudinova, T. Rijavec, A. Lapanje and R. A. Surmenev, *Mater. Sci. Eng., C*, 2019, **97**, 420–430.
19 A. Mazinani, M. J. Nine, R. Chiesa, G. Candiani, P. Tarsini, T. T. Tung and D. Losic, *Mater. Des.*, 2020, 109443, DOI: 10.1016/j.matdes.2020.109443.
20 E. Marin, M. V. Diamanti, M. Boffelli, M. Sendoh, M. P. Pedeferri, A. Mazinani, M. Moscatelli, B. Del Curto, W. Zhu, G. Pezzotti and R. Chiesa, *Mater. Des.*, 2016, **108**, 77–85.
21 W. Sun and F. G. Wu, *Chem. – Asian J.*, 2018, **13**, 3378–3410.
22 S. Liu, T. H. Zeng, M. Hofmann, E. Burcombe, J. Wei, R. Jiang, J. Kong and Y. Chen, *ACS Nano*, 2011, **5**, 6971–6980.
23 L. Mei, S. Zhu, W. Yin, C. Chen, G. Nie, Z. Gu and Y. Zhao, *Theranostics*, 2020, **10**, 757–781.
24 M. Ikram, I. Jahan, A. Haider, J. Hassan, A. Ul-Hamid, M. Imran, J. Haider, A. Shahzadi, A. Shahbaz and S. Ali, *Appl. Nanosci.*, 2020, **10**, 2339–2349.
25 K. Rasool, K. A. Mahmoud, D. J. Johnson, M. Helal, G. R. Berdiyorov and Y. Gogotsi, *Sci. Rep.*, 2017, **7**, 1598.
26 M. Li, L. Li and S. Lin, *Chin. Chem. Lett.*, 2020, **31**, 1511–1515.
27 T. I. Kim, J. Kim, I.-J. Park, K.-O. Cho and S.-Y. J. D. M. Choi, *2D Mater.*, 2019, **6**, 025025.
28 S. Begum, A. Pramanik, D. Davis, S. Patibandla, K. Gates, Y. Gao and P. C. Ray, *ACS Omega*, 2020, **5**, 3116–3130.
29 X. Lu, X. Feng, J. R. Werber, C. Chu, I. Zucker, J.-H. Kim, C. O. Osuji and M. Elimelech, *Proc. Natl. Acad. Sci.*, 2017, **114**, E9793–E9801.

30 M. J. Nine, D. N. H. Tran, A. ElMekawy and D. Losic, *Carbon*, 2017, **117**, 252–262.
31 N. Sun, S. Yin, Y. Lu, W. Zhang and X. J. J. O. M. C. B. Jiang, *J. Mater. Chem. B*, 2020, **8**, 5606–5619.
32 A. B. Khiabani, S. Rahimi, B. Yarmand and M. J. M. T. P. Mozafari, *Mater. Today*, 2018, **5**, 15603–15612.
33 A. Nourmohammadi, R. Rahighi, O. Akhavan and A. Moshfegh, *J. Alloys Compd.*, 2014, **612**, 380–385.
34 N. K. Kuromoto, R. A. Simão and G. A. Soares, *Mater. Charact.*, 2007, **58**, 114–121.
35 S. Aliasghari, P. Skeldon and G. E. Thompson, *Appl. Surf. Sci.*, 2014, **316**, 463–476.
36 D. C. Marcano, D. V. Kosynkin, J. M. Berlin, A. Sinitskii, Z. Sun, A. Slesarev, L. B. Alemany, W. Lu and J. M. Tour, *ACS Nano*, 2010, **4**, 4806–4814.
37 N. I. Zaaba, K. L. Foo, U. Hashim, S. J. Tan, W.-W. Liu and C. H. Voon, *Procedia Eng.*, 2017, **184**, 469–477.
38 M. J. Nine, A. C. Hee, T. T. Tung, K. Hassan and D. Losic, *Appl. Mater. Today*, 2020, **20**, 100764.
39 M. Alhabeb, K. Maleski, B. Anasori, P. Lelyukh, L. Clark, S. Sin and Y. Gogotsi, *Chem. Mater.*, 2017, **29**, 7633–7644.
40 F. Aslan, H. Esen and F. Yakuphanoglu, *Optik*, 2019, **197**, 163203.
41 J. Lipton, J. A. Röhr, V. Dang, A. Goad, K. Maleski, F. Lavini, M. Han, E. H. Tsai, G.-M. Weng and J. J. M. Kong, *Matter*, 2020, **3**, 546–557.
42 H. N. Lim, N. M. Huang and C. H. Loo, *J. Non-Cryst. Solids*, 2012, **358**, 525–530.
43 T. Kokubo and H. Takadama, *Biomaterials*, 2006, **27**, 2907–2915.
44 Y. Cao, Q. Deng, Z. Liu, D. Shen, T. Wang, Q. Huang, S. Du, N. Jiang, C.-T. Lin and J. Yu, *RSC Adv.*, 2017, **7**, 20494–20501.
45 S. A. Melchior, K. Raju, I. S. Ike, R. M. Erasmus, G. Kabongo, I. Sigalas, S. E. Iyuke and K. I. Ozoemena, *J. Electrochem. Soc.*, 2018, **165**, A501–A511.
46 X. Zhan, C. Si, J. Zhou and Z. Sun, *Nanoscale Horiz.*, 2020, **5**, 235–258.
47 H. Rastin, B. Zhang, A. Mazinani, K. Hassan, J. Bi, T. T. Tung and D. Losic, *Nanoscale*, 2020, **12**, 16069–16080.
48 R. Kang, Z. Zhang, L. Guo, J. Cui, Y. Chen, X. Hou, B. Wang, C.-T. Lin, N. Jiang and J. Yu, *Sci. Rep.*, 2019, **9**, 9135.
49 M. J. Nine, M. A. Cole, L. Johnson, D. N. H. Tran and D. Losic, *ACS Appl. Mater. Interfaces*, 2015, **7**, 28482–28493.
50 N. Kiran, S. Dey, B. Singh and L. J. T. C. Besra, *Coatings*, 2017, **7**, 214.
51 M. Li and C. Wang, *Renewable Energy*, 2019, **141**, 1005–1012.
52 M. J. Nine, M. Ayub, A. C. Zander, D. N. H. Tran, B. S. Cazzolato and D. Losic, *Adv. Funct. Mater.*, 2017, **27**, 1703820.
53 R. O. Hussein, X. Nie, D. O. Northwood, A. Yerokhin and A. Matthews, *J. Phys. D: Appl. Phys.*, 2010, 105203–105216.
54 C.-J. Chung, R.-T. Su, H.-J. Chu, H.-T. Chen, H.-K. Tsou and J.-L. He, *J. Biomed. Mater. Res., Part B*, 2013, **101**, 1023–1030.
55 J. Kim, S. Kwon, D.-H. Cho, B. Kang, H. Kwon, Y. Kim, S. O. Park, G. Y. Jung, E. Shin, W.-G. Kim, H. Lee, G. H. Ryu, M. Choi, T. H. Kim, J. Oh, S. Park, S. K. Kwak, S. W. Yoon, D. Byun, Z. Lee and C. Lee, *Nat. Commun.*, 2015, **6**, 8294.
56 A. Barhoum, M. L. García-Betancourt, H. Rahier and G. Van Assche, *Emerging Applications of Nanoparticles and Architecture Nanostructures*, Elsevier, 2018, pp. 255–278.
57 M. Ribeiro, F. J. Monteiro and M. P. Ferraz, *Biomatter*, 2012, **2**, 176–194.
58 M. Kıvanç, B. Barutca, A. T. Koparal, Y. Göncü, S. H. Bostancı and N. Ay, *Mater. Sci. Eng., C*, 2018, **91**, 115–124.
59 S. Pandit, K. Gaska, V. R. S. S. Mokkapati, S. Forsberg, M. Svensson, R. Kádár and I. Mijakovic, *RSC Adv.*, 2019, **9**, 33454–33459.
60 K. Rasool, M. Helal, A. Ali, C. E. Ren, Y. Gogotsi and K. A. Mahmoud, *ACS Nano*, 2016, **10**, 3674–3684.
61 K. Rasool, K. A. Mahmoud, D. J. Johnson, M. Helal, G. R. Berdiyorov and Y. Gogotsi, *Sci. Rep.*, 2017, **7**, 1598.
62 M. J. Nine, M. A. Cole, D. N. H. Tran and D. Losic, *J. Mater. Chem. A*, 2015, **3**, 12580–12602.
63 O. Akhavan and E. Ghaderi, *ACS Nano*, 2010, **4**, 5731–5736.
64 M. Haghbin Nazarpak, S. Shahabi, F. Najafi, A. Majdabadi, T. Hooshmand, B. Karimi and S. M. Fatemi, *Sci. World J.*, 2014, 9.
65 V. Malinovschi, A. Marin, V. Andrei, E. Coaca, C. Mihailescu, C. P. Lungu, C. Radulescu and I. D. J. S. Dulama, *Surf. Coat. Technol.*, 2019, **375**, 621–636.
66 L. Ren, S. Pan, H. Li, Y. Li, L. He, S. Zhang, J. Che and Y. Niu, *Sci. Rep.*, 2018, **8**, 15143.
67 X. Li, H. Qiu, X. Liu, J. Yin and W. Guo, *Adv. Funct. Mater.*, 2017, **27**, 1603181.
68 E. Wagemann, Y. Wang, S. Das and S. K. Mitra, *Phys. Chem. Chem. Phys.*, 2020, **22**, 2488–2497.
69 A. M. Forson, H. C. van der Mei and J. Sjollema, *Sci. Rep.*, 2020, **10**, 12093.
70 X. Liang, C. Liao, M. L. Thompson, M. L. Soupir, L. R. Jarboe, P. M. J. F. I. M. Dixon and F. Yang, *Front. Microbiol.*, 2017, **8**, 708.
71 A. Krasowska and K. Sigler, *Front. Cell. Infect. Microbiol.*, 2014, 4.

Comparative antibacterial activity of 2D materials coated on the porous-titania

Arash Mazinani[a,b], Hadi Rastin[a,b], Md Julker Nine[a,b], James Lee[c], Alexandra Tikhomirova[c] ,Tran Thanh Tung[a,b], Reza Ghomashchi [b,d], Stephen Kidd[c], Sarah Vreugde[e], Dusan Losic[a,b]*

a. School of Chemical Engineering and Advanced Materials, The University of Adelaide, Adelaide, SA 5005, Australia.

b. ARC Hub for Graphene Enabled Industry Transformation, The University of Adelaide, Adelaide, SA, Australia.

c. Department of Molecular and Biomedical Science, The University of Adelaide, Adelaide, SA, Australia.

d. School of Mechanical Engineering, The University of Adelaide, SA, Australia

e. Department of Surgery-Otolaryngology Head and Neck Surgery, The University of Adelaide, Woodville South, Australia

*Corresponding Author: Prof. Dusan Losic

School of Chemical Engineering and Advanced Materials, The University of Adelaide, Adelaide, SA 5005, Australia; email: dusan.losic@adelaide.edu.au

Supplementary data:

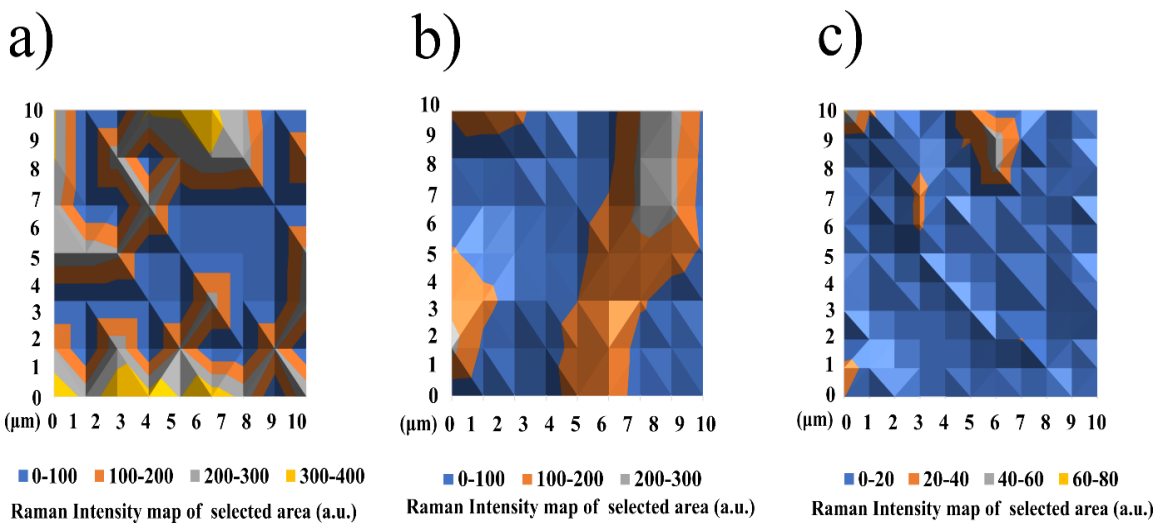

Figure S1. The Raman mapping result of deposited 2D flakes in the high concentration of (0.5 mg/ml) over PEO substrate, a) GO deposited PEO surface, b) hBN deposited PEO substrate, c) MXene deposited PEO substrate.

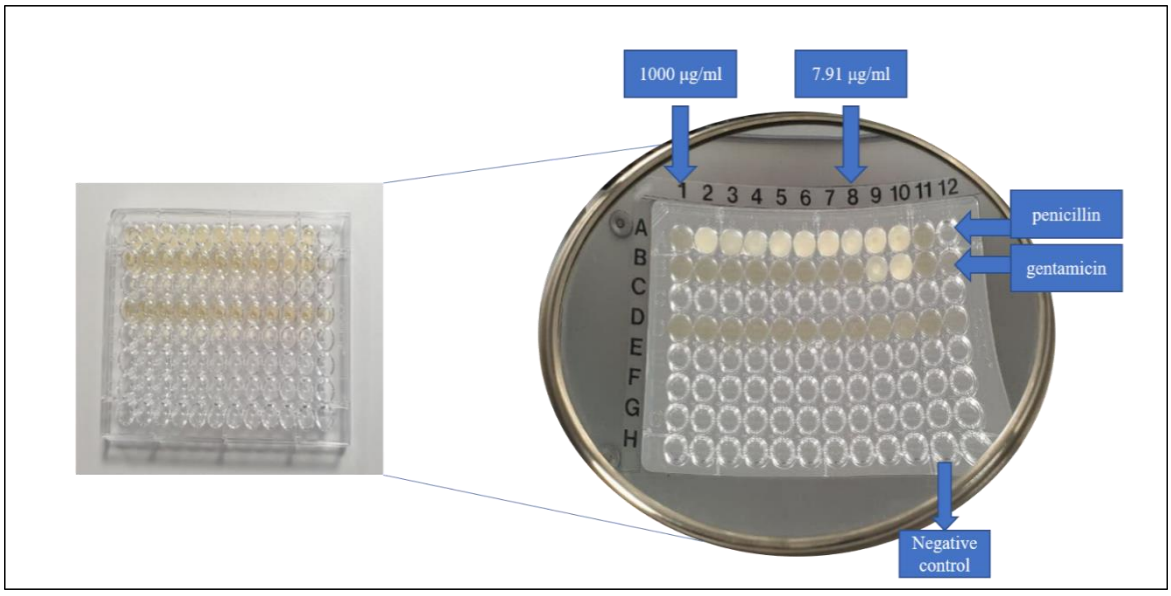

Figure S2. The result of the MIC test for Penicillin and Gentamicin against *E. coli* (JLD24) strain after 24 incubation, the initial antibiotic concentration is 1 mg/ml for both A1 and B2 test wells.

Chapter 8

Conclusions and Future works

In this chapter, the summary of key findings in this study are provided. For each chapter, a short description of the research methodology and fundamental research outcomes are highlighted. Moreover, several directions for future work have been recommended.

8.1. Conclusions

The current research contributes to the development of biomedical coating on titanium implants by application of plasma electrolytic oxidation technique and post-treatment of the surface using novel nanotechnology-based approaches to address the current complications with titanium implants, which result in implant failure. Particularly, this study investigates two fundamental approaches to modify the titanium PEO structure either by partial deposition of novel 2D materials or introducing nanostructured titania to the surface to combat the infection problem and simultaneously enhance the osseointegration ability of the orthopaedic implant.

Four fundamental research cores which this study aimed to exploit are summarized as follows:

- **Chapter 4** describes a novel method to combine the high voltage electrophoretic deposition technique (EPD) with plasma electrolytic oxidation technique (PEO), which is known as the PEO-EPD technique to deposit graphene oxide (GO) on the surface of PEO treated titanium substrate and improve the antibacterial ability of a surface. The key findings of this chapter are :
  - Partial deposition of (GO) flakes on PEO treated titanium sample is demonstrated as achievable and scalable process through PEO-EPD process in a very short period of time.
  - The most uniform pattern for GO flakes deposition obtaines within 15 seconds of the PEO-EPD process with 66% of GO surface coverage.
  - A superior antibacterial activity with 100% efficiency against *S. aureus* and around 80 % against *E.coli* bacteria is achieved.

- Good bioactivity of PEO samples after GO partial deposition is observed, evident by hydroxyapatite formation after 21 days mineralization process.
- The main significance of this study is to fabricate titanium implant with a mixture of two types of surfaces. First, PEO porous structure to improve osseointegration ability and secondly, GO patches to prevent bacterial adhesion and colonization. The main challenge with the PEO-EPD process was finding the optimum deposition time to allow partial deposition of GO on the PEO substrate and, therefore, improve the osseointegration and antibacterial activity simultaneously.

➢ **Chapter 5.** The formation of titania nanostructures by a combination of the PEO process and hydrothermal treatment is generally limited due to the formation of HAP during the HT process. HAP formation is associated with the presence of Ca and P in the PEO coating, which are usually added to the common PEO electrolytes. A new approach to replace the common PEO electrolyte with a Ca-free electrolyte that will create titania oxide film with an array of micro and nano-pores is demostrated.

- The subsequent HT process on the PEO surface is shown to fabricate additional arrays of new titania nanostructures that can be tuned to various forms such as nano-blade, nano-ribbons, nano-rods, nano-spikes, nano-pillars etc. depends on the electrolyte and HT conditions.
- The dimensions of the fabricated nanostructures with HT are highly influenced by the duration of HT process, which are showing an increasing

trend in their height from around 100 nm in the first hour of HT to about 1000 nm after 6 hours of HT process.

- The PEO treatment significantly increases the mechanical hardness of the surface (164 Hv). However, the subsequent HT decreases the mechanical stability to around 138 Hv and 108 Hv after 2 and 6 hours, respectively.
- The main significance of study presented in this chapter is demostartion of process to fabricate titania nanostructures on the PEO substrate through HT with the application of a new Ca-free electrolyte. In this new approach, a mixture of tuneable titania nanostructures such as nano-blades and nano-spikes are formed on the PEO porous micro-nano structure. The formed hierarchical micro-nano titania structure demonstrated superior bioactivity evident from the formation of HAP particles covering the whole surface area.

➢ **Chapter 6** presentes the application of different PEO electrolytes for the fabrication of Mechano-bactericidal nanostructures via combination of PEO and HT methods. Common titania PEO treated samples are bioactive but cannot address the infection issues associated with bone implants. On the other side, titania nanostructures showed great potential to fight against different types of bacteria. However, the formation of titania nanostructures over PEO treated sample via HT has been challenging due to the formation of HAP particles throughout the process. It was previously showed that the application of acidic Ca-free PEO electrolyte could lead to the formation of tuneable titania nanostructures over the surface. In the current study, a novel basic Ca-free

electrolyte is introduced, and the effect of different acidic and basic electrolyte on the formation of various types of nanostructures after different HT duration (from 1 to 24 hours) are examined. Following are the main findings of chapter 6:

- The elimination of calcium from the basic PEO electrolytes led to the formation of sodium titanate nanostructures in the forms of nano-blades, nano-needles, and micro-nano belts after the HT process using different times.
- Significantly faster formation and growth rate of nanostructures on the acidic PEO treated surface were observed compared to the basic PEO treated sample.
- Several numbers of the micropores generated by the PEO process were still detectable after 6 hours of HT on the acidic PEO substrate (A-HT_{6h}) and after 12 hours (B-HT_{12h}) on the basic PEO substrate, which can further contribute to the osseointegration enhancement.
- The application of HT after PEO notably improved the bioactivity and wettability of both acidic and basic PEO treated samples.
- The significance of study presented in this is to find the optimum condition for the fabrication of the tallest upright-oriented titania nanostructures via a combination of PEO with HT, which are assumed to damage bacteria membrane and eventually kill bacteria mechanically. In both acidic and basic PEO groups, hydrothermally treated samples after 4 hours and 6 hours demonstrated the most desirable form of nanostructures. The titania nanostructures formed by applying HT for 4

hours on the acidic PEO process showed better antibacterial activity with 88% decrease in the number of *E.coli* colonies compared to the basic PEO group (with 68% decrease in the number of CFUs) fabricated at a similar HT duration. After 6 hours of HT, acidic PEO surface exhibited superior antibacterial activity against *S. aureus* with ~ 99% colonies reduction, recorded after incubation for 24 hours.

- **Chapter 7** presents a comparative antibacterial activity improvement of PEO substrates by post drop-casting of various 2D materials. This study aims to understand and compare the antibacterial properties of the selected 2D materials (GO, HBN, MXene) at different low and high concentrations over PEO treated titanium substrates. The 2D flakes concentrations are adjusted to achieve the partial deposition of flakes on the PEO surface and ensure some extent of porous PEO substrate exposure for osseointegration enhancement, while the presence of 2D flakes would improve the antibacterial activity of the sample. Following are the main findings of this study:
  - Results show the dose-dependent nature of the deposited antibacterial agent on the PEO substrate.
  - Deposited 2D flakes on PEO substrates were mainly effective against gram-positive bacteria (*S. aureus)* compared to the gram-negative bacteria (*E. coli*). This observation can be justified by the presence of an additional protective outer membrane on gram-negative species, which could provide more effective protection against the mechano-bactericidal damage

- In the low concentration group, GO deposited PEO demonstrated the highest antibacterial activity against *S. aureus* bacteria with inactivation of 70 (±2) % of colonies. In contrast, in the higher concentration group, MXene deposited PEO samples showed the most increased antimicrobial activity with 97 (±0.5) % CFUs inactivation.
- Only about 20 % decrease in the number of *E. coli* colonies observed for higher concentration group with ~18 (±2) % CFUs decrease in the hBN-PEO sample, ~17 (±4) % for GO-PEO and ~7 (±1) % for MXene-PEO samples compared to control, demonstrating lower sensitivity of gram-negative bacteria to the antibacterial 2D materials.
- Successful formation of HAP particles over the 2D deposited PEO substrates showed good bioactivity of fabricated samples.
- The significance of results presented in this chapter is to develop new method able to generate titanium implant with a mixture of two types of surfaces. First, PEO porous titania structure to enhance the osseointegration ability, and secondly, the 2D flakes deposited on the PEO substrate to improve the antibacterial activity of the surface. This chapter provides a comparative antibacterial activity assessment of the PEO substrate partially deposited by 2D materials in different concentrations.

8.2. Recommendations for future work

This research project successfully unlocked the hidden potential of the PEO in the development of the next generation of antibacterial implants. This was achieved by combining the PEO process with subsequent nanotechnology fabrication routes, such as

nanotexturing of the surface via HT treatment or applying various 2D antibacterial materials coated by different deposition techniques.

For future direction, several pathways are recommended here to investigate other aspects of the modified PEO technology in the fabrication of antibacterial and bioactive orthopaedic and dental implants:

1. **Design of hybrids rGO-titania nanostructure via the hydrothermal treatment of GO deposited PEO-EPD surface: In previous chpaters** it was shown that GO patches deposited on PEO surface by PEO-EPD technique could improve the antibacterial activity of titania surface. However, the introduction of titania nanostructure to this system has not been thoroughly investigated. The PEO-EPD technique can partially deposit GO flakes over the PEO substrate. Further, HT of the surface is expected to form titania nanostructures over the non-covered PEO porous sites, develop the hybrid GO,rGO structure, and simultaneously improve antibacterial and bioactivity of the surface.
2. **In-vivo osseointegration and toxicity assessment of the nanotextured titania samples:** Sodium titanate nanoblades fabricated in this study demonstrated great antibacterial activity against different gram-negative and gram-positive bacteria. The initial bioactivity assessment showed a significant biomineralization ability of the surface. However, the bio-toxicity and bio-integration ability of fabricated mechano-bactericidal surface requires further investigation to ensure the safe interaction of osteoblast cells with sharp edges of titania nanostructures.
3. **Exploring the antiviral activity of titania nanostructures developed on the PEO surface**. PEO treatment is a well-known technique for the fabrication of durable and hard coating, used in different industrial and biomedical applications.

With the emergence of viral disease in current years, the development of antiviral surface has become one of the hot topics. Recently different research groups have shown the ability of nanostructured Surfaces to reduce the viability of SARS-CoV-2[1]. It is believed that the same successful mechano-bactericidal approach in killing bacteria would be effective against viruses. Particularly, sharp and slightly rendered edges of our fabricated nanoblades end to a sharp tip with approximately 10 nm width, lower than the general size range of viruses (22–150 nm)[2]. Therefore, nanostructures may pierce and slice the virus and eventually kill the viruses mechanically.

4. **Design of a hybrid GO-MXene and silver nanocomposites to improve the antibacterial activity of PEO samples.** Different studies showed high antibacterial activity of GO, MXene and silver nanoparticles against various bacteria[3-5]. However, our research revealed higher efficiency of 2D materials in killing gram-positive bacteria such as *S.aureus* compared with gram-negative ones (*E.coli*). This observation can be justified by the presence of a more protective layer in the gram-negative bacteria membrane, which makes them less susceptible to mechanical damage. Therefore, the combination of GO/MXene with a small quantity of silver nanoparticles is expected to significantly increase the antimicrobial activity against both types of gram-positive and gram-negative bacteria. The partial deposition of the mixture can be simply done with the drop-casting method on the PEO substrate.
5. **The combination of printing titniuam implants with PEO and hydrothermal process.** Recently, the 3D printing of titanium implants has received significant attention in the orthopedic field. This is mainly due to the ability of additive

manufacturing (AM) in the fabrication of shapes and geometries that cannot be developed with other conventional methods[6]. This research thesis successfully developed a new concept for the generation of antibacterial titania nanostructures achieved by combining HT with the PEO process with a specific selection of PEO electrolyte and HT duration. This novel fabrication route can be further explored on the different titanium alloys as well as 3D printed titanium samples with complex geometries.

8.3. References

1. Hasan, J., et al., *Antiviral Nanostructured Surfaces Reduce the Viability of SARS-CoV-2.* ACS biomaterials science & engineering, 2020. **6**(9): p. 4858-4861.
2. Grgacic, E.V.L. and D.A. Anderson, *Virus-like particles: Passport to immune recognition.* Methods, 2006. **40**(1): p. 60-65.
3. Rasool, K., et al., *Efficient Antibacterial Membrane based on Two-Dimensional Ti3C2Tx (MXene) Nanosheets.* Scientific Reports, 2017. **7**(1): p. 1598.
4. Sun, N., et al., *Graphene oxide-coated porous titanium for pulp sealing: an antibacterial and dentino-inductive restorative material.* Journal of Materials Chemistry B, 2020. **8**(26): p. 5606-5619.
5. Franci, G., et al., *Silver Nanoparticles as Potential Antibacterial Agents.* 2015. **20**(5): p. 8856-8874.
6. Popov, V.V., et al., *Design and 3D-printing of titanium bone implants: brief review of approach and clinical cases.* Biomedical Engineering Letters, 2018. **8**(4): p. 337-344.

Abbreviation

Description	Notation
Plasma electrolytic oxidation	PEO
Graphene oxide	GO
Hexagonal boron nitride	hBN
Hydroxyapatite	HAP
Electrophoretic deposition	EPD
Hydrothermal treatment	HT
Reduced Graphene oxide	rGO
Titanium	Ti
Diamond-like carbon	DLC
Antimicrobial peptides	AMPs
Osteomyelitis	OM
Osteoporosis	OP
Multi-drug resistant bacteria	MDR
Methicillin-resistant Staphylococcus aureus	MRSA
Passive surface modification treatments	PSM
Active surface modification	ASM
Gentamicin coating	PLLA

Appendix 1: Abbreviation

Implant-associated infection	IAI
Reactive oxygen species	ROS
Micro Arc Oxidation	MAO
Transition metal carbides and carbonitrides	MXene
Layered double hydroxides	LDHs
Ultraviolet	UV
laponite	Lap
Transition metal disulphide	TMD
Colony Forming Unit	CFU
Simulated body fluid	SBF